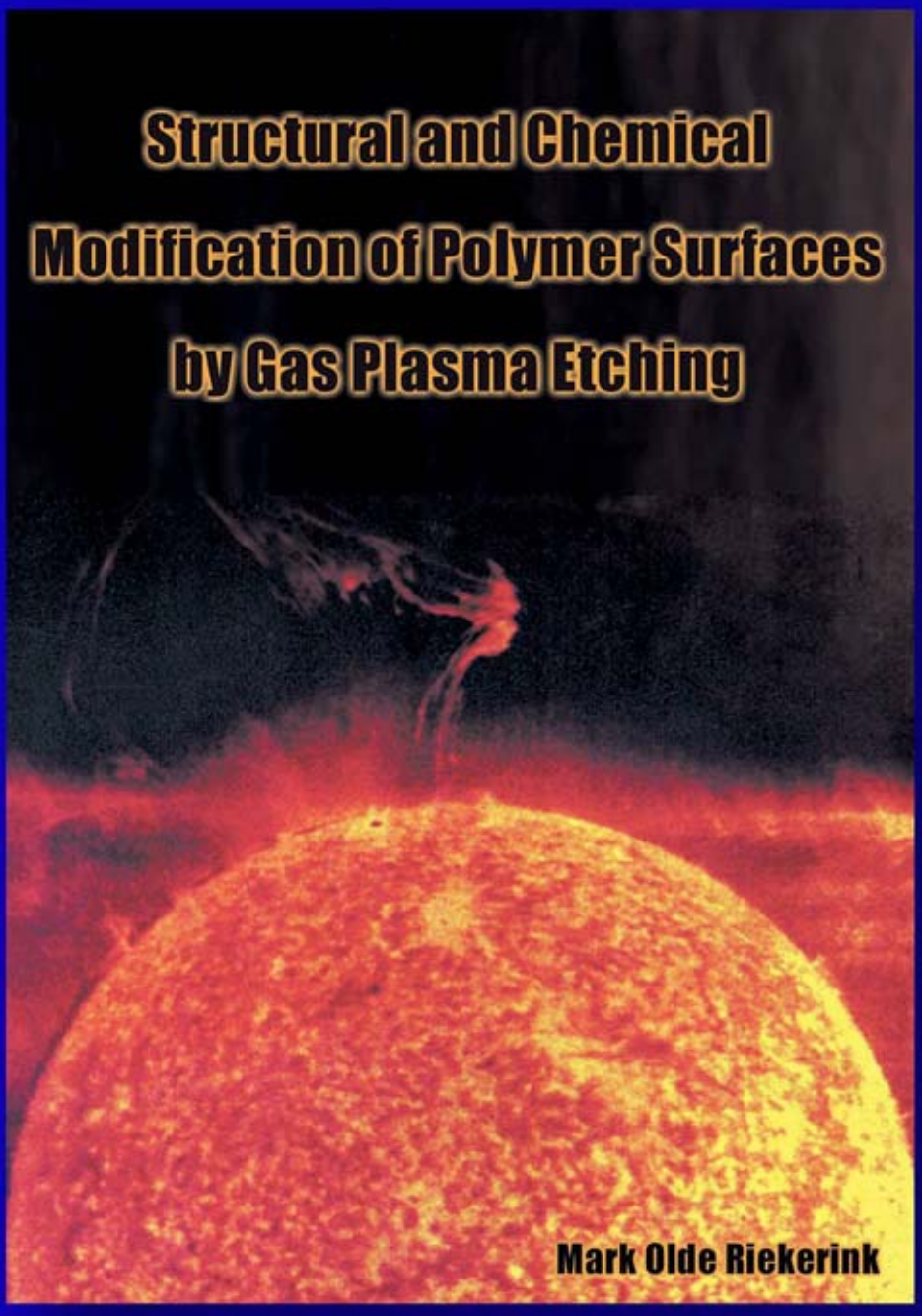
Structural and Chemical
Modification of Polymer Surfaces
by Gas Plasma Etching
Mark Olde Riekerink

STRUCTURAL AND CHEMICAL MODIFICATION OF POLYMER SURFACES BY GAS PLASMA ETCHING

PROEFSCHRIFT

ter verkrijging van
de graad van doctor aan de Universiteit Twente,
op gezag van de rector magnificus,
prof. dr. F.A. van Vught,
volgens besluit van het College voor Promoties
in het openbaar te verdedigen
op vrijdag 21 september 2001 te 16.45 uur.

door

Marinus Bernardus Olde Riekerink

geboren op 6 september 1972
te Losser

Dit proefschrift is goedgekeurd door:

Promotor:	Prof. Dr. J. Feijen
Assistent-promotor:	Dr. Ir. G.H.M. Engbers
Referent:	Dr. Ir. J.G.A. Terlingen

“Anyone who has never made a mistake has never tried anything new.”

Albert Einstein

Structural and chemical modification of polymer surfaces by gas plasma etching /
M.B. Olde Riekerink
Thesis University of Twente, Enschede, The Netherlands
With references – With summary in English, met samenvatting in het Nederlands

ISBN: 90 365 1643 9

The research described in this thesis was financed by the Netherlands Foundation for Chemical Research (NWO-CW): grant number 700-41-014.

Cover illustration: Corona and solar eruption – Courtesy of NASA.

Press: Printpartners Ipskamp, Enschede, The Netherlands, 2001

Voorwoord

Voor u ligt het eindresultaat van mijn 11 jaar durende avontuur op de Universiteit Twente. In september 1990 begon ik aan de studie Chemische Technologie en nu, september 2001, hoop ik deze leuke, interessante en zeer leerzame periode op succesvolle wijze af te kunnen sluiten met het verdedigen van dit proefschrift. Het voorwoord, dat gewoonlijk als laatste wordt geschreven maar als eerste (en vaak ook als enige) wordt gelezen, is bedoeld om allen, die de promovendus bij de totstandkoming van het proefschift hebben geholpen, te bedanken. Van die taak wil ik mij dan ook zeker kwijten. Hoewel ik bekend sta als zijnde 'lang van stof', zal ik proberen in ieder geval dit onderdeel van mijn boekje zo beknopt mogelijk te houden.

Als eerste wil ik mijn promotor, Jan Feijen, bedanken voor de gelegenheid die hij mij heeft gegeven om in zijn groep af te kunnen studeren en vervolgens verder te gaan met een promotieonderzoek. Ondanks zijn overvolle agenda heeft hij mijn onderzoek altijd met veel interesse en een kritisch oog gevolgd en met name in de slotfase ervoor gezorgd dat het geheel ook netjes op papier kwam te staan. Mijn assistent-promotor, Gerard Engbers, ben ik veel dank verschuldigd voor de enorme hoeveelheid correctiewerk, de vele nuttige discussies en de altijd aanwezige dosis gezonde humor om mijn frustraties over zijn 'opbouwende' kritiek weer wat te sussen. Naast zijn wetenschappelijke input wist hij mij ook op het sportieve vlak altijd scherp te houden bij het tweewekelijkse potje zaalvoetbal…een toque was daarbij geen overbodige luxe. Leon Terlingen, beter bekend als 'The Godfather of Plasma', heeft een belangrijke rol gespeeld tijdens de eerste fase van mijn onderzoek. Als initiator en begeleider van mijn project heeft hij zijn kennis en enthousiasme over de gasplasmatechniek op mij weten over te brengen. Zijn overstap van plasma's naar kunstmest heb ik daarom nooit helemaal begrepen.

In het nu volgende gedeelte worden normaal gesproken de studenten bedankt die de promovendus in de vorm van doctoraalopdrachten hebben geholpen bij zijn onderzoek. In mijn geval kan ik daar heel kort over zijn…ze waren er niet. Heb ik er dan in die vier jaar helemaal alleen voor gestaan? Integendeel, de diverse hoofdstukken waren niet tot stand gekomen zonder de inzet van een hele groep mensen. Allereerst heb ik een deel van mijn experimenten (hoofdstuk 5) aan de Rijksuniversiteit Groningen uitgevoerd. Henk Busscher, Henny van der Mei, Betsy v/d Belt-Gritter en alle collega-AIO's in de groep 'Biomedical Engineering' wil ik hartelijk danken voor de fijne tijd in het hoge noorden. Matthias Wessling en Erik Rolevink van de naburige vakgroep 'Membraantechnologie' hebben bijgedragen aan de totstandkoming van hoofdstuk 6. Marjan Sleijster (Isotis NV), Joop de

Vries (RUG), Dirk Grijpma en in het bijzonder Menno Claase zijn nauw betrokken geweest bij het niet onbelangrijke, laatste hoofdstuk. Oppervlakte-analyse loopt als een rode draad door dit proefschrift heen. Een drietal specialisten van het MESA+ instituut, te weten Albert v/d Berg (XPS), Mark Smithers (SEM) en Clemens Padberg (AFM), hebben hieraan een wezenlijke bijdrage geleverd. Allen hartelijk dank!

Voor de financiële, technische en administratieve ondersteuning dank ik Wim, Piet, Hetty, John, Marc en Karin. Vooral de eindeloze inzet en de altijd aanwezige lach op het gezicht van laatstgenoemde, heb ik al die jaren zeer gewaardeerd. CT-1338a, mijn werkdomein op de UT, was niet zo levendig geweest zonder de sociale inbreng van mijn kamergenoten Luuk, Alma, Paulien, Fenghua en Priscilla. Het 'hokken' van twee dames en twee kerels op één kamer was niet alleen ARBO-technisch verantwoord, maar vormde ook een uitstekende balans in de talrijke (soms diepgaande) discussies. Ook alle andere collega's van de vakgroepen PBM, RBT, STEP en MTP wil ik bedanken voor de broodnodige sociale input tijdens de koffiepauzes, borrels, BBQ's, snertfeesten, broodjes Mario en dergelijke (culinaire) uitspattingen. Naast (vr)eten, hield ik er nog andere hobby's op na tijdens mijn promotietijd. De sportievelingen waarmee ik heb getafeltennist, gezaalvoetbald, gevolleybald, gesquashed, gezeild en getriathlond zijn er te veel om op te noemen…allen bedankt voor deze welkome oplevingen in mijn bestaan als AIO.

Tot slot een dankwoord aan mijn familie en vrienden. Luuk, Ray (mijn paranimfen) en Robin hebben alledrie hun uiterste best gedaan om mijn alcoholpromillage goed op peil te houden. Door de vele biertjes en vooral 'Quatrootjes' werd ik wel eens wat loslippig…en jullie weten waartoe dat kan leiden!?! Mijn familie en schoonfamilie wil ik bedanken voor hun interesse in mijn onderzoek. Ik realiseer me dat het erg lastig moet zijn om altijd maar interessante vragen te stellen terwijl je er zelf eigenlijk geen snars van begrijpt. Met name mijn ouders en tweelingbroer Rick wil ik bedanken omdat ze me, vanaf het moment dat mijn wetenschappelijke ambities duidelijk werden, in alle opzichten altijd enorm hebben gesteund.

Rest mij nog één iemand te noemen, last but certainly not least: Annelien. Ik weet dat je echt niet van dit soort aandacht houdt en daarom zal ik me hiertoe beperken…lieverd, het is bijna 22 september…bedankt!

Mark

Contents

Chapter 1

General introduction

1.1 Introduction

Nowadays, polymeric materials are used for a wide variety of applications. The choice for a specific polymer is usually based on its bulk properties (e.g. mechanical, physical), which are mainly determined by the bulk chemistry and morphology of the processed material. For many applications the polymer's surface properties are of major importance. The desired surface properties can be obtained by modification of the surface chemistry and/or the surface structure of a polymer.

Gas plasma treatment has proven to be a versatile tool for surface modification of polymeric materials.[1-14] A gas plasma (glow discharge) is a partially ionized gas which can be generated by an electrical discharge. Thus, a highly reactive environment is created with plasma species like electrons, ions, radicals and metastables. Besides being a dry (solvent-free) and time-efficient process, the main advantage of this technique is its confinement to the surface layer of a material. By using gas plasma treatment, a variety of advantageous, interfacial properties can be introduced at a polymer surface without affecting the desired bulk properties of a material like strength, toughness and biodegradability.

Two types of gas plasma treatment, i.e. plasma etching and plasma polymerisation (deposition), are commonly used for changing the surface chemistry of a polymer. In contrast to chemical surface modification of polymers by gas plasma treatment, tailoring of the surface structure (e.g. morphology, topography, roughness) as a means of changing the material's surface properties has found far less applications. Structural and chemical surface modification of phase separated polymer systems (e.g. semi-crystalline polymers, block copolymers, organic-inorganic hybrid materials) is of importance for tailoring a wide variety of interfacial properties. Surface characteristics like wettability, adhesion, printability, friction, fouling, and biocompatibility largely determine the applicability of polymeric materials (e.g. thermoplastic objects, coatings, films, membranes, fibers, textiles, biomaterials) in various indrustial areas (e.g. automotive, packaging, filtration, clothing, biomedical technology). Furthermore,

nanostructuring of phase separated polymer systems has become increasingly important for the fast growing area of nanotechnology. Nanopatterned polymer templates have a huge potential as etching masks in nanolithographic processing.[15-22]

Preferential plasma etching is a promising method for surface nanostructuring of a phase separated polymer system.[19,23,24] This method is based on the principle that different polymers show different etching rates when exposed to a gas plasma.[25-27] Also, a substantial difference in etching rate usually exists between the crystalline and the amorphous phase of a semi-crystalline polymer.[12,28] The nanoscale architecture of the structured surfaces obtained by preferential plasma etching is governed by the phase separation of the polymer system (crystalline lamellae/spherulites, cylinders or spheres in a continuous matrix, bicontinuous structure, etc.). Therefore, by using preferential plasma etching as a surface modifying technique a diversity of nanostructured polymer and hybrid surfaces with various interfacial properties is feasible.

1.2 Objective

The objective of the study described in this thesis is to explore the possibilities of gas plasma etching as a tool to tailor the surface properties of polymeric and hybrid systems. Therefore, various plasma etchants (e.g. CF_4, CO_2, Ar) and treatment conditions (e.g. time, continuous vs. pulsed plasma) will be used throughout this study. The primary goal is to induce surface nanostructuring by preferential etching of one component from a two-phase system (e.g. crystalline vs. amorphous, organic vs. inorganic, polymer A vs. polymer B). Inherently, chemical surface modification will occur during plasma etching. After characterization of the obtained surface nanostructure (Scanning Electron Microscopy (SEM), Atomic Force Microscopy (AFM)) and chemistry (X-ray Photoelectron Spectroscopy (XPS)), their effect on the interfacial properties of the plasma etched materials (e.g. wettability, permeability, fouling, chemical selectivity, biocompatibility) will be studied in more detail.

1.3 Structure of this thesis

Gas plasma etching of polymer surfaces plays a central role in this thesis. The basic principles of this complicated process will be outlined in Chapter 2. Furthermore, the current status of developing nanostructured polymer surfaces and its (potential) applications in areas like

nanotechnology, membrane technology and biomedical technology will be discussed in this chapter.

In Chapter 3, the results of preferential etching of a semi-crystalline polymer, poly(ethylene) (PE), will be described.[29] A series of commercial PE films with varying crystallinity is treated with a CF_4 gas plasma. The surface chemical and structural modification upon plasma etching is characterized by XPS, SEM and AFM. The resulting surface wettability of the PE films is studied by water contact angle measurements.

The surface chemical and structural modification of low density PE (LDPE) upon (pulsed) CF_4 plasma treatment is described in more detail in Chapter 4. The effect of temperature rise and fluorination on the wettability and stability of LDPE films is studied as a function of the plasma treatment time.

In Chapter 5, some bio-interfacial properties of CF_4 plasma treated LDPE films are discussed. The effect of surface energy, roughness and charge on the fouling behaviour of these plasma etched films is investigated by performing *in vitro* adhesion experiments with several microbes (four different bacterial strains and one yeast strain).

Gas plasma etching of cellulose acetate membranes is described in Chapter 6. The aim of this study is to explore the possibilities to tailor the properties of these asymmetric membranes (e.g. permeability, wettability, retention, fouling) by gradual etching of the membrane's toplayer with oxidative (CO_2) or fluorinizing (CF_4) gas plasma treatment.[30]

Surface nanostructuring of a two-phase hybrid system (i.e. isolated gold nanoparticles on a continuous (polymeric) matrix) by using oxidative plasma treatment (CO_2, air) is described in Chapter 7. Protein-gold nanocolloids are adsorbed onto various substrates from an aqueous solution in a one-step procedure. After removal of the protein by preferential etching, the feasibility for selective chemical modification of these heterogeneous, nanostructured surfaces is studied by silanation and subsequent thiol chemisorption of some control substrates.

In Chapter 8, a block copolymer system is subjected to oxidative (CO_2) and mild (Ar) gas plasma etching. The effect of chemical and structural surface modification on the wettability and biocompatibility (i.e. scaffolds for bone tissue regeneration) of a series of segmented poly(ethylene oxide)/poly(butylene terephthalate) (PEO/PBT) block copolymer films is studied in this final chapter.

1.4 References

1) Suhr, H. *Applications of Nonequilibrium Plasmas to Organic Chemistry*; Hollahan, J. and Bell, A. T., Ed.; Wiley: New York, 1974, pp 57-111.

2) Yasuda, H. *J. Macromol. Sci.-Chem.* **1976**, *A10*, 383-420.
3) Liston, E. M.; Martinu, L.; Wertheimer, M. R. *Plasma surface modification of polymers for improved adhesion: a critical review*; Strobel, M., Lyons, C. and Mittal, K. L., Ed.; VSP: Utrecht, 1994, pp 3-39.
4) Chan, C. M. *Plasma Modification*; Chan, C. M., Ed.; Hanser Publishers: München, 1994, pp 225-263.
5) Piskin, E. *J. Biomater. Sci. Polym. Edn.* **1992**, *4*, 45-60.
6) Gombotz, W. R.; Hoffman, A. S. *CRC Crit. Rev. Biocompatibility* **1987**, *4*, 1-42.
7) Ratner, B. D.; Chilkoti, A.; Lopez, G. P. *Plasma Deposition and Treatment for Biomaterial Applications*; d'Agostino, R., Ed.; Academic Press, Inc.: Boston, 1990, pp 463-516.
8) Favia, P.; d'Agostino, R. *Surf. Coat. Technol.* **1998**, *98*, 1102-1106.
9) Loh, I.-H. *Medical Device Technol.* **1999**, *Jan-Febr*, 24-30.
10) Terlingen, J. G. A. *Introduction of functional groups at polymer surfaces by glow discharge techniques*; University of Twente: Enschede, The Netherlands, 1993.
11) Groenewoud, L. M. H. *Transparent and conductive polymer layers by gas plasma techniques*; University of Twente: Enschede, The Netherlands, 2000.
12) Takens, G. A. J. *Functionalization of polymeric surfaces by oxidative gas plasma treatment*; University of Twente: Enschede, The Netherlands, 1997.
13) Lens, J. P. *Gas plasma immobilization of surfactants to improve the blood compatibility of polymeric surfaces*; University of Twente: Enschede, The Netherlands, 1996.
14) Klomp, A. J. A. *Design of surface modified poly(ethylene terephthalate) non-wovens for the removal of leukocytes from platelet concentrates*; University of Twente: Enschede, The Netherlands, 1998.
15) Chou, S. Y.; Krauss, P. R.; Renstrom, P. J. *Science* **1996**, *272*, 85-87.
16) Mansky, P.; Harrison, C. K.; Chaikin, P. M.; Register, R. A.; Yao, N. *Appl. Phys. Lett.* **1996**, *68*, 2586-2588.
17) Mansky, P.; DeRouchey, J.; Russell, T. P.; Mays, J.; Pitsikalis, M.; Morkved, T.; Jaeger, H. *Macromolecules* **1998**, *31*, 4399-4401.
18) Morkved, T. L.; Lu, M.; Urbas, A. M.; Ehrichs, E. E.; Jaeger, H. M.; Mansky, P.; Russell, T. P. *Science* **1996**, *273*, 931-933.
19) Park, M.; Harrison, C.; Chaikin, P. M.; Register, R. A.; Adamson, D. H. *Science* **1997**, *276*, 1401-1404.
20) Mansky, P.; Chaikin, P.; Thomas, E. L. *J. Mater. Sci.* **1995**, *30*, 1987-1992.
21) Harrison, C.; Park, M.; Chaikin, P. M.; Register, R. A.; Adamson, D. H. *J. Vac. Sci. Technol. B* **1998**, *16*, 544-552.
22) Spatz, J. P.; Eibeck, P.; Mossmer, S.; Moller, M.; Herzog, T.; Ziemann, P. *Adv. Mater.* **1998**, *10*, 849-852.
23) Lammertink, R. G. H.; Hempenius, M. A.; van den Enk, J. E.; Chan, V. Z. H.; Thomas, E. L.; Vancso, G. J. *Adv. Mater.* **2000**, *12*, 98-103.
24) Lammertink, R. G. H.; Hempenius, M. A.; Chan, V. Z. H.; Thomas, E. L.; Vancso, G. J. *Chem. Mater.* **2001**, *13*, 429-434.
25) Taylor, G. N.; Wolf, T. M. *Polym. Eng. Sci.* **1980**, *20*, 1087-1092.
26) Pederson, L. A. *J. Electrochem. Soc.: Solid-State Sci. Technol.* **1982**, *129*, 205-208.
27) Egitto, F. D.; Vukanovic, V.; Taylor, G. N. *Plasma Etching of Organic Polymers*; d'Agostino, R., Ed.; Academic Press, Inc.: Boston, 1990, pp 321-422.
28) Herbert, S.; Shinozaki, D. M.; Collacott, R. J. *J. Mater. Sci.* **1996**, *31*, 4655-4661.
29) Olde Riekerink, M. B.; Terlingen, J. G. A.; Engbers, G. H. M.; Feijen, J. *Langmuir* **1999**, *15*, 4847-4856.
30) Olde Riekerink, M. B.; Engbers, G. H. M.; Wessling, M.; Feijen, J. *submitted to J. Colloid Interface Sci.* **2001**.

Chapter 2

Gas plasma etching as a tool for nanostructuring of polymer surfaces: A literature survey

2.1 Introduction

Tailoring of a polymer surface structure on the nanoscale level (nanostructuring) has become an important tool in the fast growing area of nanotechnology. Several innovative approaches can be found in literature to create well-ordered, nanopatterned surfaces for possible use in semi-conductor integrated circuits, electronics and optical or magnetic (nano)devices.[1-14] Some of these concepts that are aimed at nanopatterning of polymer surfaces for use as nanolithographic templates will be briefly described below.

One useful approach is based on nanoimprint lithography.[4,5] With this technique, a mold with nanometer-scale features is first pressed into a thin thermoplastic resist film cast on a substrate. The imprint pattern is formed when the temperature is above the glass transition temperature (T_g) of the thermoplast. After the mold is removed, an anisotropic etching process is used to transfer the nanopattern through the entire polymer resist thickness. In this way, compact disks with 10 nm features and a data storage density of 400 Gbits/inch^2 were fabricated (nano-CDs).[4]

Another frequently used approach is based on the orientation of thin phase separated block copolymer films, which could subsequently be used as polymer masks/templates for nanolithography.[6-8,15-18] Extensive research has been performed on the phase behaviour, (self-)ordering and surface morphology of styrenic di- and triblock copolymers (A-B, A-B-A) with the second phase (B) consisting of e.g. poly(butadiene), poly(isoprene) or poly(2-vinylpyridine).[10,11,19-41] Thin films of these block copolymers are well-known for their spontaneous self-assembly, resulting in nanoscale patterns when they are annealed above their T_g. Uniform orientation (alignment) of phase separated domains (e.g. cylinders) can further be improved by applying flow or electrical fields during film processing.[7,8,24,30,37,41] After nanopatterning of a thin copolymer film, nanolithographic templates can be created by preferential etching of one polymer phase (see also section 2.4.4). These templates can contain

nanoscale tubular or spherical holes, ridges, or tubular or spherical protuberances as shown in Figure 2.1. The size of these holes/protuberances is determined by the domains formed by the phase separated polymer system and can vary between tens of nanometers (block copolymers) and a few micrometers (polymer blends). Subsequently, these nanopatterns can be transferred into semi-conductor substrates (e.g. silicon wafers) by anisotropic etching techniques like reactive ion etching (RIE).[15]

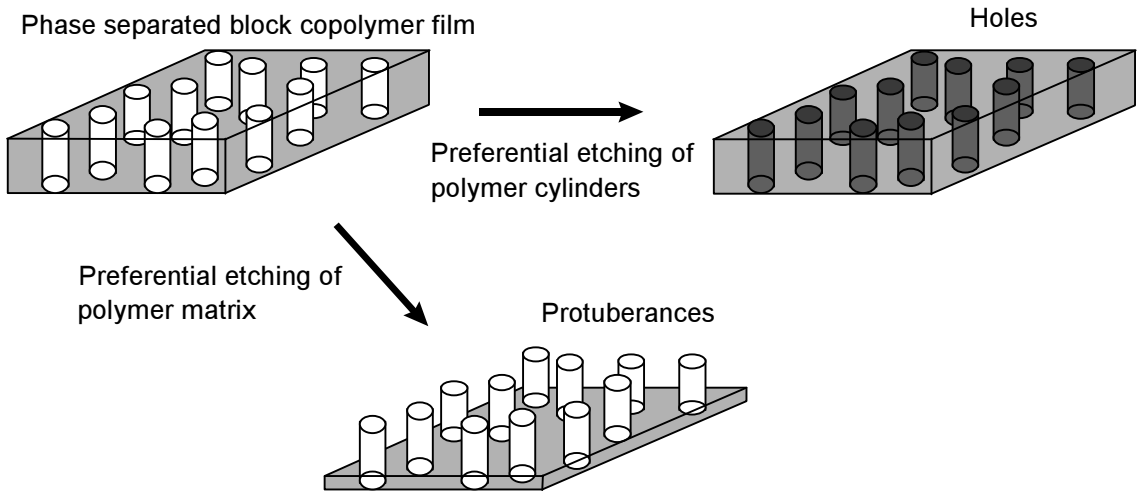

Figure 2.1: *Schematic representation of preferential etching of an oriented, phase separated block copolymer film for creation of nanolithographic templates.*

A third interesting approach is based on the self-organization of well-defined, nanosized gold islands onto a substrate.[42-48] Spatz *et al.* developed nanopatterned gold colloid surfaces by coating a monolayer of diblock copolymer micelles containing encapsulated gold nanoparticles onto an inorganic substrate (e.g. semi-conductor wafer, glass, mica).[45,47] The gold loaded micelles self-organize into a quasi-hexagonal pattern with lattice spacing between 20 and 200 nm. After removal of the organic phase (i.e. copolymer) these nanostructured gold surfaces can serve as lithographic masks for patterning of the underlying substrate.[46-48]

Although the above concepts generally lead to well-ordered surface nanostructures, a high degree of patterning can only be obtained through proper manipulation of thin polymer layers. Moreover, uniform surface patterning (e.g. hexagonal packing) is often only observed over a relatively small surface area. Besides structural manipulation of a polymer surface, tailoring of the surface chemistry would also be of great interest for nanotechnological applications. For example, the development of well-defined, chemically heterogeneous surfaces on a nanoscale (i.e. chemically different surface nanodomains) has a large potential for applications like sensing devices. When uniform surface nanopatterning is not a prerequisite (e.g. biosensing,

controlled drug release, tissue engineering, nanofiltration), gas plasma treatment is a versatile tool for simultaneous and controlled modification of a polymer's surface nanostructure and chemistry. Moreover, this surface modification technique is suitable for a large range of materials with varying geometrical properties (e.g. film thickness, size, shape). The principles and applications of gas plasma etching with respect to nanostructuring of polymer surfaces will be further discussed in the remainder of this literature survey.

2.2 Gas plasma treatment of polymer surfaces

Gas plasma treatment processes (glow discharges) are extensively used for the surface modification of polymeric materials (e.g. thermoplastic films, fibers, non-wovens, membranes, biomedical devices). The main advantage of this versatile technique is that it is confined to the surface layer of a material without affecting its bulk properties. Moreover, it is a dry (solvent-free), clean and time-efficient process with a large variety of controllable process parameters (e.g. discharge gas, power input, pressure, treatment time) within the same experimental setup. However, due to the complexity of the plasma process and the variety of chemical and physical reactions that can occur, the exact chemical and structural composition of a plasma treated surface is hard to predict. Detailed descriptions of the theory of plasma treatment processes can be found in literature.[49-58]

Gas plasmas produced by electrical discharges can be divided in two types: 'hot', equilibrium plasmas (e.g. arcs, plasma jets) and 'cold', non-equilibrium plasmas.[52] Most of the applications of plasma treatment involve the use of 'cold' plasmas, which can be defined as partially ionized gases composed of reactive species (e.g. electrons, ions, free radicals, photons, metastables) and gas molecules. In 'cold' plasmas the temperature of the electrons is much higher than the temperature of the gas molecules (non-equilibrium state), making them suitable for treatment of anorganic as well as organic materials (polymers). Non-equilibrium plasmas can be generated by a number of discharge techniques including direct-current (DC) discharges, low-frequency discharges (e.g. corona treatment[59]; kHz range), radio-frequency (RF) discharges (MHz range), and microwave discharges (GHz range).[60,61] For laboratory purposes (low-pressure) RF glow discharges are mostly used for plasma treatment of polymer surfaces.

Basically, RF gas plasma treatment can be used for three different types of polymer surface modification. Firstly, the surface chemistry of a polymer can be tailored by plasma immobilisation, i.e. the covalent grafting of pre-adsorbed molecules with functional end groups

(e.g. surfactants) onto a surface by an inert gas plasma (e.g. argon).[62-68] Plasma polymerisation (deposition) is a second way of modifying the surface chemistry of a polymer.[51,57,69,70] In this case, the plasma acts as an initiator by forming free radicals in the monomer gas and on the surface of the substrate. As a result of this process a thin polymer film is deposited on the substrate surface. Generally, by using hydrocarbon containing gases plasma polymerisation is observed. A variety of surface properties (e.g. conductivity[71], biocompatibility[72], non-fouling[70,73]) can be tailored by simply varying the type of monomer gas. Nowadays, plasma polymerisation is used for a growing number of applications in the coating industry. Finally, the surface of a polymer can be modified by plasma etching.[58,74-78] Besides changing the surface chemistry through introduction of specific chemical groups (e.g. OH, COOH, NH_2, F)[49,78,79], the surface structure (e.g. morphology, topography, roughness) will also be affected by plasma etching. Gases which can induce etching of polymer surfaces are noble gases (e.g. helium, neon, argon), hydrogen, nitrogen, oxygen, carbon dioxide, air, water, ammonia, tetrafluoromethane, or mixtures (e.g. CF_4/O_2).

Besides gas plasma etching, several other etching techniques are used for surface modification of polymers. Wet chemical etching by oxidative acids (e.g. permanganate[80-84], chromic acid[81,85-92], fuming nitric acid[93-95], perchloric acid[86]) is often used for revealing surface morphological features of semi-crystalline polymers (e.g. poly(ethylene)).[95] Moreover, printability of non-polar polymer surfaces and adhesion of polymer fibers/laminates (e.g. UHMW-PE) to other compounds like epoxy resins can be largely improved by wet oxidative etching, due to surface roughening (mechanical interlocking) and the introduction of polar surface groups (chemical anchors).[81,85,87-91,93] One disadvantage of wet chemical etchants is its detrimental effect on the mechanical (bulk) properties of thin polymer films/fibers.[91] Other etching techniques found in literature are: ultrasonic etching[96], electron or ion beam etching[97-101], excimer laser etching[102-104], ultraviolet (UV) etching[102,105], ozone etching (ozonolysis)[6,17,106], and a combination of the two latter techniques.[107,108] Although these etching techniques all have a long history in the field of surface technology, they will not be further discussed here.

This chapter will focus on RF gas plasma etching of polymer surfaces without aiming for a complete review of (plasma) etching technology. Some basic principles of this versatile technique and its applications in polymer (nano)technology will be discussed in the following sections.

2.3 Plasma etching mechanisms

Plasma etching is the practice of etching or gasifying substrate material in a plasma.[75] Plasma etching has been extensively used for improving the adhesive properties of polymer surfaces.[92,109,110] Other important applications of plasma etching of polymers are found in the semi-conductor and lithographic industry.

In spite of the wide application field of plasma etching the exact mechanisms which affect the rates, (an)isotropicity and selectivity of the polymer etching process are still not completely understood. For a given substrate, the parameters that play a role in plasma etching can be divided in two categories: apparatus parameters (e.g. reactor type, frequency, electrodes) and discharge parameters (e.g. type of gas (etchant), discharge power, gas flow rate, pressure, treatment time).

Basically, plasma etching can proceed through three different pathways. Firstly, a polymer substrate is etched by chemical reaction of reactive plasma species (e.g. radicals, ions) with the surface, referred to as chemical etching. Secondly, ion bombardment on a polymer surface causes sputtering of the surface, which is a physical process. Finally, UV radiation from the plasma phase causes dissociation of chemical bonds, which leads to formation of low molecular weight (LMW) material. In general, these three etching mechanisms occur simultaneously during the plasma treatment of a polymer and induce a flow of volatile (LMW) products from the substrate to the plasma. This causes a gradual weight loss of the treated polymeric material (Figure 2.2). The three pathways mentioned above will be separately discussed in the following sections. A more detailed description is found in literature.[49,74-76,111-116]

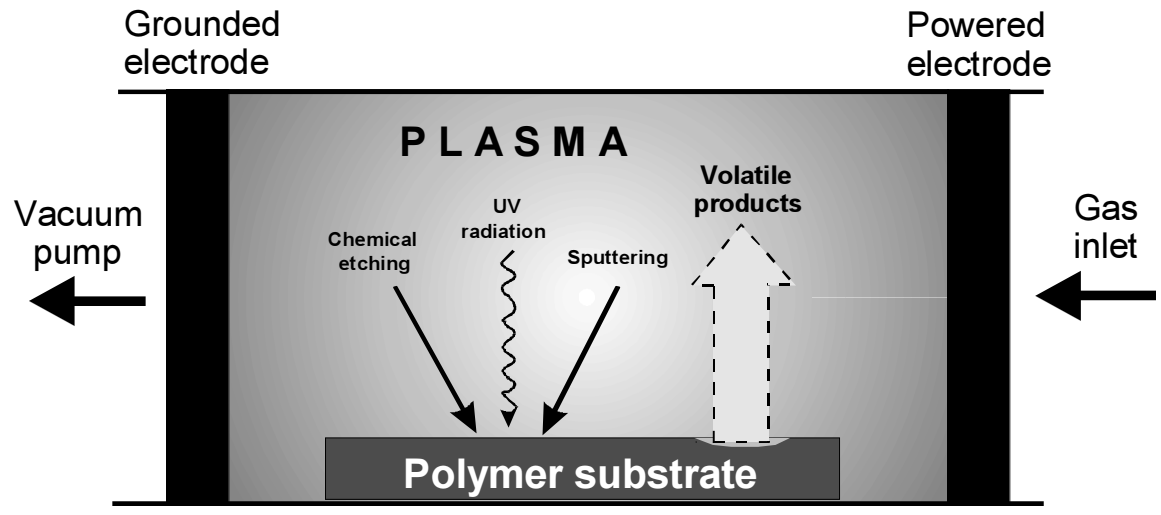

Figure 2.2: *Schematic representation of the plasma etching process.*

2.3.1 Chemical etching

In chemical etching, activated gas phase species merely react with a surface resulting in the formation of volatile products. The reactive etchant species are created by the plasma through collisions of accelerated, energetic free electrons with gas molecules, which induces dissociation or excitation of the feed gas (e.g. O_2, CF_4, Ar). These inelastic electron-neutral collisions maintain the supply of ions, metastables and radicals which are continuously lost by reaction and recombination. Examples of reactions which can occur in the plasma phase are found in literature.[49,51,54,56,75,76]

Oxygen gas plasmas are known to be very reactive etchants. This reactivity is due to the reaction of atomic oxygen with a polymer surface, which is the starting point for the etching process. Attack of a polymer by atomic oxygen can proceed through a variety of mechanisms including abstraction (Figure 2.3: 1-3), addition to unsaturated moieties (Figure 2.3: 4), or to a lesser extent by absorption of the O_2 dissociation energy (Figure 2.3: 5).[112]

After atomic oxygen attack the radical site can be subsequently attacked by molecular oxygen leading to significantly weakened C-C bonds. A possible autoxidation process (Figure 2.3: 6) leading to bond weakening was proposed by Moss *et al.*.[117] From these structures polymer backbone chain scissions can occur (Figure 2.3: 7), eventually leading to volatile etch products such as CO and CO_2.

In order to enhance etching of polymers in pure oxygen plasmas, the dissociation of O_2 to atomic oxygen should be optimized. An efficient way to increase the atomic oxygen concentration in O_2 plasmas is by addition of fluorine containing gases.[74] In literature several examples are known of increasing plasma etching rates after addition of some CF_4 to the O_2 gas feed.[112,114,118-120] Atomic oxygen is mainly produced through electron-induced dissociation processes.[49] Therefore, the enhancement of oxygen atom production upon addition of CF_4 is probably due to increases of the electron density and/or electron energy in the plasma. In addition, atomic fluorine can react chemically with a polymer, leading to reactive radical sites (Figure 2.3: 8-9). These sites can further react with atomic or molecular oxygen, inducing polymer backbone cleavage by β-scission of the formed alkoxy radicals (Figure 2.3: 6-7). Although fluorine containing gases like CF_4 can enhance degradation of polymers through facile generation of polymer radical sites, excess fluorine in the O_2/CF_4 plasma can serve to inhibit etching by competing with oxygen for these sites (radical sites are lost through fluorination).

Compared to oxygen and fluorine containing gases, chemical etching is of minor importance when noble gases (e.g. argon) are used as etchants. In these cases other mechanisms determine the etching process (discussed below).

Abstraction by oxygen:

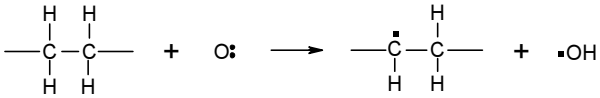

(1)

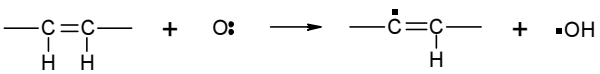

(2)

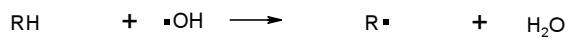

(3)

Oxygen addition:

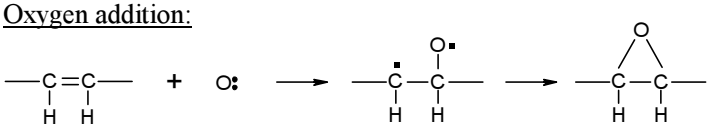

(4)

Dissociation by oxygen:

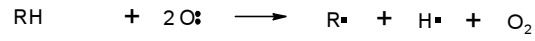

(5)

Oxidation:

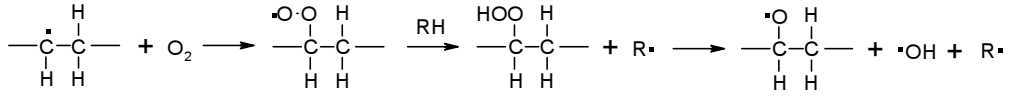

(6)

Chain scission:

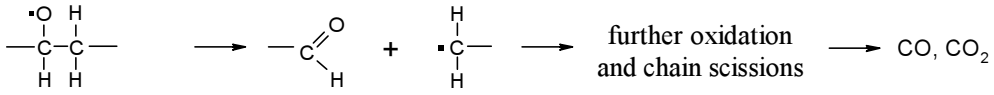

(7)

Abstraction by fluorine:

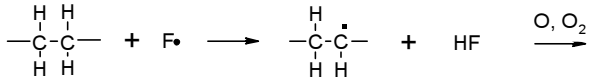

(8)

Fluorine addition:

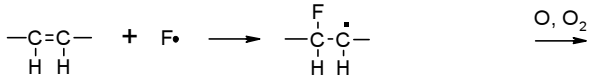

(9)

Figure 2.3: *Scheme of several reactions that can occur during chemical etching in an O_2 and/or CF_4 gas plasma.*

2.3.2 Sputtering

During gas plasma etching the surface of a polymer is slowly sputtered by a bombardment of ions from the plasma phase. When a substrate is exposed to a plasma, it will directly be negatively charged by accelerated electrons. As a result, low energetic positive ions are

accelerated through the plasma sheath towards the substrate surface. In this way, material fragments are ejected from the surface, which makes sputtering a purely physical process. Sputtering is inherently unselective, because the energy of the accelerated ions is much higher than the energy required for breaking specific surface chemical bonds.[111]

Compared to chemical etching, etching through sputtering is generally slow. Higher sputter rates can be achieved by lowering the pressure (< 50 mTorr) and by properly biasing the substrate (negative potential). In this way, redeposition of sputtered species is suppressed and the energy of the ions is greatly increased in the direction of the substrate (see also section 2.3.4).

2.3.3 UV radiation

Besides energetic species like ions, radicals and metastables, a gas plasma is also a source of electromagnetic radiation (e.g. ultraviolet (UV) radiation, visible light, infrared (IR) radiation). The energetic UV radiation has several effects on polymers. Firstly, vacuum UV radiation with wavelengths of less than 178 nm can cause photo-ionization.[121,122] Furthermore, UV radiation can cause dissociation of bonds yielding free radicals:[55,74,116,123]

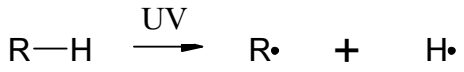

These radicals can cause crosslinking in the substrate's surface layer or can react with species from the plasma phase. For example, subsequent reaction with atomic or molecular oxygen can lead to polymer backbone cleavage (Figure 2.3: 6-7). A substantial amount of research on VUV-induced oxidation/degradation of polymer surfaces in low-pressure plasmas has been performed by Holländer *et al.*.[105,115,124-126] Terlingen *et al.* have shown that VUV radiation (λ < 150 nm) causes decarboxylation of poly(acrylic acid) (PAAc) during argon plasma treatment:[127]

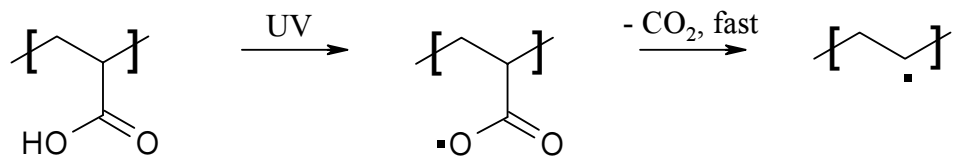

This decarboxylation, inducing surface free radicals, is largely responsible for the relatively high etching rate of PAAc in an argon plasma (see section 2.4). The removal of pendant groups (e.g. COOH, Cl) from the polymer backbone (e.g. PAAc, PVC) induced by VUV

radiaton emitted from an argon plasma was also found by Groenewoud *et al.*.[128] Obviously, UV radiation can play a major role in plasma etching of polymers. However, its etching impact is largely dependent on the polymer's chemical structure and the plasma conditions, which also counts for chemical etching and sputtering.

2.3.4 Reactive ion etching (RIE)

Besides the three etching pathways discussed above, an intermediate type of plasma etching can be distinguished. Reactions between a polymer substrate and neutral species from the plasma phase (chemical etching) can be accelerated by ion bombardment (ion enhanced etching).[111] For example, oxygen plasma etching of polymers proceeds at relatively low rates in the absence of energetic ions. The combined action of chemically reactive and accelerated ions results in anisotropical etching of the polymer surface. This combined process, which is also commonly referred to as reactive ion etching (RIE), is often used for patterning of surfaces in the semiconductor and (nano)lithographic industry.[5,17,46,76,123,129-134] Anisotropicity (directionality) can only be achieved when the substrate is properly biased, i.e. when the substrate functions as the cathode with a (self-)bias voltage. This important feature distinguishes RIE from other plasma etching techniques. RIE does not affect all polymers equally. Some polymers exhibit a higher etching rate than others and the etching rate for a given polymer depends on the plasma conditions.

2.4 Factors that determine the plasma etching rate of a polymer

In the previous section it was shown that polymers can be etched in a gas plasma according to several mechanisms that occur simultaneously. The etching rate (Å/min) of a polymer largely depends on the plasma treatment conditions (e.g. discharge gas, pressure, discharge power, substrate temperature, treatment time) and on the polymer's chemical and physical properties. These three aspects will be briefly discussed in the following paragraphs. Based on a difference of etching rates, the most susceptible polymer segments in a phase separated polymer system (e.g. block copolymers, semi-crystalline polymers, polymer blends) can be preferentially removed by plasma etching. This will be discussed in paragraph 2.4.4.

2.4.1 Etching rate vs. plasma treatment conditions

The etching rate for a given polymer can vary considerably with changes in plasma treatment conditions. Probably, the most important discharge parameter is the type of gas (etchant)

being used. Oxygen plasmas are known to be very reactive etchants. Addition of CF_4 to an oxygen plasma will even further increase the etching rate of a polymer (see paragraph 2.3.1). Although inert gases like argon (Ar) generally induce relatively low etching rates compared to oxidative and fluorinizing plasmas (rule of thumb: Ar<CF_4<CO_2<air<O_2), Ar plasma etching can be highly selective. Terlingen *et al.* studied the etching rates of poly(ethylene) (PE) and PAAc in different gas plasmas.[135] They showed that the Ar plasma etching rate of PAAc was more than 30 times higher than that of PE (see also Table 2.1). The selectivity of plasma etching with CF_4 or air turned out to be much lower (PAAc/PE etch ratios of 3 and 2, respectively).

The plasma etching rate of a given polymer increases with discharge power.[100,136] Upon higher energy input, the density of plasma reactive species as well as their acceleration towards the substrate will increase, resulting in more severe etching of the substrate's surface.

The etching rate of a polymer substrate also increases upon temperature elevation during plasma treatment.[74] Similar to chemical reactions this temperature dependence is often described by the Arrhenius equation, relating the etching rate to an apparent (total) activation energy for the polymer etching reactions (ln[etching rate] ~ $-E_a/RT$). Besides accelerated etching reactions, LMW etch products will evaporate more easily at higher substrate temperatures which may further increase the etching rate. While higher temperatures induce higher plasma etching rates, plasma etching in its turn leads to an increase of surface temperature.[59,137,138] A continuous surface bombardment of plasma reactive species induces heat development, while exothermic surface chemical reactions will also generate energy. Due to the low heat conductivity of most polymers, the surface temperature can be raised considerably during continuous plasma etching. Besides influencing the etching rate this increase in temperature might also have a major effect on the polymer surface structure. In this respect, an interesting parameter that could influence the etching rate and the structural development of polymers is the use of pulsed plasma etching. When the etching process is periodically interrupted, the increase in temperature is likely to be less extreme than during continuous etching. Because of this milder temperature effect the etching rate will probably be lower and the surface structure of the polymer might be less affected.

The etching rate of polymers can be significantly enhanced when a bias voltage is applied to the polymer substrate (cathode), due to a bombardment of higher energetic ions (RIE, paragraph 2.3.4). For CF_4/O_2 RIE, the dependence of the etching rate on the bias voltage can be roughly considered as linear.[120] Bias voltages might also be used to drive polymer surface reactions in specific directions.[120]

Another discharge parameter that can influence the etching rate of polymers is the position of the substrate in the reactor during plasma treatment. Normand *et al.* investigated the functionalization and degradation of high density PE (HDPE), poly(propylene) (PP) and poly(caprolactone) in an oxygen microwave discharge.[139] They concluded that the functionalization level is higher in the afterglow than in the plasma itself, without any significant etching of the polymer surface. Takens determined the etching rates of LDPE film in a RF CO_2 gas plasma and in its afterglow.[78] He found that the LDPE etching rate in the afterglow is on the order of 50-100 times lower than etching in the plasma. The high etching rates in the plasma region are caused by a relatively high reactive particle density and a bombardment of charged species (e.g. electrons, ions) onto the substrate. In the afterglow region the substrate is exposed only to a small fraction of long-living, neutral plasma species (e.g. radicals), which significantly suppresses the etching rate. However, even if the etching rate is almost negligible in the afterglow treatment, its actual value still depends on the susceptibility of the polymer chains to bond cleavage by these long-living radicals.

Although the plasma pressure is an important discharge parameter, its effect on the etching rate is ambiguous. Upon rising plasma pressures increases as well as decreases of etching rate have been observed.[100,134,136] A plausible explanation can be found in the fact that higher pressures increase the plasma gas concentration, but also decrease the electron density. The concentration of plasma reactive species, which directly influences the etching rate, results from the superposition of these counteracting effects. Furthermore, the energy of the ions impinging on the substrate decreases with rising pressure, which reduces the sputtering effect.

In general, plasma etching will reach an equilibrium state (i.e. constant etching rate) in the course of treatment time. Initial fluctuations of the etching rate may arise due to changes of surface temperature (see above) and surface chemistry. For example, crosslinking in the surface layer of the substrate during plasma treatment (e.g. CASING[140-142]) could suppress the initial etching rate of a polymer.

2.4.2 Etching rate vs. chemical structure

The chemical structure of polymers has a major influence on the etching rate. Many studies have been aimed at providing more understanding about the relation between etch resistance and a polymer's chemical structure.[113,114,118,143-147] One of the first studies in this field was performed by Taylor and Wolf who studied the oxygen plasma etching behaviour of 40 different polymers.[143,144] They found that the strength of polymer backbone bonds mainly determines the rate of weight loss in most cases. Weak backbone bonds enhance polymer removal, while weak backbone-side chain bonds also enhance degradation. Weak bonds not

immediately pendant to the main polymer chain have little effect on the etching rate. They also concluded that aromatic functional side groups and certain polar functional side groups promote etch resistance, possibly by enhancing deactivation of normally reactive species. Finally, they found that organometallic polymers such as poly(dimethyl siloxane) exhibit extremely good etch resistance, most likely due to the formation of a thin metal oxide layer that protects the polymer from further etching.

Table 2.1: Etching rates of various polymers in relation to their chemical structure and the plasma treatment conditions.

Polymer	Structure characteristics	Plasma treatment conditions	Etching rate (Å/min)	Ref.
PE	Saturated; -C-C- and -C-H	Ar, CF_4, air RF plasma; 44 W; 0.07 mbar	6 (Ar) 70 (CF_4) 600 (air)	135
PAAc	Weak side chain; -COOH	Ar, CF_4, air RF plasma; 44 W; 0.07 mbar	200 (Ar) 200 (CF_4) 1200 (air)	135
PS	Aromatic	O_2 plasma; 100 W; 0.55 Torr	270	133
PMMA	Weak side chain; -$COOCH_3$	O_2 plasma; 100 W; 0.55 Torr	640	133
Poly(butene-1 sulfone)	Weak sulfone backbone	O_2 plasma; 100 W; 0.55 Torr	1920	133
POM	Weak backbone; -C-O-C-	He plasma; 30 W; 0.10 Torr	1360 *	146
PP	Saturated; -C-CH_3	He plasma; 30 W; 0.10 Torr	90 *	146
PET	Aromatic; -COOC- (weak)	He plasma; 30 W; 0.10 Torr	120 *	146
PVC	Weak bonds; -C-Cl	O_2 plasma; 100 W; 0.55 Torr	3500	143
MMA/MAAc Copolymer	Weak side chains; -$COOCH_3$, -COOH	CF_4/O_2 RF plasma; 200 W; 0.55 Torr	>3200	147
Cellulose	Weak backbone; a lot of R-O-R	CF_4/O_2 RF plasma; 200 W; 0.55 Torr	>7000	147
PU Oxime	Weak backbone	CF_4/O_2 RF plasma; 200 W; 0.55 Torr	>1700	147
PC (Lexan®)	Aromatic; -OCOO- (weak)	CF_4/O_2 RF plasma; 200 W; 0.55 Torr	750	147

* Etching rate calculated from weight loss rate ($mg.cm^{-2}.min^{-1}$) with $\rho_{POM} = 1.25\ g.cm^{-3}$, $\rho_{PP} = 0.9\ g.cm^{-3}$, and $\rho_{PET} = 1.38\ g.cm^{-3}$.

In general, some basic guidelines can be formulated concerning the etching behaviour of polymers in relation to their chemical structure:

- Aromatic polymers have lower etching rates than their aliphatic analogues.[74,113,114,123,147]
- Polymers containing little (or no) oxygen and no halogen other than fluorine are most resistant to oxygen plasma etching.[123]
- Polymers containing chlorine are rapidly eroded in an oxygen plasma (weak C-Cl bonds).[123]
- Cyano (-CN) and fluorine substituents in the polymer enhance the etch resistance, due to strong bonding to the backbone chains.[74]

In the past, a wide variety of homopolymers and copolymers have been tested for their plasma etch resistance.[74,100,113,114,118,123,133,135,136,139,143-153] Table 2.1 shows a survey of the etching rates of some characteristic polymers. Although this table is far from complete, it gives a clear picture of the varying etching rates of different polymers in relation to their chemical structure and the plasma treatment conditions.

2.4.3 Etching rate vs. physical properties

Besides the chemical structure, the physical properties (e.g. T_m, T_g, crystallinity) of a polymer also influence the etching rate. Polymers with a high thermal stability (i.e. high T_m or T_g) are likely to be less susceptible than low-melting polymers, since a substantial temperature rise can be expected at the polymer's surface during plasma etching (discussed in section 2.4.1).

For semi-crystalline polymers it is generally known that the crystalline regions are more etch-resistant than the amorphous segments.[108,154-156] Herbert *et al.* studied the etching process of a PE surface using ultraviolet radiation in the presence of ozone.[108] They found that the amorphous regions of PE were preferentially etched during this treatment resulting in a fine scale surface topography. Okuno *et al.* investigated the correlation between crystallinity and plasma susceptibility of PET and nylon 66 fibers.[154] The weight loss after exposure to an air plasma decreased with increasing crystallinity up to a threshold crystallinity, above which slight increases of weight loss were observed.

The most plausible explanation for the etch selectivity in semi-crystalline polymers is found in the fact that the permeability of plasma reactive species into a dense, crystalline structure is lower than into loosely packed, amorphous material.[78] The diffusion of reactive particles into a polymer is known to be an important factor in the chemical etching processes of materials.[157]

2.4.4 Preferential etching of phase separated polymer systems

As discussed in the previous sections, the etching behaviour of a polymer is dependent on a number of factors. Phase separated polymer systems (e.g. semi-crystalline polymers, block copolymers, polymer blends) consist of two (or more) polymer phases, each phase forming their own domains on a micro- or nanoscale. When exposing such a system to a plasma treatment, the etching rate of the distinct polymer phases will be determined by their respective chemical and physical properties. Under specific plasma treatment conditions one polymer phase will be more susceptible to etching than the other, resulting in preferential etching. The efficiency of preferential plasma etching will be enhanced when the disparity of etching rates between the different components is enlarged (i.e. high etch ratio). A schematic representation of preferential etching of a phase separated polymer system has been shown earlier (Figure 2.1).

From previous studies it is known that semi-crystalline polymers can show preferential etching behaviour (see also previous section).[108,154-156] In these cases preferential etching of the amorphous phase was observed. This difference in etching rates allows the examination of the crystalline structure (e.g. lamellae, spherulites) after the amorphous phase has been removed.[158]

Preferential plasma etching can also be used for investigating the morphological properties of polymer blends in which the etching rates of the blend components are substantially different. Ramesh *et al.* studied the size distribution of poly(butadiene) (PB) particles in a continuous poly(styrene) (PS) matrix.[159] They found that PB was etched about three times faster than PS when exposed to an oxygen plasma. Owing to this etch ratio the PB particles covering PS were removed first, revealing the internal morphology of high-impact PS. Similar studies were performed by Yang *et al.*, Takamatsu *et al.* and Nishimura *et al.*.[158,160,161] They evaluated particle dispersions in polymer blends/composites by means of preferential oxygen plasma etching. Moreover, the latter investigated the phase structure of poly(urethane) with this etching technique. Thermoplastic poly(urethane) is known to be composed of soft and hard segments.[162,163] The authors found that the etching rate of the soft segments is nearly seven times larger than that of the hard segments. Preferential oxygen plasma etching was also reported by King *et al.*, who studied the morphology of water trees that were grown in low density PE.[164]

More recently, preferential etching techniques have been applied to block copolymer films in order to create nanolithographic masks for semi-conductor applications.[6,15] Pattern transfer from the polymer mask into the underlying silicon substrate was performed by anisotropic plasma etching (RIE). Since the unaltered organic blocks (PS, PB) can not be etched at highly

different rates under RIE conditions, two different processing techniques were applied prior to RIE to enhance the etching selectivity of the block copolymer films. Ozonolysis was used to remove the PB phase from the PS matrix by selective attack of the backbone's double bonds.[6,15] This highly selective etching technique has also been succesfully applied by other investigators.[106,165,166] A reverse etching effect was obtained by pre-treatment of the PS-PB film with OsO_4.[15] Selective staining of the PB phase (double bonds) lowered the etching rate of PB compared to unstained PS, resulting in a PS:PB etch ratio of ~2:1. A drawback of OsO_4 staining as well as ozonolysis is that both techniques are confined to processing block copolymers that contain one component with unsaturated double bonds. Moreover, the complete etching process (incl. pattern transfer by RIE) involves several steps. A versatile, one-step approach for obtaining high etch ratios and direct pattern transfer is the incorporation of silicon-containing or organometallic blocks into the copolymer.[106,166-170] With this type of block copolymers etching selectivity is obtained through formation of a thin, etch resistant oxide layer at the surface of the inorganic block during O_2 RIE. In this way, organic:inorganic etch ratios up to 50:1 were obtained.[106,170]

2.5 Applications of nanostructured polymer surfaces

Preferential plasma etching as a tool for nanostructuring of polymer surfaces can be used in a wide area of applications. Although initially this surface modification technique was mainly applied to polymeric materials as a useful pre-treatment for studying their (phase separated) morphology with electron microscopy[158-161,164], its versatile potential has far outgrown this restricted area.

Due to the rapid development and large economic potential of nanotechnology, the use of preferential plasma etching as a nanolithographical processing technique in the semi-conductor industry (see previous section) is an area that has gained a lot of interest in the past few years. Phase separated polymer templates have already been succesfully applied as etching masks for nanopattern transfer[15,47,169], although further optimization is still essential (e.g. aspect ratio ↑, large-area patterning).

An interesting area that has received increasing attention is the development of nanoporous membranes for advanced applications in filtration technology.[166,171,172] By preferential plasma etching of nanopores into thin (polymer) films the membrane's properties could be tailored to serve a variety of applications ranging from ultrafiltration to controlled release. Moreover, simultaneous chemical surface modification of the membrane's toplayer during

plasma etching may add advantageous properties to the membrane like low-fouling or wettability.[173-175]

Nanostructuring of polymer surfaces by preferential plasma etching can also be of great use to biomedical technology, an area with fast growing importance in modern society. A wide variety of applications involving bioadhesion, cell-substrate interactions, controlled drug release and biosensing could be developed or improved by structural and chemical tailoring of the biomaterial's surface. Den Braber showed that cell proliferation and orientation on biomaterials can be manipulated by microtexturing of the biomaterial's surface.[176] Liu *et al.* developed diblock copolymer films with well-defined nanochannels (chemical valves) that can be useful in chemical sensing devices and controlled drug release.[172] Furthermore, nanotemplates could be created for immobilization of active biomolecules or cells by simultaneous nanostructuring and chemical functionalization of a substrate. Finally, a general point of interest in biomedical surface science is the improvement of the biocompatibility of polymer surfaces. The adhesion of cells, microbes or proteins onto biomaterials could be enhanced or reduced by tailoring a biomaterial's surface structure and chemistry with plasma etching.

Summarizing, gas plasma etching can be of great use for tailoring the surface characteristics (nanostructure and chemistry) of polymers in order to enhance their potential in several application areas. For a given material, a diversity of interfacial properties can be obtained with this one-step technique simply by varying the treatment conditions (e.g. discharge gas, treatment time, continuous vs. pulsed treatment). A number of these possibilities will be explored in this thesis. Four different polymeric systems (i.e. semi-crystalline polymers, asymmetric membranes, organic-inorganic hybrid surfaces, segmented block copolymers) that are of interest to areas like biomedical, membrane or nanotechnology will be subjected to gas plasma etching. The effect of surface nanostructuring and chemical surface modification upon plasma etching on the system's interfacial properties (e.g. wettability, permeability, fouling, chemical selectivity, biocompatibility) will be described in the following chapters.

2.6 References

1) Xia, Y. N.; Rogers, J. A.; Paul, K. E.; Whitesides, G. M. *Chem. Rev.* **1999**, *99*, 1823-1848.
2) Wallraff, G. M.; Hinsberg, W. D. *Chem. Rev.* **1999**, *99*, 1801-1821.
3) Walheim, S.; Schaffer, E.; Mlynek, J.; Steiner, U. *Science* **1999**, *283*, 520-522.
4) Chou, S. Y.; Krauss, P. R.; Zhang, W.; Guo, L. J.; Zhuang, L. *J. Vac. Sci. Technol. B* **1997**, *15*, 2897-2904.

5) Chou, S. Y.; Krauss, P. R.; Renstrom, P. J. *Science* **1996**, *272*, 85-87.
6) Mansky, P.; Harrison, C. K.; Chaikin, P. M.; Register, R. A.; Yao, N. *Appl. Phys. Lett.* **1996**, *68*, 2586-2588.
7) Mansky, P.; DeRouchey, J.; Russell, T. P.; Mays, J.; Pitsikalis, M.; Morkved, T.; Jaeger, H. *Macromolecules* **1998**, *31*, 4399-4401.
8) Morkved, T. L.; Lu, M.; Urbas, A. M.; Ehrichs, E. E.; Jaeger, H. M.; Mansky, P.; Russell, T. P. *Science* **1996**, *273*, 931-933.
9) Stocker, W. *Macromolecules* **1998**, *31*, 5536-5538.
10) Spatz, J. P.; Sheiko, S.; Moller, M. *Adv. Mater.* **1996**, *8*, 513-517.
11) Spatz, J. P.; Moller, M.; Noeske, M.; Behm, R. J.; Pietralla, M. *Macromolecules* **1997**, *30*, 3874-3880.
12) Boltau, M.; Walheim, S.; Mlynek, J.; Krausch, G.; Steiner, U. *Nature* **1998**, *391*, 877-879.
13) Burmeister, F.; Schafle, C.; Keilhofer, B.; Bechinger, C.; Boneberg, J.; Leiderer, P. *Adv. Mater.* **1998**, *10*, 495-497.
14) Lammertink, R. G. H. *Poly(ferrocenyldimethylsilanes) at the Interface of Chemistry and Materials Science: Synthesis, Structure-Properties and Thin Film Applications*; University of Twente: Enschede, The Netherlands, 2000.
15) Park, M.; Harrison, C.; Chaikin, P. M.; Register, R. A.; Adamson, D. H. *Science* **1997**, *276*, 1401-1404.
16) Mansky, P.; Chaikin, P.; Thomas, E. L. *J. Mater. Sci.* **1995**, *30*, 1987-1992.
17) Harrison, C.; Park, M.; Chaikin, P. M.; Register, R. A.; Adamson, D. H. *J. Vac. Sci. Technol. B* **1998**, *16*, 544-552.
18) Spatz, J. P.; Eibeck, P.; Mossmer, S.; Moller, M.; Herzog, T.; Ziemann, P. *Adv. Mater.* **1998**, *10*, 849-852.
19) Annis, B. K.; Schwark, D. W.; Reffner, J. R.; Thomas, E. L.; Wunderlich, B. *Makromol. Chem.* **1992**, *193*, 2589-2604.
20) Zhao, Y. *Macromolecules* **1992**, *25*, 4705-4711.
21) Scott, D. B.; Waddon, A. J.; Lin, Y. G.; Karasz, F. E.; Winter, H. H. *Macromolecules* **1992**, *25*, 4175-4181.
22) Schwark, D. W.; Vezie, D. L.; Reffner, J. R.; Thomas, E. L.; Annis, B. K. *J. Mater. Sci. Lett.* **1992**, *11*, 352-355.
23) Winter, H. H.; Scott, D. B.; Waddon, A. J.; Lin, Y. G.; Karasz, F. E. *Flow-Induced Ordering and Anisotropy of a Triblock Copolymer Styrene-Butadiene-Styrene with Cylindrical Domain Morphology*; Moldenaers, P. and Keunings, R., Ed.; Elsevier Science Publishers B.V.: Brussels, Belgium, 1992; Vol. 1, pp 405-407.
24) Albalak, R. J.; Thomas, E. L. *J. Polym. Sci. B: Polym. Phys.* **1993**, *31*, 37-46.
25) Morrison, F. A.; Mays, J. W.; Muthukumar, M.; Nakatani, A. I.; Han, C. C. *Macromolecules* **1993**, *26*, 5271-5273.
26) Morrison, F. A.; Mays, J. W.; Nakatani, A.; Han, C. C. *Polym. Prepr.* **1993**, *34*, 678-679.
27) Sakurai, S.; Iwane, K.; Nomura, S. *Macromolecules* **1993**, *26*, 5479-5486.
28) Xie, R.; Sun, G.; Yang, B.; Jiang, B. *Macromolecules* **1994**, *27*, 3444-3446.
29) Jackson, C. L.; Muthukumar, M.; Barnes, K. A.; Morrison, F. A.; Mays, J. W.; Nakatani, A. I.; Han, C. C. *Polym. Prepr.* **1994**, *35*, 624-625.
30) Albalak, R. J.; Thomas, E. L. *J. Polym. Sci. B: Polym. Phys.* **1994**, *32*, 341-350.
31) Berg, R. v. d.; Groot, H. d.; Dijk, M. A. v.; Denley, D. R. *Polymer* **1994**, *35*, 5778-5781.
32) Thomas, E. L.; Lescanec, R. L. *Phil. Trans. R. Soc. Lond. A* **1994**, *348*, 149-166.
33) Gattiglia, E.; Turturro, A.; Ricci, D.; Bonfiglio, A. *Macromol. Rapid Commun.* **1995**, *16*, 919-925.
34) Dijk, M. A. v.; Berg, R. v. d. *Macromolecules* **1995**, *28*, 6773-6778.

35) Sakurai, S.; Umeda, H.; Taie, K.; Nomura, S. *J. Chem. Phys.* **1996**, *105*, 8902-8908.
36) Adams, J. L.; Quiram, D. J.; Graessley, W. W.; Register, R. A.; Marchand, G. R. *Macromolecules* **1996**, *29*, 2929-2938.
37) Albalak, R. J.; Thomas, E. L.; Capel, M. S. *Polymer* **1997**, *38*, 3819-3825.
38) Laurer, J. H.; Hajduk, D. A.; Smith, S. D.; Gruner, S. M.; Agard, D. A.; Spontak, R. J. *Macromolecules* **1997**, *30*, 3938-3941.
39) Kim, G.; Libera, M. *Macromolecules* **1998**, *31*, 2670-2672.
40) Kim, G.; Libera, M. *Macromolecules* **1998**, *31*, 2569-2577.
41) Albalak, R. J.; Capel, M. S.; Thomas, E. L. *Polymer* **1998**, *39*, 1647-1656.
42) Morkved, T. L.; Wiltzius, P.; Jaeger, H. M.; Grier, D. G.; Witten, T. A. *Appl. Phys. Lett.* **1994**, *64*, 422-424.
43) Roescher, G. A. *Stabilization of Colloidal Noble Metals by Block Copolymers*; University of Twente: Enschede, The Netherlands, 1995.
44) Spatz, J. P.; Mößmer, S.; Möller, M. *Chem. Eur. J.* **1996**, *2*, 1552-1555.
45) Spatz, J. P.; Mößmer, S.; Möller, M.; Herzog, T.; Plettl, A.; Ziemann, P. *J. Luminesc.* **1998**, *76&77*, 168-173.
46) Lewis, P. A.; Ahmed, H.; Sato, T. *J. Vac. Sci. Technol. B* **1998**, *16*, 2938-2941.
47) Spatz, J. P.; Herzog, T.; Mossmer, S.; Ziemann, P.; Moller, M. *Adv. Mater.* **1999**, *11*, 149-153.
48) Koslowski, B.; Strobel, S.; Herzog, T.; Heinz, B.; Boyen, H. G.; Notz, R.; Ziemann, P.; Spatz, J. P.; Moller, M. *J. Appl. Phys.* **2000**, *87*, 7533-7538.
49) Terlingen, J. G. A. *Introduction of functional groups at polymer surfaces by glow discharge techniques*; University of Twente: Enschede, The Netherlands, 1993.
50) Gombotz, W. R.; Hoffman, A. S. *CRC Crit. Rev. Biocompatibility* **1987**, *4*, 1-42.
51) Biederman, H.; Osada, Y. *Adv. Polym. Sci.* **1990**, *95*, 59-109.
52) Suhr, H. *Applications of Nonequilibrium Plasmas to Organic Chemistry*; Hollahan, J. and Bell, A. T., Ed.; Wiley: New York, 1974, pp 57-111.
53) Yasuda, H. *J. Macromol. Sci.-Chem.* **1976**, *A10*, 383-420.
54) Bell, A. T. *Fundamentals of Plasma Chemistry*; Hollahan, J. and Bell, A. T., Ed.; Wiley: New York, 1974, pp 1-56.
55) Liston, E. M.; Martinu, L.; Wertheimer, M. R. *Plasma surface modification of polymers for improved adhesion: a critical review*; Strobel, M., Lyons, C. and Mittal, K. L., Ed.; VSP: Utrecht, 1994, pp 3-39.
56) Chan, C. M. *Plasma Modification*; Chan, C. M., Ed.; Hanser Publishers: München, 1994, pp 225-263.
57) Yasuda, H. *Plasma polymerization*; Academic Press, Inc.: Orlando, 1985.
58) Chapman, B. *Glow Discharge Processes - Sputtering and Plasma Etching*; John Wiley & Sons: New York, 1980.
59) Overney, R. M.; Lüthi, R.; Haefke, H.; Frommer, J.; Meyer, E.; Güntherodt, H. J.; Hild, S.; Fuhrmann, J. *Appl. Surface Sci.* **1993**, *64*, 197-203.
60) Kasemura, T.; Ozawa, S.; Hattori, K. *J. Adhesion* **1990**, *33*, 33-44.
61) Badey, J. P.; Urbaczewski-Espuche, E.; Jugnet, Y.; Sage, D.; Duc, T. M.; Chabert, B. *Polymer* **1994**, *35*, 2472-2479.
62) Terlingen, J. G. A.; Feijen, J.; Hoffman, A. S. *J. Biomater. Sci.-Polym. Edn.* **1992**, *4*, 31-33.
63) Terlingen, J. G. A.; Feijen, J.; Hoffman, A. S. *J. Colloid Interface Sci.* **1993**, *155*, 55-65.
64) Terlingen, J. G. A.; Brenneisen, L. M.; Super, H. T. J.; Pijpers, A. P.; Hoffman, A. S.; Feijen, J. *J. Biomater. Sci.-Polym. Edn.* **1993**, *4*, 165-181.
65) Lens, J. P.; Terlingen, J. G. A.; Engbers, G. H. M.; Feijen, J. *Langmuir* **1997**, *13*, 7052-7062.
66) Lens, J. P.; Harmsen, P. F. H.; TerSchegget, E. M.; Terlingen, J. G. A.; Engbers, G. H. M.; Feijen, J.

J. Biomater. Sci.-Polym. Edn. **1997**, *8*, 963-982.

67) Lens, J. P.; Terlingen, J. G. A.; Engbers, G. H. M.; Feijen, J. *Polymer* **1998**, *39*, 3437-3444.

68) Lens, J. P.; Terlingen, J. G. A.; Engbers, G. H. M.; Feijen, J. *J. Biomater. Sci.-Polym. Edn.* **1998**, *9*, 357-372.

69) Groenewoud, L. M. H.; Engbers, G. H. M.; Terlingen, J. G. A.; Wormeester, H.; Feijen, J. *Langmuir* **2000**, *16*, 6278-6286.

70) Os, M. T. v. *Surface modification by plasma polymerization: film deposition, tailoring of surface properties and biocompatibility*; University of Twente: Enschede, The Netherlands, 2000.

71) Groenewoud, L. M. H. *Transparent and conductive polymer layers by gas plasma techniques*; University of Twente: Enschede, The Netherlands, 2000.

72) Panchalingam, V.; Poon, B.; Huo, H. H.; Savage, C. R.; Timmons, R. B.; Eberhart, R. C. *J. Biomater. Sci.-Polym. Edn.* **1993**, *5*, 131-145.

73) Wu, Y. L. J.; Timmons, R. B.; Jen, J. S.; Molock, F. E. *Colloid Surf. B-Biointerfaces* **2000**, *18*, 235-248.

74) Egitto, F. D.; Vukanovic, V.; Taylor, G. N. *Plasma Etching of Organic Polymers*; d'Agostino, R., Ed.; Academic Press, Inc.: Boston, 1990, pp 321-422.

75) Flamm, D. L.; Herb, G. K. *Plasma Etching Technology-An Overview*; Manos, D. M. and Flamm, D. L., Ed.; Academic Press, Inc.: Boston, 1989, pp 1-89.

76) Jansen, H. V. *Plasma Etching in Microtechnology*; University of Twente: Enschede, The Netherlands, 1996.

77) Sugawara, M. *Plasma Etching - Fundamentals and Applications*; Oxford University Press: Oxford, 1998.

78) Takens, G. A. J. *Functionalization of polymeric surfaces by oxidative gas plasma treatment*; University of Twente: Enschede, The Netherlands, 1997.

79) Klomp, A. J. A. *Design of surface modified poly(ethylene terephthalate) non-wovens for the removal of leukocytes from platelet concentrates*; University of Twente: Enschede, The Netherlands, 1998.

80) Dong, Y. M.; Yuan, Q.; Wu, Y. S.; Wang, M. *Polym. Bull.* **2000**, *44*, 85-91.

81) Mercx, F. P. M.; Benzina, A.; Vanlangeveld, A. D.; Lemstra, P. J. *J. Mater. Sci.* **1993**, *28*, 753-759.

82) Olley, R. H.; Hodge, A. M.; Bassett, D. C. *J. Polym. Sci. B-Polym. Phys.* **1979**, *17*, 627-643.

83) Olley, R. H.; Bassett, D. C. *Polymer* **1982**, *23*, 1707-1710.

84) Shahin, M. M.; Olley, R. H.; Blissett, M. J. *J. Polym. Sci. B-Polym. Phys.* **1999**, *37*, 2279-2286.

85) Bag, D. S.; Kumar, V. P.; Maiti, S. *J. Appl. Polym. Sci.* **1999**, *71*, 1041-1048.

86) Ghosh, I.; Konar, J.; Bhowmick, A. K. *J. Adhes. Sci. Technol.* **1997**, *11*, 877-893.

87) Sheng, E.; Sutherland, I.; Brewis, D. M.; Heath, R. J. *J. Adhes. Sci. Technol.* **1995**, *9*, 47-60.

88) Silverstein, M. S.; Breuer, O. *J. Mater. Sci.* **1993**, *28*, 4718-4724.

89) Silverstein, M. S.; Breuer, O. *Composites Sci. Technol.* **1993**, *48*, 151-157.

90) Silverstein, M. S.; Breuer, O.; Dodiuk, H. *J. Appl. Polym. Sci.* **1994**, *52*, 1785-1795.

91) Silverstein, M. S.; Sadovsky, J. *J. Adhes. Sci. Technol.* **1995**, *9*, 1193-1208.

92) Silverstein, M. S.; Sadovsky, J.; Alon, D.; Wahad, V. *J. Appl. Polym. Sci.* **1999**, *72*, 405-418.

93) Bag, D. S.; Kumar, V. P.; Maiti, S. *Angew. Makromol. Chem.* **1997**, *249*, 33-46.

94) Glennon, D.; Nevell, T. G.; Tsibouklis, J.; Ewen, R. J. *Mater. Res. Bull.* **1998**, *33*, 1139-1142.

95) Uehara, H.; Nakae, M.; Kanamoto, T.; Ohtsu, O.; Sano, A.; Matsuura, K. *Polymer* **1998**, *39*, 6127-6135.

96) Zhao, Y. Y.; Bao, C. G.; Feng, R.; Mason, T. J. *J. Appl. Polym. Sci.* **1998**, *68*, 1411-1416.

97) Svorcik, V.; Micek, I.; Rybka, V.; Palmetshofer, L.; Hnatowicz, V. *J. Appl. Polym. Sci.* **1998**, *69*, 1257-1261.

98) Svorcik, V.; Rybka, V.; Hnatowicz, V.; Novotna, M.; Vognar, M. *J. Appl. Polym. Sci.* **1997**, *64*, 2529-2533.
99) Golub, M. A. *Langmuir* **1996**, *12*, 3360-3361.
100) Sprang, N.; Theirich, D.; Engemann, J. *Surf. Coat. Technol.* **1995**, *74-75*, 689-695.
101) Busscher, H. J.; Stokroos, I.; Mei, H. C. v. d.; Rouxhet, P. G.; Schakenraad, J. M. *J. Adh. Sci. Technol.* **1992**, *6*, 347-356.
102) Zhang, J. Y.; Esrom, H.; Kogelschatz, U.; Emig, G. *Modification of polymers with UV excimer radiation from lasers and lamps*; Mittal, K. L., Ed.; VSP: Utrecht, 1995, pp 153-184.
103) Hiraoka, H.; Sendova, M.; Lee, C. H.; Lätsch, S.; Wong, T. M.; Sung, J.; Hung, C. T.; Smith, T. *SPIE* **1995**, *2547*, 260-266.
104) Williams, R. L.; Tavakoli, S. M.; Hunt, J. A.; Riches, S. T. *Laser surface modification of polymers to improve biocompatibility*; 12th Eur. Conf. Biomater.: Porto, 1995, pp 103.
105) Fozza, A.; Roch, J.; Klemberg-Sapieha, J. E.; Kruse, A.; Holländer, A.; Wertheimer, M. R. *Polym. Prepr.* **1997**, *38*, 1097-1098.
106) Avgeropoulos, A.; Chan, V. Z.-H.; Lee, V. Y.; Ngo, D.; Miller, R. D.; Hadjichristidis, N.; Thomas, E. L. *Chem. Mater.* **1998**, *10*, 2109-2115.
107) Walzak, M. J.; Flynn, S.; Foerch, R.; Hill, J. M.; Karbashewski, E.; Lin, A.; Strobel, M. *UV and ozone treatment of polypropylene and poly(ethylene terephthalate)*; Mittal, K. L., Ed.; VSP: Utrecht, 1995, pp 253-272.
108) Herbert, S.; Shinozaki, D. M.; Collacott, R. J. *J. Mater. Sci.* **1996**, *31*, 4655-4661.
109) Choi, D. M.; Park, C. K.; Cho, K.; Park, C. E. *Polymer* **1997**, *38*, 6243-6249.
110) Wu, S. *Polymer Interface and Adhesion*; Marcel Dekker, Inc.: New York, 1982.
111) Flamm, D. L. *Introduction to Plasma Chemistry*; Manos, D. M. and Flamm, D. L., Ed.; Academic Press, Inc.: Boston, 1989, pp 91-183.
112) Egitto, F. D. *Pure & Appl. Chem.* **1990**, *62*, 1699-1708.
113) Moss, S. J.; Jolly, A. M.; Tighe, B. J. *Plasma Chem. Plasma Process.* **1986**, *6*, 401-416.
114) Moss, S. J. *Polym. Degrad. Stab.* **1987**, *17*, 205-222.
115) Holländer, A.; Klemberg-Sapieha, J. E.; Wertheimer, M. R. *Macromolecules* **1994**, *27*, 2893-2895.
116) Morosoff, N.; Crist, B.; Bumgarner, M.; Hsu, T.; Yasuda, H. *J. Macromol. Sci.-Chem.* **1976**, *A10*, 451-471.
117) Moss, S. J.; Jolly, A. M.; Tighe, B. J. *Oxygen plasma stripping rates in relation to polymer structure*; Boulos, M. I. and Munz, R. J., Ed.; Int. Union Pure Appl. Chem.: Montreal, 1983, pp 621-626.
118) Cain, S. R.; Egitto, F. D.; Emmi, F. *J. Vac. Sci. Technol. A* **1987**, *5*, 1578-1584.
119) Turban, G.; Rapeaux, M. *J. Electrochem. Soc.: Solid-State Sci. Technol.* **1983**, *130*, 2231-2236.
120) Occhiello, E.; Garbassi, F.; Coburn, J. W. *Etching of Polymers by CF_4/O_2 Discharges*; Akashi, K. and Kinbara, A., Ed.; Proc. 8th Int. Symp. Plasma Chem.: Tokyo, 1987, pp 947-952.
121) Partridge, R. H. *J. Chem. Phys.* **1966**, *45*, 1685-1690.
122) Clark, D. T.; Dilks, A. *J. Polym. Sci. A-Polym. Chem.* **1977**, *15*, 2321-2345.
123) Blevins, R. W.; Daly, R. C.; Turner, S. R. *Lithographic Resists*; Kroschwitz, J. I., Ed.; John Wiley & Sons: New York, 1987; Vol. 9, pp 97-138.
124) Hollander, A.; Klembergsapieha, J. E.; Wertheimer, M. R. *J. Polym. Sci. A-Polym. Chem.* **1995**, *33*, 2013-2025.
125) Hollander, A.; KlembergSapieha, J. E.; Wertheimer, M. R. *J. Polym. Sci. A-Polym. Chem.* **1996**, *34*, 1511-1516.
126) Holländer, A.; Behnisch, J. *Polym. Prepr.* **1997**, *38*, 1051-1052.

127) Terlingen, J. G. A.; Takens, G. A. J.; Gaag, F. J. v. d.; Hoffman, A. S.; Feijen, J. *J. Appl. Polym. Sci.* **1994**, *52*, 39-53.

128) Groenewoud, L. M. H.; Terlingen, J. G. A.; Engbers, G. H. M.; Feijen, J. *Langmuir* **1999**, *15*, 5396-5402.

129) Jurek, M. J.; Tarascon, R. G.; Reichmanis, E. *Polym. Mater. Sci. Eng.* **1989**, *60*, 376-380.

130) Haring, R. A.; Nunes, S. L.; McGouey, R. P.; Galligan, E. A.; Volksen, W.; Hedrick, J. L.; Labadie, J. *J. Mater. Res.* **1995**, *10*, 1028-1037.

131) Baggerman, J. A. G.; Visser, R. J.; Collart, E. J. H. *J. Appl. Phys.* **1994**, *75*, 758-769.

132) Samukawa, S.; Mieno, T. *Plasma Sources Sci. Technol.* **1996**, *5*, 132-138.

133) Taylor, G. N.; Wolf, T. M.; Moran, J. M. *J. Vac. Sci. Technol.* **1981**, *19*, 872-880.

134) Richter, K.; Orfert, M.; Drescher, K. *Surf. Coat. Technol.* **1997**, *97*, 481-487.

135) Terlingen, J. G. A.; Hoffman, A. S.; Feijen, J. *J. Appl. Polym. Sci.* **1993**, *50*, 1529-1539.

136) Zeuner, M.; Meichsner, J.; Poll, H. U. *Plasma Sources Sci. Technol.* **1995**, *4*, 406-415.

137) Durandet, A.; Joubert, O.; Pelletier, J.; Pichot, M. *J. Appl. Phys.* **1990**, *67*, 3862-3866.

138) ter Beek, M. *Immobilisatie van enzymen aan oppervlakte gemodificeerde polyethyleen membranen (not published)*; University of Twente: Enschede, The Netherlands, 1994.

139) Normand, F.; Granier, A.; Leprince, P.; Marec, J.; Shi, M. K.; Clouet, F. *Plasma Chem. Plasma Process.* **1995**, *15*, 173-198.

140) Hansen, R. H.; Schonhorn, H. *J. Polym. Sci. B* **1966**, *4*, 203-209.

141) Schonhorn, H.; Hansen, R. H. *J. Appl. Polym. Sci.* **1967**, *11*, 1461-1474.

142) Yao, Y.; Liu, X.; Zhu, Y. *J. Adh. Sci. Technol.* **1993**, *7*, 63-75.

143) Taylor, G. N.; Wolf, T. M. *Oxygen Plasma Removal of Thin Polymer Films*: Ellenville, New York, 1979, pp 175-201.

144) Taylor, G. N.; Wolf, T. M. *Polym. Eng. Sci.* **1980**, *20*, 1087-1092.

145) Gerenser, L. J. *XPS studies of in situ plasma-modified polymer surfaces*; Strobel, M., Lyons, C. and Mittal, K. L., Ed.; VSP: Utrecht, 1994, pp 43-64.

146) Yasuda, H.; Lamaze, C. E.; Sakaoku, K. *J. Appl. Polym. Sci.* **1973**, *17*, 137-152.

147) Pederson, L. A. *J. Electrochem. Soc.: Solid-State Sci. Technol.* **1982**, *129*, 205-208.

148) Rybkin, V. V.; Titov, V. A.; Kuvaldina, E. V.; Terekhina, E. A.; Serova, N. Y. *High Energy Chem.* **1995**, *29*, 199-202.

149) Rybkin, V. V.; Titov, V. A.; Kuvaldina, E. V.; Terekhina, E. A. *High Energy Chem.* **1995**, *29*, 122-125.

150) Grant, J. L.; Dunn, D. S.; McClure, D. J. *J. Vac. Sci. Technol. A* **1988**, *6*, 2213-2220.

151) Ueno, N.; Doi, Y.; Sugita, K.; Sasaki, S.; Nagata, S. *J. Appl. Polym. Sci.* **1987**, *34*, 1677-1691.

152) Jones, R. G.; Cragg, R. H.; Davies, R. D. P.; Brambley, D. R. *J. Mater. Chem.* **1992**, *2*, 371-377.

153) Clouet, F.; Shi, M. K. *J. Appl. Polym. Sci.* **1992**, *46*, 1955-1966.

154) Okuno, T.; Yasuda, T.; Yasuda, H. *Textile Res. J.* **1992**, *62*, 474-480.

155) Friedrich, J.; Gähde, J.; Frommelt, H.; Wittrich, H. *Faserforsch. Textiltechnik* **1976**, *27*, 604-608.

156) Friedrich, J.; Gähde, J. *Acta Polymerica* **1980**, *31*, 52-58.

157) Roosmalen, A. J. v.; Baggerman, J. A. G.; Brader, S. J. H. *Dry etching for VLSI*; Plenum Press: New York, 1991.

158) Nishimura, H.; Yarita, T.; Noshiro, M. *Asahi Garasu Kenkyu Hokoku* **1983**, *33*, 151-160.

159) Ramesh, N. S.; Padiyath, R.; Campbell, G. A.; Babu, S. V. *J. Polym. Sci. B: Polym. Phys.* **1991**, *29*, 1031-1034.

160) Yang, A. C. M.; Allen, R. D.; Reiley, T. C. *J. Appl. Polym. Sci.* **1992**, *46*, 757-762.

161) Takamatsu, S.; Kobayashi, T.; Komoto, T.; Sugiura, M.; Ohara, K. *Polymer* **1994**, *35*, 3598-3603.

162) Bonart, R.; Müller, E. H. *J. Macromol. Sci.-Phys.* **1974**, *B10*, 177-189.

163) Chang, Y. J. P.; Wilkes, G. L. *J. Polym. Sci. B: Polym. Phys.* **1975**, *13*, 455-476.
164) King, J. A.; Grundmeyer, M.; Stepp, D.; Hugo, D. *IEEE Trans. Electr. Insul.* **1993**, *28*, 415-419.
165) Hashimoto, T.; Tsutsumi, K.; Funaki, Y. *Langmuir* **1997**, *13*, 6869-6872.
166) Chan, V. Z. H.; Hoffman, J.; Lee, V. Y.; Iatrou, H.; Avgeropoulos, A.; Hadjichristidis, N.; Miller, R. D.; Thomas, E. L. *Science* **1999**, *286*, 1716-1719.
167) Gabor, A. H.; Lehner, E. A.; Mao, G. P.; Schneggenburger, L. A.; Ober, C. K. *Chem. Mater.* **1994**, *6*, 927-934.
168) Gabor, A. H.; Ober, C. K. *Silicon-containing block copolymer resist materials*; Microelectronics Technology, 1995; Vol. 614, pp 281-298.
169) Lammertink, R. G. H.; Hempenius, M. A.; van den Enk, J. E.; Chan, V. Z. H.; Thomas, E. L.; Vancso, G. J. *Adv. Mater.* **2000**, *12*, 98-103.
170) Lammertink, R. G. H.; Hempenius, M. A.; Chan, V. Z. H.; Thomas, E. L.; Vancso, G. J. *Chem. Mater.* **2001**, *13*, 429-434.
171) van Rijn, C. J. M.; Veldhuis, G. J.; Kuiper, S. *Nanotechnology* **1998**, *9*, 343-345.
172) Liu, G.; Ding, J. *Adv. Mater.* **1998**, *10*, 69-71.
173) Johansson, J.; Yasuda, H. K.; Bajpai, R. K. *Appl. Biochem. Biotechnol.* **1998**, *70-2*, 747-763.
174) Gancarz, I.; Pozniak, G.; Bryjak, M. *Eur. Polym. J.* **1999**, *35*, 1419-1428.
175) Gancarz, I.; Pozniak, G.; Bryjak, M. *Eur. Polym. J.* **2000**, *36*, 1563-1569.
176) den Braber, E. T. *Microtextured surfaces*; University of Nijmegen: Nijmegen, The Netherlands, 1997.

Chapter 3

Selective etching of semi-crystalline polymers: CF_4 gas plasma treatment of poly(ethylene) *

M. B. Olde Riekerink [1], J. G. A. Terlingen [2], G. H. M. Engbers [1], J. Feijen [1]

[1] *Department of Chemical Technology, Section Polymer Chemistry and Biomaterials and Institute for Biomedical Technology, University of Twente, P.O. Box 217, 7500 AE Enschede, The Netherlands*

[2] *Scotts International BV, Nyverheidsweg 5, 6422 PD Heerlen, The Netherlands*

A series of poly(ethylene) (PE) films with different degrees of crystallinity was treated with a radiofrequency (RF) tetrafluoromethane (CF_4) gas plasma (48-49W, 0.06-0.07 mbar, continuous vs. pulsed treatment). The etching behaviour and surface chemical and structural changes of the PE films were studied by weight measurements, X-ray Photoelectron Spectroscopy (XPS), static and dynamic water contact angle measurements, Scanning Electron Microscopy (SEM) and Atomic Force Microscopy (AFM).
With increasing crystallinity (14-59%) of PE a significant and almost linear decrease of the etching rate was found, ranging from 50 Å/min for linear low density poly(ethylene) (LLDPE) to 35 Å/min for high density poly(ethylene) (HDPE). XPS analysis revealed that after CF_4 plasma treatment the PE surfaces were highly fluorinated up to F/C ratios of 1.6. Moreover, CF_4 plasma treatment of PE resulted in extremely hydrophobic surfaces. Advancing water contact angles up to 150° were measured for treated LDPE films. Both SEM and AFM analysis revealed that pronounced surface restructuring took place during prolonged continuous plasma treatment (≥ 15 min). The lamellar surface structure of LDPE changed into a nanoporous-like structure with uniform pores and grains on the order of tens of nanometers. This phenomenon was not observed during plasma treatment of HDPE films. Apart from surface roughening due to selective etching, pulsed plasma treatment did not result in significant surface structural changes either. Therefore, the restructuring of continuously plasma treated surfaces was attributed to a combined effect of etching and an increase of surface temperature, resulting in phase separation of PE-like and poly(tetrafluoroethylene)-like material of which the latter is surface oriented.

3.1 Introduction

Gas plasma treatment processes are extensively used for the chemical modification of polymer surfaces.[1-3] Also, plasma etching treatments have been used to increase surface roughness without aiming for a well-defined surface structure, for instance to improve properties such as

* The contents of this chapter has been published in *Langmuir* **1999**, *15*, 4847-4856.

adhesion.[4,5] However, defined restructuring of a polymer surface on the nanoscale level is of interest for several areas such as biomedical technology, membrane technology and the micro-chip industry.

In principle, gas plasma treatment can be used for tailoring the surface structure of phase separated polymeric systems, i.e. semi-crystalline homopolymers, polymer blends or block copolymers. This application of plasma technology is based on selective etching, i.e. removal of one polymer phase in preference to another. The architecture of the resulting surfaces is determined by the initial phase separated surface/bulk structure and the difference of etching rate between the two polymer phases. Using this approach, it is envisaged that surfaces can be created which contain tubular or spherical holes, ridges, or tubular or spherical protuberances. The size of these holes/protuberances will be determined by the domains present in the phase separated polymer system and can vary between tens of nanometers and a few micrometers.

For semi-crystalline polymers it is known that the amorphous phase is preferentially removed during an etching treatment.[6-9] Herbert *et al.* studied the process of ablation of the surface of poly(ethylene) (PE) using ultraviolet radiation in the presence of ozone.[6] They found that the amorphous regions of PE were preferentially etched during this treatment resulting in a fine scale surface topography. Okuno *et al.* investigated the correlation between crystallinity and plasma susceptibility of poly(ethylene terephthalate) and nylon 66 fibers.[7] The weight loss after exposure to an air plasma decreased with increasing crystallinity up to a threshold crystallinity, above which appreciable increases in weight loss were observed.

The aim of this study is to develop 'nanoscale' structured polymer surfaces by selective plasma etching of semi-crystalline polymers. Therefore, a series of commercial grade PE films, varying in crystallinity, is treated with a radio frequency (RF) tetrafluoromethane (CF_4) plasma. Compared to oxidizing plasmas a CF_4 plasma is known as a mild etchant. Still, it is much more 'aggressive' than an Ar plasma, which is an inert gas resulting in very low etching rates. Moreover, the etching characteristics of a CF_4 plasma are well known.[10-15] For example, Meichsner *et al.* showed that during CF_4 plasma treatment of low density PE a stationary equilibrium between fluorine incorporation and etching is reached after a short time (< 1 min).[15]

Furthermore, a comparison is made between continuous and pulsed CF_4 plasma treatment in order to obtain more information about the temperature effects of the different processes that occur simultaneously during plasma etching.

The chemical composition and the wetting properties of the surface of the treated materials are studied by X-ray Photoelectron Spectroscopy (XPS) and water contact angle measurements using the sessile drop method, respectively. In addition, Scanning Electron Microscopy (SEM)

and Atomic Force Microscopy (AFM) are used to investigate the surface structure and topography of the films before and after plasma treatment.

3.2 Experimental

3.2.1 Materials

Seven types of blown extruded PE films were kindly supplied by DSM Polyethylenes, Geleen, The Netherlands. Poly(tetrafluoroethylene) film (PTFE) was purchased from Goodfellow, Cambridge, England. The film characteristics of the used polymers are shown in Table 3.1.

Table 3.1: Film characteristics of the used polymers.

Polymer code / Tradename	PE Type	Additives	Film thickness (μm)	Density (g/cm^3)
LLDPE1 / Stamylex TMX 1000 F	linear low density (C_2/C_8 copolymer)	anti-oxidant **	45	0.902 *
LLDPE2 / Stamylex 08-026 F	linear low density (C_2/C_8 copolymer)	anti-oxidant **	50	0.910 *
LDPE1 / Stamylan LD 2100TN00	low density	-	55	0.921 *
LDPE2 / Stamylan LD 2600TC00	low density	-	130	0.926 *
LDPE / Stamylan LD type 2300	low density	-	200	0.93
LMDPE / Stamylex 4026 F	linear medium density (C_2/C_8 copolymer)	anti-oxidant **	55	0.936 *
HDPE / Stamylan HD 7751 FC	high density	anti-oxidant, processing aid **	10	0.950 *
PTFE / Teflon®	-	-	500	2.2

* These data were obtained from DSM (test method ISO 1183 (A)).
** The amount of additives in the PE films is small and will be neglected.

Dichloromethane (purity ≥ 99.5%) and acetone (purity ≥ 99.5%) were obtained from Merck, Darmstadt, Germany. Tetrafluoromethane (CF_4) gas (Freon-14; purity ≥ 99.95%) was purchased from Hoekloos, Amsterdam, The Netherlands. For all experiments except for the water contact angle measurements, ultra-pure water obtained from a Milli-Q Plus System (Millipore) was used. For the contact angle measurements distilled water was used.

3.2.2 Methods

Cleaning of polymer films

PE and PTFE films were cut into 4x4 cm pieces. These films were cleaned ultrasonically, successively in dichloromethane (10 min, three times), in acetone (10 min, three times), in water (10 min, three times) and again in acetone (10 min), after which the films were dried *in vacuo* at room temperature (RT) and stored at RT in the dark.

Determination of the PE crystallinity

The crystallinity of the various (untreated) PE films was determined by Differential Scanning Calorimetry (DSC) according to a standard procedure.[16] The empirical heat of fusion for 100% crystalline PE was set at 293 J/g.[17] The measurements were performed with a Perkin Elmer DSC 7 apparatus.

CF_4 plasma treatment of polymer films

Cleaned films (4) were mounted in a glass holder (exposed surface area per film: 14 cm^2) which was placed in the center region of a gas plasma tubular reactor (length 80 cm, internal diameter 6.5 cm). Three externally placed capacitively coupled copper electrodes were attached to the reactor: a 'hot' electrode in the center and a 'cold' electrode at both sides of the 'hot' electrode at 10 cm distance. The electrodes were connected to a RF (13.56 MHz) generator through a matching network. A detailed description of the plasma apparatus is given elsewhere.[18]

The reactor was evacuated to a pressure of 0.01 mbar. Subsequently, a CF_4 gas flow of 10 cm^3/min (STP) was established through the reactor for 15 min (pre-delay). The polymer films were then exposed to the plasma (0.06-0.07 mbar, 48-49 W) for either 15 or 180 min while maintaining a constant gas flow (10 cm^3/min) through the reactor. Subsequently, the gas flow was maintained for another 2 min (post-delay). Finally, the reactor was brought to atmospheric pressure with air and the films were removed.

Moreover, pulsed plasma treatment was carried out at the same conditions as mentioned above. This treatment consisted of 900 plasma pulses of 1 s separated by dark periods of 10 s.

In order to suppress aging effects (i.e. changes of surface chemistry over the course of time due to the mobility of surface functional groups), the treated films were stored at –20 °C prior to analysis.[2]

Determination of etching rates

Before plasma treatment, the polymer films were weighed on an analytical balance (Mettler AT261 Deltarange). Directly after a three-hour plasma treatment the films were weighed again. The weight decrease was converted into an average etching rate, using the formula:

$$v_E = \frac{\Delta m}{tA\rho} \tag{3.1}$$

where v_E is the etching rate [cm/min] of the polymer films, Δm is the weight decrease [g], t is the plasma treatment time [min], A is the exposed surface area [cm^2] and ρ is the density [g/cm^3] of the polymer films.

When the etching rate is calculated with this formula it is assumed that the weight decrease caused by etching is linear over the course of time.[15] The initial mass increase due to fluorine incorporation is not taken into account here, since it is negligible when compared to the total weight loss after 3 h of plasma etching.

Thermal post-treatment of plasma treated LDPE films

Part of the plasma treated PE films (LDPE type 2300, either treated continuously for 15 min or pulsed for 900 x 1 s) was subjected to a thermal post-treatment. Untreated LDPE films were thermally post-treated as a reference. The films were exposed to temperatures of 50, 100 or 150 °C during a period of 30 s or 30 min at atmospheric pressure. After this treatment the films were allowed to cool at RT before storage at –20 °C.

XPS analysis

The chemical surface composition of the plasma treated polymer films was investigated by X-ray Photoelectron Spectroscopy (XPS). The measurements were performed with a Kratos XSAM-800 apparatus (Manchester, United Kingdom) using a Mg K_α source (15kV, 15 mA). A spot size of 3x6 mm was analysed. The pressure during the measurements was $1x10^{-7}$ - $1x10^{-8}$ mbar. Survey scans (0-1100 eV) were recorded for all samples to qualitatively determine the elements present at the surface. Detail scans (20-30 eV windows) were recorded to quantify the elemental surface composition. The measured peak areas were converted into atomic percentages by using sensitivity factors known from literature.[19]

Contact angle measurements

Plasma treated films were characterized by static and dynamic water contact angle measurements using the sessile drop method. The measurements were performed with a KRÜSS Contact Angle Measuring System G10/G40 (Hamburg, Germany).

First, static contact angles were measured by placing a water droplet onto the sample with an electronically regulated syringe. Subsequently, a fresh droplet was placed onto the sample and dynamic contact angles were measured by increasing and decreasing the droplet volume with the syringe, resulting in advancing and receding contact angles, respectively. The dynamic contact angle measurement was started directly after the droplet had reached a constant shape and the liquid-solid interface started to move along the polymer surface.

Every contact angle was determined at least ten times during each measurement, resulting in an average value. For every sample, measurements were carried out in threefold using fresh water for each new droplet.

SEM analysis

The surface morphology of the polymer films was studied by Scanning Electron Microscopy (SEM). Prior to SEM analysis the samples were sputtered with a 20 Å thick gold-palladium layer. The coated samples were analysed with a Hitachi S-800 Field Emission SEM (6 kV, 20° tilt). SEM pictures were taken at 40,000 times magnification.

AFM analysis

Atomic Force Microscopy (AFM) was used to study the surface topography of the polymer films. The samples were analysed with a Nanoscope III microscope (Digital Instruments Inc., Santa Barbara, USA). AFM images were recorded in tapping mode at RT in air using silicon cantilevers (Digital Instruments). For each sample both height and phase images were recorded with the maximum available number of pixels (512x512). For image analysis the recorded scans were "flattened" using the Nanoscope image processing software. In addition, the mean surface roughness (R_a) was calculated for the scanned area (5x5 μm) by applying the formula:

$$R_a = \sqrt{\sum_{x,y=1}^{N} \frac{(Z_{x,y} - Z_{average})^2}{N^2}} \qquad (3.2)$$

Here, the roughness is defined as the normalized standard deviation calculated from the local heights ($Z_{x,y}$) and the average height ($Z_{average}$) determined over all x,y coordinates (N) measured in the AFM image.

3.3 Results and Discussion

3.3.1 Etching behaviour of PE in a CF_4 plasma

The crystallinity of the various PE grades increased with density from 14% (LLDPE1) to 59% (HDPE) as was determined by DSC. All films were treated with a CF_4 plasma for 3 h in order to determine the etching rate. The relation between etching rate and crystallinity is shown in Figure 3.1. For the (L)LDPE grades (crystallinity ≤ 36%) the etching rate decreased almost linearly with increasing crystallinity. For PE grades with a higher crystallinity the further decrease of the etching rate was less pronounced.

The etching rate of PTFE in a CF_4 plasma was also determined. A value of 46 ± 1 Å/min was found after three measurements, which is in the range of the etching rates shown in Figure 3.1.

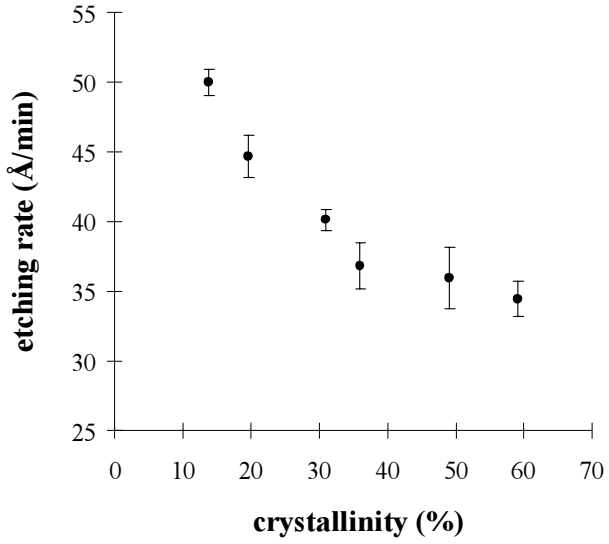

Figure 3.1: *Etching rate as a function of crystallinity of a series of PE grades in a CF_4 plasma (n=3, ±sd).*

The decrease of the etching rate with increasing crystallinity of PE indicates that in a CF_4 plasma the amorphous phase of PE is etched faster than the crystalline phase. At low crystallinity (≤ 36%) the PE etching rate showed a linear dependence resulting in the relation:

$$v_E = cv_{E,C} + (1-c)v_{E,A} = (v_{E,C} - v_{E,A})c + v_{E,A} \qquad (3.3)$$

in which v_E refers to the total etching rate, $v_{E,C}$ and $v_{E,A}$ refer to the etching rate of the crystalline phase and the amorphous phase, respectively, and c refers to the crystalline fraction (C/100).

This simple model of etching of a two-phase material was also applied by Herbert *et al.* to explain the linear dependence of the etching rate of PE on crystallinity when using an ultraviolet-ozone treatment.[6] In this model it is assumed that the etching rates of the crystalline and the amorphous phase have a constant value during the etching process. The difference between these values determines the selectivity of the etching process. When this linear relation is applied to the (L)LDPE grades, it can be calculated that $v_{E,C}$ = 1 Å/min and $v_{E,A}$ = 57 Å/min. Although this calculation is somewhat speculative and many important aspects involved in the etching process (e.g. temperature effects, surface fluorination, surface roughness, surface vs. bulk composition, surface restructuring) are not taken into account, it indicates a preferential etching behaviour of PE in a CF_4 plasma.

A significant deviation from the linear etching behaviour is found for LMDPE and HDPE films. This illustrates that indeed other factors must play an important role during the etching process. A reasonable explanation for the deviating behaviour could be found when realising that the surface characteristics (e.g. morphology, roughness and chemistry) of the (L)LDPE films differ from those of higher density PE. For instance, a HDPE surface is rougher than a LDPE surface (Table 3.4) resulting in a larger exposed surface area during plasma treatment. Therefore, a higher etching rate than that derived from relation 3.3 (extrapolating the (L)LDPE linear decrease would result in a HDPE etching rate of 24 Å/min) can be expected. The impact of the surface structure on the plasma etching process will be discussed in section 3.3.4.

3.3.2 Surface chemical changes of PE during CF_4 plasma treatment

The surface of the 3 h plasma treated PE films (CF_4-180) was characterized by XPS. Untreated PTFE samples were taken as a reference. The results are shown in Table 3.2.

XPS analysis revealed that during CF_4 plasma treatment the PE surfaces were highly fluorinated. For LLDPE, F/C ratios up to 1.6 were found. Moreover, there seems to be a correlation between the degree of fluorination and the crystallinity. With increasing PE crystallinity the F/C ratio slightly decreased. Besides fluorination, the PE surfaces were somewhat oxidized during plasma treatment.

Table 3.2: XPS data of PE films treated with a CF_4 plasma for 3 h (n=3, ±sd).*

Sample	C (at.%)	O (at.%)	F (at.%)	F/C ratio
LLDPE1; CF_4-180	37.6 ± 0.8	2.0 ± 0.2	58.5 ± 0.5	1.6 ± 0.1
LLDPE2; CF_4-180	38.8 ± 0.9	1.9 ± 0.4	57.4 ± 1.2	1.5 ± 0.1
LDPE1; CF_4-180	38.2 ± 0.6	2.1 ± 0.4	57.2 ± 0.6	1.5 ± 0.1
LDPE2; CF_4-180	38.8 ± 1.9	2.1 ± 0.1	56.8 ± 1.0	1.5 ± 0.1
LMDPE; CF_4-180	39.2 ± 1.5	2.0 ± 0.1	55.8 ± 0.4	1.4 ± 0.1
HDPE; CF_4-180	38.7 ± 0.6	2.1 ± 0.5	56.0 ± 0.6	1.4 ± 0.1
PTFE; untreated	30.9 ± 0.6	-	69.1 ± 0.6	2.2 ± 0.1

* Untreated PE films contain less than 0.5% oxygen and no fluorine at all.

In order to study the difference in treatment between continuous and pulsed CF_4 plasmas, all PE grades were either treated continuously for 15 min (CF_4-15) or treated with 900 plasma pulses of 1 s (CF_4-900 x 1 s). When the actual plasma discharge time is kept constant (900 s), a reasonable comparison can be made between continuous and pulsed CF_4 plasma treatment. However, it should be noted that 'dark' period effects might occur during pulsed treatment due to the presence of long living radicals and/or metastables. These effects are not taken into account here. The XPS results of these treatments are shown in Table 3.3.

Table 3.3: XPS data of PE films treated with a continuous (15 min) or a pulsed (900 x 1 s) CF_4 plasma (n=1).

Sample	C (at.%)	O (at.%)	F (at.%)	F/C ratio
LLDPE1; CF_4-15	41.7	2.6	55.7	1.3
LLDPE1; CF_4-900 x 1 s	43.9	2.9	53.2	1.2
LLDPE2; CF_4-15	41.8	2.5	55.7	1.3
LLDPE2; CF_4-900 x 1 s	43.4	2.9	53.6	1.2
LDPE1; CF_4-15	41.0	2.2	56.8	1.4
LDPE1; CF_4-900 x 1 s	43.6	2.1	54.2	1.2
LDPE2; CF_4-15	42.4	2.2	55.3	1.3
LDPE2; CF_4-900 x 1 s	43.0	2.6	54.3	1.3
LMDPE; CF_4-15	43.2	2.4	54.4	1.3
LMDPE; CF_4-900 x 1 s	44.6	2.3	53.1	1.2
HDPE; CF_4-15	43.5	2.8	53.7	1.2
HDPE; CF_4-900 x 1 s	43.9	2.6	53.4	1.2

Table 3.3 clearly shows that almost complete fluorination occurred within 15 min of plasma treatment. For all PE grades a small difference in the degree of fluorination is found between continuous and pulsed treatment, the latter causing somewhat less fluorination. This difference seems to be most pronounced for the (L)LDPE grade films. Again, fluorination is accompanied by some oxidation during CF_4 plasma treatment.

The high degree of surface fluorination that occurred during CF_4 plasma treatment is not surprising, since it is well known that fluorine radicals are the most reactive species in a CF_4 plasma yielding high F/C ratios at the polymer surface.[20-23]

An interesting feature is the slight decrease of F/C ratio with increasing crystallinity. One reason for the varying F/C ratios might be a difference in the depth of modification. However, this cannot be shown by XPS due to the relatively high roughness of PE surfaces. Another explanation would be that during CF_4 plasma treatment the crystalline phase of PE is somewhat less fluorinated than the amorphous phase. When considering that the crystalline phase is less susceptible to chemical or physical changes and therefore better resistant to etching (Figure 3.1), this result could indeed be expected.

Another interesting feature shown in Table 3.3 is the small difference of fluorination between continuously and pulsed treated films. However, from previous experiments (data not shown) it is known that for longer plasma treatment times (30 min) this difference disappears. Comparing the data in Table 3.2 with those in Table 3.3 shows that fluorination has practically reached its equilibrium value after 15 min of treatment. If the hydrogen atoms in the PE backbone were completely substituted by fluorine, a theoretically maximal F/C ratio of 2 would be found. However, this maximal value is not reached probably due to the presence of a fluorine gradient at the surface and/or due to the equilibrium between etching (F $\downarrow$) and fluorination (F $\uparrow$). Furthermore, the occurrence of crosslinking during plasma treatment will limit the F/C ratio.

According to Tables 3.2 and 3.3, fluorination of PE is accompanied by some oxidation. During plasma treatment some oxygen containing species are present in the plasma phase due to reaction of fluorine radicals with the inner glass wall of the reactor (Si_xO_y) yielding Si_xF_y fragments and atomic oxygen.[24] However, the small amount of surface oxidation can also be explained by post-reactions of surface free radicals, which are still present after plasma treatment, with oxygen in air.

3.3.3 Wettability of CF_4 plasma treated PE films

Water contact angle measurements were carried out using the sessile drop method. Static and dynamic contact angle data of all treated and untreated PE samples are presented in Figures

3.2 and 3.3, respectively. For comparison, the value of the water contact angles of PTFE are represented by dotted lines.

Figures 3.2 and 3.3 clearly show that CF_4 plasma treatment of PE resulted in a significant decrease of wettability by water. Advancing angles up to 150° were measured for plasma treated LDPE (crystallinity ≤ 36%), which is significantly higher than the corresponding value for PTFE (129°). For most PE films no significant difference was found between 15 min and 3 h of treatment. However, a striking difference was observed between continuously treated and pulsed treated (L)LDPE films, the latter being less hydrophobic. Another remarkable result shown in Figure 3.3 is the high contact angle hysteresis (here defined as $\theta_{advancing} - \theta_{receding}$) found for plasma treated PE. The largest effect is observed for LDPE films for which hysteresis increased from 17° for untreated films to values of 77° for continuously plasma treated films.

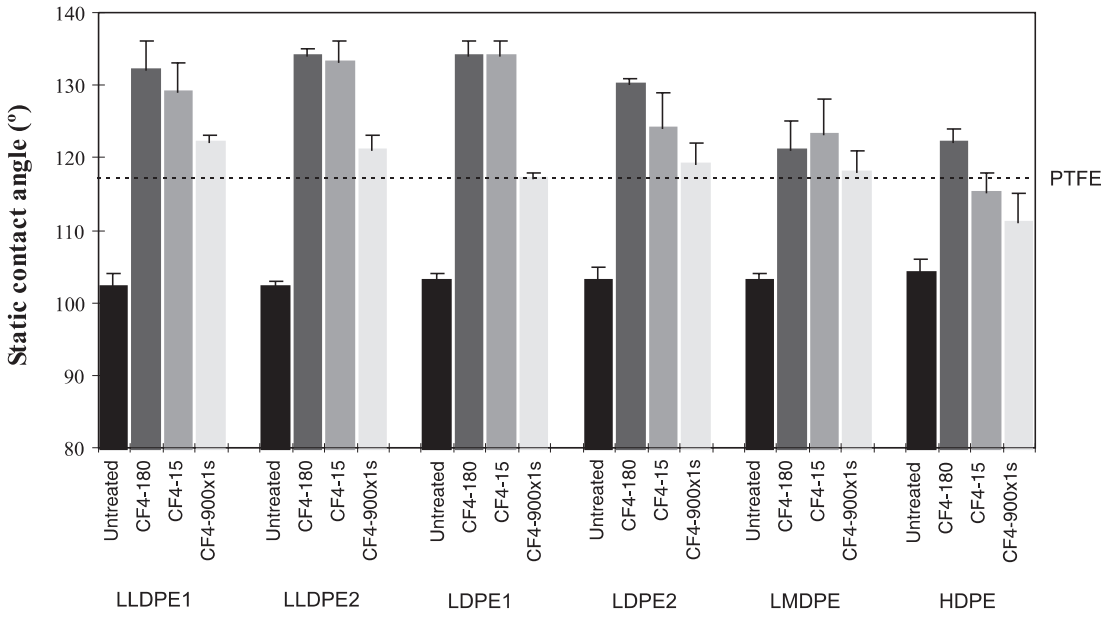

Figure 3.2: *Static water contact angles of untreated and CF_4 plasma treated PE. The series of PE films were all treated either for 3 h (CF_4-180), 15 min (CF_4-15) or with 900 pulses of 1 s (CF_4-900 x 1 s). The dotted line represents the static water contact angle of untreated PTFE (n=3, ±sd).*

Clearly, prolonged CF_4 plasma treatment of PE resulted in extremely hydrophobic surfaces. Similar superhydrophobic surfaces were prepared by Busscher *et al.* by argon ion etching of FEP-Teflon followed by an oxygen plasma treatment.[25] These surfaces have water contact angles higher than 140°.

The high hydrophobicity of the plasma treated PE surfaces is at least partly due to the large amount of surface fluorination. The occurrence of an equilibrium state for fluorine incorporation is indicated by the fact that no large differences of wettability were found between surfaces treated for 15 and 180 min. This is in good agreement with the corresponding amounts of fluorination discussed in the previous section. However, surface fluorination is only part of the explanation for superhydrophobicity since the water contact angles of an untreated PTFE surface are much lower. Therefore, other factors must have a significant influence on the hydrophobicity of these films. In principal, the equilibrium contact angle at a solid-liquid-air interface is dependent not only on the surface chemistry of the solid, but also on its surface structure (e.g. roughness, heterogeneity, porosity).[26-31] An explanation for the extremely high contact angles could be found in the porous character of the plasma treated LDPE surfaces (Figure 3.4; discussed in the next section).

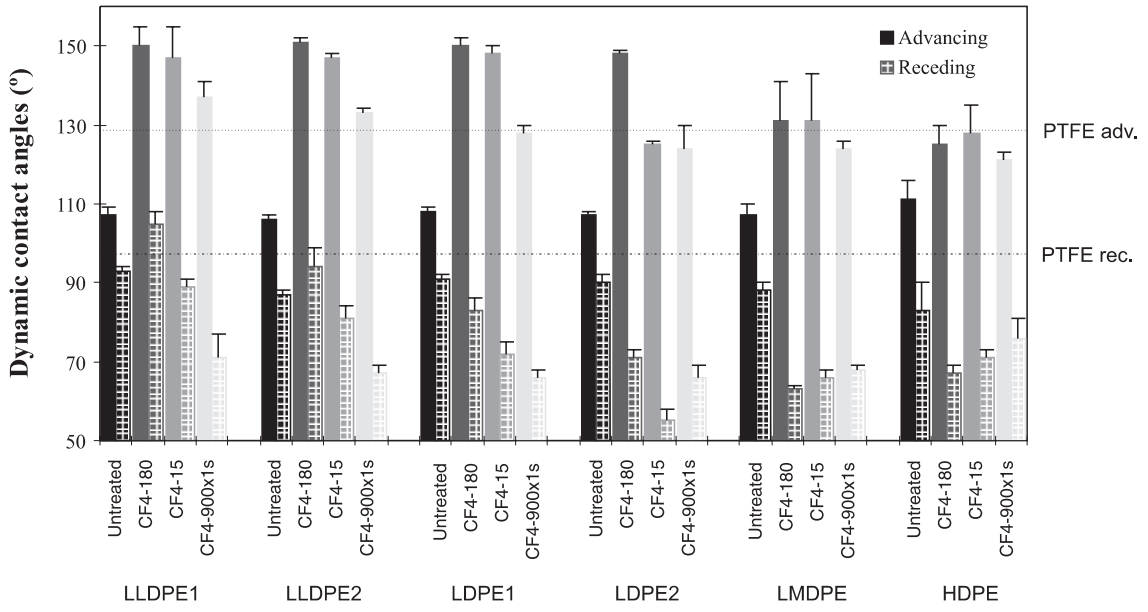

Figure 3.3: *Dynamic water contact angles of untreated and CF_4 plasma treated PE. The series of PE films were all treated either for 3 h (CF_4-180), 15 min (CF_4-15) or with 900 pulses of 1 s (CF_4-900 x 1 s). The dotted lines represent the dynamic water contact angles of untreated PTFE (n=3, ±sd).*

Cassie and Baxter derived an equation for the apparent contact angle (θ_A) of a uniform porous surface, based on thermodynamics: [26]

$$\cos\theta_A = f_1 \cos\theta_1 - f_2 \qquad (3.4)$$

In this equation, f_1 and f_2 are the area fractions of solid-liquid and liquid-air interfaces on the solid, respectively. θ_1 represents the contact angle (advancing or receding) for the solid-liquid interface. On the basis of this theory a rough estimation can be made of the area fractions f_1 and f_2 for PE surfaces after CF_4 plasma treatment. For plasma treated LDPE1 surfaces an apparent advancing water contact angle of 150° (θ_A) was found (Figure 3.3). The advancing contact angle for the solid-liquid interface (θ_1) is set at 129°, which is the advancing contact angle of 'solid' PTFE (Figure 3.3). From these values it can be calculated that $f_1 = 0.36$ and $f_2 = 0.64$. Although this calculation is merely qualitative, it indicates that a surface structural change has indeed taken place during plasma treatment of LDPE surfaces, as will be discussed in the next section.

For plasma treated HDPE surfaces, θ_A is similar or even lower than the assumed value for θ_1 (Figure 3.3). This suggests that θ_1 probably has a lower value, which seems reasonable when it is realised that the surface chemistry of 'solid' fluorinated PE is not exactly equal to that of 'solid' PTFE ($\theta_1 = \theta_A = 129°$).

Another interesting result shown in Figures 3.2 and 3.3 is the significant difference between continuously treated and pulsed treated (L)LDPE films. It is not expected that this difference was only caused by the small difference of surface fluorination (Table 3.3), but it must also be attributed to changes of surface structure.

3.3.4 Surface structural changes of PE during CF_4 plasma treatment

SEM pictures were made of the surfaces of untreated and plasma treated PE films. Figures 3.4 and 3.5 show the surface morphology of two different PE grades (LDPE1 and HDPE, respectively) before and after CF_4 plasma treatment.

The SEM pictures in Figure 3.4 clearly show that the morphology of the LDPE surface changed significantly during prolonged, continuous CF_4 plasma treatment. Very similar pictures were obtained for the other (L)LDPE films (crystallinity ≤ 36%).

The untreated LDPE surface consists of randomly oriented lamellae. The crystalline lamellae are surrounded by amorphous PE, the major phase of the material. During plasma treatment this lamellar surface structure changed into a nanoporous-like surface structure (Figures 3.4B and C). The pores/grains that appeared at the surface have a quite uniform size on the order of tens of nanometers.

This pronounced change of surface structure (i.e. surface restructuring) was not found for pulsed plasma treated LDPE films (Figure 3.4D). Although the surface morphology was affected to some extent, the lamellar structure is still present at the PE surface after pulsed plasma treatment.

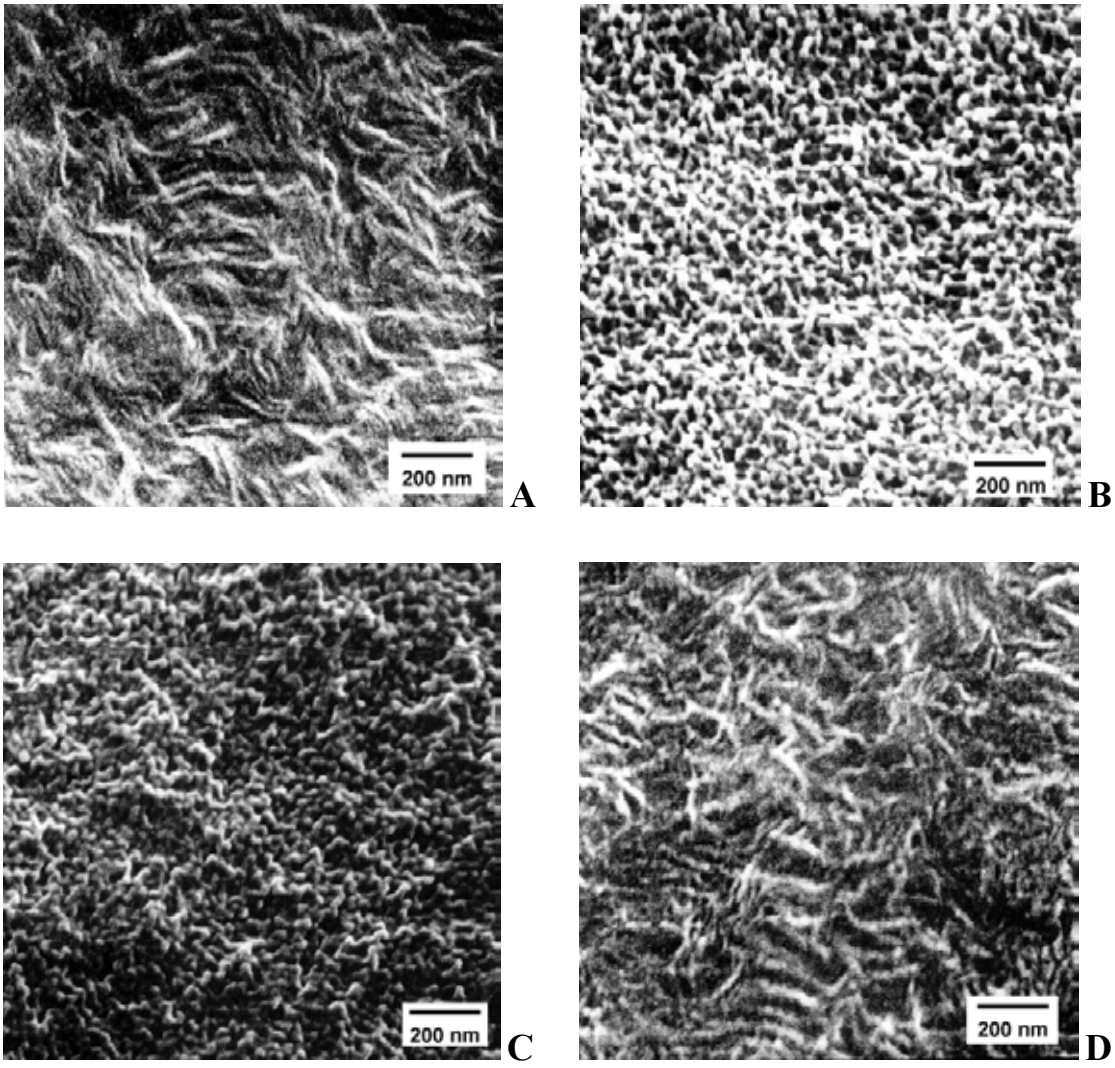

Figure 3.4: *SEM pictures of untreated and CF_4 plasma treated LDPE1 surfaces; (A) untreated, (B) treated for 3 h, (C) treated for 15 min, (D) treated with 900 pulses (1 s).*

In the case of plasma treated HDPE films a completely different effect of plasma treatment on the surface structure was found, as can be seen in Figure 3.5. The untreated surface is characterized by organised lamellae. The lamellae are oriented perpendicular to the microscopic film texture, which is possibly induced by the film blow procedure. During prolonged plasma treatment this oriented lamellar surface structure largely disappeared (Figure 3.5B). For shorter plasma treatment times the surface restructuring was less significant and oriented lamellae are still visible (Figure 3.5C). Pulsed plasma treatment hardly seemed to affect the surface structure of HDPE (Figure 3.5D).

Similar effects were found for plasma treated LMDPE films, although in this case the surface lamellae are not oriented in one direction.

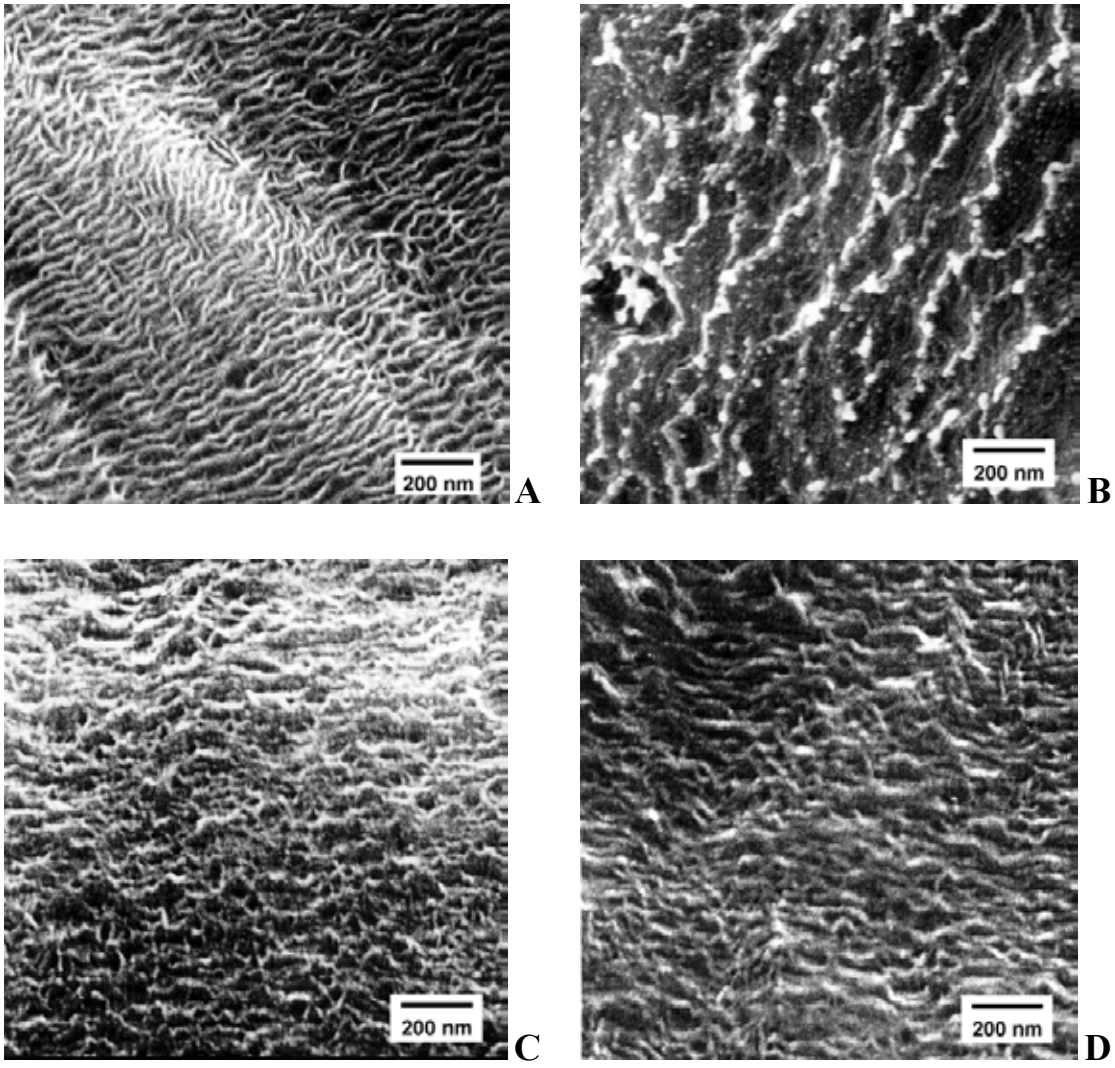

Figure 3.5: *SEM pictures of untreated and CF_4 plasma treated HDPE surfaces; (A) untreated, (B) treated for 3 h, (C) treated for 15 min, (D) treated with 900 pulses (1 s).*

Tapping mode AFM analysis was also used to study the surface topography of untreated and plasma treated PE films. Height and phase images were recorded simultaneously and the results of LDPE1 and HDPE films are shown in Figures 3.6 and 3.7. The values of the mean surface roughness (R_a) of these films are shown in Table 3.4.

Although the untreated LDPE surface is quite rough (Figure 3.6A), the surface roughness further increased upon plasma treatment (Table 3.4). When Figure 3.6A is compared with Figures 3.6B and C a pronounced surface restructuring is visible similar to that observed in Figure 3.4. The surface lamellae disappeared and were replaced by a granular structure. Figure 3.6D shows that the LDPE surface structure remained quite intact during pulsed plasma treatment, although the lamellae are not as clearly visible as those in Figure 3.6A.

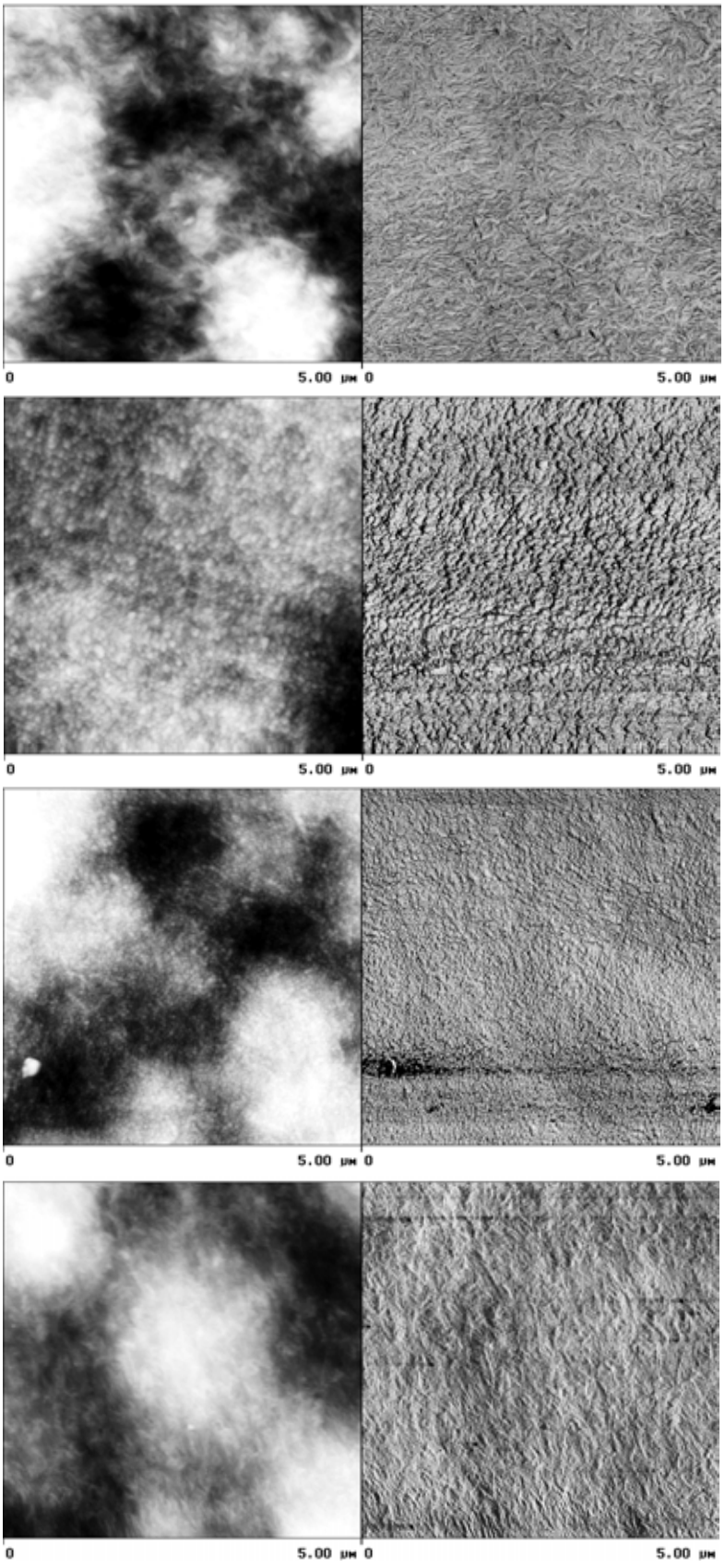

Figure 3.6: *Tapping mode AFM images (height (left) and phase (right) imaging) of untreated and CF_4 plasma treated LDPE1 surfaces; (A) untreated, (B) treated for 3 h, (C) treated for 15 min, (D) treated with 900 pulses (1 s).*

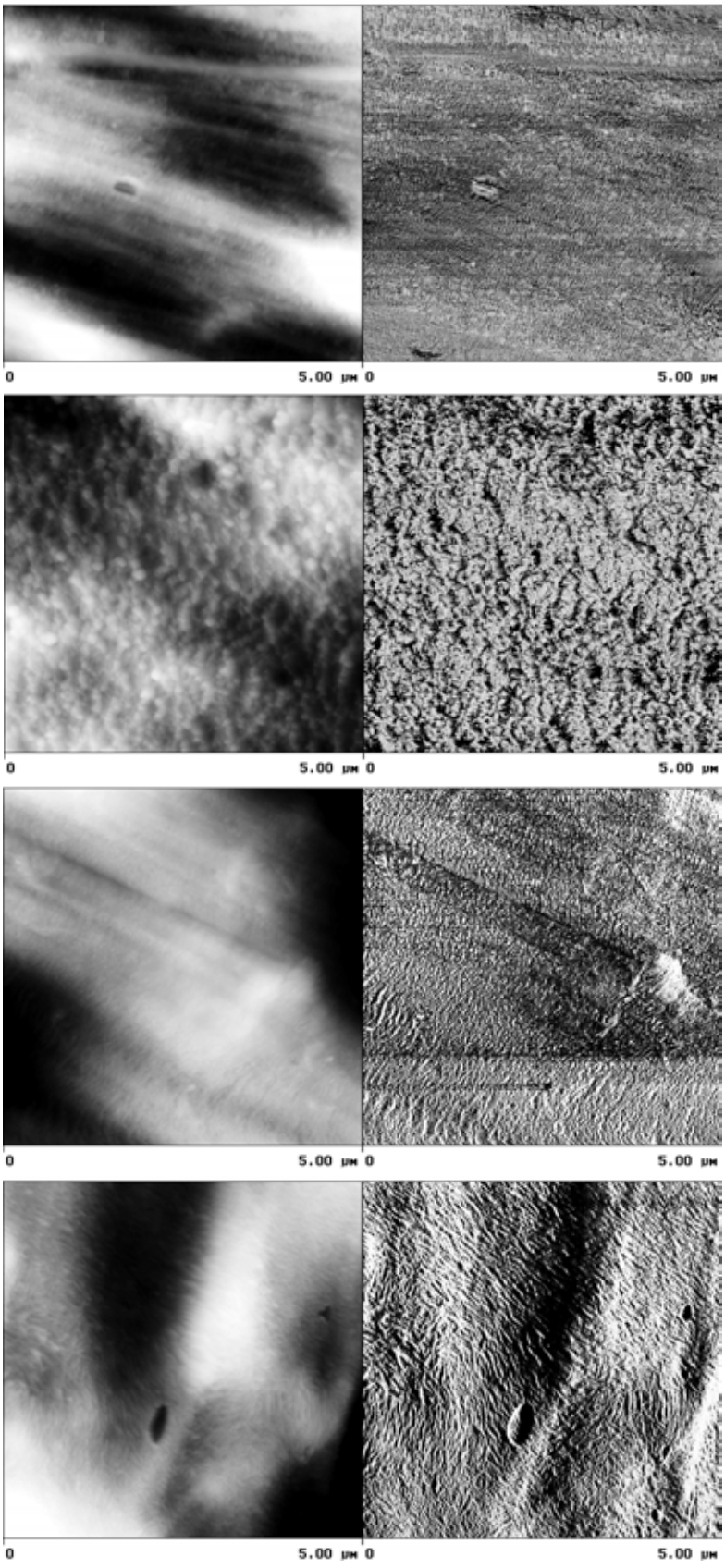

Figure 3.7: *Tapping mode AFM images (height (left) and phase (right) imaging) of untreated and CF_4 plasma treated HDPE surfaces; (A) untreated, (B) treated for 3 h, (C) treated for 15 min, (D) treated with 900 pulses (1 s).*

Table 3.4: Mean surface roughness (R_a) of untreated and CF_4 plasma treated PE films as calculated from AFM results. The films were treated either for 3 h (CF_4-180), 15 min (CF_4-15) or with 900 pulses of 1 s (CF_4-900 x 1 s).

Sample	R_a (nm) *
LDPE1; untreated	23
LDPE1; CF_4-180	30
LDPE1; CF_4-15	45
LDPE1; CF_4-900x1s	49
HDPE; untreated	38
HDPE; CF_4-180	60
HDPE; CF_4-15	87
HDPE; CF_4-900x1s	91

* Scanned surface area = 5x5 μm (n=1).

Figure 3.7A clearly illustrates the microscale texture of untreated HDPE induced by film processing (height image) in combination with a nanoscale lamellar morphology (phase image) perpendicularly oriented to the microscale texture. During the 3 h plasma treatment the lamellae were severely damaged and a rough, undefined structure is obtained (Figure 3.7B). After shorter treatment times (Figure 3.7C) and after pulsed treatment (Figure 3.7D) the microscale texture with its perpendicular lamellar morphology is retained, although substantial surface roughening has occurred (Table 3.4).

Generally, the observed surface structural changes in Figures 3.6 and 3.7 are in good agreement with the results found by SEM analysis (Figures 3.4 and 3.5). It should be noted that the nanopores seen in Figures 3.4B and C cannot be directly imaged as such by AFM since the radius of the AFM tip (~30 nm) is on the same order of magnitude as the size of the pores. Thus, the tip cannot penetrate into the pores resulting in a type of granular structure as shown in Figure 3.6B.

The SEM pictures in Figure 3.4 and the AFM images in Figure 3.6 clearly show that the LDPE surface is structurally changed during continuous plasma treatment. On the contrary, the surface lamellar structure of pulsed treated films was hardly affected although significant surface roughening took place. This is clearly shown by the hysteresis data in the previous section (Figure 3.3) and the surface roughness data obtained from AFM analysis in Table 3.4. The increase of surface roughness and the preservation of the lamellar surface structure nicely show that CF_4 pulsed plasma treatment is a selective etching process.

Still, the question remains how the striking difference of surface structure between continuously treated and pulsed treated films can be explained. Two possible causes can be responsible for this structural difference.

First, a continuous bombardment by reactive species (e.g. electrons, ions, fluorine radicals) can cause more surface damage than pulsed bombardment. During the dark periods used in the pulsed plasma treatment the polymer surface is able to recover, for example by recombination of dissociated chain bonds and by termination of surface radicals. Although the actual time of discharge (900 s) is equal for continuous and pulsed plasma treatment, the treatment conditions in the latter case seem to be milder.

Second, temperature effects probably play an important role during the etching process.[32] During continuous plasma treatment an increase of surface temperature is expected due to heat development caused by fluorination, which is an exothermic reaction. Moreover, a continuous bombardment of reactive species onto the substrate raises the surface temperature significantly.[33,34] The overall temperature increase might be such that during plasma treatment the melting temperature of PE is reached at the surface. Together with surface fluorination and preferential etching this could very well lead to restructuring of the surface. In the case of pulsed plasma treatment the heat developed at the surface will flow away during the dark periods, thereby preventing a major temperature increase and a subsequent surface restructuring.

In order to investigate whether temperature effects indeed play a key role in explaining the difference between continuously and pulsed treated PE films, thermal post-treatments were carried out with LDPE. One type of LDPE film (type 2300) was subjected to a thermal treatment after exposure to a CF_4 plasma (either continuously for 15 min or pulsed for 900 x 1 s). The LDPE films were exposed to a temperature of 50, 100 or 150 ºC either for 30 s or 30 min.

SEM analysis (pictures not shown here) clearly pointed out that at temperatures of 50 and 100 ºC for 30 s and 30 min no change of surface structure was found after (pulsed) plasma treatment. The surface structures seemed to be quite stable and did not reorganise at temperatures just below the melting temperature of LDPE (110-115 ºC). Moreover, the untreated reference material did not show any change during thermal post-treatment at these temperatures.

However, after thermal treatment above the melting temperature (150 ºC) the (un)treated LDPE films recrystallised from the melt and the macroscale structure was changed drastically. The films did not retain their film characteristics since the bulk of the films was also affected. This dramatic macroscale change of surface and bulk structures can be easily explained when it

is realised that during PE film processing (blown extrusion) a specific morphology is created which simply cannot be recovered after melting and recrystallisation of the films. With respect to this extreme thermal post-treatment it should be noted that during plasma treatment these macroscale changes were not observed. This implies that, although a surface temperature increase is inevitable, the melting temperature will not be reached in the bulk during plasma treatment. A similar conclusion was drawn earlier from experiments with UHMWPE membranes that were treated with a CO_2 plasma.[34] The increase of surface temperature during CF_4 plasma treatment of LDPE films is further discussed elsewhere.[35]

The question remains whether and how temperature effects influence the surface structure of PE films during plasma treatment. Based on the results obtained so far, the most reasonable explanation for the pronounced surface structural change is a combined effect of preferential etching, fluorination and an increase of surface temperature. While the amorphous regions are preferentially removed from the surface, fluorination and heat development may induce phase separation at the PE surface segregating fluorine-rich domains from fluorine-poor domains. The outside of the granular structures seen in Figures 3.4B,C and 3.6B,C probably consists of fluorine-rich domains, thus realising a minimal surface energy. In the case of pulsed treatment the temperature increase is not sufficient and therefore no phase separation will occur.

Figures 3.5 and 3.7 show that the etching process has a completely different effect on HDPE surfaces. Hardly any difference can be seen between the surface structure of continuously and pulsed treated films (Figures 3.5C,D and 3.7C,D), which is in agreement with the contact angle data shown in Figures 3.2 and 3.3. Apparently, the surface lamellar structure of HDPE is less affected by a temperature increase during plasma treatment which would lead to phase separation (see above). Still, preferential etching of the amorphous phase induced a major increase of surface roughness for all HDPE surfaces (Table 3.4).

Clearly, the crystallinity of PE does have a major influence on the surface structural changes during plasma treatment. The (L)LDPE grades all show very similar changes, while the etching behaviour of LMDPE and HDPE films leads to deviating and undefined structures. This also explains the deviating results for wettability and etching rates of plasma treated LMDPE and HDPE as compared to (L)LDPE seen in Figures 3.1 to 3.3. Obviously, changes of surface structure during CF_4 plasma treatment have a large influence on the wettability and the etching rate of PE films.

3.4 Conclusions

This study showed that selective plasma etching can be a versatile tool for creating nanostructured polymer surfaces. Both continuous and pulsed CF_4 plasma treatment of PE resulted in a preferential etching process, the original amorphous phase being etched faster than the crystalline phase.

Moreover, the PE films were highly fluorinated during treatment (F/C ratios up to 1.6) and extremely hydrophobic surfaces were formed with advancing water contact angles of up to 150º.

Besides fluorination, a pronounced surface restructuring took place during continuous plasma treatment of (L)LDPE films as was revealed by SEM and AFM analysis. The lamellar surface structure was converted into a nanoporous-like structure with uniform domains on the order of tens of nanometers. The change of surface structure was attributed to a combined effect of etching and an increase of surface temperature inducing phase separation of PE-like and PTFE-like material, of which the latter is surface oriented. These surface structural changes were not observed after plasma treatment of LMDPE and HDPE films, which can most likely be attributed to differences in surface etching behaviour. In all cases, the surface roughness increased substantially during plasma treatment resulting in a large hysteresis.

During pulsed CF_4 plasma treatment of PE films the initial lamellar morphology remained intact but the surface roughness increased considerably. Therefore, selective etching by pulsed plasma treatment is most suitable when preservation of surface morphology is desired.

3.5 Acknowledgements

Albert v/d Berg, Mark Smithers and Clemens Padberg (MESA+ Institute, University of Twente) are acknowledged for performing the XPS, SEM and AFM measurements, respectively. Prof. G.J. Vancso (Materials Science and Technology of Polymers, University of Twente) is acknowledged for valuable discussion of the paper. This study was financially supported by the Netherlands Foundation for Chemical Research (NWO-CW).

3.6 References

1) Terlingen, J. G. A. *Introduction of functional groups at polymer surfaces by glow discharge techniques*; University of Twente: Enschede, The Netherlands, 1993.
2) Takens, G. A. J. *Functionalization of polymeric surfaces by oxidative gas plasma treatment*; University of Twente: Enschede, The Netherlands, 1997.
3) Dewez, J. L.; Humbeek, E.; Everaert, E.; Doren, A.; Rouxhet, P. G. *Plasma treated polymer films: Relationship between surface composition and surface hydrophilicity*; Pireaux, J. J., Bertrand, P. and Brédas, J. L., Ed.; IOP Publishing Ltd: Bristol, 1992, pp 463-474.
4) Wu, S. *Polymer Interface and Adhesion*; Marcel Dekker, Inc.: New York, 1982.
5) Choi, D. M.; Park, C. K.; Cho, K.; Park, C. E. *Polymer* **1997**, *38*, 6243-6249.
6) Herbert, S.; Shinozaki, D. M.; Collacott, R. J. *J. Mater. Sci.* **1996**, *31*, 4655-4661.
7) Okuno, T.; Yasuda, T.; Yasuda, H. *Textile Res. J.* **1992**, *62*, 474-480.
8) Friedrich, J.; Gähde, J.; Frommelt, H.; Wittrich, H. *Faserforsch. Textiltechnik* **1976**, *27*, 604-608.
9) Friedrich, J.; Gähde, J. *Acta Polymerica* **1980**, *31*, 52-58.
10) Hopkins, J.; Badyal, J. P. S. *Langmuir* **1996**, *12*, 3666-3670.
11) Egitto, F. D.; Vukanovic, V.; Taylor, G. N. *Plasma Etching of Organic Polymers*; d'Agostino, R., Ed.; Academic Press, Inc.: Boston, 1990, pp 321-422.
12) Egitto, F. D.; Matienzo, L. J.; Schreyer, H. B. *J. Vac. Sci. Technol. A* **1992**, *10*, 3060-3064.
13) Occhiello, E.; Garbassi, F.; Coburn, J. W. *Etching of Polymers by CF_4/O_2 Discharges*; Akashi, K. and Kinbara, A., Ed.; Proc. 8th Int. Symp. Plasma Chem.: Tokyo, 1987, pp 947-952.
14) Turban, G.; Rapeaux, M. *J. Electrochem. Soc.: Solid-State Sci. Technol.* **1983**, *130*, 2231-2236.
15) Meichsner, J.; Nitschke, M.; Rochotzki, R.; Zeuner, M. *Surf. Coat. Technol.* **1995**, *74-75*, 227-231.
16) Bershtein, V. A.; Egorov, V. M. *Differential Scanning Calorimetry of Polymers - Physics, Chemistry, Analysis, Technology*; Ellis Horwood: New York, 1994.
17) Wunderlich, B. *Macromolecular Physics*; Academic Press: New York, 1980; Vol. 3.
18) Terlingen, J. G. A.; Hoffman, A. S.; Feijen, J. *J. Appl. Polym. Sci.* **1993**, *50*, 1529-1539.
19) Briggs, D.; Seah, M. P. *Practical Surface Analysis: by Auger and X-ray Photo-electron Spectroscopy*; Wiley: Chichester, 1983.
20) Hopkins, J.; Boyd, R. D.; Badyal, J. P. S. *Polym. Prepr.* **1997**, *38*, 1093-1094.
21) Terlingen, J. G. A.; Takens, G. A. J.; Gaag, F. J. v. d.; Hoffman, A. S.; Feijen, J. *J. Appl. Polym. Sci.* **1994**, *52*, 39-53.
22) Egitto, F. D. *Pure & Appl. Chem.* **1990**, *62*, 1699-1708.
23) Sigurdsson, S.; Shishoo, R. *J. Appl. Polym. Sci.* **1997**, *66*, 1591-1601.
24) Breitbarth, F. W.; Berg, D.; Dumke, K.; Tiller, H. J. *Plasma Chem. Plasma Process.* **1997**, *17*, 39-57.
25) Busscher, H. J.; Stokroos, I.; Mei, H. C. v. d.; Rouxhet, P. G.; Schakenraad, J. M. *J. Adhes. Sci. Technol.* **1992**, *6*, 347-356.
26) Cassie, A. B. D.; Baxter, S. *Trans. Faraday Soc.* **1944**, *40*, 546-551.
27) Zisman, W. A. *Relation of the Equilibrium Contact Angle to Liquid and Solid Constitution*; Fowkes, F. M., Ed.; ACS: Washington DC, 1964; Vol. 43 (Advances in Chemistry Series), pp 1-51.
28) Chan, C. M. *Contact Angle Measurement*; Chan, C. M., Ed.; Hanser Publishers: München, 1994, pp 35-76.
29) Schulze, R. D.; Possart, W.; Kamusewitz, H.; Bischof, C. *J. Adhes. Sci. Technol.* **1989**, *3*, 39-48.
30) Miyama, M.; Yang, Y.; Yasuda, T.; Okuno, T.; Yasuda, H. K. *Langmuir* **1997**, *13*, 5494-5503.
31) Everaert, E. P.; Chatelier, R. C.; Mei, H. C. v. d.; Busscher, H. J. *Plasmas & Polymers* **1997**, *2*, 41-51.

32) Overney, R. M.; Lüthi, R.; Haefke, H.; Frommer, J.; Meyer, E.; Güntherodt, H. J.; Hild, S.; Fuhrmann, J. *Appl. Surface Sci.* **1993**, *64*, 197-203.
33) Durandet, A.; Joubert, O.; Pelletier, J.; Pichot, M. *J. Appl. Phys.* **1990**, *67*, 3862-3866.
34) ter Beek, M. *Immobilisatie van enzymen aan oppervlakte gemodificeerde polyethyleen membranen (not published)*; University of Twente: Enschede, The Netherlands, 1994.
35) Olde Riekerink, M. B.; Engbers, G. H. M.; Feijen, J. *Chapter 4 of this thesis.*

Chapter 4

CF_4 gas plasma treatment of low density poly(ethylene): Changes of surface temperature, chemistry and structure

M. B. Olde Riekerink, G. H. M. Engbers, J. Feijen

Department of Chemical Technology, Section Polymer Chemistry and Biomaterials and Institute for Biomedical Technology, University of Twente, P.O. Box 217, 7500 AE Enschede, The Netherlands

In this study changes of surface temperature and chemistry during CF_4 plasma treatment of poly(ethylene) films were invesigated in relation to changes of surface structure. Low density poly(ethylene) (LDPE) films were treated with a radiofrequency (RF) tetrafluoromethane (CF_4) gas plasma (48-49 W, 0.06-0.07 mbar) for various treatment times ranging from 0.1 s to 120 min. The films were characterized by angle dependent X-ray Photoelectron Spectroscopy (XPS), Scanning Electron Microscopy (SEM) and contact angle measurements to study the development of surface chemistry, structure and wettability, respectively, in the course of treatment time. Moreover, *in situ* fluoroptic temperature measurements were carried out during continuous and pulsed plasma treatment. Finally, aging of the plasma treated films was studied by contact angle measurements after storage up to 100 days at RT.

Initially, the surfaces were rapidly fluorinized (< 15 s) leading to increased surface heterogeneity. Substantial surface restructuring took place between 5 and 15 min of treatment. This drastic change of surface structure was attributed to a temperature induced phase separation (or demixing) of fluorinated and non-modified LDPE domains. In contrast to continuous treatment, no substantial surface temperature increase was observed during pulsed treatment, thus preventing surface restructuring. After 30 min of continuous treatment an equilibrium of surface structure and chemistry was reached. The plasma treated films were superhydrophobic ($\theta_{w,adv.}$=152°) and not susceptible to aging. However, they showed a large hysteresis (81°) which was ascribed to an increased surface heterogeneity and roughness.

4.1 Introduction

Gas plasma processes are extensively used for the chemical modification of polymer surfaces.[1-3] Tetrafluoromethane (CF_4) is often chosen as discharge gas due to its mild etching and highly fluorinating characteristics.[4-7] Several fundamental studies on characterization of CF_4 plasma treated surfaces and/or analysis of the CF_4 plasma phase can be found in

literature.[5,8-17] Meichsner *et al.* have shown that major chemical changes occurred at the surface of a low density poly(ethylene) (LDPE) film already after a few seconds of CF_4 plasma treatment.[8] Besides chemical modification, it is generally known that gas plasma etching leads to an increase of temperature at the substrate.[18-20] A surface bombardment of plasma reactive species (e.g. ions, electrons, radicals) causes heat development, while exothermic surface chemical reactions can also generate thermal energy. Due to the low thermal conductivity of most polymers, the surface temperature can easily be raised considerably during plasma treatment. The extent of surface temperature increase could play an important role in the development of surface structure during plasma treatment of polymer films.

Recently, it was shown that prolonged CF_4 plasma etching of LDPE films resulted in a remarkable surface structural change combined with a high degree of surface fluorination.[4] In this way, extremely hydrophobic surfaces with advancing water contact angles up to 150º were obtained. A combined effect of etching, fluorination and an increase of surface temperature, inducing phase separation of PE-like and Teflon-like material, was proposed as a possible explanation for the pronounced surface restructuring of the LDPE films.

The aim of the present study is to further investigate this hypothesis by studying the development of surface chemistry (fluorination) and temperature during CF_4 plasma treatment in relation to surface restructuring of LDPE films. Therefore, the films are subjected to a radio frequency (RF) CF_4 gas plasma for various treatment times ranging from 0.1 s to 120 min. *In situ* temperature measurements are carried out at the LDPE surface during continuous and pulsed plasma treatment. The surface chemical changes of the films during treatment are studied by X-ray Photoelectron Spectroscopy (XPS). Scanning Electron Microscopy (SEM) is used to investigate the changes of surface structure of the films in the course of treatment time. The effect of surface chemical and structural changes on the wettability of the plasma treated LDPE surfaces is studied by static and dynamic water contact angle measurements using the sessile drop method. In addition, contact angle measurements are used to study surface aging of the plasma treated films (<100 days), since this phenomenon is known to occur after gas plasma treatment of polymer surfaces.[2,21]

4.2 Experimental

4.2.1 Materials

Low density poly(ethylene) film (LDPE; Stamylan LD) was kindly supplied by DSM Polyethylenes, Geleen, The Netherlands. Dichloromethane (purity ≥ 99.5%) and acetone (purity ≥ 99.5%) were obtained from Merck,

Darmstadt, Germany. Tetrafluoromethane (CF_4) gas (Freon-14; purity ≥ 99.95%) was purchased from Hoekloos, Amsterdam, The Netherlands. For all experiments ultra-pure water obtained from a Milli-Q Plus System (Millipore) was used.

4.2.2 Methods

Cleaning of LDPE films

LDPE films were cleaned ultrasonically, successively in dichloromethane (10 min, three times), in acetone (10 min, three times), in water (10 min, three times), and again in acetone (10 min). After cleaning, the films were dried *in vacuo* at room temperature (RT) and stored at RT in the dark.

Gas plasma treatment of LDPE films

Cleaned LDPE films were mounted in glass holders, which were placed in the center region of a gas plasma tubular reactor (length 80 cm, internal diameter 6.5 cm). Three externally placed capacitively coupled copper electrodes were attached to the reactor: a 'hot' electrode in the center and a 'cold' electrode at both sides of the 'hot' electrode at 10 cm distance. The glass holders were positioned between the 'hot' and 'cold' electrodes. The electrodes were connected to a RF (13.56 MHz) generator through a matching network. A detailed description of the plasma apparatus is given elsewhere.[22]

The reactor was evacuated to a pressure of 0.01 mbar. Subsequently, a CF_4 gas flow of 10 cm^3/min (STP) was established through the reactor for 15 min (pre-delay). The films were then exposed to the plasma (0.06-0.07 mbar, 48-49 W) for various treatment times ranging from 0.1 s to 120 min while maintaining a constant gas flow (10 cm^3/min) through the reactor. Subsequently, the gas flow was maintained for another 2 min (post-delay). Finally, the reactor was brought to atmospheric pressure with air and the films were removed.

Moreover, pulsed plasma treatment was carried out at the same conditions as mentioned above. The treatment consisted of 1800 plasma pulses of 1 s separated by dark periods of 10 s.

In order to suppress aging effects, the plasma treated films were stored at -20°C prior to analysis (except the films that were used for the aging experiments).[2]

Temperature measurements during gas plasma treatment of LDPE films

In situ temperature measurements were carried out during continuous and pulsed CF_4 plasma treatment of LDPE films. The temperature was measured continuously by a fluoroptic temperature probe (Model 790, Luxtron Corporation, Santa Clara, USA) connected to an SSC-2 cable and an SIWR tip. The tip was placed on top of the LDPE surface in the plasma tube and connected to the external cable at the tube entrance. A schematic representation of the contact area is shown in Figure 4.1.

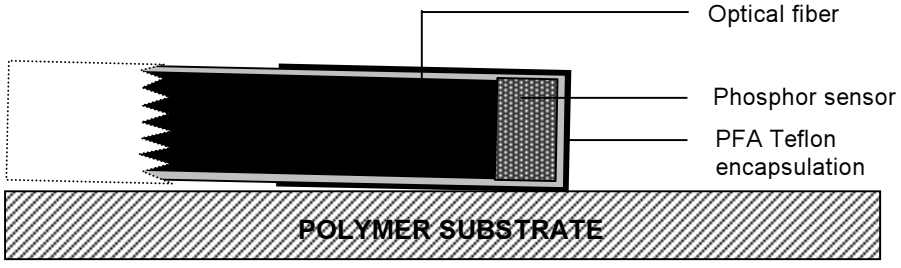

Figure 4.1: *Schematic representation of the setup for in situ temperature measurements with the fluoroptic temperature probe. The encapsulated tip is in contact with the polymer substrate.*

The increase of temperature during pulsed and continuous plasma treatment was recorded at regular time intervals. In the case of pulsed treatment, the temperature increase was recorded directly after a plasma pulse (T_{max}).

XPS analysis

The chemical surface composition of the plasma treated LDPE films was investigated by X-ray Photoelectron Spectroscopy (XPS). The measurements were performed with an XSAM-800 apparatus (Kratos, Manchester, UK) using a Mg K_α source (15kV, 15 mA). A spot size of 3x6 mm was analysed. The pressure during the measurements was $1x10^{-7}$ - $1x10^{-8}$ mbar. Survey scans (0-1100 eV) were recorded for all samples to qualitatively determine the elements present at the surface. Detail scans (20-30 eV windows) were recorded to quantify the elemental surface composition. The measured peak areas were converted into atomic percentages by using sensitivity factors known from literature.[23] Moreover, angle dependent XPS measurements were carried out on plasma treated LDPE films at take off angles (toa) of 90° (default), 30° and 20° relative to the surface.

A high resolution XPS spectrum of plasma treated LDPE was recorded on a PHI Quantum 2000 Scanning ESCA Microprobe (Physical Electronics, Minneapolis, USA) using a monochromatic Al K_α source (92.8 W, 11.75 eV). A spot size of 100 μm (ϕ) was analysed at a take off angle of 10° relative to the surface.

SEM analysis

The surface structure of the plasma treated LDPE films was studied by Scanning Electron Microscopy (SEM). Prior to SEM analysis the samples were sputtered with a 20 Å thick gold-palladium layer (Polaron SEM Sputtering System, VG Microtek, East-Grinstead, UK). The coated samples were analysed with an S-800 Field Emission SEM (Hitachi, Tokyo, Japan; 5-7 kV, 20° tilt, 40,000x magnification).

Contact angle measurements

Plasma treated LDPE films were characterized by static and dynamic water contact angle measurements using the sessile drop method. The measurements were performed with a Contact Angle Measuring System G10/G40 (KRÜSS, Hamburg, Germany).

First, static contact angles were measured by placing a water droplet (±1 μl) onto the sample with an electronically regulated syringe. Subsequently, a fresh droplet was placed onto the sample and dynamic contact angles were measured by increasing and decreasing the droplet volume with the syringe, resulting in advancing and receding contact angles, respectively. The dynamic contact angle measurement was started directly after the droplet had reached a constant shape and the liquid-solid interface started to move along the polymer surface. Every contact angle was determined at five different spots on the sample using fresh water for each new droplet.

Aging experiments were carried out with a series of plasma treated LDPE films. After plasma treatment these films were stored at RT in the dark. Static water contact angles (n=5; droplets of ±1 μl) were measured on these samples successively 2, 22, 49 and 100 days after plasma treatment.

4.3 Results and Discussion

4.3.1 Surface temperature changes during CF_4 plasma treatment of LDPE

To obtain more information about the temperature changes at an LDPE surface during (pulsed) CF_4 plasma treatment, *in situ* measurements were carried out in this study. In the past, several studies have been aimed at determination of the substrate temperature during plasma treatment by using optical[18], infrared[24], pyrometric[25], or other techniques.[26,27] Although these kind of *in situ* measurements have shown that substantial surface temperature rises up to 200ºC can occur during plasma etching, these measurements were all carried out on silicon wafers. Similar temperature studies on polymer surfaces could not be found in literature. The low thermal conductivity of most polymers compared to semi-conductors like silicon does not allow a direct extrapolation of these temperature data to the present system. Preliminary measurements during CF_4 plasma treatment of LDPE films with an infrared thermal microscanner were not succesful, due to strong disturbance by the plasma. Also, measurements with thermosensitive indicators (discoloration at a specific temperature) did not result in accurate surface temperature data during plasma treatment. In an attempt to overcome the practical problems encountered with *in situ* surface temperature measurements during plasma treatment of polymer films, fluoroptic measurements were carried out in this study. The Teflon® encapsulated fluorescent sensor that was used for these measurements (Figure 4.1) is self-calibrating with an accuracy of ± 2 ºC. Furthermore, the temperature could be measured with a rapid response (0.25 s) without disturbing or heat sinking the polymer film. Figure 4.2 shows temperature curves that were measured during continuous and pulsed plasma treatment of LDPE.

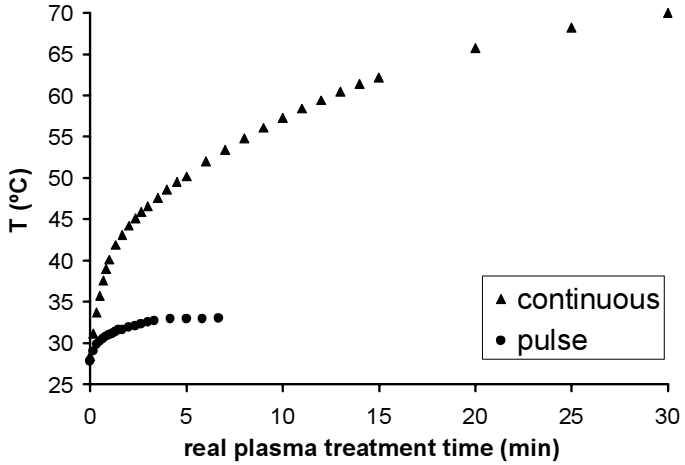

Figure 4.2: *Surface temperature during CF_4 plasma treatment as measured with a fluoroptic temperature probe on top of the polymer substrate.*

Clearly, substantial differences were found between the temperature increase during continuous and that during pulsed plasma treatment. During continuous treatment the temperature rapidly increased up to 50ºC within 5 min, after which a more gradual temperature increase was observed. The measurement was stopped at 70ºC after 30 min of plasma treatment. Pulsed plasma treatment resulted in a much milder temperature development. After an initial rapid temperature increase, an equilibrium was reached within 250 pulses of plasma treatment. The measurement was stopped after 400 plasma pulses (T_{max} = 33ºC), the absolute temperature increase (ΔT) being only 5ºC. It should be noted that the temperature increase was plotted as a function of the net plasma treatment time (here: 400 s), while the total pulsed treatment took 73 min. This essential time difference was caused by the relatively long, intermediate dark periods (10 s). The dark periods prevented a major surface temperature increase, since the heat developed at the surface during an 'on' cycle (1 s) could dissipate during the following 'off' cycle (10 s).

According to the temperature data in Figure 4.2, the melting point of LDPE (T_m = 110-115ºC) was not approached in either plasma treatment. As a control for the surface temperature measurements the temperature was also measured in the plasma above the LDPE surface (± 2 cm). For pulsed plasma treatment the 'plasma' equilibrium temperature was a little higher (ΔT = 2ºC) than the temperature measured at the LDPE surface, while for continuous treatment this temperature difference was much more significant (T_{plasma}-$T_{surface}$ = 10-15ºC). The higher 'plasma' temperature could be explained by the strong heat built up at the temperature probe in the vacuum (no heat sink). When the tip is in contact with the polymer substrate (Figure 4.1) the latter could function as a heat sink, thereby reducing the probed temperature. Thus, these experiments strongly suggest that the actual surface temperature was not accurately measured during plasma treatment. A higher surface temperature was expected, induced by continuous ion bombardment (sputtering) and exothermic chemical reactions. Apparently, the highly localized surface temperature is difficult to probe with the used fluoroptical setup. Although the absolute surface temperature could not be measured accurately, the observed temperature development in Figure 4.2 is considered to be indicative for the actual temperature increase at the polymer surface. More importantly, the substantial temperature difference between continuous and pulsed plasma treatment strongly suggests that local surface melting due to exceeding of T_m is only plausible during continuous plasma treatment.

Besides a substantial surface temperature increase, surface fluorination was also proposed to be responsible for surface restructuring during continuous CF_4 plasma treatment of LDPE.[4] Therefore, the next section will address changes of surface chemistry in the course of (continuous) plasma treatment.

4.3.2 Changes of surface chemistry during CF_4 plasma treatment of LDPE

The surface chemical composition of LDPE films was studied as a function of plasma treatment time by angle dependent XPS measurements. The data in Figure 4.3 show that rapid fluorination of LDPE occurred during CF_4 plasma treatment. The strongest increase of fluorine incorporation was found within the first 15 s of treatment (47 at.% at 90º). Longer treatment times caused a further, gradual increase of surface fluorine until an equilibrium value of 57-58 at.% was reached after 30 min (Table 4.1). Pulsed plasma treatment resulted in a similar surface chemistry compared to its continuous equivalent after 30 min (Table 4.1).

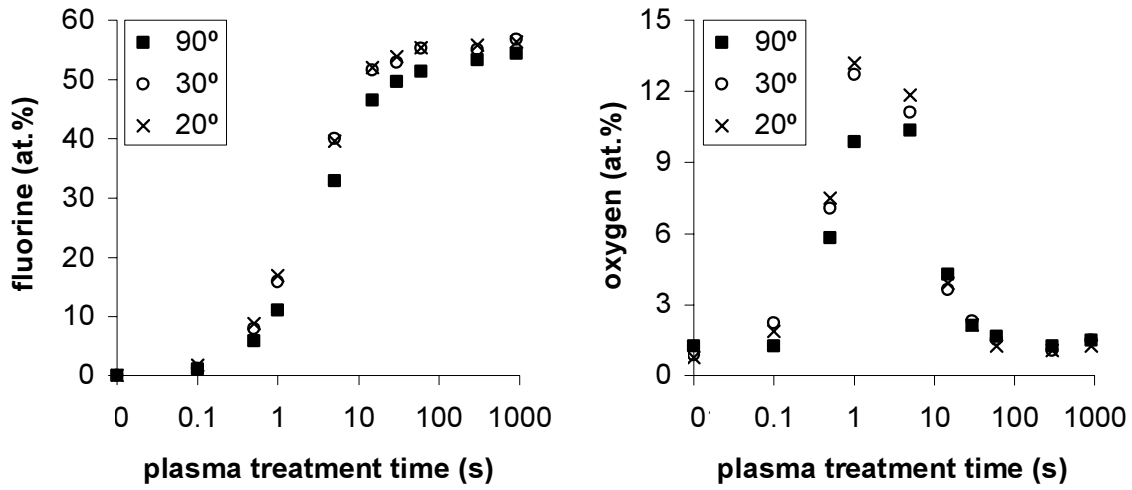

Figure 4.3: *Angle dependent XPS data of continuous CF_4 plasma treated LDPE films. Fluorine (left) and oxygen (right) atomic percentages were determined at take off angles of 90º, 30º and 20º relative to the surface.*

Besides rapid surface fluorination, a substantial amount of oxygen was introduced at the LDPE surface after short treatment times (< 5 s; Figure 4.3). After reaching a maximum value of 10 at.% (toa = 90º), surface oxidation rapidly decreased upon prolonged CF_4 plasma etching. Since a CF_4 plasma does not generate oxygen reactive species, the surprisingly high amounts of surface oxygen after short treatment times were most probably caused by post-oxidation reactions. In the initial stage of plasma treatment (< 1 s) a lot of surface free radicals were created by abstraction of hydrogen from the polymer backbone by plasma reactive species (mainly F-radicals). After plasma treatment the surfaces were exposed to air and immediate surface oxidation could take place at the generated free radical sites. The second stage of plasma treatment (1-15 s) mainly consisted of fluorine incorporation at the surface free radical sites (F↑), leaving less sites available for post-oxidation (O↓). Prolonged CF_4

plasma treatment saturated the LDPE surface with fluorine, thereby further suppressing post-oxidation.

Table 4.1: XPS data of continuous and pulsed CF_4 plasma treated LDPE films (n=1).

Sample	C (at.%)	O (at.%)	F (at.%)	F/C ratio
Untreated	98.8	1.2	-	-
30 min	40.4	2.2	57.3	1.4
60 min	39.9	1.7	58.4	1.5
120 min	41.1	2.4	56.5	1.4
1800 x 1 s	39.1	2.2	58.6	1.5

Although angle dependent XPS measurements are a valuable tool to obtain information about the chemical differentiation in the surface layer, great care should be taken when interpreting the data of rough surfaces. When looking ahead at Figure 4.5, it becomes difficult to define the surface layer in terms of the XPS analysis depth due to the high surface roughness of the LDPE films. To check the reliability of the angle dependent data in Figure 4.3, control experiments were carried out with smooth poly(styrene) surfaces (data not shown). The results of angle dependent XPS analysis were similar to those found for plasma treated LDPE films, supporting the proposed mechanism of successive radical formation, fluorination and post-oxidation as was derived from Figure 4.3.

Decreasing the take off angle showed that a fluorine gradient was present at the plasma treated LDPE surface. This gradient was most obvious during the second stage of plasma treatment (1-15 s) when fluorine was rapidly incorporated at the surface. Naturally, the outer surface was fluorinated first during this stage of treatment. Upon prolonged treatment (30 min) the gradient largely disappeared due to saturation of the complete surface layer (~10 nm). Furthermore, higher amounts of oxygen (up to 13 at.%) were detected in the upper part of the surface layer (toa = 20°) after short plasma treatment times. Since post-oxidation is mainly expected directly at the air/polymer interface, the highest amount of oxygen should indeed be located in the upper part of the surface layer.

In addition to angle dependent XPS measurements, a high resolution XPS spectrum was recorded of a 30 min plasma treated LDPE surface to obtain more information on the type of chemical bonds that were created during plasma treatment. The results of C1s peak deconvolution are presented in Figure 4.4 and Table 4.2.

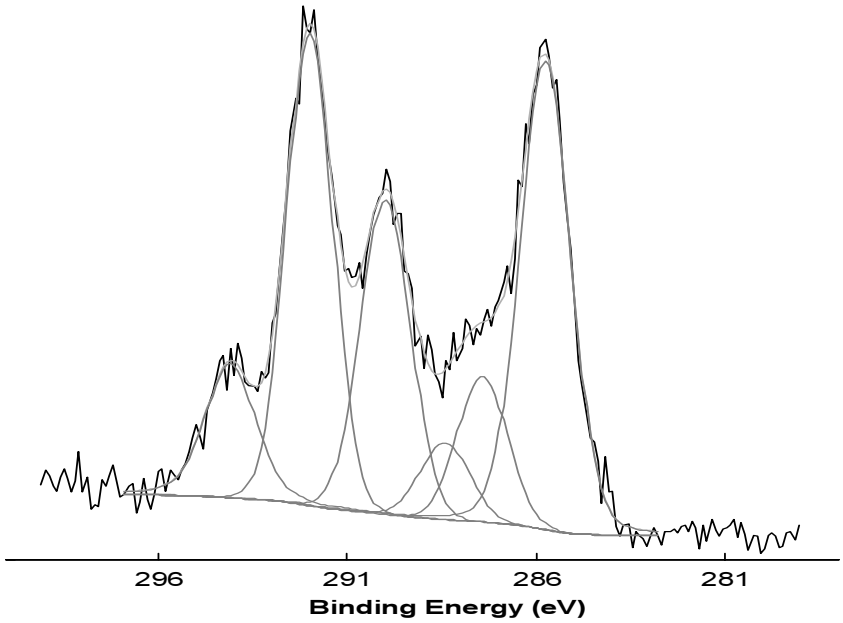

Figure 4.4: *Deconvolution of a high resolution XPS C1s spectrum of a 30 min CF_4 plasma treated LDPE film. The lowest C1s binding energy was set at 285.7 eV.*

Table 4.2: Deconvolution of a high resolution XPS C1s spectrum of a 30 min CF_4 plasma treated LDPE film. Binding energies were derived from literature.[28]

Binding Energy (eV)	Carbon bond	Area (%)
285.7	$\underline{C}H_2$-CF	29.8
287.3-288.5	$\underline{C}F$	14.3
289.9	$\underline{C}F$-CF_n *	19.0
291.9	$\underline{C}F_2$	28.2
294.1	$\underline{C}F_3$	8.8

Normally, the C1s peak of a saturated hydrocarbon is set at 285.0 eV.[28] Based on the high fluorination of the LDPE surface (F/C ratio = 1.4) after CF_4 plasma treatment, it is reasonable to assume that no nonsubstituted hydrocarbon parts (CH_2-CH_2) were left in the outer surface layer. Therefore, the main C1s peak in Figure 4.4 was set at 285.7 eV, which was assigned to hydrocarbon bonds next to a monofluorinated carbon ($\underline{C}H_2$-CF). Five additional subpeaks with increasing binding energy were deconvoluted from the C1s spectrum, corresponding to mono-, di-, and trifluorinated carbons, respectively (CF, CF_2 and CF_3; Table 4.2). For comparison, an XPS spectrum of poly(tetrafluoroethylene) (PTFE) displays only one C1s peak at 292.5 eV (CF_2-CF_2). Clearly, the plasma treated LDPE surface consisted of a number of different functionalities. Roughly, 30% of the carbon atoms was nonfluorinated, 30% was

monofluorinated and 30% was difluorinated. Additionally, a substantial amount of CF_3 functionalities was detected at the surface (9%). These various CF_n functionalities can be explained by the repetition of the abstraction/fluorination mechanism at the polymer backbone in a CF_4 plasma.[29] Additionally, formation of surface radicals by polymer chain/bond rupture may also be attributed to the vacuum ultraviolet (VUV) irradiation component of the gas plasma.[30] Furthermore, VUV irradiation is known to cause crosslinking of polymer chains during plasma treatment.[31] Besides chain rupture and crosslinking, the branched character of LDPE also contributes to the diversity of the CF_n moieties created upon CF_4 plasma treatment. Also, the surface structural changes (e.g. roughness, phase separation) upon plasma treatment, discussed in the next section, have probably influenced the development of the heterogeneous surface chemistry.

Overall, the complexity of the discussed C1s spectrum (Figure 4.4) combined with the angle dependent XPS data in Figure 4.3 clearly indicates that the development of surface chemistry during CF_4 plasma treatment of LDPE films is not straightforward. Therefore, care should be taken when simply comparing these fluorinated surfaces to well-known fluorinated materials like PTFE.

4.3.3 Changes of surface structure during CF_4 plasma treatment of LDPE

The surface structure of a series of plasma treated LDPE films was studied by SEM analysis. The resulting pictures are shown in Figure 4.5.

The SEM pictures in Figure 4.5 show that up to 5 min of plasma treatment the original lamellar surface structure of LDPE was largely preserved. Substantial surface restructuring started to occur after longer treatment times (Figure 4.5D). A drastic surface transformation from lamellae to pores and grains was observed between 5 and 15 min of plasma treatment.

Apparently, the restructuring process is induced at some point during the plasma treatment by significant changes of the surface conditions (e.g. temperature, chemistry). The temperature data in Figure 4.2, showing the largest ΔT within the first 5 min of treatment, support the idea of inducing surface restructuring at a certain 'threshold' temperature. However, this surface temperature increase could not have been solely responsible for the disappearance of the lamellar structure, as was shown earlier by thermal treatment of LDPE films.[4] The surface chemical changes observed in Figure 4.3, showing that fluorination approached its equilibrium after 15 min of plasma treatment, also played a crucial role in the restructuring process. The discussed surface temperature and chemical changes strongly support the hypothesis of surface restructuring being the result of a temperature induced phase separation of outward directed, fluorinated LDPE domains and underlying, unmodified LDPE. A different way of explaining

surface restructuring could be by assuming that some kind of demixing process took place between fluorinated and nonfluorinated polymer during cooling of the plasma treated surface from a molten state to RT. Since the surfaces were analysed after plasma treatment at RT, it is impossible to retrieve the exact moment of surface restructuring (either during plasma treatment (T↑) or during cooling after plasma treatment (T↓)).

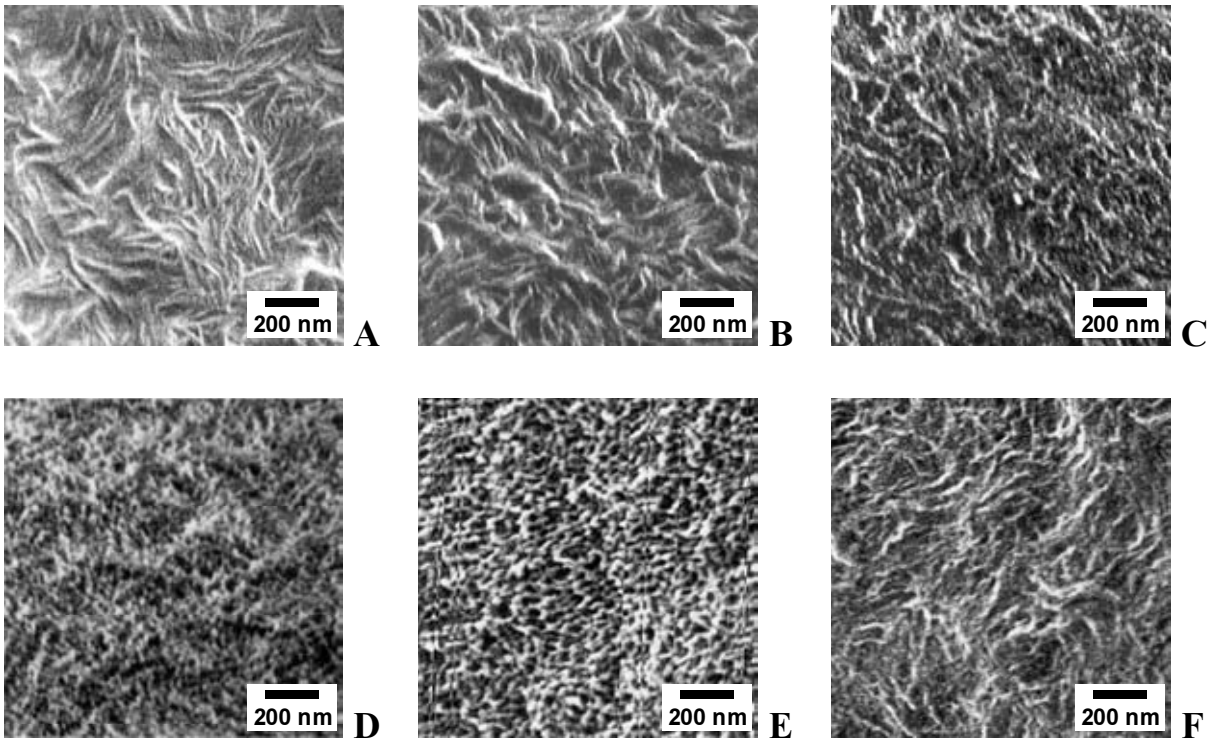

Figure 4.5: *SEM pictures of a series of CF_4 plasma treated LDPE films. Untreated (A), 1 min (B), 5 min (C), 15 min (D), 30 min (E) and 1800 x 1 s (F).*

The 'threshold' temperature for surface restructuring was not reached during prolonged pulsed treatment, resulting in preservation of the surface lamellar structure (Figure 4.5F) despite the high surface fluorination (Table 4.1). Although this was already observed before[4], it can now be better understood when looking back at the pulsed plasma temperature data in Figure 4.2.

The nanoporous-like structure, first seen after 15 min of continuous treatment, was fully developed after 30 min of treatment. Prolonged plasma etching (>30 min) did not lead to further changes of surface structure (not shown). Clearly, the surface structure reached its equilibrium state after 30 min of plasma etching, which corresponds well with the surface chemical equilibrium (Table 4.1). The drastic change of surface structure upon continuous CF_4 plasma treatment of LDPE will undoubtedly have a large impact on the surface properties of the films. Two important properties, surface wettability and stability, will be discussed next.

4.3.4 Wettability and aging of CF_4 plasma treated LDPE

A series of CF_4 plasma treated LDPE films was subjected to wettability and aging experiments. Wettability was studied by static and dynamic water contact angle measurements, the results are presented in Figure 4.6. A gradual decrease of wettability was observed with increasing plasma treatment times. Wettability reached a minimum after 30 min of treatment at a static angle of 131° and an advancing angle of 152°. In contrast to the trend observed for static and advancing angles, the receding angles decreased upon plasma treatment and remained relatively low (±70°) for longer treatment times. This resulted in a high hysteresis which reached a maximum after 30 min of treatment ($\theta_{adv.}$-$\theta_{rec.}$= 81°). The large increase of hysteresis, compared to a value of 20° for untreated LDPE, was attributed earlier to a substantial increase of surface roughness.[4] Besides surface roughness, surface heterogeneity can also cause hysteresis.[32-34] Therefore, the large hysteresis observed in Figure 4.6 should also be attributed to an increase of surface heterogeneity during plasma treatment. After all, high hysteresis values were already measured after 30 s of treatment ($\theta_{adv.}$-$\theta_{rec.}$= 59°) before a large increase of surface roughness caused by etching was observed. Furthermore, changes occurring in the liquid-solid interface during the contact angle measurement, including surface water uptake and surface mobility (reorientation) of functional groups, can cause hysteresis.[32] However, on the basis of the surface characteristics (e.g. chemistry) this kind of contact angle hysteresis is not expected for CF_4 plasma treated LDPE films.

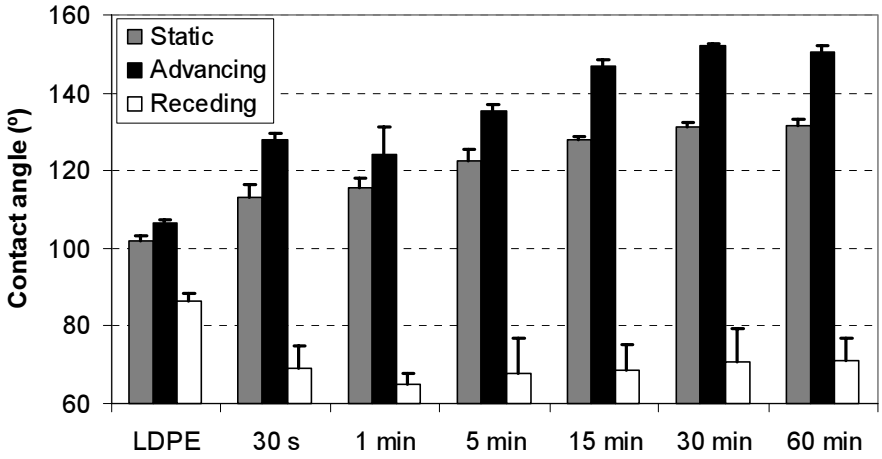

Figure 4.6: *Static and dynamic water contact angles of a series of CF_4 plasma treated LDPE films (n=5, ±sd).*

The surface chemical data in Figure 4.3 and Table 4.2 support the hysteresis data with respect to an increase of surface (chemical) heterogeneity. Summarizing, it can be concluded that

surface fluorination in an early stage (< 1 min) and surface restructuring in a later stage (Figure 4.5) were both responsible for the superhydrophobicity and the large hysteresis of the plasma treated LDPE films.

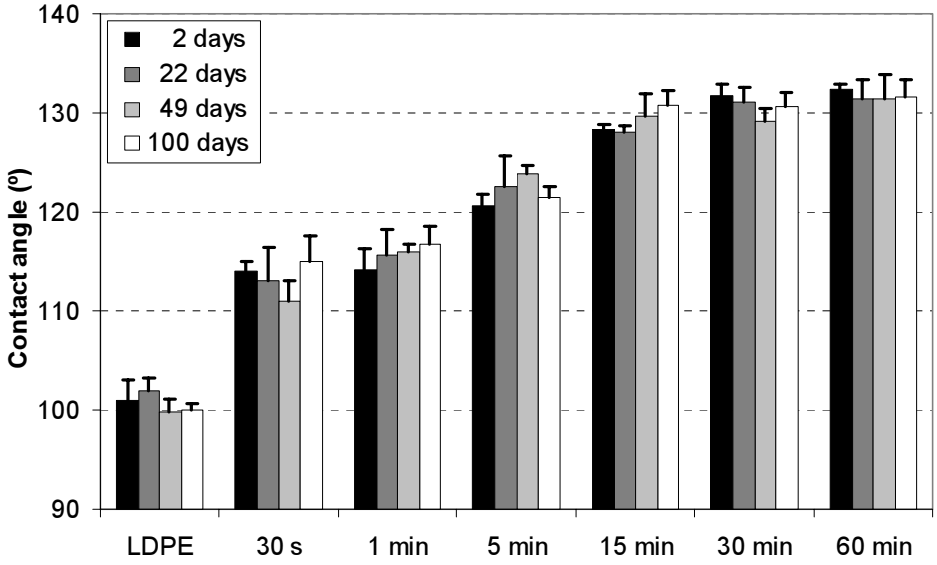

Figure 4.7: *Static water contact angles of a series of CF_4 plasma treated LDPE films measured successively 2, 22, 49 and 100 days after plasma treatment (n=5, ±sd).*

The stability of the superhydrophobic, fluorinated LDPE films was studied by aging experiments. Static contact angles were measured of stored films up to 100 days after plasma treatment. Figure 4.7 shows that the superhydrophobicity of plasma treated LDPE films was maintained upon storage. No significant decrease of contact angle was observed for any of the fluorinated surfaces in the course of storage time. These results are consistent with basic thermodynamics, which states that every material will strive for the lowest attainable surface free energy. Since fluorinated LDPE films have a much lower surface energy than the original material, the former will be energetically more stable. Aging problems, frequently encountered after oxidative plasma treatment of polymer films[2,21], are therefore not expected after CF_4 plasma treatment.

4.4 Conclusions

This study has shown that CF_4 plasma treatment of LDPE surfaces could be divided in several stages. Initially, a lot of radicals were formed which reacted with oxygen in air (< 5 s) after plasma treatment. The second stage mainly consisted of rapid fluorination (1-15 s), which

increased the water contact angle and the corresponding hysteresis of the LDPE surface. Prolonged plasma treatment saturated the surface with fluorine and substantial surface restructuring was observed (5-15 min). After 30 min of plasma treatment an equilibrium of surface structure and chemistry was reached. The plasma treated surfaces contained a number of different fluorine functionalities (e.g. CF, CF_2, CF_3) inducing surface heterogeneity. The nanoporous-like surface structure combined with the high degree of fluorination (F/C ratio = 1.4-1.5) resulted in superhydrophobic films ($\theta_{w,adv.}$=152º), while surface roughness and heterogeneity caused a large hysteresis (81º). No significant aging of the plasma treated films was observed up to 100 days after treatment.

The surface temperature and chemical changes during continuous CF_4 plasma treatment of LDPE strongly support the proposed mechanism of surface restructuring. The substantial temperature increase measured at the LDPE surface most probably induced some kind of phase separation or demixing of fluorinated (low-energy) and non-modified (high-energy) LDPE domains. The low surface temperature rise during pulsed treatment was not sufficient to trigger such a process, thus surface restructuring was not observed.

4.5 Acknowledgements

Albert v/d Berg and Mark Smithers (MESA+ Institute, University of Twente) are acknowledged for performing the XPS and SEM measurements, respectively. Physical Electronics (Minneapolis, USA) is acknowledged for performing the high resolution XPS measurement. This study was financed by the Netherlands Foundation for Chemical Research (NWO-CW).

4.6 References

1) Terlingen, J. G. A. *Introduction of functional groups at polymer surfaces by glow discharge techniques*; University of Twente: Enschede, The Netherlands, 1993.
2) Takens, G. A. J. *Functionalization of polymeric surfaces by oxidative gas plasma treatment*; University of Twente: Enschede, The Netherlands, 1997.
3) Dewez, J. L.; Humbeek, E.; Everaert, E.; Doren, A.; Rouxhet, P. G. *Plasma treated polymer films: Relationship between surface composition and surface hydrophilicity*; Pireaux, J. J., Bertrand, P. and Brédas, J. L., Ed.; IOP Publishing Ltd: Bristol, 1992, pp 463-474.
4) Olde Riekerink, M. B.; Terlingen, J. G. A.; Engbers, G. H. M.; Feijen, J. *Langmuir* **1999**, *15*, 4847-4856.
5) Sigurdsson, S.; Shishoo, R. *J. Appl. Polym. Sci.* **1997**, *66*, 1591-1601.

6) Terlingen, J. G. A.; Takens, G. A. J.; Gaag, F. J. v. d.; Hoffman, A. S.; Feijen, J. *J. Appl. Polym. Sci.* **1994**, *52*, 39-53.
7) Egitto, F. D.; Vukanovic, V.; Taylor, G. N. *Plasma Etching of Organic Polymers*; d'Agostino, R., Ed.; Academic Press, Inc.: Boston, 1990, pp 321-422.
8) Meichsner, J.; Nitschke, M.; Rochotzki, R.; Zeuner, M. *Surf. Coat. Technol.* **1995**, *74-75*, 227-231.
9) Hopkins, J.; Badyal, J. P. S. *Langmuir* **1996**, *12*, 3666-3670.
10) d'Agostino, R.; Cramarossa, F.; Colaprico, V.; d'Ettole, R. *J. Appl. Phys.* **1983**, *54*, 1284-1288.
11) Shirafuji, T.; Stoffels, W. W.; Moriguchi, H.; Tachibana, K. *J. Vac. Sci. Technol. A* **1997**, *15*, 209-215.
12) Denpoh, K.; Nanbu, K. *J. Vac. Sci. Technol. A* **1998**, *16*, 1201-1206.
13) Li, J.; McConkey, J. W. *J. Vac. Sci. Technol. A* **1996**, *14*, 2102-2105.
14) Mantzaris, N. V.; Gogolides, E.; Boudouvis, A. G. *Plasma Chem. Plasma Process.* **1996**, *16*, 301-327.
15) McMillin, B. K.; Zachariah, M. R. *J. Vac. Sci. Technol. A* **1997**, *15*, 230-237.
16) Wang, W.; Poncin-Epaillard, F.; Brosse, J. C.; Ausserre, D. *Plasmas & Polymers* **1996**, *1*, 65-85.
17) Poncin-Epaillard, F.; Pomepui, B.; Brosse, J. C. *J. Polym. Sci. A: Polym. Chem.* **1993**, *31*, 2671-2680.
18) Durandet, A.; Joubert, O.; Pelletier, J.; Pichot, M. *J. Appl. Phys.* **1990**, *67*, 3862-3866.
19) ter Beek, M. *Immobilisatie van enzymen aan oppervlakte gemodificeerde polyethyleen membranen (not published)*; University of Twente: Enschede, The Netherlands, 1994.
20) Overney, R. M.; Lüthi, R.; Haefke, H.; Frommer, J.; Meyer, E.; Güntherodt, H. J.; Hild, S.; Fuhrmann, J. *Appl. Surface Sci.* **1993**, *64*, 197-203.
21) Takens, G. A. J.; Terlingen, J. G. A.; Engbers, G. H. M.; Feijen, J. *On the Stability of (Gas) Plasma Oxidized Polymer Surfaces*; 5th World Biomater. Congr.: Toronto, 1996; Abstract books, pp 635.
22) Terlingen, J. G. A.; Hoffman, A. S.; Feijen, J. *J. Appl. Polym. Sci.* **1993**, *50*, 1529-1539.
23) Briggs, D.; Seah, M. P. *Practical Surface Analysis: by Auger and X-ray Photo-electron Spectroscopy*; Wiley: Chichester, 1983.
24) Patel, V.; Patel, M.; Ayyagari, S.; Kosonocky, W. F.; Misra, D.; Singh, B. *Appl. Phys. Lett.* **1991**, *59*, 1299-1301.
25) Richter, K.; Drescher, K. *Surf. Coat. Technol.* **1995**, *74-5*, 546-551.
26) Luckman, G. *J. Vac. Sci. Technol. B* **1993**, *11*, 99-107.
27) Gabriel, C. T.; Yeh, E. K. *Solid State Technol.* **1999**, *42*, 99.
28) Beamson, G.; Briggs, D. *High resolution XPS of organic polymers: the Scienta ESCA300 database*; Wiley: Chichester, 1992.
29) Hopkins, J.; Boyd, R. D.; Badyal, J. P. S. *Polym. Prepr.* **1997**, *38*, 1093-1094.
30) Holländer, A.; Klemberg-Sapieha, J. E.; Wertheimer, M. R. *Macromolecules* **1994**, *27*, 2893-2895.
31) Groenewoud, L. M. H.; Terlingen, J. G. A.; Engbers, G. H. M.; Feijen, J. *Langmuir* **1999**, *15*, 5396-5402.
32) Chan, C. M. *Contact Angle Measurement*; Chan, C. M., Ed.; Hanser Publishers: München, 1994, pp 35-76.
33) Morra, M.; Occhiello, E.; Garbassi, F. *Surf. Interface Anal.* **1990**, *16*, 412-417.
34) Garbassi, F.; Morra, M.; Occhiello, E.; Barino, L.; Scordamaglia, R. *Surf. Interface Anal.* **1989**, *14*, 585-589.

Chapter 5

Microbial adhesion onto superhydrophobic fluorinated low density poly(ethylene) films

M. B. Olde Riekerink [1], G. H. M. Engbers [1], H. C. van der Mei [2], H. J. Busscher [2], J. Feijen [1]

[1] *Department of Chemical Technology, Section Polymer Chemistry and Biomaterials and Institute for Biomedical Technology, University of Twente, P.O. Box 217, 7500 AE Enschede, The Netherlands*

[2] *Department of Biomedical Engineering, Section Bioadhesion, University of Groningen, A. Deusinglaan 1, 9713 AV Groningen, The Netherlands*

A convenient method has been developed to obtain superhydrophobic surfaces by means of gas plasma treatment. Low density poly(ethylene) (LDPE) films were treated with a radiofrequency (RF) tetrafluoromethane (CF_4) gas plasma (48-49 W, 0.05-0.07 mbar, 30 min). The films were characterized by Scanning Electron Microscopy (SEM), Atomic Force Microscopy (AFM), X-ray Photoelectron Spectroscopy (XPS), contact angle measurements and streaming potential measurements to obtain information about surface structure, roughness, chemistry, wettability and charge, respectively. Subsequently, the films were screened on their fouling behaviour by adhesion of several microbes (e.g. *Staphylococcus epidermidis, Streptococcus oralis, Escherichia coli, Pseudomonas aeruginosa, Candida albicans*). The microbial adhesion experiments were performed in a parallel-plate flow chamber during a period of three hours using two different suspension buffers (phosphate buffer and phosphate buffered saline). Microbial adhesion onto superhydrophobic fluorinated LDPE was compared to adhesion onto three reference materials (untreated LDPE, fluorinated ethylene propylene copolymer (FEP) and poly(ethylenimine) coated LDPE).
SEM and AFM analysis revealed that a remarkable surface structural change occurred during plasma treatment of LDPE. A rough, nanoporous-like surface structure was formed which was highly fluorinated (F/C = 1.2) and superhydrophobic (θ_{water} = 135°). Surprisingly, in most cases superhydrophobization of LDPE films did not lead to a substantial decrease of microbial adhesion. Changes of surface roughness and energy did not seem to affect the bioadhesive properties of the films, whereas inverting the film surface charge (from – to +) led to a much higher initial microbial adhesion.

5.1 Introduction

Gas plasma treatment processes are extensively used for the chemical modification of polymer surfaces.[1-3] Plasma etching treatments have also been used to increase surface roughness without aiming for a specific surface structure, for instance to improve properties such as

adhesion.[4,5] Restructuring of polymer surfaces on the nanoscale level is of interest for several areas such as biomedical engineering and membrane technology. Recently, it was shown that selective gas plasma etching of semi-crystalline polymers like low density poly(ethylene) (LDPE) can lead to interesting nanostructures under specific plasma treatment conditions.[6]

In a previous paper it was shown that hydrophobic, fluorinated surfaces showed less microbial adhesion compared to the non-fluorinated starting material.[7] Also, human skin fibroblasts spreaded significantly less on superhydrophobic FEP-Teflon surfaces with a high surface roughness compared to untreated FEP-Teflon.[8] In this study, a novel approach is used to obtain superhydrophobic fluorinated surfaces which, due to their highly non-wetting properties, could be of interest for use as a non-fouling biomaterial.

LDPE films are treated with a radio frequency (RF) tetrafluoromethane (CF_4) plasma. Scanning Electron Microscopy (SEM) and Atomic Force Microscopy (AFM) are used to investigate the surface structure and roughness of the films, respectively. Furthermore, the surface chemical composition and wetting properties of the films are studied by X-ray Photoelectron Spectroscopy (XPS) and water contact angle measurements, respectively. To obtain information about the surface charge of the films, zeta potentials are determined.

After characterization, the superhydrophobic surfaces are screened on their fouling behaviour by microbial adhesion experiments. Four bacterial strains of different species and one yeast strain that play an important role in biomaterial infections are selected. *Staphylococcus epidermidis* and *Pseudomonas aeruginosa* bacteria are generally found at infections caused by biomaterials (e.g. prostheses, heart valves), *Escherichia coli* is a bacterium mainly responsible for urinary tract infections[9], *Streptococcus oralis* is a natural mouth bacterium, and *Candida albicans* is a yeast causing biomaterial infections in the head/throat area (e.g. voice prostheses[7,10], dentures). The microbial adhesion experiments are performed in a parallel-plate flow chamber system. With this system direct observation of the microbial adhesion process *in situ* is possible.

Besides untreated and plasma treated LDPE films, fluorinated ethylene propylene copolymer (FEP) film, a well-known hydrophobic biomaterial, and poly(ethylenimine) (PEI) coated LDPE film, which is positively charged, are studied as reference materials. In this way, more information about the effects of surface chemistry, roughness and charge on the bioadhesive properties of the films can be obtained.

5.2 Experimental

5.2.1 Materials

Low density poly(ethylene) (LDPE) film (Stamylan LD 2100TN00) was kindly supplied by DSM Polyethylenes, Geleen, The Netherlands. Fluorinated ethylene propylene copolymer (FEP) film was purchased from Goodfellow, Cambridge, England. Poly(ethylenimine) (PEI branched; M_w=70,000 g/mol) aqueous solution (30%) was purchased from Polysciences Europe GmbH, Eppelheim, Germany. Dichloromethane (purity ≥ 99.8%), n-hexane (purity ≥ 96%), and acetone (purity ≥ 99.8%) were purchased from Biosolve BV, Valkenswaard, The Netherlands. Ethylene glycol (purity ≥ 99%) and 1N hydrochloric acid (HCl) were obtained from Merck, Darmstadt, Germany. Methylene iodide (purity = 99%) and 1-bromonaphthalene (purity = 98%) were purchased from Sigma-Aldrich Chemie GmbH, Steinheim, Germany. Phosphate buffered saline (PBS) solution (used for washing polymer films) was purchased from NPBI, Emmer-Compascuum, The Netherlands. Tetrafluoromethane (CF_4) gas (Freon-14; purity ≥ 99.95%) was purchased from Hoekloos, Amsterdam, The Netherlands. For all experiments ultra-pure water obtained from a Milli-Q Plus System (Millipore) was used.
For zeta potential measurements and microbial adhesion experiments two different, freshly made buffers were used: Phospate buffer (denoted as: kpi) containing 10 mM potassium phosphate (pH=7) in deionized water, and phosphate buffered saline (denoted as: PBS) containing 10 mM potassium phosphate and 150 mM sodium chloride (pH=7) in deionized water.

5.2.2 Methods

Cleaning of polymer films
LDPE films (4x10 cm) were cleaned ultrasonically, successively in dichloromethane (10 min, three times), in acetone (10 min, three times), in water (10 min, three times), and again in acetone (10 min). FEP films (5x8 cm) were cleaned ultrasonically, successively in hexane (10 min, three times), in acetone (10 min, three times), in water (10 min, three times), and again in acetone (10 min). Subsequently, all films were dried *in vacuo* at room temperature (RT) and stored at RT in the dark.

CF_4 plasma treatment of LDPE films
Cleaned LDPE films (2) were mounted in glass holders (i.e. two stacked glass plates of which the upper plate contained an area of 3.5 x 9.5 cm to expose one side of the film), which were placed in the center region of a gas plasma tubular reactor (length 80 cm, internal diameter 6.5 cm). Three externally placed capacitively coupled copper electrodes were attached to the reactor: a 'hot' electrode in the center and a 'cold' electrode at both sides of the 'hot' electrode at 15 cm distance. The glass holders were positioned between the 'hot' and 'cold' electrodes. The electrodes were connected to a RF (13.56 MHz) generator through a matching network. A detailed description of the plasma apparatus is given elsewhere.[11]
The reactor was evacuated to a pressure of 0.01 mbar. Subsequently, a CF_4 gas flow of 10 cm^3/min (STP) was established through the reactor for 15 min (pre-delay). The LDPE films were then exposed to the plasma (0.05-0.07 mbar, 48-49 W) for 30 min while maintaining a constant gas flow (10 cm^3/min) through the reactor. Subsequently, the gas flow was maintained for another 2 min (post-delay). Finally, the reactor was brought to atmospheric pressure with air and the films were removed.

In order to suppress aging effects, the treated films were stored at -20°C prior to analysis.[2]

Coating of PEI onto LDPE films

PEI solution (30%) was diluted to 1% with water and subsequently acidified to pH=6 by addition of 1N HCl solution. LDPE films were incubated in this solution (50 ml) overnight to allow PEI adsorption to take place. The PEI solution was then removed and the coated LDPE films were washed successively with water (15 min, three times), PBS (15 min, three times) and water (15 min, three times). Subsequently, the washed films were dried *in vacuo* at room temperature (RT) and stored at RT.

SEM analysis

The surface morphology of the polymer films was studied by Scanning Electron Microscopy (SEM). Prior to SEM analysis the samples were sputtered with a 20 Å thick gold-palladium layer (Polaron SEM Sputtering System, VG Microtek, East-Grinstead, UK). The coated samples were analysed with an S-800 Field Emission SEM (Hitachi, Tokyo, Japan; 7 kV, 20° tilt). SEM pictures were taken at 40,000 times magnification.

AFM analysis

Atomic Force Microscopy (AFM) was used to calculate the mean surface roughness (R_a) of the polymer films. The samples were analysed with a Nanoscope III microscope (Digital Instruments Inc., Santa Barbara, USA). AFM images were recorded in tapping mode at RT in air using silicon cantilevers (Digital Instruments). For each sample, height images were recorded with the maximum available number of pixels (512x512). For image analysis the recorded scans were "flattened" using the Nanoscope image processing software. Finally, R_a was calculated for the scanned area (5x5 μm) by applying the formula:

$$R_a = \sqrt{\sum_{x,y=1}^{N} \frac{\left(Z_{x,y} - Z_{average}\right)^2}{N^2}} \qquad (5.1)$$

Here, the roughness is defined as the normalized standard deviation calculated from the local heights ($Z_{x,y}$) and the average height ($Z_{average}$) determined over all x,y coordinates (N) measured in the AFM image.

XPS analysis

The chemical surface composition of the plasma treated polymer films was investigated by X-ray Photoelectron Spectroscopy (XPS). The measurements were performed with an XSAM-800 apparatus (Kratos, Manchester, UK) using a Mg K_α source (15kV, 10 mA). A spot size of 6 mm (ϕ) was analysed. The pressure during the measurements was $1x10^{-7}$ - $1x10^{-8}$ mbar. Survey scans (0-1100 eV) were recorded for all samples to qualitatively determine the elements present at the surface. Detail scans (20-30 eV windows) were recorded to quantify the elemental surface composition. The measured peak areas were converted into atomic percentages by using sensitivity factors known from literature.[12]

Contact angle measurements and determination of surface free energy

All polymer films were characterized by static and dynamic water contact angle measurements using the sessile drop method. The measurements were performed with a Contact Angle Measuring System G10/G40 (KRÜSS, Hamburg, Germany).

First, static contact angles were measured by placing a water droplet (1-3 μl) onto the sample with an electronically regulated syringe. Subsequently, a fresh droplet was placed onto the sample and dynamic contact angles were measured by increasing and decreasing the droplet volume with the syringe, resulting in

advancing and receding contact angles, respectively. The dynamic contact angle measurement was started directly after the droplet had reached a constant shape and the liquid-solid interface started to move along the polymer surface. For each sample, contact angles were determined at five different spots (n=5) using fresh water for each new droplet.

In addition, the sessile drop method was used to determine the surface free energy (γ_s) of the films. Static contact angles (n=5) were measured with the polar liquids water and ethylene glycol and the apolar liquids methylene iodide and 1-bromonaphthalene. In this way, four different combinations of liquids (i.e. one polar and one apolar) could be made to calculate γ_s by using the Owens-Wendt-Kaelble (OWK) equation:[13]

$$\cos\theta = 2\frac{\sqrt{\gamma_l^{LW}\gamma_s^{LW}}}{\gamma_l} + 2\frac{\sqrt{\gamma_l^{AB}\gamma_s^{AB}}}{\gamma_l} - 1 \qquad (5.2)$$

in which θ is the measured contact angle, γ_l^{AB} is the polar or acid-base component of the surface tension of the liquid, γ_l^{LW} is the apolar or Lifshitz-van der Waals component of the surface tension of the liquid, γ_s^{AB} and γ_s^{LW} are the polar and apolar components of the surface free energy of the solid, respectively. The surface tensions of the used liquids are shown in Table 5.1.

Table 5.1: Surface tension and its components of several liquids used for contact angle measurements. Data are taken from Bos *et al.*.[14]

Liquid	γ_l (mJ/m^2)	γ_l^{LW} (mJ/m^2)	γ_l^{AB} (mJ/m^2)
Water	72.8	21.8	51.0
Ethylene glycol	48.0	29	19.0
Formamide	58	39	19
Methylene iodide	50.8	50.8	~0
1-Bromonaphthalene	44.4	44.4	~0

First, γ_s^{LW} was determined by measuring the contact angle with one apolar liquid (γ_l^{AB}~0). Then, γ_s^{AB} could be determined by measuring the contact angle with one polar liquid. Finally, γ_s was calculated by addition of γ_s^{LW} and γ_s^{AB}. This procedure was performed four times (n=4) by using a different combination of apolar and polar liquids for each calculation.

Zeta potential measurements

Zeta potentials of the polymer films were determined in a parallel-plate flow chamber containing two platinum electrodes (5x25 mm) at both ends of the chamber. The films (26x76 mm) were attached to PS plates (26x76 mm) with double-sided tape. Two plates were mounted in the flow chamber (top and bottom) separated by a 0.2 mm Teflon® gasket. Subsequently, the chamber was filled with buffer (e.g. kpi or PBS) making sure that no air was left in the chamber. Measurements were carried out by applying pressure to the flow chamber (100 mbar, -100 mbar, 200 mbar, -200 mbar.... 500 mbar, -500 mbar). Zeta potentials (ζ) of the film surfaces were derived from the pressure dependence of the streaming potentials ($\Delta E_{str}/\Delta P$).[15] For each sample, measurements were carried out in threefold using new films every time.

Culturing and harvesting of microbial strains

In this study four bacterial strains of different species and one yeast strain were used: *Staphylococcus epidermidis* 3399 (SE) cultured in trypticase soy broth, *Streptococcus oralis* J22 (SO) cultured in Todd Hewitt broth, *Escherichia coli* O2K2 (EC) cultured in brain heart infusion broth, *Pseudomonas aeruginosa* AK1 (PA) cultured in nutrient broth, and *Candida albicans* GB 1/2 (CA) cultured in brain heart infusion broth.

All microbes were inoculated from an agar plate into a batch culture. After incubation for 24 h at 37 °C under aerobic conditions this culture was used to inoculate a second culture, which was grown for ± 16 h at 37 °C under aerobic conditions prior to harvesting.

The microbes were harvested by centrifugation (5 min at 5,000 g for the bacterial strains and 10,000 g for the yeast strain), washed twice with water, and resuspended in buffer (kpi or PBS). Bacteria were resuspended to a concentration of $3x10^8$/ml and yeasts to a concentration of $1x10^6$/ml as determined in a Bürker-Türk counting chamber (Tamson, Zoetermeer, The Netherlands).

Characterization of the microbial strains

The microbial strains were characterized by contact angle measurements and electrophoresis to determine the zeta potentials. The contact angle measurements were performed in an earlier study of which the results are presented in Table 5.6.[16] These contact angles are merely used as indicative values for the various microbial strains, since biological variations may cause deviating results. Unfortunately, no data of the yeast strain (CA) were available since no stable contact angles could be measured on yeasts. From the contact angle data γ_s of the bacteria was calculated according to equation 5.2, using water and formamide as polar liquids and methylene iodide and 1-bromonaphthalene as apolar liquids (see Table 5.1).[16]

The zeta potentials of the microbial strains were determined in kpi or PBS buffer by particulate microelectrophoresis.[17,18] Microbes were resuspended (± $5x10^7$ cells/ml) in buffer and their electrophoretic mobility was measured immediately after resuspending at 150 V using a Lazer Zee Meter 501 (PenKem, USA) and converted into zeta potentials assuming that the Helmholtz-Smoluchowski equation is valid. All microbial suspensions used for these measurements were taken from the same batch as was used for the adhesion experiments in order to rule out biological variations.

Microbial adhesion onto polymer films

The microbial adhesion experiments were performed in a parallel-plate flow chamber system as shown in Figure 5.1.[14,19] The chamber consists of a metal casing which encloses two transparent plates having the dimensions 76x50 mm, separated from one another by two 0.6 mm Delrin® spacers. The construction of the flow chamber is such that a laminar flow is obtained. In one experiment two different polymer films (25x75 mm each) were attached next to each other (parallel to the flow direction) on the bottom plate with double-sided tape. In this way, both films were exposed to exactly the same flow conditions, which makes comparison more accurate. The entire flow chamber was placed on the stage of a phase-contrast microscope which was coupled to a CCD camera and connected to an image analyser.

During a period of three hours a constant flow (2 ml/min) of microbial suspension was maintained through the flow chamber. Images were recorded at regular time intervals (i.e. 5, 10, 15, 30, 45, 60, 90 120, 150 and 180 min) at three different, arbitrary spots on each film.

Image analysis consisted of enumeration of the total number of adhering microbes viewed in one recorded image. The magnification of the system is such that the total image area is $1.76x10^{-4}$ cm^2 for bacteria and $29.9x10^{-4}$ cm^2 for yeasts (four times lower magnification due to the larger size of yeasts). To distinguish between adherent and in focus moving microbes, ten successively grabbed images were added to obtain one net image. Furthermore, to reduce noise and to amplify the gray value difference between microbes and background, a Laplace filter procedure was carried out on the net image. An additional Gauss filter procedure,

prior to the Laplace filter, was necessary for the images recorded during the adhesion of yeasts. The net image was then "thresholded" and enumeration of the adherent microbes was carried out by the image analysis software. Finally, an average number of adherent microbes at a specific time was calculated from the three values obtained at different spots on the film. A more detailed description of the used parallel-plate flow chamber system and the image analysis procedure can be found elsewhere.[14,19]

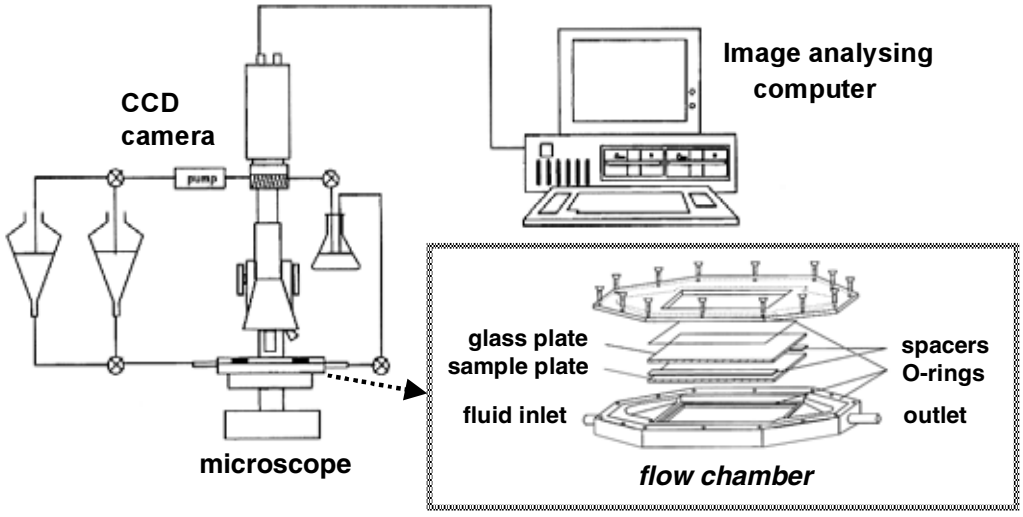

Figure 5.1: *Schematic overview of the parallel-plate flow chamber system and detailed view of the chamber itself.*[14,19]

5.3 Results and Discussion

5.3.1 Characterization of polymer surfaces

SEM and AFM analysis were used to study the surface structure and roughness of the polymer films. The results are shown in Figure 5.2. The surface structure of PEI coated LDPE films was very similar to that of untreated LDPE (picture not shown).

The SEM pictures clearly show that the morphology of the LDPE surface changed significantly during plasma treatment. The lamellar surface structure of LDPE changed into a nanoporous-like surface structure. The pores/grains that appeared at the surface have a quite uniform size, on the order of tens of nanometers. This remarkable change of surface structure during CF_4 plasma treatment was assigned to a combined effect of surface fluorination and a surface temperature increase, which was discussed extensively in a previous paper.[6]

Besides the surface structural change of LDPE, the surface roughness increased almost twofold during plasma treatment. FEP films were quite smooth and did not show any surface

nanostructure at all (Figure 5.2C). This can be ascribed to the amorphous character of the fully transparent films combined with the method of film processing.

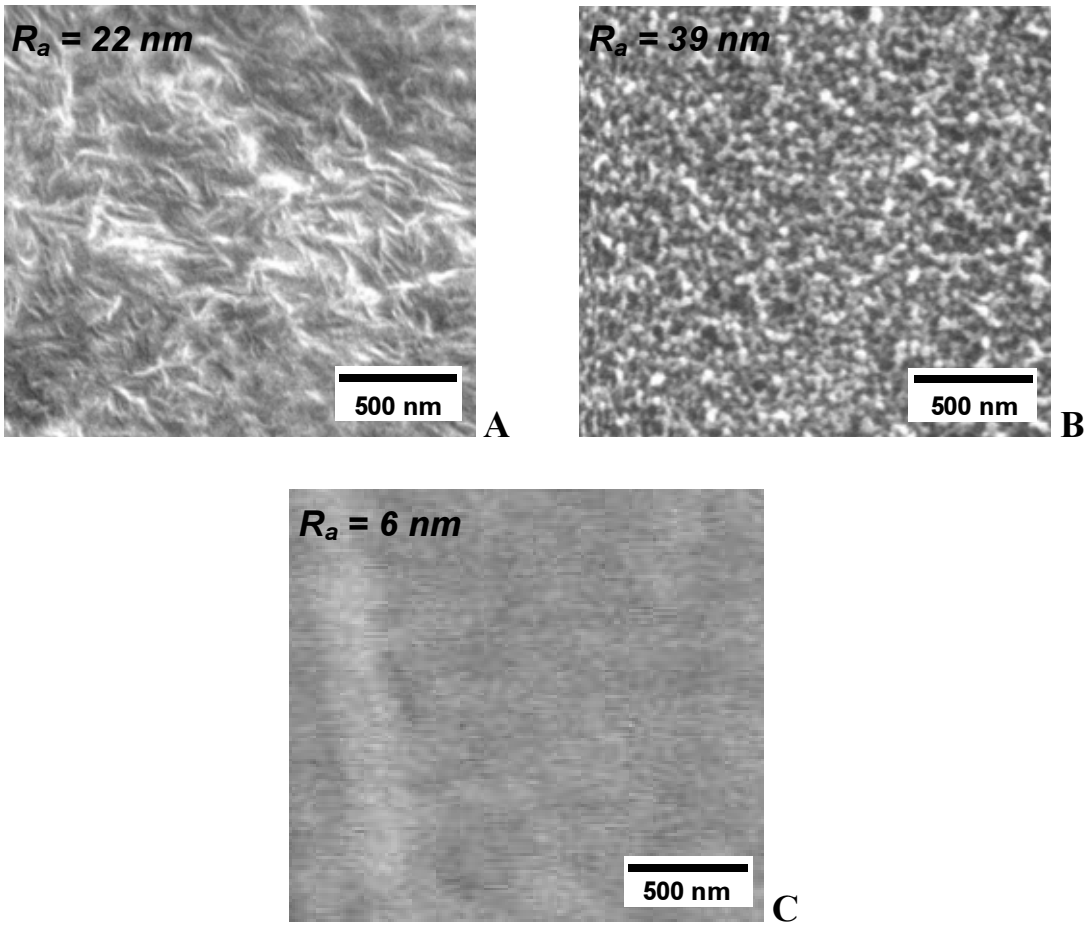

Figure 5.2: *SEM pictures of untreated LDPE (A), plasma treated LDPE (B), and FEP (C) surfaces. R_a was determined by AFM analysis for a scanned surface area of 5x5 μm.*

XPS analysis was used to determine the surface chemical composition of the polymer films. The results are shown in Table 5.2. The untreated LDPE surface was somewhat oxidized, which is a normal phenomenon for this type of film not containing any additives. During CF_4 plasma treatment the LDPE surface was highly fluorinated resulting in an F/C ratio of 1.2. The surface chemistry of these plasma treated films is comparable to that of FEP films with a measured F/C ratio of 1.9 (theoretical ratio = 2). The high degree of fluorination during CF_4 plasma treatment can be explained by the very reactive fluorine radicals which are present in a CF_4 plasma.[6,20-23] Some oxygen was again present after plasma treatment of LDPE, which can be attributed to post-reactions of surface free radicals with oxygen in air. The small

amount of sodium at the surface can not directly be explained (possible surface contamination).

Table 5.2: Chemical surface composition of polymer films as determined by XPS (n=3, ±sd).

Sample	C (at.%)	F (at.%)	O (at.%)	N (at.%)	Na / Si (at.%)
LDPE; untreated	98.3 ± 0.9	-	1.7 ± 0.9	-	-
LDPE; CF_4 plasma	44.3 ± 3.4	52.6 ± 2.7	2.4 ± 1.4	-	0.6 ± 0.3 (Na)
FEP	34.4 ± 0.4	65.0 ± 0.5	0.7 ± 0.2	-	-
LDPE; PEI coated	89.0 ± 2.1	-	6.3 ± 1.2	1.5 ± 0.3	3.2 ± 1.2 (Si)

The surface chemistry of PEI coated LDPE seems somewhat surprising. PEI has a theoretical N/C ratio of 0.5. If the LDPE surface was covered with a thick PEI layer (>10 nm), this ratio would be expected. On the contrary, a very low N/C ratio of 0.02 was found for PEI coated LDPE. This indicates that the adsorbed PEI layer was very thin. From literature it is known that on unmodified PE and other hydrophobic surfaces only a rather limited adsorption of PEI takes place, i.e. similar N/C ratios for PEI coated PE surfaces were found by Gölander *et al.*.[24] However, due to the extensive rinsing procedure after PEI adsorption (water 3x, PBS 3x, water 3x) it is reasonable to assume that the thin PEI layer is attached firmly to the LDPE surface and can not easily be removed during the flow experiments, which will be discussed in the last section.

The high amount of oxygen at the PEI coated LDPE surface can only be partly explained by some surface oxidation of the untreated LDPE (see above), and possibly by some oxygen containing groups associated with the presence of amide condensation products in the PEI.[24] However, a major part of the surface oxygen probably originated from some sort of surface contamination as indicated by the rather high amount of silicium that was also detected. This surface contamination was either introduced during the PEI adsorption procedure or already present as an impurity in the used PEI solution. Several attempts to get rid of this contamination were not successful. Therefore, the characterization of the PEI coated LDPE film should be interpreted with great care, keeping in mind that the unidentified silicon contamination may very well have influenced some of the surface properties.

Water contact angle measurements were performed on all polymer films. The results are shown in Table 5.3. Clearly, CF_4 plasma treatment of LDPE resulted in a significant decrease of wettability by water. These superhydrophobic films also show a much larger hysteresis (62°)

than untreated LDPE (19º). Since the water contact angle of an untreated FEP surface is much lower than that of CF_4 plasma treated LDPE, surface fluorination during plasma treatment is only part of the explanation for superhydrophobicity. Obviously, surface structural changes during plasma treatment also have a major effect on the hydrophobicity of the films. The nanoporous character of the plasma treated films (Figure 5.2) explains both the high water contact angles as well as the large hysteresis. The water contact angle of PEI coated LDPE is slightly lower than that of untreated LDPE, whereas a much larger difference was expected as a result of the polar amine groups present in the PEI.[24] Still, the increase of hysteresis after PEI adsorption (19º→ 36º), primarily attributed to a significant decrease of $\theta_{receding}$, supports the presence of a (contaminated) PEI layer.

Table 5.3: Static and dynamic water contact angles of polymer films as determined by the sessile drop method (n=5, ±sd).

Sample	θ_{static} (º)	$\theta_{advancing}$ (º)	$\theta_{receding}$ (º)	hysteresis (º)*
LDPE; untreated	103 ± 1	107 ± 1	88 ± 3	19
LDPE; plasma	135 ± 5	155 ± 2	93 ± 19	62
FEP	111 ± 1	120 ± 1	102 ± 1	18
LDPE; PEI coated	98 ± 1	102 ± 3	66 ± 5	36

* hysteresis = $\theta_{advancing}$ - $\theta_{receding}$

Table 5.4: Surface energy and its components of polymer films as calculated from contact angle measurements with four different liquids (n=4, ±sd).

Sample	γ_s (mJ/m^2)	γ_s^{LW} (mJ/m^2)	γ_s^{AB} (mJ/m^2)
LDPE; untreated	38.4 ± 6.1	38.2 ± 5.8	0.2 ± 0.3
LDPE; plasma	8.5 ± 4.2	8.1 ± 3.6	0.5 ± 0.8
FEP	19.0 ± 6.6	18.4 ± 7.0	0.6 ± 0.5
LDPE; PEI coated	38.1 ± 6.9	37.8 ± 6.9	0.3 ± 0.3

Table 5.4 shows the surface energies of all polymer films, calculated from contact angles determined with water (polar), ethylene glycol (polar), methylene iodide (apolar) and 1-bromonaphthalene (apolar). Generally, the calculated value of the surface energy is dependent on the method (here: equation 5.2) and the liquids used. Varying the combination of liquids (one apolar and one polar, 4 combinations) to calculate γ_s led to rather high fluctuations.

However, a similar trend, i.e. γ_s(LDPE; plasma) < γ_s(FEP) < γ_s(LDPE), was found for every single calculation. Therefore, when looking at Table 5.4 most attention should be paid to this general trend rather than to the absolute values of γ_s.

The superhydrophobic fluorinated LDPE films have a very low surface energy, less than half of the value for FEP films. This indicates that these surfaces are energetically highly stable under ambient conditions. Indeed, aging studies have pointed out that hardly any changes occur in surface wettability in the course of time (data not shown).

For all polymer films the surface energy mainly consists of an apolar part. With the exception of PEI coated LDPE this result nicely agrees with the fact that, besides a minor amount of surface oxidized groups, no polar groups are present at the surface. The surface energy components of PEI coated LDPE are identical to those of untreated LDPE, whereas amine groups present in the former surface should have led to a much higher polar energy component. Since contact angle measurements characterize the outermost surface layer of the films, the lack of difference between untreated and PEI coated LDPE can most likely be attributed to apolar silicon surface contaminations (discussed above).

For microbial adhesion studies it is useful to obtain information about the surface charge of the polymer films, besides studying surface structure (Figure 5.2), chemistry (Table 5.2), wettability (Table 5.3), and energy (Table 5.4). Therefore, zeta potential measurements were carried out in the same buffers that were used for microbial adhesion (kpi and PBS). The results are shown in Table 5.5.

Table 5.5: Zeta potentials of polymer films as determined by streaming potential measurements in kpi and PBS buffer (n=3, ±sd).

Sample	ζ_{kpi} (mV)	ζ_{PBS} (mV)
LDPE; untreated	-31 ± 3	-20 ± 5
LDPE; plasma	-30 ± 5	-21 ± 3
FEP	-32 ± 4	-16 ± 6
LDPE; PEI coated	2 ± 1	n.d.

With the exception of PEI coated LDPE all polymer films have a highly negative zeta potential, indicating a negative surface charge. As expected, in PBS buffer the zeta potentials are less negative due to the high ionic strength of the medium. Despite the large differences in surface structure and chemistry, the surface charges of (un)treated LDPE and FEP films do not differ significantly in either of the two buffers. However, PEI coated LDPE has a slightly

positive surface charge due to the presence of basic amine groups and is therefore clearly distincted from the rest. Also, the large difference between untreated and PEI coated LDPE is an indirect proof for the presence of a PEI layer on the LDPE film. More importantly, the adsorbed PEI layer seemed to withstand the flow conditions during the ζ-measurement which are comparable to the conditions during microbial adhesion. The positive charge of the PEI coated LDPE does make these films suitable for studying the effect of surface charge on microbial adhesion, despite the presence of surface contaminating species.

The characterization of the polymer films used in this study shows that substantial differences in surface structure, roughness, chemistry, wettability, and charge were found which will influence the microbial adhesion on these films. Before discussing these results, the characterization data of the used microbial strains will be presented.

5.3.2 Characterization of microbial strains

The calculated surface energies of the bacterial strains, based on contact angle data taken from literature[16], are presented in Table 5.6. The bacterial strains vary quite a lot in hydrophobicity, from 24° for the *S. oralis* strain to 106° for the *P. aeruginosa* strain. This was one of the selection criteria for the bacterial strains used in this screening study. This variation was also found to some extent for the surface energy of the bacterial strains. The *P. aeruginosa* strain has the lowest surface energy due to its very low polar component. In that respect it resembles the surface properties of the polymer films best. The other bacterial strains have a much more polar character with some minor mutual differences. The apolar surface energy component is roughly the same for all strains and similar to that of untreated LDPE films. Again, it should be noted that the high standard deviations are caused by the various combinations of liquids that were used to calculate γ_s.

Table 5.6: Surface energy and its components of bacterial strains as calculated from contact angle data taken from literature (n=4, ±sd).[16]

Sample	θ_{water} (°)*	γ_s (mJ/m^2)	γ_s^{LW} (mJ/m^2)	γ_s^{AB} (mJ/m^2)
Staphylococcus epidermidis 3399	29	52.2 ± 16.8	33.0 ± 2.4	19.2 ± 16.8
Streptococcus oralis J22	24	60.1 ± 11.5	36.2 ± 1.6	24.0 ± 11.5
Escherichia coli O2K2	57	50.4 ± 1.7	32.9 ± 4.4	17.5 ± 3.6
Pseudomonas aeruginosa AK1	106	37.0 ± 3.4	34.1 ± 1.1	2.9 ± 3.3

* van der Mei *et al.*[16]

Also, zeta potentials of the microbial strains were determined in the same buffers used for the adhesion experiments. Table 5.7 shows that all strains have a negative surface charge under the studied conditions, although there are certainly some mutual differences. The *S. epidermidis* and *E. coli* strains are most negatively charged in both buffers. In this respect, they resemble the surface properties of the negatively charged polymer films. The *S. oralis* and *C. albicans* strains are much less negatively charged and approach neutrality in PBS buffer. Again, for all strains zeta potentials are much less negative in PBS buffer due to its higher ionic strength. However, this effect of buffer seems to be more pronounced for the microbial strains than for the polymer films (Table 5.5).

Table 5.7: Zeta potentials of microbial strains as determined by particulate micro-electrophoresis in kpi and PBS buffer.

Sample	ζ_{kpi} (mV)	ζ_{PBS} (mV)
Staphylococcus epidermidis 3399	-37 ± 6	-13 ± 6
Streptococcus oralis J22	-19 ± 4	-7 ± 4
Escherichia coli O2K2	-36 ± 4	-15 ± 6
Pseudomonas aeruginosa AK1	-29 ± 9	-10 ± 4
Candida albicans GB 1/2	-19 ± 6	-3 ± 4

The negative surface charge of both the microbial strains and the polymer films implies an electrostatic repulsive effect, especially in buffers with a low ionic strength (e.g. kpi). Therefore, in principle a higher microbial adhesion is expected in PBS buffer due to minor electrostatic repulsion. The microbial adhesion experiments will be discussed in the next section.

5.3.3 Microbial adhesion experiments

The microbial adhesion experiments that were performed in this screening study can be divided in two parts. First, the effect of film superhydrophobicity on microbial adhesion was studied. In this (most extensive) part adhesion experiments with five different microbial strains were carried out on untreated and plasma treated LDPE films in two different buffers (kpi and PBS). The resulting ten microbial adhesion curves are shown in Figure 5.3. Secondly, the role of surface roughness, energy and charge of the polymer films was investigated in more detail. In this part adhesion experiments with the *S. epidermidis* strain (SE) were carried out on untreated, plasma treated and PEI coated LDPE films and FEP films in kpi buffer. For these

experiments, the initial increase in the number of adhering bacteria with time was expressed in a so-called initial deposition rate j_0 (i.e. slope of the adhesion curve at t=0). The number of bacteria adhering after 3 h, n_{3h}, was taken as an estimate for long-term bacterial adhesion. The initial (j_0) and long-term (n_{3h}) adhesion data are shown in Figure 5.4.

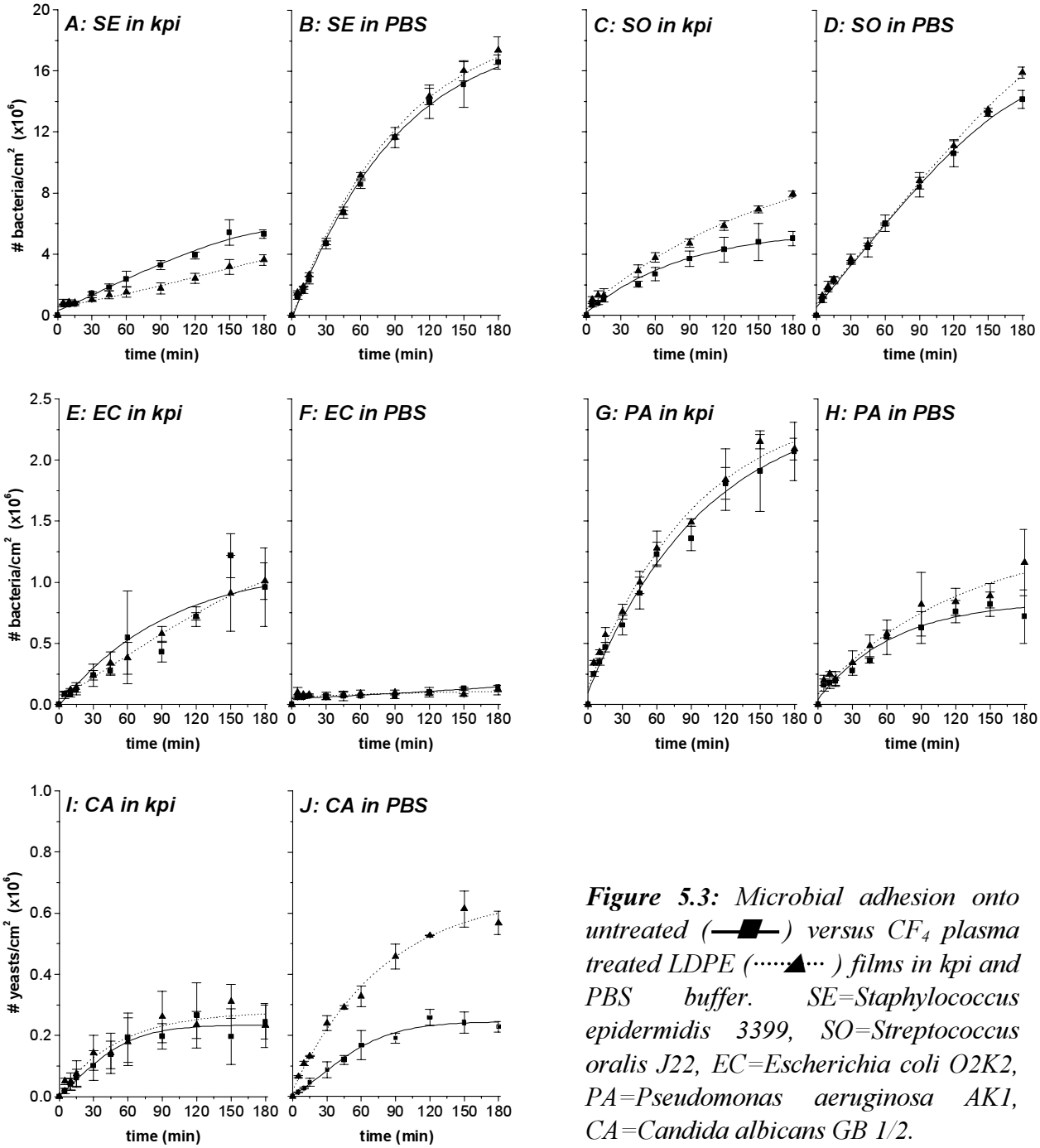

Figure 5.3: *Microbial adhesion onto untreated (—■—) versus CF_4 plasma treated LDPE (·····▲····) films in kpi and PBS buffer. SE=Staphylococcus epidermidis 3399, SO=Streptococcus oralis J22, EC=Escherichia coli O2K2, PA=Pseudomonas aeruginosa AK1, CA=Candida albicans GB 1/2.*

It is remarkable that in general no significant differences in initial bacterial adhesion (t<15 min) were found between untreated and plasma treated LDPE films, irrespective of the type of

bacterial strain and the type of buffer (Figure 5.3A-H). This suggests that the differences in surface properties between untreated and plasma treated LDPE films have no effect on the initial adhering behaviour of the bacteria. Apparently, bacteria cannot discriminate between hydrophobic LDPE and superhydrophobic, fluorinated LDPE. Long-term adhesion (t>60 min) did show significant differences in a few cases. SE in kpi adhered significantly less onto plasma treated LDPE, whereas SO in kpi showed a reverse effect. In both cases no long-term differences were found in PBS buffer, although bacterial adhesion was much higher than in kpi buffer which was expected due to a much lower electrostatic repulsion. The EC and PA strains hardly showed any differences in long-term adhesion onto untreated and plasma treated LDPE, neither in kpi nor in PBS buffer. Remarkably, these strains adhered much less in PBS than in kpi buffer which is contradictory to the electro-repulsive theory. No direct explanation could be found for this deviating adhering behaviour.

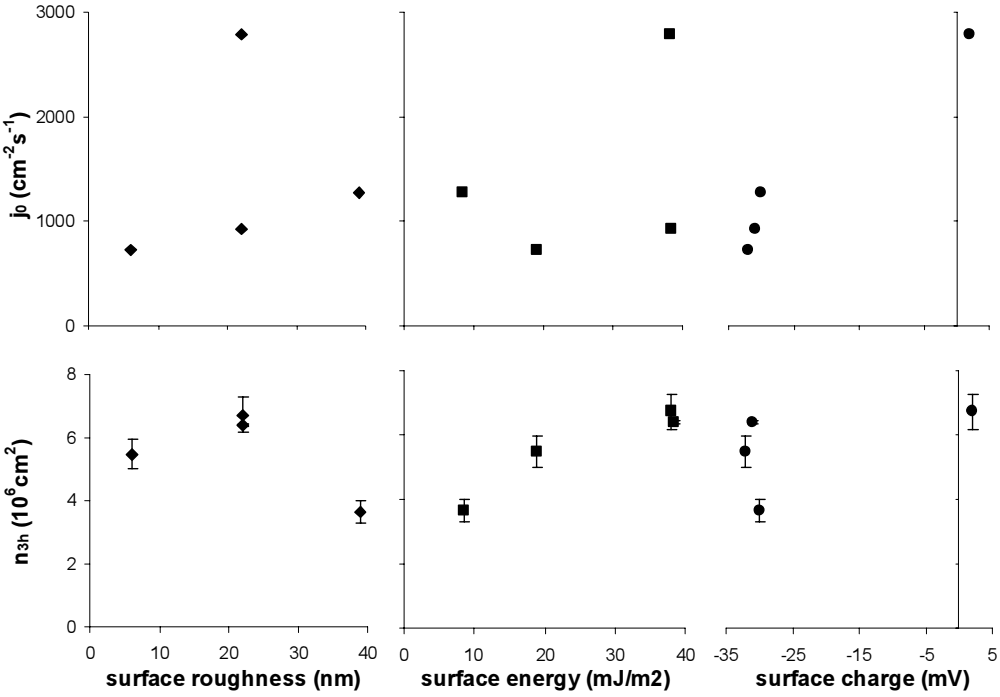

Figure 5.4: *Effect of surface roughness (◆), surface energy (■) and surface charge (●) of polymer films on the initial deposition rate (j_0) and the number of adhering Staphylococcus epidermidis 3399 in kpi buffer after 3 h (n_{3h}).*

The adhesion of yeasts onto untreated and plasma treated LDPE shows a very different development from that of bacteria (Figure 5.3I,J). In kpi buffer no differences in initial and long-term adhesion were found, whereas in PBS buffer yeasts adhered much more onto plasma treated LDPE. This remarkable difference occurred directly after starting the

experiment and became even larger during long-term adhesion. Since the zeta potentials of untreated and plasma treated LDPE are similar and PBS suppresses most of the electrostatic repulsion, the preferential adhesion of yeasts onto plasma treated LDPE can only be explained by a difference of surface chemistry or structure.

The effect of various surface properties was further studied by plotting j_0 and n_{3h} of SE in kpi as a function of the surface roughness (R_a), the surface energy (γ_s) and the surface charge (ζ) of the polymer films, respectively (Figure 5.4). Generally, no clear trends were observed in the effect of film surface roughness and energy on the adhesion of SE. Still, initial adhesion effects (j_0) clearly differed from long-term adhesion effects (n_{3h}). For example, the roughest surface (plasma treated LDPE) initially showed a higher deposition rate than the smooth FEP surface, whereas an inverse effect was found after long-term adhesion.

In contrast to surface roughness and energy, the effect of surface charge on bacterial adhesion did show a clear trend. Initially, SE adhered preferentially onto the positively charged surface with a deposition rate up to four times higher than onto negatively charged surfaces. Clearly, surface charge has a major effect on initial bacterial adhesion in buffers with a low ionic strength, which is in agreement with results found earlier by Harkes *et al.*.[25] However, after long-term adhesion the initial difference largely disappeared. This could be explained by the fact that the main driving force for adhesion, electrostatic attraction, becomes smaller once the positively charged surface is covered with negatively charged bacteria. In a recent study, Gottenbos *et al.* have shown that PA in PBS initially adhered twice as fast on a positively charged polymer surface compared to a chemically similar, negative surface.[26] This proves that film surface charge also influences initial bacterial adhesion in buffers with a high ionic strength, although the effect is somewhat smaller.

One aspect that has not been discussed is the tendency of the microbes to form clusters (aggregates) once the surface becomes saturated after long-term adhesion. Although, this natural phenomenon has been observed more or less on all studied polymer films, there was no clear indication that microbes preferentially clustered on one type of surface. Therefore, no further attention was paid to the causes and effects of microbial surface aggregation.

Unfortunately, when listing all the microbial adhesion results it is not possible to find one general trend in the effect of film surface properties on the adhering behaviour of microbes. Clearly, the various strains of microbes used in this screening study showed different adhering behaviour, but in most cases no substantial difference of adhesion could be found for superhydrophobic, fluorinated LDPE and hydrophobic, untreated LDPE. Nonetheless, surface charge does play an important role in the adhesion process, especially in buffers with a low ionic strength. Keeping the surface charge of the films highly negative (like in this study) will

reduce initial microbial adhesion due to electrostatic repulsion, taking into account that most microbial strains are negatively charged.

5.4 Conclusions

Superhydrophobic low-energy surfaces can be prepared by CF_4 plasma treatment of LDPE films. The superhydrophobicity is caused by a combination of fluorination and surface structural changes during CF_4 plasma treatment. In this way, energetically stable surfaces with high F/C ratios (1.2) and low wettability (θ_{water} = 135°) were obtained.
The bioadhesive properties of these films were tested by microbial adhesion experiments with four bacterial strains of different species and one yeast strain. Surprisingly, this screening study showed there is no general trend that superhydrophobization of LDPE films leads to lower microbial adhesion. On all negatively charged surfaces initial microbial adhesion ($t < 15$ min) is relatively low and is not affected by surface structure (e.g. roughness) or chemistry (e.g. energy). However, on positively charged surfaces like PEI coated LDPE films the initial deposition rate of bacteria is up to four times higher than on negatively charged surfaces.

5.5 Acknowledgements

Albert v/d Berg, Mark Smithers and Clemens Padberg (MESA+ Institute, University of Twente) are acknowledged for performing the XPS, SEM and AFM measurements, respectively. Betsy v/d Belt-Gritter (Department of Biomedical Engineering, University of Groningen) is acknowledged for culturing of the microbial strains and assisting with the adhesion experiments. This study was financed by the Netherlands Foundation for Chemical Research (NWO-CW).

5.6 References

1) Terlingen, J. G. A. *Introduction of functional groups at polymer surfaces by glow discharge techniques*; University of Twente: Enschede, The Netherlands, 1993.
2) Takens, G. A. J. *Functionalization of polymeric surfaces by oxidative gas plasma treatment*; University of Twente: Enschede, The Netherlands, 1997.

3) Dewez, J. L.; Humbeek, E.; Everaert, E.; Doren, A.; Rouxhet, P. G. *Plasma treated polymer films: Relationship between surface composition and surface hydrophilicity*; Pireaux, J. J., Bertrand, P. and Brédas, J. L., Ed.; IOP Publishing Ltd: Bristol, 1992, pp 463-474.
4) Wu, S. *Polymer Interface and Adhesion*; Marcel Dekker, Inc.: New York, 1982.
5) Choi, D. M.; Park, C. K.; Cho, K.; Park, C. E. *Polymer* **1997**, *38*, 6243-6249.
6) Olde Riekerink, M. B.; Terlingen, J. G. A.; Engbers, G. H. M.; Feijen, J. *Langmuir* **1999**, *15*, 4847-4856.
7) Everaert, E. P. J. M.; van der Mei, H. C.; Busscher, H. J. *Colloid Surf. B-Biointerfaces* **1998**, *10*, 179-190.
8) Busscher, H. J.; Stokroos, I.; Golverdingen, J. G.; Schakenraad, J. M. *Cell Mater.* **1991**, *1*, 243-249.
9) Harkes, G. *Interaction of Escherichia coli with Solid Surfaces; Adhesion, Growth and Migration*; University of Twente: Enschede, The Netherlands, 1991.
10) Busscher, H. J.; Geertsema-Doornbusch, G. I.; van der Mei, H. C. *J. Biomed. Mater. Res.* **1997**, *34*, 201-209.
11) Terlingen, J. G. A.; Hoffman, A. S.; Feijen, J. *J. Appl. Polym. Sci.* **1993**, *50*, 1529-1539.
12) Briggs, D.; Seah, M. P. *Practical Surface Analysis: by Auger and X-ray Photo-electron Spectroscopy*; Wiley: Chichester, 1983.
13) Chan, C. M. *Contact Angle Measurement*; Chan, C. M., Ed.; Hanser Publishers: München, 1994, pp 35-76.
14) Bos, R.; van der Mei, H. C.; Busscher, H. J. *Fems Microbiol. Rev.* **1999**, *23*, 179-230.
15) van Wagenen, R. A.; Andrade, J. D. *J. Colloid Interface Sci.* **1980**, *76*, 305-314.
16) van der Mei, H. C.; Bos, R.; Busscher, H. J. *Colloid Surf. B-Biointerfaces* **1998**, *11*, 213-221.
17) Noordmans, J.; Kempen, J.; Busscher, H. J. *J. Colloid Interface Sci.* **1993**, *156*, 394-399.
18) Hiemenz, P. C. *Electrophoresis and other electrokinetic phenomena*; 2nd ed.; Hiemenz, P. C., Ed.; Marcel Dekker: New York, 1986; Vol. 4, pp 737-790.
19) Busscher, H. J.; Mei, H. C. v. d. *Use of Flow Chamber Devices and Image Analysis Methods to Study Microbial Adhesion*; Doyle, R. J. and Ofek, I., Ed.; Academic Press: San Diego, 1995; Vol. 253, pp 455-477.
20) Hopkins, J.; Boyd, R. D.; Badyal, J. P. S. *Polym. Prepr.* **1997**, *38*, 1093-1094.
21) Terlingen, J. G. A.; Takens, G. A. J.; Gaag, F. J. v. d.; Hoffman, A. S.; Feijen, J. *J. Appl. Polym. Sci.* **1994**, *52*, 39-53.
22) Egitto, F. D. *Pure & Appl. Chem.* **1990**, *62*, 1699-1708.
23) Sigurdsson, S.; Shishoo, R. *J. Appl. Polym. Sci.* **1997**, *66*, 1591-1601.
24) Gölander, C. G.; Eriksson, J. C. *J. Colloid Interface Sci.* **1987**, *119*, 38-48.
25) Harkes, G.; Feijen, J.; Dankert, J. *Biomaterials* **1991**, *12*, 853-860.
26) Gottenbos, B.; Van der Mei, H. C.; Busscher, H. J.; Grijpma, D. W.; Feijen, J. *J. Mater. Sci.-Mater. Medicin* **1999**, *10*, 853-855.

Chapter 6

Tailoring the properties of asymmetric cellulose acetate membranes by gas plasma etching *

M. B. Olde Riekerink [1], G. H. M. Engbers [1], M. Wessling [2], J. Feijen [1]

[1] *Department of Chemical Technology, Section of Polymer Chemistry and Biomaterials and Institute for Biomedical Technology, University of Twente, P.O. Box 217, 7500 AE Enschede, The Netherlands*

[2] *Department of Chemical Technology, Membrane Technology Group, University of Twente, P.O. Box 217, 7500 AE Enschede, The Netherlands*

Cellulose triacetate (CTA) ultrafilters and cellulose acetate blend (CAB) desalination membranes were treated with a radio frequency (RF) gas plasma (tetrafluoromethane (CF_4) or carbon dioxide (CO_2), 47-49 W, 0.04-0.08 mbar). Treatment times were varied between 15 s and 120 min. The plasma treated toplayer of the membranes was characterized by Scanning Electron Microscopy (SEM), X-ray Photoelectron Spectroscopy (XPS) and contact angle measurements to obtain information about surface structure, chemistry and wettability, respectively. The membrane properties (e.g. permeability, selectivity, fouling) were studied by waterflux measurements, molecular weight cutoff (MWCO) measurements and fouling experiments with bovine serum albumin (BSA).

CO_2 plasma treatment resulted in gradual etching of the membrane's dense toplayer. Permeation and selectivity changed significantly for treatment times of 0-15 min for CTA and 5-60 min for CAB membranes. Moreover, CTA membranes were hydrophilized during CO_2 plasma treatment whereas CF_4 plasma treatment led to hydrophobic surfaces due to strong fluorination of the toplayer. This study shows that gas plasma etching can tailor the properties of asymmetric cellulose acetate membranes by simultaneously modifying the chemistry and structure of the toplayer. The low fouling properties of CTA membranes were thereby largely maintained.

6.1 Introduction

Gas plasma treatment processes are extensively used for the chemical modification of polymer surfaces.[1-3] This powerful surface modification technique has also often been used to improve the specific properties of ultrafiltration (UF) and reverse osmosis (RO) membranes (e.g. permeation, selectivity, biocompatibility).[4-15] In this respect, a lot of attention has been paid to hydrophilization of membrane surfaces in order to reduce fouling.[7,13,15] Besides chemical

* The contents of this chapter has been submitted to J. Colloid Interface Sci. **2001**

modification, gas plasma etching was also used as a tool to obtain more information about the membrane structure.[16,17]

A major part of all these studies was focussed on plasma treatment of poly(sulfone) and poly(acrylonitrile) membranes.[4-12] A few other studies report on plasma modification of poly(ethylene) and track-etched poly(ethylene terephthalate) membranes.[13,18]

Cellulose acetate is a moderately hydrophilic, cheap polymer frequently used for production of high performance asymmetric UF and RO membranes.[19-23] However, hardly any research was aimed at improving the membrane properties of cellulose acetate by gas plasma treatment. Recently, Bhat *et al.* used ammonia plasma treatment to modify the surface of homogeneous cellulose triacetate membranes.[14] Besides an increase of hydrophilicity, pervaporation studies for separation of an isopropanol-aqueous mixture showed that these membranes have excellent selectivity for water.

In the present study, gas plasma etching will be used to modify the surface chemical and structural properties of asymmetric cellulose acetate membranes. Controlled structural modification of the membrane's toplayer on the nanoscale level, thereby simultaneously modifying the surface chemistry, could be a versatile one-step tool to tailor the membrane properties for a wide range of applications.

One type of UF and one type of RO cellulose acetate membrane have been selected for this study. Cellulose triacetate (CTA) ultrafilters are well-known for their low fouling properties and cellulose acetate blend (CAB) membranes are widely used for desalination. These membranes are treated with a radio frequency (RF) plasma. Carbon dioxide (CO_2) and tetrafluoromethane (CF_4) are used as discharge gas. The former is an oxidative etchant[2], while the latter is known as a mild, highly fluorinizing etchant.[24] After gas plasma etching the toplayer structure of the membranes is analysed by Scanning Electron Microscopy (SEM). Furthermore, the chemical composition and the wetting properties of the surface of the treated CTA membranes are studied by X-ray Photoelectron Spectroscopy (XPS) and water contact angle measurements using the sessile drop method, respectively.

The permeability of the membranes after plasma etching is studied by waterflux measurements in a 'dead end' flow cell. The CTA membrane's selectivity is studied by calculation of the molecular weight cutoff (MWCO) from the results of gel permeation chromatography (GPC) measurements, using a polydisperse dextran solution. Finally, the effect of CO_2 plasma treatment on the fouling properties of CTA membranes is studied by filtration experiments with a 'fouling' solution of bovine serum albumin (BSA).

6.2 Experimental

6.2.1 Materials

Cellulose triacetate (CTA) ultrafilter discs (ø=25 mm) with a molecular weight cutoff (MWCO) of 5,000 g/mol were purchased from Sartorius AG, Goettingen, Germany. The CTA filters contain Aerosil®, i.e. synthetic silicic acid which is added to the casting solution during membrane production.[22] Cellulose acetate blend (CAB) desalination membrane sheets were kindly supplied by Hydranautics, Almelo, The Netherlands. These membranes consist of a mixture of cellulose di- and triacetate casted on a non-woven PET support. Tetrafluoromethane (CF_4) gas (Freon-14; purity ≥ 99.95%) and carbon dioxide (CO_2) gas (purity ≥ 99.995%) were purchased from Hoekloos, Amsterdam, The Netherlands. Dextran ($M_{w,avg}$ = 71,400 g/mol; M_w/M_n = 4.5-5.0) and bovine serum albumin (BSA; purity = 96%) were purchased from Sigma-Aldrich Chemie GmbH, Steinheim, Germany. Micro BCA Protein Assay Reagent Kit was purchased from Pierce, Rockford, USA. Phosphate buffered saline (PBS) was purchased from NPBI, Emmer-Compascuum, The Netherlands. For rinsing, membrane storage and contact angle measurements, ultra-pure water obtained from a Milli-Q Plus System (Millipore) was used. For waterflux measurements deionized water was used.

6.2.2 Methods

Preparation of CAB membrane discs

Discs of 25 mm (ø) were punched from CAB membrane sheets and subsequently cleaned ultrasonically with water (10 min, three times). After cleaning, the discs were stored in water at 4 °C. CTA ultrafilter discs were used as received.

Gas plasma treatment of CTA and CAB membranes

Prior to plasma treatment the wet CAB membranes were dried *in vacuo* overnight at ± 40 °C. During the drying process the asymmetric membranes have a strong tendency to roll up. Therefore, the wet membranes were fixed in a glass holder (i.e. two stacked glass plates of which the upper plate contained three holes of 20 mm (ø) to expose the membranes) to prevent curling during drying.

The glass holders, either containing at most three dried CAB membranes or three original CTA membranes, were placed in the center region of a gas plasma tubular reactor (length 80 cm, internal diameter 6.5 cm). Three externally placed capacitively coupled copper electrodes were attached to the reactor: a 'hot' electrode in the center and a 'cold' electrode at both sides of the 'hot' electrode at 10 cm distance. The glass holders were positioned between the 'hot' and 'cold' electrodes. The electrodes were connected to a RF (13.56 MHz) generator through a matching network. A detailed description of the plasma apparatus is given elsewhere.[25]

The reactor was evacuated to a pressure of 0.01 mbar. Subsequently, a CO_2 or CF_4 gas flow of 10 cm^3/min (STP) was established through the reactor for 15 min (pre-delay). The membranes were then exposed to the plasma (0.04-0.08 mbar, 47-49 W) for various treatment times ranging from 15 s to 120 min while maintaining a constant gas flow (10 cm^3/min) through the reactor. Subsequently, the gas flow was maintained for another 2 min (post-delay). Finally, the reactor was brought to atmospheric pressure with air and the membranes were removed. Pulsed plasma treatments (900 plasma pulses of 1 s separated by dark periods of 10 s) were carried out at the same conditions as mentioned above.

After plasma treatment the membranes were rinsed with water. For CTA membranes rinsing was necessary to remove residual glycerin which was originally present to prevent the pores from collapsing. To maintain the membranes' porous structure, the rinsed membranes were finally stored in water at 4 °C prior to further characterization.

SEM analysis

The surface structure of the toplayer of the membranes was studied by Scanning Electron Microscopy (SEM). Prior to SEM analysis the CTA membranes were saturated with a 10% glycerin solution in water for ± 48 h to maintain the porous structure after drying. All membranes were dried in air and subsequently sputtered with a 20 Å thick gold-palladium layer (Polaron SEM Sputtering System, VG Microtek, East-Grinstead, UK). The coated samples were analysed with an S-800 Field Emission SEM (Hitachi, Tokyo, Japan; 6-8 kV, 20° tilt, 20,000x magnification). Additionally, SEM pictures of cross sections of an untreated CTA membrane were made (6 kV, 800x and 15,000x magnification).

XPS analysis

The chemical surface composition of the toplayer of plasma treated, dried CTA membranes was investigated by X-ray Photoelectron Spectroscopy (XPS). The measurements were performed with an XSAM-800 apparatus (Kratos, Manchester, UK) using a Mg K_α source (15kV, 10 mA). A spot size of 3 mm (ϕ) was analysed. The pressure during the measurements was $1x10^{-7}$ - $1x10^{-8}$ mbar. Survey scans (0-1100 eV) were recorded for all samples to qualitatively determine the elements present at the surface. Detail scans (20-30 eV windows) were recorded to quantify the elemental surface composition. The measured peak areas were converted into atomic percentages by using sensitivity factors known from literature.[26]

Contact angle measurements

Plasma treated and rinsed CTA membranes were dried in air and subsequently characterized by static water contact angle measurements using the sessile drop method. The measurements were performed with a Contact Angle Measuring System G10/G40 (KRÜSS, Hamburg, Germany). Contact angles were measured by placing a water droplet (1-2 µl) onto the membrane with an electronically regulated syringe. For each membrane, contact angles were determined at five different spots (n=5) using fresh water for each new droplet.

Waterflux measurements

Waterflux measurements were carried out on plasma treated CTA and CAB membranes using the following setup. The rinsed membranes were placed in a 'dead end' flow cell (∅ = 25 mm) and fixed on a glass filter support (P3) by a silicone rubber ring. In this way, a total flux area of 3.14 cm^2 (∅ = 20 mm) was created. The flow cell was then filled with water and a pressure of 3 bar was applied to the flow system. The waterflux was determined gravimetrically over a period of 90 min. For a series of CO_2 plasma treated CTA membranes measurements were carried out in threefold, using a new membrane for each measurement. Single measurements were performed on all other membranes.

MWCO measurements

For MWCO measurements the same flow setup was used as for waterflux measurements. After mounting the membrane, the flow cell was filled with a freshly prepared dextran solution (0.3% dextran + 0.03% ethylene glycol in water) and a pressure of 3 bar was applied to the system. The feed solution was stirred at 500 rpm and the permeate was collected in a test tube. After filtration of at least 2 ml permeate a 1 ml sample was collected for further analysis.

The collected sample (± 1 ml) was injected into a GPC apparatus (Polymer Standards Service GmbH, Mainz, Germany) consisting of two successive PSS Suprema columns (type 1000 and type 30). The eluent, a 0.05M $NaNO_3$ solution containing 0.005% NaN_3, was pumped through the columns with a rate of 1 ml/min. Chromatograms were successively recorded of the permeate and the feed solution. Using the PSS WINGPC software a sieve curve was calculated according to the standard procedure provided by the manufacturer. This sieve curve shows the concentration of permeate relative to the feed solution curve as a function of molecular weight. The molecular weight at which the sieve curve reaches a value of 10% (i.e. 90% retention) is defined as the membrane's cutoff (MWCO).

Fouling measurements

Untreated and 15 s CO_2 plasma treated CTA membranes were screened on their fouling behaviour by using the following setup. Prior to fouling, the waterflux of the membranes was determined as described before ($J_{w,pre}$; unstirred, P = 3 bar, t = 45 min). Subsequently, water was replaced by PBS and the membranes were pre-conditioned for 30 min (stirred at 500 rpm, P = 3 bar). The resulting PBS flux was taken as initial value (J_0). PBS was then replaced by ± 35 ml BSA solution (5 g/l in PBS) and the weight increase (Δm) of the permeate output was measured until it reached a total value of 4 g. At this point, stirring (500 rpm) was stopped and filtration was continued until a final output of 6 g was reached. After the filtration, samples were taken of the feed, permeate and retentate for UV/VIS analysis. The fouled membranes were removed from the flow cell and stored in water overnight at 4 °C. The next day, the waterflux of the membranes was determined one more time ($J_{w,post}$; unstirred, P =3 bar, 45 min).

UV/VIS spectroscopy

UV/VIS spectroscopy was used to determine the BSA concentration in the feed, permeate and retentate of the fouling measurements. The measurements were performed with a Cary 300 Bio UV-Visible Spectrophotometer (Varian, Victoria, Australia). The feed and retentate samples were diluted (1:2) with PBS and the BSA absorbance was measured directly at 285 nm using PBS as blanc solution. A calibration curve of BSA in PBS was made to convert the BSA absorbance into a BSA concentration. The permeate samples were diluted (1:1) with PBS and subsequently Micro BCA reagent was added (1:1). The reagent mixture was incubated at 60 °C for 1 h and cooled down to RT. Absorbance was then measured at 563 nm using a Micro BCA/PBS mixture (1:1) as blanc solution. A calibration curve of Micro BCA reacted BSA in PBS was made to convert the absorbance into a BSA concentration.

6.3 Results and Discussion

6.3.1 Surface analysis of the membranes' toplayer

SEM analysis was used to study the surface structure of the toplayer of (un)treated CTA and CAB membranes. SEM pictures of untreated CTA membrane cross sections are shown in Figure 6.1. The toplayer pictures of plasma treated CTA membranes are shown in Figure 6.2 and Figure 6.3.

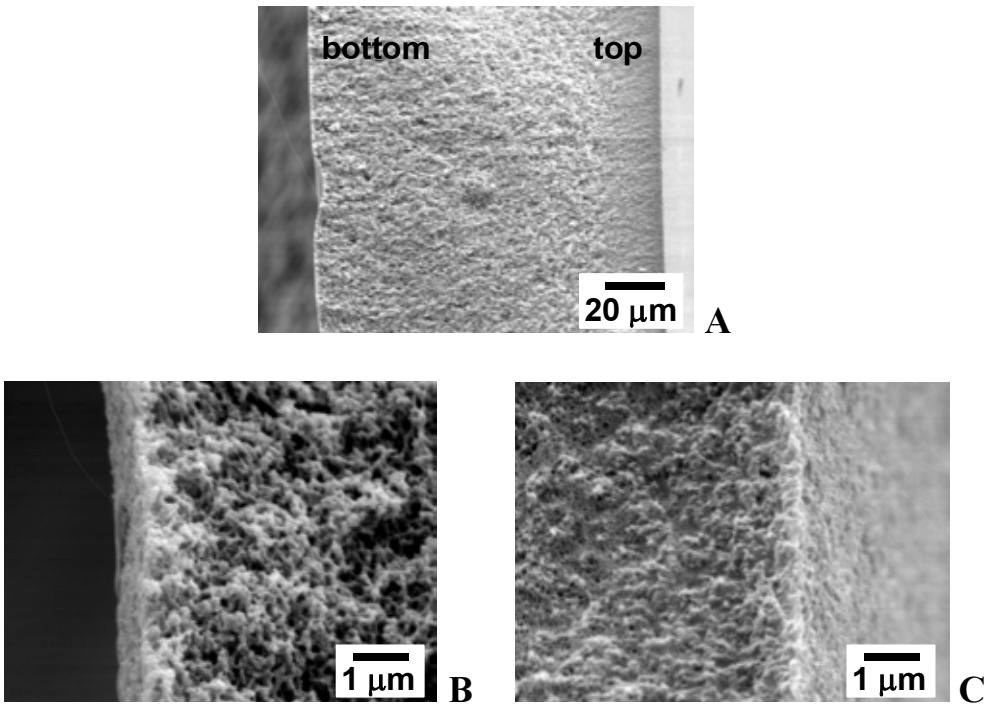

Figure 6.1: *SEM pictures of cross sections of an untreated CTA membrane. Overview (A), bottom side (B), top side (C).*

The untreated, asymmetric CTA membranes have quite a dense cross sectional structure. The nanoporous top side of the membrane (Figure 6.1C) gradually changes into a microporous structure (Figure 6.1B). Pores could not be observed in the toplayer (Figure 6.2A), which is normal for this kind of asymmetric UF membranes. Furthermore, the toplayer of untreated CTA membranes is quite rough, which is caused by the presence of Aerosil® fumed silica in the membrane.[22] After 15 s of CO_2 plasma treatment no surface structural changes could yet be observed. During longer plasma treatments (> 1 min) the surface roughness of the toplayer increased as a result of etching. The silica particles were further exposed at the surface (white spots in Figure 6.2C and D) and some pores started to appear. Substantial surface structural changes took place between 5 and 15 min of treatment time, due to gradual etching of the toplayer, until the toplayer was completely removed (≥ 15 min) and the microporous sublayer of the CTA membranes became visible. No significant differences of surface structure could be found between pulse treated (900x1 s) and continuously treated (15 min) CTA membranes. This indicates that, the actual plasma time of both treatments being the same (900 s), the total etch effect on the surface structure is also similar, despite the fact that the conditions for pulsed treatment were much milder.[24]

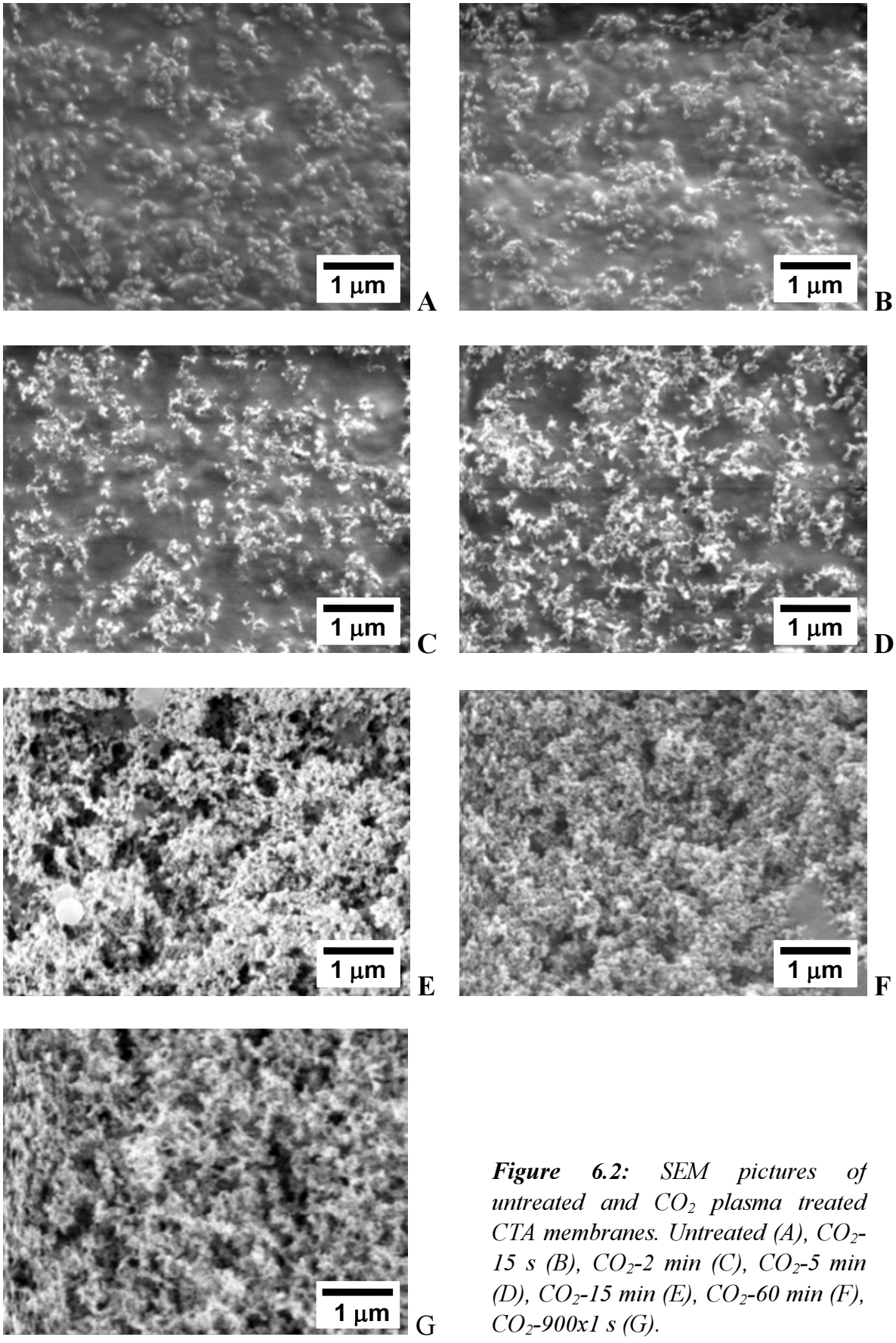

Figure 6.2: *SEM pictures of untreated and CO_2 plasma treated CTA membranes. Untreated (A), CO_2-15 s (B), CO_2-2 min (C), CO_2-5 min (D), CO_2-15 min (E), CO_2-60 min (F), CO_2-900x1 s (G).*

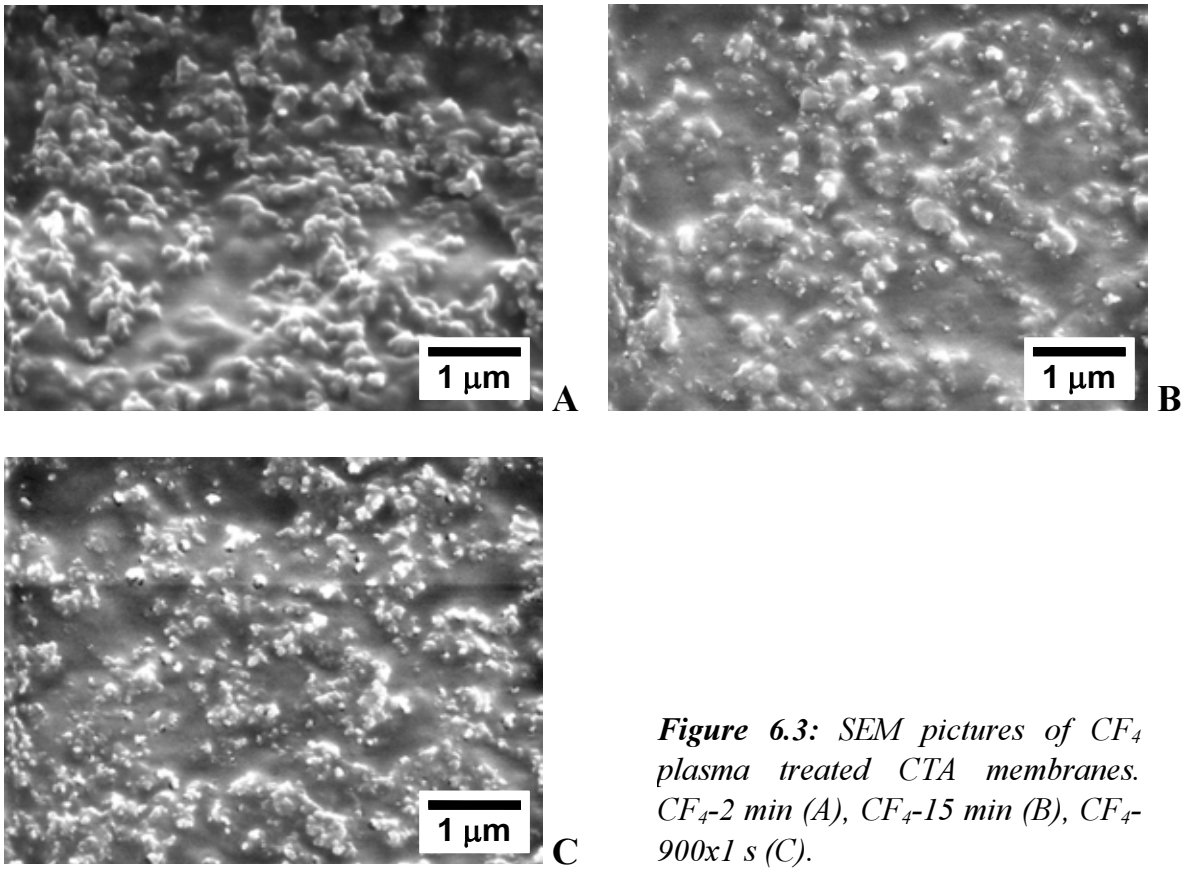

Figure 6.3: *SEM pictures of CF_4 plasma treated CTA membranes. CF_4-2 min (A), CF_4-15 min (B), CF_4-900x1 s (C).*

Figure 6.3 shows that CF_4 plasma treatment had a completely different effect on the surface structure of the membrane's toplayer. Even after 15 min of plasma treatment the toplayer seemed to be quite intact, although some pores were clearly introduced by etching. Again, no substantial differences of surface structure could be found between pulse treated and continuously treated CTA membranes (Figure 6.3B and C).

Figure 6.4 shows that the changes of surface structure of CAB membranes during CO_2 plasma treatment were quite different from that of CTA membranes. The untreated dense toplayer is very smooth. After 15 min of CO_2 plasma treatment small pores (50-100 nm) are visible which were created by the oxidative etching process. This nanoporous structure gradually developed in the course of treatment time (Figure 6.4D) until parts of the toplayer were ablated and the microporous sublayer became visible (Figure 6.4E,F). Prolonged plasma etching (> 60 min) completely removed the toplayer of the CAB membrane and thereby all its characteristic properties were lost. Clearly, the most interesting phase for surface structural modification of CAB membranes is found at longer treatment times (15-30 min) as compared to CO_2 plasma treatment of CTA membranes. Moreover, by accurately increasing the treatment time the structure of the toplayer could be nicely tailored from non-porous to nanoporous, up to complete removal of the skin (microporous).

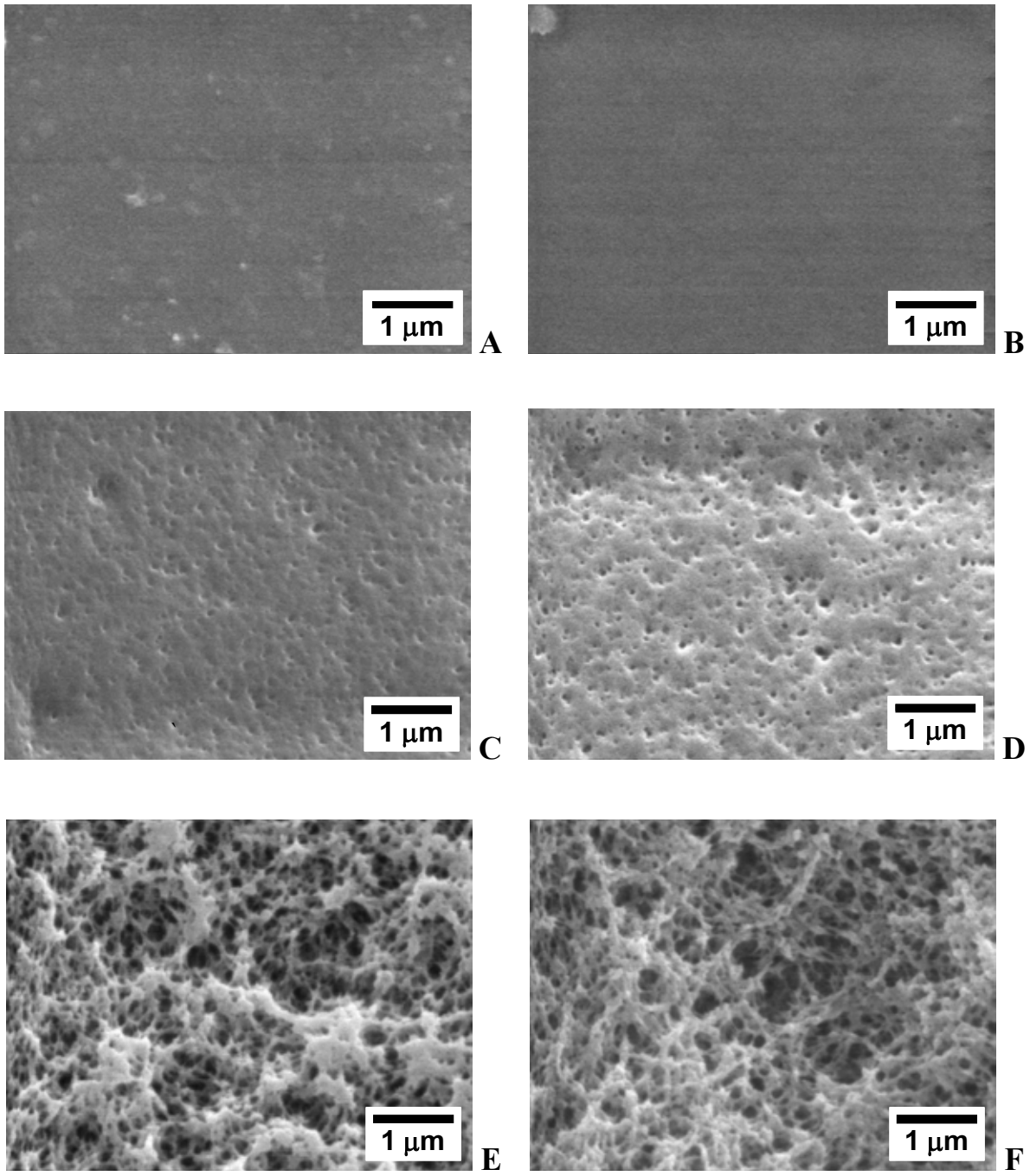

Figure 6.4: *SEM pictures of untreated and CO_2 plasma treated CAB membranes. Untreated (A), CO_2-5 min (B), CO_2-15 min (C), CO_2-30 min (D), CO_2-45 min (E), CO_2-60 min (F).*

The surface chemical composition of plasma treated CTA membranes was studied by XPS. The resulting data are shown in Table 6.1. The experimentally determined O/C ratio of untreated CTA is 0.6 which agrees reasonably well with the theoretical value of 0.7. At first sight, it seems that the CTA toplayer was strongly oxidized during CO_2 plasma treatment since the O/C ratio increased up to values of 2 (900x1 s). However, the increased O/C ratio must have been caused to a large extent by the exposure of silica particles (Aerosil®; SiO_2) to the

surface, since the amount of silicium increased substantially with increasing treatment time. The chemical surface composition of continuously treated (15 min) and pulse treated (900x1 s) CTA is quite similar, although somewhat more silica was exposed at the latter surface.

Table 6.1: XPS data of untreated and plasma treated CTA membranes (n=1).

Sample	C (at.%)	O (at.%)	F (at.%)	Si (at.%)
CTA; untreated	62.4	35.8	-	1.8
CTA; CO_2-15 s	60.3	37.6	-	2.1
CTA; CO_2-2 min	59.4	37.1	-	3.5
CTA; CO_2-5 min	50.5	41.7	-	7.8
CTA; CO_2-15 min	31.9	47.6	-	20.5
CTA; CO_2-900x1 s	25.6	51.3	-	23.1
CTA; CF_4-2 min	51.5	16.1	32.4	-
CTA; CF_4-15 min	53.0	19.8	27.2	-
CTA; CF_4-900x1 s	52.0	25.3	20.3	2.4

The silica particles have a theoretical O/Si ratio of 2, suggesting that 20% of silicium at the surface should be accompanied by 40% of oxygen. This calculation makes clear that a major part of surface oxygen can be attributed to silica after prolonged etching (15 min). Subtracting this contribution from the total amount of surface oxygen results in an 'organic' O/C ratio for etched CTA which is likely to be less than the original value of 0.6. From a chemical point of view this could be explained by cleavage of the acetate side functionalities from the cellulose ring during plasma etching, which reduces the overall O/C ratio.

A decrease of O/C ratio was also found for CF_4 plasma treated CTA membranes, but in this case it is not coupled with a surface oxygen increase due to exposure of silica. In fact, during continuous CF_4 plasma treatment silica was not exposed at the membrane's surface at all. Instead, a substantial amount of fluorine was incorporated in the membrane's toplayer. A maximum F/C ratio of 0.6 was already reached after 2 min of plasma treatment. Prolonged CF_4 plasma treatment suppressed the F/C ratio, possibly due to an equilibrium between etching and fluorination. At the surface of CF_4 pulse treated CTA the amount of fluorine was lower than for continuously treated membranes. Results from a previous paper on CF_4 plasma treatment of low density poly(ethylene) (LDPE) films confirm that pulsed treatment causes somewhat less fluorination.[24] Also, some silicium was exposed at the surface of the pulse

treated CTA membrane, which is similar to the values found for untreated or short CO_2 plasma treated membranes (< 2 min).

From literature it is known that fluorine radicals present in a CF_4 plasma can react with Si_xO_y yielding volatile Si_xF_y fragments and atomic oxygen.[27] Although this could induce some silica ablation at the surface during CF_4 plasma etching, it does not fully explain the complete lack of silicium at the surface of continuously treated CTA membranes. Another reason can be found when comparing the surface structure of CF_4 pulse treated CTA (Figure 6.3C) with that of 2 min CO_2 plasma treated CTA (Figure 6.2C). Although the treatments were very different the resulting surface structures are almost identical. The exposure of silica is roughly the same (3.5% vs. 2.4%) for both membranes. Clearly, the ablation of the membrane's toplayer is much slower in a CF_4 plasma making it a milder etchant than a CO_2 plasma.[8,28] Perhaps the most plausible reason for the lack of silicium at the treated membrane's surface is found in surface restructuring during CF_4 plasma treatment. The surface nanopores could fuse together due to a local temperature rise caused by etching and fluorination (exothermic).[24] Thus, the silica particles remain covered by a thin, restructured and fluorinated polymer layer.

Table 6.2: Static water contact angles of untreated and plasma treated CTA membranes (n=5, ±sd).

Sample	θ (°)
CTA; untreated	66 ± 2
CTA; CO_2-15 s	63 ± 2
CTA; CO_2-2 min	64 ± 1
CTA; CO_2-5 min	56 ± 2
CTA; CO_2-15 min	n.a.
CTA; CO_2-900x1 s	n.a.
CTA; CF_4-2 min	102 ± 1
CTA; CF_4-15 min	96 ± 2
CTA; CF_4-900x1 s	104 ± 2

n.a.=droplet was absorbed by the membrane

Water contact angles were measured on plasma treated CTA membranes and the results are shown in Table 6.2. It should be noted beforehand that some care must be taken when interpreting these data, due to the porous structure of the plasma treated membranes. Clearly, the differences in surface chemical composition and structure between CO_2 and CF_4 plasma

treated CTA membranes had a major impact on their wettability. A gradual increase of wettability was found when increasing the CO_2 plasma treatment time. Based on a previous study on CO_2 plasma treatment of LDPE films, a more pronounced increase of wettability was expected.[2] Besides a possible hydrophobizing effect of air (θ = 180°) which is trapped in the surface nanopores during measurement[24,29], the limited increase of wettability may also be explained by the counteracting contribution of the hydrophobically rendered silica particles[22] that are exposed at the surface upon CO_2 plasma etching. Once the toplayer was completely ablated (see also Figure 6.2E and G), contact angles were impossible to measure since the water droplets were quickly absorbed by the microporous surface.

An inverse effect on wettability was found for CF_4 plasma treated membranes. The original, moderately hydrophilic CTA membrane was quickly hydrophobized by fluorination of the toplayer. Longer treatment times did not further decrease wettability which is in agreement with the data presented in Table 6.1. Surprisingly, the contact angle of a pulse treated CTA membrane is somewhat higher than the value found for continuously treated material. This seems to contradict the lower amount of fluorination after pulsed treatment (Table 6.1), assuming that fluorinated groups are responsible for the membrane's hydrophobicity. Possibly, the minor differences of surface structure observed in Figure 6.3B and C could be responsible for the varying hydrophobicity.[24]

It is obvious from the results discussed so far that plasma treatment of CTA and CAB membranes substantially changes their surface characteristics. The extent of surface structural and chemical changes can be tailored by varying the plasma treatment conditions like the type of gas and the treatment time. These changes of surface properties will undoubtedly have a major impact on the membrane's properties like permeation (flux), retention (MWCO) and susceptibility to fouling. These properties will be discussed in the next section.

6.3.2 Characterization of the membranes' properties

The permeation of plasma treated CTA and CAB membranes was studied by waterflux measurements. The results are presented in Table 6.3 and Figure 6.5. CO_2 plasma treatment strongly influenced the permeation of both types of membranes. A longer treatment time clearly resulted in a higher flux although the effects on CTA and CAB membranes are quite different. In the case of CTA membranes a tenfold increase of flux was observed within the first two minutes of plasma treatment. Prolonged plasma treatment (> 2 min) induced a further fourfold flux increase up to an equilibrium value of 0.8 g/cm^2.min. Unfortunately, the errors are quite large due to critical plasma conditions, but it should be noted that the same trend was found for every single series of treated membranes. A rather large difference was found

between the permeation of continuously and pulse treated CTA membranes. Based on the resemblance of surface chemical and structural characteristics discussed in the previous section, similar permeation behaviour was expected.

Table 6.3: Waterflux of plasma treated CTA membranes (n=1).

Sample	J_w (g/cm^2.min)
CTA; untreated	0.02 *
CTA; CO_2-15 s	0.08 *
CTA; CO_2-2 min	0.21 *
CTA; CO_2-5 min	0.48 *
CTA; CO_2-15 min	0.71 *
CTA; CO_2-900x1 s	0.42
CTA; CF_4-2 min	0.01
CTA; CF_4-15 min	0.03
CTA; CF_4-900x1 s	0.05

* see also Figure 6.5 (n=3)

CAB membranes needed longer plasma treatments (15 min) to obtain a measureable waterflux. When realising that these membranes are normally applied at much higher pressures (20-40 bar) for desalination, it was not surprising to measure zero waterflux at 3 bar. However, once a substantial waterflux was established it increased rapidly with treatment time.

CF_4 plasma treatment had much less impact on the permeation of CTA membranes. Prolonged treatment was necessary to obtain a relatively small flux increase (Table 6.3). In contrast to CO_2 pulsed plasma treatment, CF_4 pulsed treatment resulted in a higher flux than continuous treatment (15 min). During pulsed treatment the surface temperature increase inducing surface restructuring (i.e. fusing of the pores; see previous section) is expected to be lower than during continuous treatment[24], which could explain the measured flux difference.

In general, the permeation data of CTA and CAB membranes match well with the observed surface structural changes shown in Figure 6.2 to Figure 6.4. For CTA membranes, permeation can be tailored up to 15 min of CO_2 plasma treatment by gradual etching of the toplayer. CAB membranes show a controllable region up to 30 min of treatment time (nanoporous toplayer), after which the waterflux rapidly increased due to complete ablation of the toplayer (microporous sublayer).

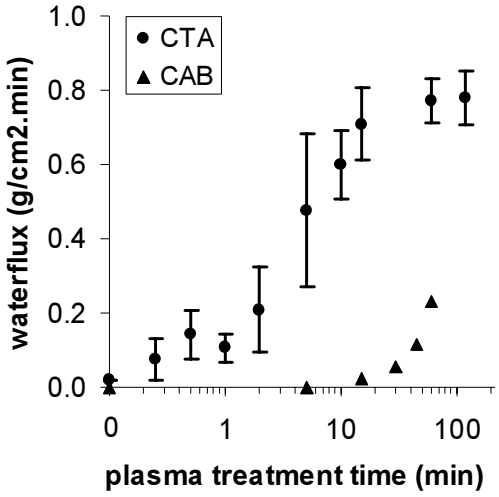

Figure 6.5: *Waterflux of CO_2 plasma treated CTA and CAB membranes as a function of plasma treatment time (CTA: n=3, ±sd; CAB: n=1).*

In addition to permeation experiments it is interesting to study the retention behaviour of the plasma treated membranes. For practical reasons (i.e. extremely low flux at UF conditions) CAB membranes were not included in these experiments. Table 6.4 and Figure 6.6 show MWCO data of a series of CO_2 and CF_4 plasma treated CTA membranes. In order to test the reproducibility of the presented data (n=1), four equally treated CTA membranes (CO_2-2 min) were independently studied on their retention behaviour. A standard deviation of 10% was found, which is a good indication of the fluctuation of the membrane's properties after plasma treatment (see also Figure 6.5).

Table 6.4: MWCO data of untreated and plasma treated CTA membranes (n=1).

Sample	MWCO (kD)
CTA; untreated	10 *
CTA; CO_2-15 s	20 *
CTA; CO_2-2 min	166 *
CTA; CO_2-5 min	350 *
CTA; CO_2-15 min	x **
CTA; CO_2-900x1 s	x **
CTA; CF_4-2 min	27
CTA; CF_4-15 min	230
CTA; CF_4-900x1 s	260

* see also Figure 6.6
** no retention of feed

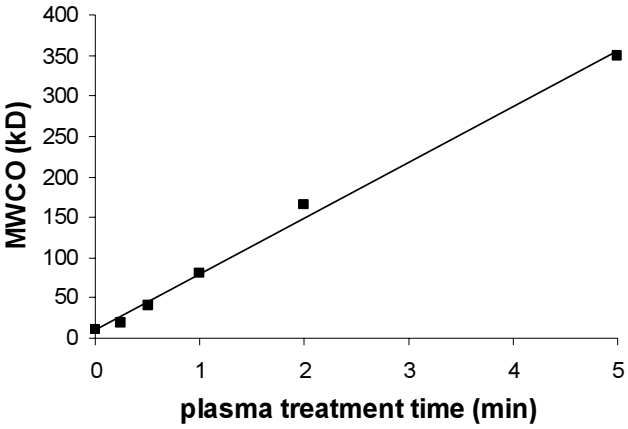

Figure 6.6: *MWCO of CO_2 plasma treated CTA membranes as a function of plasma treatment time (n=1).*

Using a dextran solution (71.4 kD) with a polydispersity of 4.5-5.0, untreated CTA membranes have a measured MWCO which is twice the value given by the manufacturer (5 kD). It is generally known that MWCO values strongly depend on the type of measurement and the conditions used. Therefore, absolute values should be interpreted with some caution and more attention should be paid to the relative retention differences between the plasma treated membranes. Obviously, CO_2 as well as CF_4 plasma treatment caused an increase of the membrane's MWCO. The membrane's selectivity for the used dextran was completely lost after 15 min of CO_2 plasma treatment (continuous and pulsed), whereas CF_4 plasma treatment was less destructive. Within the first 5 min of CO_2 plasma treatment an almost linear increase of MWCO with treatment time was observed (Figure 6.6). Thus, selectivity of plasma treated CTA membranes can be nicely tailored up to 350 kD by accurately increasing treatment time. This agrees well with the observed surface structural changes (Figure 6.2A-D) showing preservation of the 'selective' toplayer up to 5 min of plasma treatment.

The slightly higher MWCO of the CF_4 pulse treated membrane compared to continuous treatment is in accordance with the flux difference of these membranes (Table 6.3). This supports the fact that a surface temperature rise during plasma etching may have influenced the nanoporosity of the membranes as discussed earlier (restructuring). A lack of temperature rise during pulsed treatment could have prevented the nanopores from fusing together, resulting in a higher membrane permeation (Table 6.3) and lower selectivity (Table 6.4) than measured for continuously treated membranes.

Finally, (un)treated CTA membranes were screened on their fouling behaviour. Untreated CTA membranes are characterized by their moderate hydrophilicity and very low non-specific

protein binding. Therefore, they are very suitable for UF applications like protein removal. In the previous section it was shown that the membrane's properties can be tailored by chemical and structural modification of the toplayer during plasma etching. The aim of this screening experiment is to study the effect of CO_2 plasma treatment on the fouling properties of CTA membranes. An untreated and a CO_2 plasma treated (15 s) membrane were selected. Despite differences of permeability (Table 6.3), the MWCO values (Table 6.4) indicate that the fouling agent (BSA; M_w = 67 kD) will be largely retained at the membrane's surface in both cases, which makes the fouling conditions comparable. Moreover, the total volume input and output was kept the same for both fouling measurements. The results of these fouling experiments are presented in Figure 6.7. Graph A shows the permeate output (m) of the two membranes as a function of time. From these data the normalized flux (J/J_0) of the membranes could be calculated, which was plotted against the permeate output in graph B.

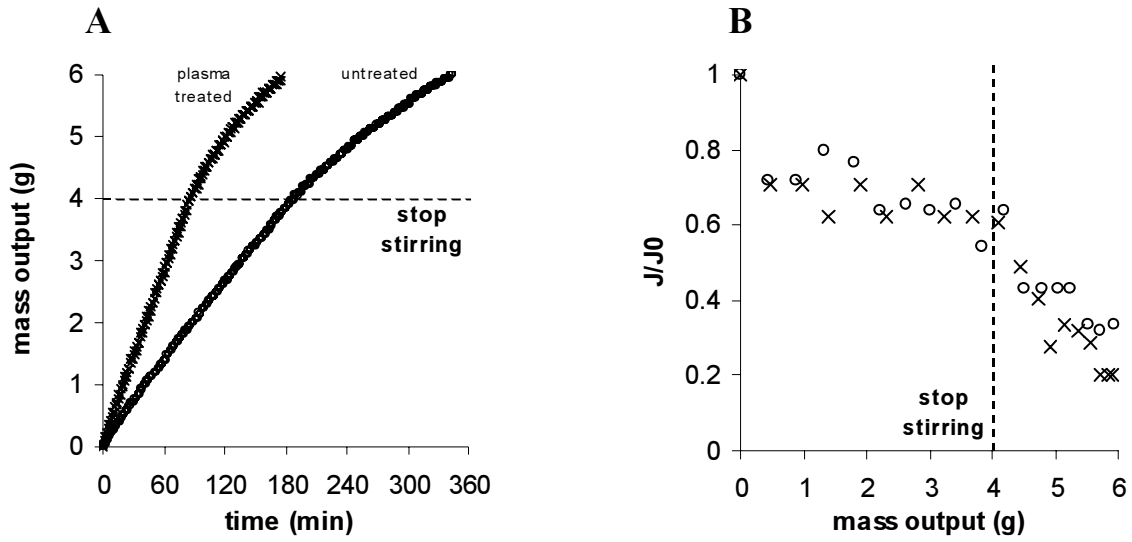

Figure 6.7: *Fouling curves (mass output vs. time (A) and normalized flux vs. mass output (B)) of untreated (o) and 15 s CO_2 plasma treated (×) CTA membranes. J_0 = PBS pre-conditioning flux.*

The fouling curves can be divided in two parts, stirred and unstirred fouling. For both membranes the normalized flux decreased during fouling, but there was a slightly different effect of stirring. The gradual, normalized flux decline of the untreated membrane hardly seemed to change after stirring was stopped. In fact, the overall flux decline is quite linear and ends at a value of 30% of the initial PBS flux (J_0). The normalized flux of the CO_2 plasma treated membrane largely resembled that of the untreated membrane, although a clear flux

drop was observed after stirring was stopped. During stirring the permeate flux was almost constant at 60-70% of J_0, but it decreased to a final value of 20% during unstirred fouling.
In order to quantify the fouling conditions for the membranes, the BSA concentrations in the feed, retentate and permeate were determined by UV/VIS spectroscopy (results not shown). The BSA concentration in the feed was equal for both experiments (4.7 mg/ml), as was the BSA concentration in the retentate (5.3-5.4 mg/ml). Since BSA was retained at the membrane's surface, its concentration in the retentate was slightly higher than in the feed. Indeed, the BSA concentrations in the permeate were negligible in both cases (4-9 μg/ml), confirming that the membranes' MWCO values were much lower than the molecular weight of BSA.

Table 6.5: Waterflux ratio of untreated and CO_2 plasma treated CTA membranes as a result of BSA fouling (n=1).

Sample	$J_{w,post}$ / $J_{w,pre}$
CTA; untreated	0.61
CTA; CO_2-15 s	0.65

After the fouling experiment the waterflux was measured again to determine the final impact of the fouling process on the permeability of the membranes. Table 6.5 shows the waterflux ratio of both membranes as a result of fouling ($J_{w,post}/J_{w,pre}$). The recovery of the untreated and CO_2 plasma treated membrane was comparable (61-65%). Together with the fouling curves in Figure 6.7 these data show that the low fouling properties of CTA membranes were largely maintained after CO_2 plasma treatment.

6.4 Conclusions

This study has shown that gas plasma etching can be used to tailor the surface characteristics and properties of asymmetric CTA and CAB membranes. CO_2 plasma treatment resulted in gradual etching of the dense toplayer, thereby modifying the surface porosity. In this way, the membrane properties (permeation, selectivity) could be tailored up to 15 min of CO_2 plasma treatment for CTA membranes and up to 30 min of treatment for CAB membranes. Furthermore, CTA membranes were hydrophilized during CO_2 plasma treatment, whereas CF_4

plasma treatment resulted in hydrophobic CTA membranes due to strong fluorination of the toplayer.

Screening experiments with high concentrations of BSA (5 g/l) have shown that the low fouling properties of CTA UF membranes were largely maintained after CO_2 gas plasma modification. Thus, by accurately choosing the plasma treatment conditions these membranes could be of great use for several biological applications (e.g. deproteinization, sterilization, cell harvesting, and biomolecule concentration).

6.5 Acknowledgements

Albert v/d Berg and Mark Smithers (MESA+ Institute, University of Twente) are acknowledged for performing the XPS and SEM measurements, respectively. Erik Rolevink (Membrane Technology Group, University of Twente) is acknowledged for performing the GPC measurements. This study was financed by the Netherlands Foundation for Chemical Research (NWO-CW).

6.6 References

1) Terlingen, J. G. A. *Introduction of functional groups at polymer surfaces by glow discharge techniques*; University of Twente: Enschede, The Netherlands, 1993.
2) Takens, G. A. J. *Functionalization of polymeric surfaces by oxidative gas plasma treatment*; University of Twente: Enschede, The Netherlands, 1997.
3) Dewez, J. L.; Humbeek, E.; Everaert, E.; Doren, A.; Rouxhet, P. G. *Plasma treated polymer films: Relationship between surface composition and surface hydrophilicity*; Pireaux, J. J., Bertrand, P. and Brédas, J. L., Ed.; IOP Publishing Ltd: Bristol, 1992, pp 463-474.
4) Gancarz, I.; Pozniak, G.; Bryjak, M. *Eur. Polym. J.* **2000**, *36*, 1563-1569.
5) Gatin, E.; Alexandreanu, D.; Berlic, C.; Popescu, A.; Barna, E.; Moja, D. *Physica Medica* **2000**, *16*, 3-6.
6) Belfort, G. *Abstr. Papers ACS* **1995**, *209*, 311-POLY.
7) Ulbricht, M.; Belfort, G. *J. Membr. Sci.* **1996**, *111*, 193-215.
8) Hopkins, J.; Badyal, J. P. S. *Langmuir* **1996**, *12*, 3666-3670.
9) Bryjak, M.; Gancarz, I.; Krajciewicz, A.; Piglowski, J. *Angew. Makromol. Chem.* **1996**, *234*, 21-29.
10) Wolff, J.; Steinhauser, H.; Ellinghorst, G. *J. Membr. Sci.* **1988**, *36*, 207-214.
11) Gancarz, I.; Pozniak, G.; Bryjak, M. *Eur. Polym. J.* **1999**, *35*, 1419-1428.
12) Ulbricht, M.; Belfort, G. *J. Appl. Polym. Sci.* **1995**, *56*, 325-343.
13) Bryjak, M.; Gancarz, I. *Angew. Makromol. Chem.* **1994**, *219*, 117-124.
14) Bhat, N. V.; Wavhal, D. S. *J. Appl. Polym. Sci.* **2000**, *76*, 258-265.
15) Johansson, J.; Yasuda, H. K.; Bajpai, R. K. *Appl. Biochem. Biotechnol.* **1998**, *70-2*, 747-763.
16) Altena, F. W.; Henis, J. M. S.; Brooks, A. A.; Tripodi, M. K.; ISPC-7: Eindhoven, 1985, paper P-13-5.

17) Hof, J. A. v. t. *Wet Spinning of Asymmetric Hollow Fibre Membranes for Gas Separation*; University of Twente: Enschede, The Netherlands, 1988.
18) Dmitriev, S. N.; Kravets, L. I.; Sleptsov, V. V. *Nucl. Instr. Meth. Phys. Res. B- Beam Interact. Mater. Atoms* **1998**, *142*, 43-49.
19) Altena, F. W. *Phase Separation Phenomena in Cellulose Acetate Solutions in relation to Asymmetric Membrane Formation*; University of Twente: Enschede, The Netherlands, 1982.
20) Vasarhelyi, K.; Ronner, J. A.; Mulder, M. H. V.; Smolders, C. A. *Desalination* **1987**, *61*, 211-235.
21) Bogan, R. T.; Brewer, R. J. *Cellulose Esters, Organic*; Mark, H. F., Bikales, N. M., Overberger, C. G. and Menges, G., Ed.; John Wiley & Sons: New York, 1985; Vol. 3, pp 158-181.
22) Franken, W.; Nussbaumer, D.; Perl, H.; Weickhardt, L. *Asymmetrical ultrafiltration membrane on the basis of cellulose triacetate*; Eur. Patent nr. EP0004943; Sartorius GmbH, Goettingen, Germany, 1981.
23) Sivakumar, M.; Mohanasundaram, A. K.; Mohan, D.; Balu, K.; Rangarajan, R. *J. Appl. Polym. Sci.* **1998**, *67*, 1939-1946.
24) Olde Riekerink, M. B.; Terlingen, J. G. A.; Engbers, G. H. M.; Feijen, J. *Langmuir* **1999**, *15*, 4847-4856.
25) Terlingen, J. G. A.; Hoffman, A. S.; Feijen, J. *J. Appl. Polym. Sci.* **1993**, *50*, 1529-1539.
26) Briggs, D.; Seah, M. P. *Practical Surface Analysis: by Auger and X-ray Photo-electron Spectroscopy*; Wiley: Chichester, 1983.
27) Breitbarth, F. W.; Berg, D.; Dumke, K.; Tiller, H. J. *Plasma Chem. Plasma Process.* **1997**, *17*, 39-57.
28) Meichsner, J.; Nitschke, M.; Rochotzki, R.; Zeuner, M. *Surf. Coat. Technol.* **1995**, *74-75*, 227-231.
29) Cassie, A. B. D.; Baxter, S. *Trans. Faraday Soc.* **1944**, *40*, 546-551.

Chapter 7

Gas plasma etching of adsorbed protein-gold colloids as a tool for surface nanostructuring: Surface preparation and chemical modification

M. B. Olde Riekerink, G. H. M. Engbers, J. Feijen

Department of Chemical Technology, Section of Polymer Chemistry and Biomaterials and Institute for Biomedical Technology, University of Twente, P.O. Box 217, 7500 AE Enschede, The Netherlands

Albumin-gold colloids (AGC; 10 nm) and protein A-gold colloids (PAGC; 20 nm) were adsorbed onto various substrates (e.g. glass, silicon, poly(styrene) (PS), low density poly(ethylene) (LDPE)) from phosphate buffered saline (PBS) solution. After rinsing with PBS and water the adsorbed substrates were treated with a radio frequency (RF) gas plasma (carbon dioxide (CO_2) or air, 48-50 W, 0.06-0.08 mbar) for 30 min. Some chemical modification experiments were carried out on plasma etched glass and gold control substrates by silanation and thiol chemistry with octadecyltrichlorosilane (ODS) and fluorinated amide thiol (FAT).

The adsorbed, etched and/or chemically modified substrates were characterized by Scanning Electron Microscopy (SEM), Atomic Force Microscopy (AFM) and X-ray Photoelectron Spectroscopy (XPS) to study the surface nanoparticle distribution, topography and chemistry, respectively. Additionally, sizing of the protein-gold colloids was performed by Transmission Electron Microscopy (TEM) and Photon Correlated Spectroscopy (PCS).

Adsorption of AGC and PAGC was succesful on most substrates, the surface nanoparticle density being highest for AGC adsorbed glass. On all substrates AGC was randomly distributed at the surface. After adsorption, the protein shell was selectively removed from the gold nanoparticles by oxidative gas plasma etching. Selective chemical modification of these heterogeneous surfaces is feasible as was shown by succesful, selective thiol adsorption onto silanized gold control surfaces. Still, higher gold nanoparticle densities and highly accurate surface analysis techniques are necessary to successfully analyse the heterogeneous, nanostructured surfaces.

7.1 Introduction

Tailoring of surface chemical and structural properties on a nanoscale level is an essential tool in the fast growing area of nanotechnology. One promising approach within this wide spectrum of possibilities is found in the generation of chemically heterogeneous and ordered surfaces by introduction of metal nanoparticles. These type of nanopatterned surfaces are of

great interest for areas like the semiconductor industry. Several studies have been focussed on the creation of metallic hybrid surfaces with ordered nanoscale patterns.[1-7] These nanopatterned surfaces can subsequently be used as lithographic masks[1,3,8,9] or in applications like data storage devices and sensors.[7] Spatz *et al.* developed patterned gold nanoparticle surfaces by starting with a micellar system.[1,2] The micelles consisted of poly(styrene)-*block*-poly(2-vinylpyridine) diblock copolymers and the gold nanocolloids were synthesized within the micellar core.[10,11] After coating a monolayer of micelles on a substrate using the Langmuir-Blodgett technique, the block copolymer was removed by oxygen plasma etching leaving the desired gold nanoparticle surface. However, a difficult step in this process is the reduction of the gold salt into particles within the micellar core. Furthermore, the coating conditions have to be chosen with great accuracy to obtain a monomicellar film over a large surface area. Morkved *et al.* studied self-assembly of gold islands on diblock copolymer films.[4] By evaporation of gold metal onto the films, nanoscale island arrays were created that replicated the ordering of the underlying polymer blocks. High vacuum gold evaporation and prolonged annealing of the polymer films are drawbacks of this technique.

This study reports on a novel, two-step approach to obtain nanostructured surfaces with well separated gold nanodomains that could be of great use for a wide range of applications in nanotechnology. Besides lithographical applications, these chemically heterogeneous surfaces can be selectively modified by different types of chemistry. For example, the gold particles could serve as nanotemplates for selective thiol chemistry. In this way, functional sites can be created for immobilization of active (bio)molecules or cells (e.g. nanosensors). Gold nanoparticle covered surfaces with alternate hydrophobic and hydrophilic nanodomains would be another interesting possibility (e.g. hydrophobized gold nanodomains adsorbed onto a hydrophilized substrate or vice versa).

For this two-step approach commercially available protein-gold nanocolloidal dispersions are used as a starting material. These kind of gold probes have a long history as cytochemical markers for electron and light microscopy.[12-24] The commercial preparation of the probes is an uncomplicated two-step procedure. First the colloidal gold sol is produced, in most cases by chemical reduction of chloroauric acid ($HAuCl_4$).[25] Then, virtually any protein can be adsorbed onto the surface of the gold particles.[12]

In the present study two different protein-gold colloidal dispersions, i.e. albumin-gold colloids (AGC; $\varnothing_{gold}$ = 10 nm) and protein A-gold colloids (PAGC; $\varnothing_{gold}$ = 20 nm), are used. First, the protein-gold colloids are adsorbed onto various substrates (e.g. glass, silicon, poly(styrene), low density poly(ethylene)) by a simple procedure in an aqeous environment at room temperature (RT). The protein serves in two ways, as an adsorbate and as a spacer between

the adsorbed gold nanoparticles. In this way, a heterogeneous surface with well-separated and randomly distributed gold nanoparticles is expected. Second, this surface is treated with an oxidative radio frequency (RF) gas plasma (carbon dioxide or air) to remove the protein from the gold nanoparticles. Besides selective protein removal, gas plasma etching also serves as a chemical modification technique for the substrate. This additional tool makes the heterogeneous surface directly suitable for selective chemistry.

The gold nanoparticle distribution and the surface topography of protein-gold adsorbed and plasma etched substrates are analysed by Scanning Electron Microscopy (SEM) and Atomic Force Microscopy (AFM). The chemical surface composition of these substrates is studied by X-ray Photoelectron Spectroscopy (XPS). Finally, the feasibility of using gold nanoparticle covered surfaces as nanotemplates for selective chemistry is studied by surface modification of two plasma etched model substrates (gold and glass) with silane and thiol chemistry.

7.2 Experimental

7.2.1 Materials

Albumin-10 nm Colloidal Gold Labeled (AGC; 1.8×10^{13} particles/ml; suspension 50% glycerol containing 0.15M NaCl, 0.01M Tris, 0.02% PEG 20,000, 0.02% sodium azide, pH 7.6) and Protein A-20 nm Colloidal Gold Labeled (PAGC; 3.9×10^{12} particles/ml; suspension 50% glycerol containing 0.15M NaCl, 0.01M sodium phosphate, 0.02% PEG 20,000, 0.02% sodium azide, pH 7.4) were purchased from Sigma Chemical Company, St. Louis, USA. Glass slides (∅ = 15 mm) were purchased from Knittel, Braunschweig, Germany. Glass slides (∅ = 25 mm) with a sputtered gold layer were obtained from the FFW division, Department of Physics and Electrical Engineering, University of Twente, Enschede, The Netherlands. Silicon wafers (4") were supplied by MESA+ Institute, University of Twente, Enschede, The Netherlands. Low density poly(ethylene) film (LDPE type 2300) was kindly supplied by DSM Polyethylenes, Geleen, The Netherlands. Poly(ethylene glycol) (PEG; M_w = 6,000 g/mol) was purchased from Merck, Darmstadt, Germany. Dichloromethane (purity ≥ 99.8%), n-hexane (purity ≥ 96%), acetone (purity ≥ 99.8%), toluene (purity ≥ 99.7%), isopropanol (purity ≥ 99.8%) and methanol (purity ≥ 99.8%) were purchased from Biosolve BV, Valkenswaard, The Netherlands. n-Heptane (purity ≥ 99%) was obtained from Merck-Schuchardt, Hohenbrunn, Germany. Carbon dioxide (CO_2) gas (purity ≥ 99.995%) and compressed air were purchased from Hoekloos, Amsterdam, The Netherlands. Poly(styrene) (PS; M_w = 280,000) and octadecyltrichlorosilane (ODS; purity ≥ 90%) were purchased from Sigma-Aldrich Chemie GmbH, Steinheim, Germany. Fluorinated amide thiol (FAT: HS-$(CH_2)_2$-NH-CO-$(CF_2)_7$-CF_3) was synthesized by Schönherr[26] and kindly supplied for this study. Phosphate buffered saline (PBS) was purchased from NPBI, Emmer-Compascuum, The Netherlands. For all experiments ultra-pure water obtained from a Milli-Q Plus System (Millipore) was used.

7.2.2 Methods

Preparation and cleaning of substrates

LDPE films were cleaned ultrasonically, successively in dichloromethane (10 min, three times), in acetone (10 min, three times), in water (10 min, three times), and again in acetone (10 min). After cleaning, the films were dried *in vacuo* at room temperature (RT) and stored at RT in the dark. Glass substrates were cleaned ultrasonically, successively in hexane (10 min, three times), in acetone (10 min, three times), in water (10 min, three times), and again in acetone (10 min). After cleaning, the substrates were dried and stored in an oven at 120°C. Silicon substrates (∅ = 15 mm) were cut from 4" wafers and subsequently cleaned ultrasonically, successively in isopropanol (10 min, two times), in methanol (10 min, two times), and in acetone (10 min, two times). The substrates were then dried *in vacuo* at RT and stored at RT in the dark. PS substrates were prepared by spincoating a 10% (w/v) PS solution in toluene on cleaned glass substrates at 2000 rpm for 2 min with a home-made device.

Adsorption of protein-gold colloids onto substrates

Cleaned substrates (e.g. glass, Si, PS, LDPE) were mounted in a 24-wells culture plate ($\varnothing_{well}$ = 16 mm) and incubated in 475 μl PBS solution containing 0.05% PEG 6,000 (recommended by the manufacturer as diluent buffer for the nanocolloidal suspension). Subsequently, 25 μl (P)AGC was added to the solution and incubation took place for 30 or 300 min. After adsorption, the substrates (excluding PS) were carefully rinsed by stepwise addition and removal of 2 ml PBS (three times) and 2 ml water (three times). Finally, the solution remnant (500 μl) was removed from the substrates and the samples were dried in air at RT.

Gas plasma treatment of protein-gold adsorbed substrates

The protein-gold adsorbed substrates were mounted in glass holders, which were placed in the center region of a gas plasma tubular reactor (length 80 cm, internal diameter 6.5 cm). Three externally placed capacitively coupled copper electrodes were attached to the reactor: a 'hot' electrode in the center and a 'cold' electrode at both sides of the 'hot' electrode at 10 cm distance. The glass holders were positioned between the 'hot' and 'cold' electrodes. The electrodes were connected to a RF (13.56 MHz) generator through a matching network. A detailed description of the plasma apparatus is given elsewhere.[27]

The reactor was evacuated to a pressure of 0.01 mbar. Subsequently, a CO_2 or air gas flow of 10 cm^3/min (STP) was established through the reactor for 15 min (pre-delay). The substrates were then exposed to the plasma (0.06-0.08 mbar, 48-50 W) for 30 min to selectively etch the adsorbed protein while maintaining a constant gas flow (10 cm^3/min) through the reactor. Subsequently, the gas flow was maintained for another 2 min (post-delay). Finally, the reactor was brought to atmospheric pressure with air and the substrates were removed.

Sizing of protein-gold colloids

The size of the protein-gold colloids was determined in two different ways. The actual size of the bare gold particles was measured by Transmission Electron Microscopy (TEM). TEM samples were prepared by putting a drop of (P)AGC suspension onto a carbon coated copper grid which was in direct contact with a soaking tissue to remove excessive suspension immediately. The (P)AGC adsorbed grids were subsequently analysed with a CM30 Twin Scanning TEM (Philips, Eindhoven, The Netherlands; 300 kV, 260,000x magnification). The diameter of ten different gold nanoparticles was measured on the obtained TEM picture.

Secondly, Photon Correlated Spectroscopy (PCS) was used to determine the hydrodynamic diameter of the protein-gold colloidal complexes. (P)AGC suspension was analysed with a Zetasizer 4000 (Malvern

Instruments, Malvern, UK) at 20°C and an angle of 90°. The hydrodynamic diameter was determined five times for each suspension using the monomodal analysis mode.

SEM analysis

The surface structure of the protein-gold adsorbed substrates was studied by Scanning Electron Microscopy (SEM). Prior to SEM analysis a thin carbon layer (± 5 nm) was coated on the substrates by evaporation using carbon rods. The coated samples were analysed with an S-800 Field Emission SEM (Hitachi, Tokyo, Japan; 6-15 kV, 20° tilt, 40,000x magnification).

AFM analysis

Atomic Force Microscopy (AFM) was used to study the surface topography of protein-gold adsorbed silicon substrates. The samples were analysed with a Nanoscope III microscope (Digital Instruments Inc., Santa Barbara, USA). AFM images were recorded in tapping mode at RT in air using silicon cantilevers (Digital Instruments). For each sample height images were recorded with the maximum available number of pixels (512x512). For image analysis the recorded scans were "flattened" using the Nanoscope image processing software.

XPS analysis

The chemical surface composition of the protein-gold adsorbed substrates was investigated by X-ray Photoelectron Spectroscopy (XPS). The measurements were performed with an XSAM-800 apparatus (Kratos, Manchester, UK) using a Mg K_α source (15kV, 10 mA). A spot size of 6 mm (ϕ) was analysed. The pressure during the measurements was $1x10^{-7}$-$1x10^{-8}$ mbar. Survey scans (0-1100 eV) were recorded for all samples to qualitatively determine the elements present at the surface. Detail scans (20-30 eV windows) were recorded to quantify the elemental surface composition. The measured peak areas were converted into atomic percentages by using sensitivity factors, either known from literature[28] (e.g. Au, Si) or determined by calibration measurements on various polymer samples with known surface chemical composition (e.g. C, O, N, F, S).

Chemical modification of CO_2 plasma etched gold and glass substrates

Plasma etched gold and glass substrates were chemically modified by silanation and/or thiol chemistry. The silanation was performed under nitrogen flow at RT. ODS was dissolved in dry distilled n-heptane (5-10 mM). The (un)treated substrates were incubated in the ODS solution for 30 min. Subsequently, the substrates were removed from the solution and immediately rinsed with an excess of dry, distilled heptane. Finally, the substrates were dried under nitrogen flow.

For thiol chemistry, FAT was dissolved in dichloromethane (±1 mM) and the substrates were incubated in the FAT solution overnight at RT. Subsequently, the substrates were removed from the solution and immediately rinsed with an excess of dichloromethane. Finally, the substrates were dried under nitrogen flow and stored at RT.

7.3 Results and Discussion

7.3.1 Adsorption of (P)AGC onto various substrates

Two different protein-gold colloids (AGC and PAGC) were selected with different gold nanoparticle size (10 and 20 nm) in order to obtain surfaces with different nanoparticle densities after adsorption. During the adsorption process the protein serves as the adsorbate. Since adsorption/desorption of proteins at a surface is a random, thermodynamically driven process, no large-scale surface ordering (e.g. hexagonal packing) of the nanoparticles should be expected. Besides its adsorbing character, the protein has another important function in the formation of a nanoparticle surface structure. The protein shell formed around the gold nanoparticles stabilizes the suspension and prevents the colloids from aggregating during the adsorption process. In this way, the protein acts as a spacer molecule for the gold nanoparticles. Thus, it is envisaged that a dense (random) packing of isolated gold nanoparticles can be obtained at the surface, the nanoparticle density not only being dependent on the size of the gold nanoparticles but also on the thickness of the shielding protein layer.
Although the size of the (uncovered) gold nanoparticles is known from TEM analysis (Table 7.1), it is also useful to have some idea of the size of the protein-gold colloid as a whole. This makes estimation of the maximal surface nanoparticle density possible. Therefore, PCS was used to determine the hydrodynamic diameter of the protein-gold colloids. The results of these measurements are shown in Table 7.1.

Table 7.1: Sizing of protein-gold colloids by TEM (n=10) and PCS (n=5).

Sample	d_{Sigma} (nm)	d_{TEM} (nm)	d_{PCS} (nm)*
AGC	9.6 ± 0.9	8.6 ± 0.6	23.7 ± 0.6
PAGC	18.4 ± 1.5	16.8 ± 0.9	50.4 ± 1.2

* PI = 0.4

The bare gold particle size as provided by the manufacturer was checked by TEM analysis. The measured values for AGC as well as PAGC agreed reasonably well with the data obtained from Sigma. The measured hydrodynamic diameter of the colloids (PCS) was almost three times the actual diameter of the bare gold particles, which indicates the presence of a protein shell. The value of the polydispersity index (PI = 0.4) shows that the size distribution of the protein-gold colloids was relatively broad (note that PI ranges from 0 (monodisperse) to 1 (polydisperse)). Since the gold nanoparticles have a uniform size (monodisperse), the

polydispersity can be mainly attributed to the presence of the protein shell. This clearly suggests that a high degree of nanoparticle ordering can not be obtained at the protein-gold adsorbed surface. In this respect, an alternative might be to coat the gold colloids with a self-assembled (dense) monolayer (SAM) of aliphatic, end-functionalized thiols.[29] Such a uniform, well-defined SAM may replace the protein's functions of acting as an adsorbate (i.e. by interaction of functional end groups) as well as a spacer (i.e. the intercolloidal distance is determined by the length of the aliphatic thiol chain).

Based on the measured hydrodynamic diameter a rough estimation can be made of the maximal nanoparticle density at the surface, assuming an ideal hexagonal packing of the nanoparticles. Moreover, in this calculation the three-dimensional colloids are projected as two-dimensional discs at the surface and it is assumed that no overlap of the 'hydrodynamic' colloids can take place. Thus, for AGC a maximal surface nanoparticle density of $2.1 \times 10^{11}/cm^2$ was calculated and for PAGC a value of $4.5 \times 10^{10}/cm^2$ was found. The actual surface nanoparticle density will be determined from the results of the adhesion experiments, which are discussed below.

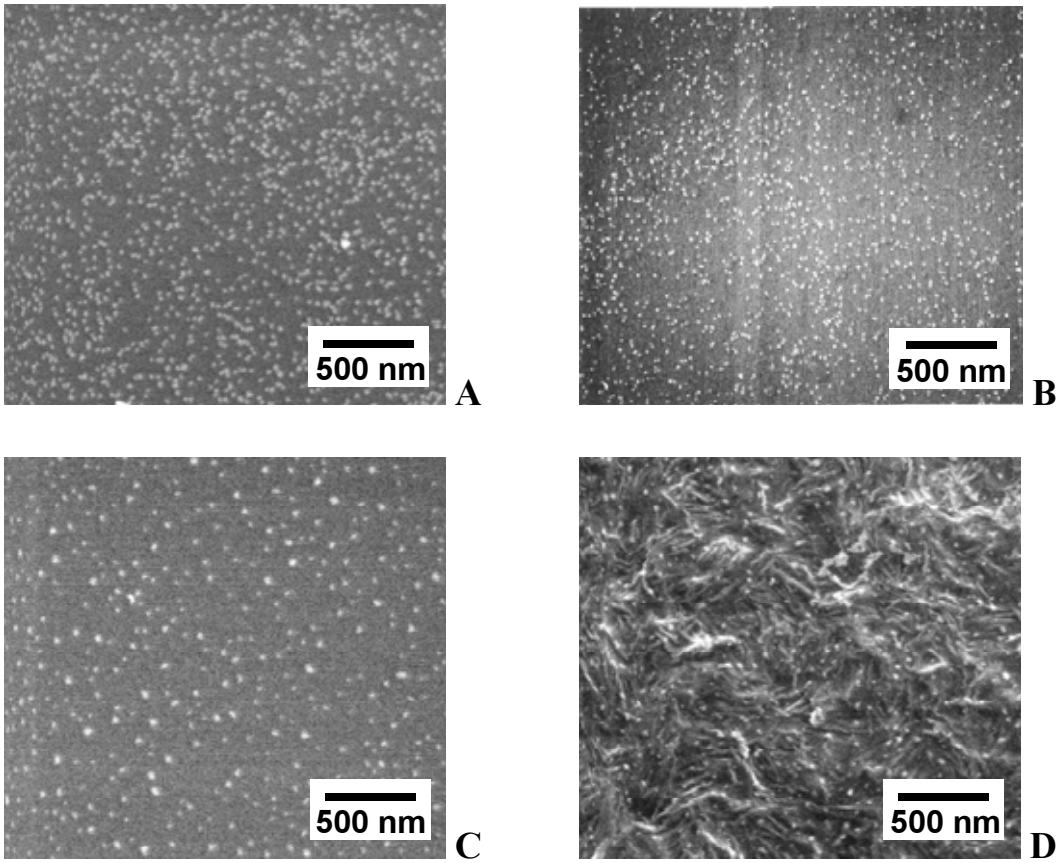

Figure 7.1: *SEM pictures of various AGC adsorbed substrates (incubation time 30 min). Glass (A), silicon (B), PS (C), LDPE (D).*

AGC and PAGC were adsorbed onto various substrates (e.g. glass, silicon, PS, LDPE). SEM pictures of the resulting surfaces are shown in Figure 7.1 and Figure 7.2. AGC adsorbed well onto all substrates, the nanoparticle density being highest on glass and silicon. Moreover, the gold nanoparticles were randomly distributed on the surface without substantial aggregation. No substantial increase of AGC nanoparticle density was observed after longer incubation times (e.g. 300 min). Furthermore, varying the AGC concentration during adsorption hardly seemed to influence the nanoparticle density (pictures not shown). From Figure 7.1A the actual surface nanoparticle density of AGC on glass was calculated to be $3.7 \times 10^{10}/cm^2$, which is about 5-6 times less than the theoretical, maximal nanoparticle density (see above). This difference clearly points out that a maximal surface coverage can not be obtained by this procedure. At this point it should be noted that the substrates (excluding PS) were extensively rinsed with PBS and water after AGC adsorption had taken place. Loosely adsorbed colloids were probably removed from the substrate during this washing procedure, leaving the firmly adsorbed particles at the surface. In this respect, a question might be whether it is not more convenient to directly adsorb uncovered (bare) gold nanoparticles to a substrate in a similar way. Some screening tests (not presented) have made clear that the nanoparticles do not stick to the substrate well enough to survive the rinsing procedure. Clearly, the protein acts as the adsorbate suppressing colloid desorption during rinsing. Another explanation for the relatively low nanoparticle density might be found in a competition between colloid and free protein adsorption. The albumin concentration in the colloidal suspension is based on the estimation of protein required to stabilize gold. A simple calculation, based on this albumin concentration provided by the manufacturer (1.4×10^{-11} μg albumin per particle ≈ 4.5 $\mu g/cm^2$) and the theoretical end-on albumin monolayer coverage of a surface (0.9 $\mu g/cm^2$)[30], learns that the protein shell around the gold colloids must consist of a multilayer. This justifies the possible presence of free albumin in the colloidal suspension. Screening experiments with varying concentrations of (free) albumin added to the AGC suspension prior to adsorption have shown that the nanoparticle density is indeed reduced upon increasing the amount of albumin (data not shown). These results support the proposed explanation for the relatively low nanoparticle density.

The AGC nanoparticle density on PS and LDPE substrates was somewhat less than on glass and silicon (Figure 7.1). Some data in literature confirm that the surface activity of albumin on a PE surface is low.[31] However, in general proteins adsorb more strongly onto hydrophobic surfaces than onto hydrophilic surfaces. This is due to a relatively large gain in entropy caused by desorption of water molecules from the surface of both the protein molecule and the solid surface upon protein adsorption, a phenomenon known as hydrophobic interaction.[32] On the

other hand, it is known that adsorption of proteins onto solid surfaces is dependent on a number of different factors (e.g. surface charge, protein conformation, amino acid sequence, etc.)[31], which makes a straightforward explanation of the observed differences in Figure 7.1 difficult. Still, once a protein does adsorb to a hydrophobic surface like PE or PS, it will most likely be irreversibly adsorbed.

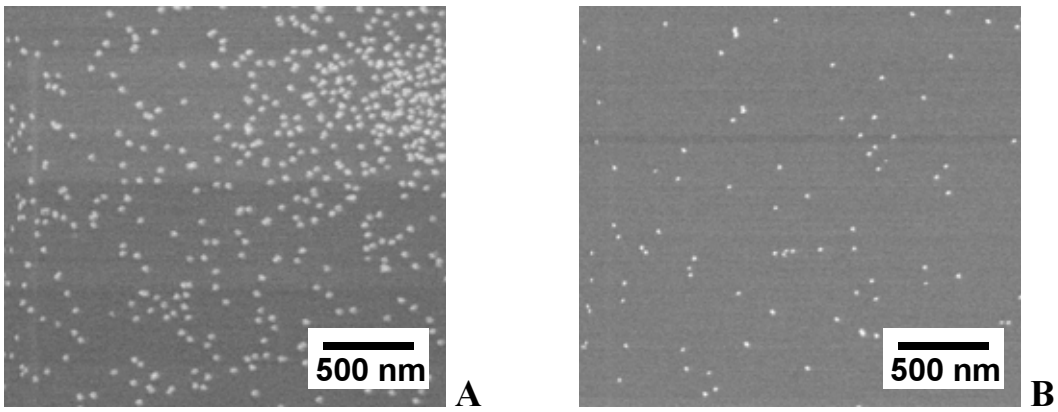

Figure 7.2: *SEM pictures of PAGC adsorbed substrates (incubation time 300 min). Glass (A), silicon (B).*

PAGC adsorption onto glass was less pronounced than AGC adsorption, even after 300 min of incubation (Figure 7.2). Initially, a lower nanoparticle density was expected based on the larger diameter of the PAGC colloids (Table 7.1). A rough estimation of the average surface nanoparticle density on glass results in a value of $9.1 \times 10^9/cm^2$. This is about 5 times less than the theoretical, maximal value (see above), which is the same ratio as was found for AGC adsorbed onto glass. However, the distribution of PAGC nanoparticles onto glass was not optimal. Figure 7.2A suggests that the PAGC colloids tended to form clusters at certain spots on the surface, which was not observed for AGC on glass (Figure 7.1A). In this respect, albumin seems to be a more suitable adsorbate for obtaining a uniform surface distribution of gold nanoparticles than protein A. PAGC adsorption onto silicon substrates was very low compared to PAGC adsorption onto glass. This difference (not observed for AGC) seems somewhat strange, since both surfaces are hydrophilic and have a similar surface chemistry. It does point out that the adsorption behaviour of proteins onto a solid surface can not always be predicted in a straightforward way.

From the above it can be concluded that adsorption of protein-gold colloids is a suitable, one-step procedure to obtain a uniform distribution of isolated gold nanoparticles at a surface.

However, adsorption is a random process and highly ordered surface nanostructures (e.g. hexagonal packing) can therefore not be achieved.

7.3.2 Gas plasma etching of (P)AGC adsorbed substrates

After (P)AGC adsorption the substrates were etched with a CO_2 or air plasma for 30 min. Glass was chosen as the substrate, since its (anorganic) surface chemical composition is hardly affected by gas plasma etching. This simplifies the interpretation of the XPS data, i.e. surface chemical changes during etching can be largely attributed to the adsorbed protein-gold colloids. XPS data of (P)AGC adsorbed and plasma etched glass substrates are presented in Table 7.2.

Table 7.2: XPS data of (P)AGC adsorbed (30 min) and plasma etched glass substrates (n=1).

Sample	Si (at.%)	O (at.%)	Au (at.%)	C (at.%)	N (at.%)
Glass	26.2	64.5	-	4.8	-
Glass;AGC	19.3	60.2	0.4	15.9	2.3
Glass;AGC;CO_2	22.4	70.1	0.5	4.8	0.6
Glass;AGC;Air	23.1	69.1	0.4	4.6	1.7
Glass;PAGC	17.5	62.0	0.1	16.5	1.4
Glass;PAGC;CO_2	23.2	68.6	0.1	4.8	0.7

NOTE: Minor amounts of sodium and potassium (total < 4%) were also detected on the glass substrates.

Glass mainly consists of SiO_x with some carbon contaminating species at the surface due to the highly energetic nature of cleaned glass. Adsorption of AGC substantially changes the surface chemical composition, SiO_x being suppressed in favor of carbon, nitrogen and oxygen originating from adsorbed albumin. The amount of gold detected at the surface was remarkably low. Based on the actual surface nanoparticle density ($3.7x10^{10}/cm^2$) a gold surface percentage of 3% was estimated for AGC adsorbed glass (2-dimensional projection). The measured values in Table 7.1 were 6-7 times lower suggesting that some unidentified factor influenced the XPS measurement. A logical explanation could be the protein shell masking the gold nanoparticles from XPS detection. Looking at the XPS data of AGC adsorbed and plasma etched substrates quickly proves that this can not be the major reason for the small amount of gold detected at the surface, since the gold percentage did not increase substantially upon etching (e.g. protein removal). Indeed, the protein must have been largely

removed from the gold nanoparticles during plasma treatment, since the surface percentages of carbon and nitrogen (typical protein elements) largely decreased upon plasma etching. The nitrogen that was still present at the CO_2 plasma etched samples can be attributed to residual etch products rather than to residual (intact) albumin. The nitrogen present at the air plasma etched sample is attributed to reaction of active nitrogen plasma species with the substrate. However, once the protein is removed the highly energetic surface (i.e. cleaned glass covered with gold nanoparticles) is exposed to organic surface contaminations from the air (discussed above; see also Table 7.3). A thin contaminating layer on the gold covered glass substrate will substantially reduce the gold detection. The residual carbon detected at the surface after CO_2 plasma etching (4.8%) confirms the presence of this type of surface contamination. Besides this masking layer, the mean free path of the photoelectrons in gold could play an important role. Only the outer layer (±2 nm) of the nanoparticles (10-20 nm) is detected by XPS, reducing the total gold signal. A final explanation could be related to geometrical effects at the surface. The high Au surface sensitivity factor (4.95), used to convert the measured Au4f peak area into an atomic percentage, is derived from flat gold surfaces. Colloidal gold structures at the surface might suppress this sensitivity factor, resulting in an actual higher gold percentage than initially calculated. However, determination of this colloid sensitivity factor with XPS calibration measurements is difficult if not impossible.

PAGC adsorbed and plasma etched glass substrates showed a similar surface chemical change as was observed for AGC adsorbed substrates, with the exception of the detected amount of gold. Based on the calculated average surface nanoparticle density (Figure 7.2A) a gold surface percentage of 3% was estimated, similar to that of AGC. Apparently, the overall surface nanoparticle density of PAGC on glass must have been less than the estimated value. The substantially higher gold percentage on AGC adsorbed glass compared to PAGC adsorbed glass indicates that AGC is a more suitable protein-gold marker for surface analysis than PAGC.

Although the detected gold percentages were generally very low, they did not decrease upon plasma etching. Thus, the gold nanoparticles were maintained at the surface during plasma treatment while the protein was largely removed. This was confirmed by AFM and SEM analysis as shown in Figure 7.3 and Figure 7.4. When looking closely at Figure 7.3A a vague ring can be observed around most of the gold nanoparticles which is attributed to the protein A shell. This ring disappeared after plasma etching (Figure 7.3B) indicating the removal of protein A. Despite removal of the adsorbate, the surface nanoparticle density was not affected by plasma etching (Figure 7.4). This suggests that some kind of interaction between the gold nanoparticles and the substrate must still be present after etching, which prevented particle

removal from taking place. Possibly, traces of residual protein that were shielded from plasma etching (and XPS detection) by the gold nanoparticles may still be responsible for anchoring these particles to the substrate.

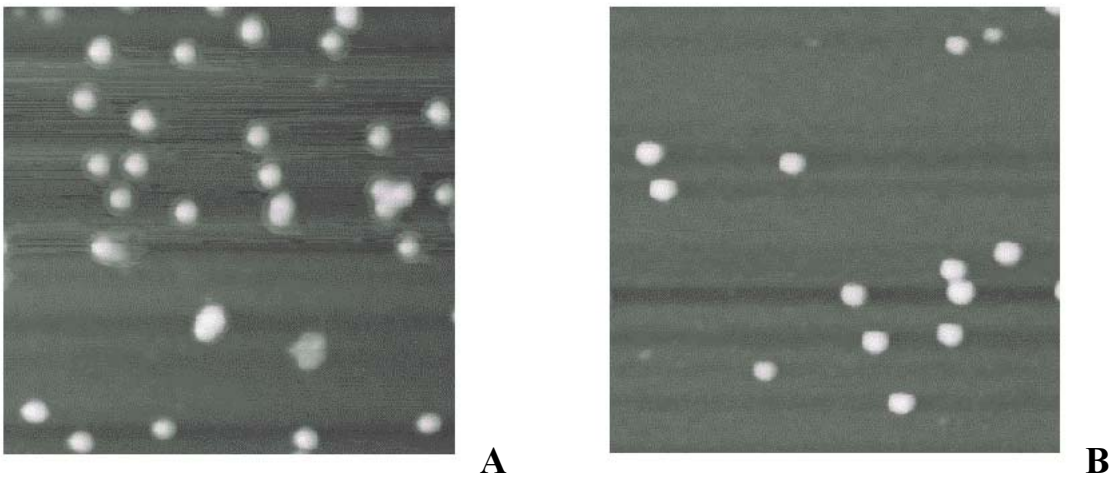

Figure 7.3: *AFM height images of PAGC adsorbed (300 min; A) and air plasma etched (B) silicon substrates. The scanned area is 750x750 nm.*

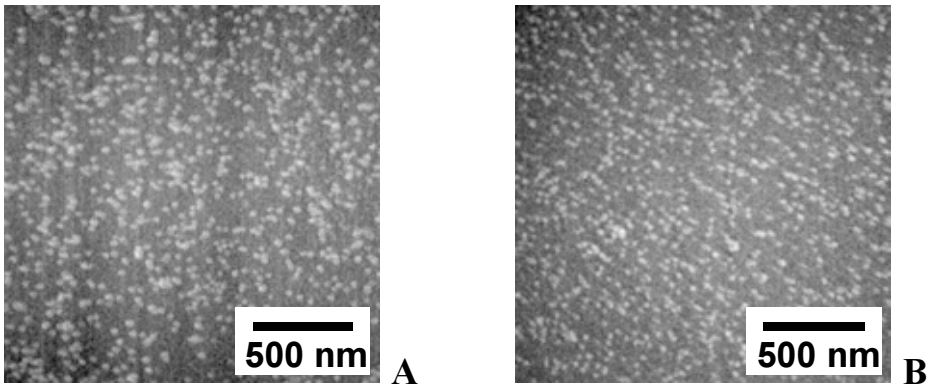

Figure 7.4: *SEM pictures of AGC adsorbed (A) and CO_2 plasma etched (B) glass substrates.*

The above results show that gas plasma etching is a versatile tool to selectively ablate organic material from an inorganic/organic complex without changing the surface distribution and density of the anorganic nanodomains. When polymer substrates are used (e.g. PS, PE) an optimal etching time should be found, after which the protein is completely removed but the polymer surface structure is still intact.

7.3.3 Chemical modification of CO_2 plasma etched substrates

Besides selective protein ablation, plasma etching also modifies the polymer surface chemistry. This additional effect could be of great use for preparation of selectively modified, nanostructured polymer hybrid systems. For example, CO_2 plasma etching hydrophilizes a polymer substrate filled with gold nanoparticles which are subsequently selectively hydrophobized by thiol chemistry.

In order to study the feasibility of selective chemistry on gold nanoparticle adsorbed and plasma etched substrates, two control surfaces were tested. Smooth gold substrates (e.g. gold sputtered glass slides) were used for thiol chemistry. Glass substrates were used as a control surface for non-selective thiol adsorption. Both control substrates were treated with a CO_2 plasma similar to the previously described experiments. Subsequently, they were both modified by thiol chemistry using a fluorinated amide thiol (FAT). This thiol was chosen for its high content of fluorine (F/C ratio = 1.5), which is a unique and easily detectable marker for the presence of thiol at the surface. Table 7.3 shows the XPS data of plasma etched and thiol functionalized gold and glass substrates. Plasma etched gold (high surface energy) was highly reactive towards organic substances from the air, as indicated by the high surface carbon percentage (25.9%). Moreover, surprisingly high amounts of surface oxygen were detected, which could be originating from different sources like surface contamination, oxidative degradation products and oxidized gold (Au_2O_3). The latter is known to occur even when gold surfaces are treated with mild oxidative plasmas.[33-35] Despite surface oxidation and contamination, FAT chemisorbed onto plasma etched gold in large amounts (F = 42.9%), confirming the high reactivity of gold (and also gold oxide[34,35]) towards thiols. Even substantial amounts of nitrogen and sulfur, present in FAT, were detected. The strong decrease of detected gold to merely 18% strongly suggests that a uniform and relatively thick FAT layer was formed on top op the reactive gold surface.

Plasma treated glass showed relatively high amounts of surface carbon and nitrogen. This is most probably caused by contaminations due to the high surface energy of plasma treated glass (similar to plasma treated gold). The nitrogen might be attributed to slight compositional changes of the type of glass used. More importantly, plasma treated glass did adsorb substantial amounts of FAT as indicated by the increased carbon percentage and the detected fluorine at the surface (6.6%). Apparently, extensive rinsing with solvent was not sufficient to remove the physisorbed FAT. A reasonable explanation for this non-selective, irreversible adsorption can be found in strong polar interactions between amide groups of the FAT adsorbate and high surface energy groups of the glass substrate.

Table 7.3: XPS data of CO_2 plasma etched and chemically modified glass and gold substrates (n=1).

Sample	Si (at.%)	O (at.%)	Au (at.%)	C (at.%)	N (at.%)	S (at.%)	F (at.%)
Gold;CO_2	-	31.9	40.3	25.9	-	-	-
Gold;CO_2;FAT	-	6.4	17.9	28.6	2.6	1.6	42.9
Gold;CO_2;ODS	3.7	25.7	26.0	41.9	-	-	-
Gold;CO_2;ODS;FAT	4.8	15.2	19.4	28.3	1.2	2.3	28.9
Glass;CO_2	24.6	59.8	-	10.2	1.6	-	-
Glass;CO_2;FAT	21.0	51.3	-	16.0	1.6	-	6.6
Glass;CO_2;ODS	25.8	56.2	-	14.3	1.1	-	-
Glass;CO_2;ODS;FAT	23.7	53.5	-	19.5	0.8	-	-

NOTE: Minor amounts of sodium, potassium, boron and chlorine (total < 4%) were also detected on the substrates.

The above results show that selective FAT chemistry on protein-gold adsorbed and plasma etched glass substrates will not be possible in one step, due to non-selective, physisorption of FAT onto plasma etched glass. Silanation is a well known and straightforward chemical tool to lower the surface energy of glass. ODS was used to silanize the surface of plasma etched glass substrates. Plasma etched gold substrates were also silanized to check the efficacy of thiol adsorption after silanation. Table 7.3 shows that silanation of plasma etched gold did affect the efficacy of thiol adsorption to some extent. About 2/3 of the initial amount of fluorine (non-silanized) was detected at the surface after silanation, while the presence of silicium indicates that ODS was still present at the surface after thiol chemisorption. Logically, thiol chemisorption had to compete with physisorbed silane for the available surface active sites, resulting in an overall lower thiol surface coverage. Still, silanation did certainly not prevent thiol adsorption from taking place, confirming that thiol chemistry is a versatile tool to modify gold surfaces.

Silanation of plasma etched glass was succesful in preventing physisorption of FAT, since no fluorine was detected at the surface of successively silanized and thiol treated glass substrates (Table 7.3). These results show that selective chemical modification of both phases of the gold/glass hybrid system is feasible by silanation of the glass followed by selective thiol modification of the gold domains.

An attempt was made to apply this two-step selective chemistry on AGC adsorbed and plasma etched glass using the same procedure as for the control substrates. Unfortunately, the initial

results (data not presented) did not clearly indicate selective thiol modification of the gold nanoparticles yet. At this moment, this deficiency is attributed to the relatively low gold percentages at the surface of protein-gold adsorbed and etched substrates. Extrapolating the F/Au ratio of a chemically modified gold surface (Table 7.3: F/Au=1.5) to selectively modified gold nanoparticles learns that only minor amounts of fluorine should be expected at the hybrid surface. Therefore, a higher gold nanoparticle density is necessary at the surface to detect a significant marker signal (here: fluorine) with surface analysis techniques like XPS. An interesting alternative could be to chemically map the heterogeneous surfaces on the nanoscale by AFM analysis with chemically modified tips.[26] With this recently developed technique different surface functionalities can be imaged at a high resolution.

Finally, it should be noted that silanation of the glass substrates might become an unnecessary modification step when apolar thiols are used to avoid non-selective thiol physisorption onto the plasma etched surface. Furthermore, selective chemical modification of polymer substrates can already be achieved during the plasma etching procedure (e.g. CO_2, CF_4), thereby avoiding the need for glass specific silanation.

7.4 Conclusions

This study has shown that protein-gold colloids can be easily adsorbed onto various substrates by a one-step procedure, leading to a random distribution of isolated gold nanoparticles at the surface. After adsorption the protein shell could be selectively removed by oxidative gas plasma etching without affecting the gold nanoparticle distribution and density.

Selective chemical modification of both the substrate and the gold nanoparticles is feasible as was shown by successive silanation and thiol chemistry on glass and gold control surfaces. Still, higher gold nanoparticle densities and highly accurate surface analysis techniques are necessary to successfully analyse these chemically heterogeneous, nanostructured surfaces.

7.5 Acknowledgements

Albert v/d Berg, Mark Smithers and Clemens Padberg (MESA+ Institute, University of Twente) are acknowledged for performing the XPS, SEM/TEM and AFM measurements, respectively. This study was financed by the Netherlands Foundation for Chemical Research (NWO-CW).

7.6 References

1) Spatz, J. P.; Herzog, T.; Mossmer, S.; Ziemann, P.; Moller, M. *Adv. Mater.* **1999**, *11*, 149-153.
2) Spatz, J. P.; Mößmer, S.; Möller, M.; Herzog, T.; Plettl, A.; Ziemann, P. *J. Luminesc.* **1998**, *76&77*, 168-173.
3) Spatz, J. P.; Eibeck, P.; Mossmer, S.; Moller, M.; Herzog, T.; Ziemann, P. *Adv. Mater.* **1998**, *10*, 849-852.
4) Morkved, T. L.; Wiltzius, P.; Jaeger, H. M.; Grier, D. G.; Witten, T. A. *Appl. Phys. Lett.* **1994**, *64*, 422-424.
5) Baker, B. E.; Natan, M. J.; Zhu, H.; Beebe, T. P. *Supramol. Sci.* **1997**, *4*, 147-154.
6) Grabar, K. C.; Allison, K. J.; Baker, B. E.; Bright, R. M.; Brown, K. R.; Freeman, R. G.; Fox, A. P.; Keating, C. D.; Musick, M. D.; Natan, M. J. *Langmuir* **1996**, *12*, 2353-2361.
7) Petit, C.; Taleb, A.; Pileni, M. P. *Adv. Mater.* **1998**, *10*, 259-261.
8) Lewis, P. A.; Ahmed, H.; Sato, T. *J. Vac. Sci. Technol. B* **1998**, *16*, 2938-2941.
9) Koslowski, B.; Strobel, S.; Herzog, T.; Heinz, B.; Boyen, H. G.; Notz, R.; Ziemann, P.; Spatz, J. P.; Moller, M. *J. Appl. Phys.* **2000**, *87*, 7533-7538.
10) Spatz, J. P.; Mößmer, S.; Möller, M. *Chem. Eur. J.* **1996**, *2*, 1552-1555.
11) Roescher, G. A. *Stabilization of Colloidal Noble Metals by Block Copolymers*; University of Twente: Enschede, The Netherlands, 1995.
12) Beesley, J. E. *Proceed. Royal Microsc. Soc.* **1985**, *20*, 187-196.
13) Roth, J. *The Colloidal Gold Marker System for Light and Electron Microscopic Cytochemistry*; Bullock, G. R. and Petrusz, P., Ed.; Academic Press: London, 1983; Vol. 2.
14) Ackerman, G. A.; Yang, J.; Wolken, K. W. *J. Histochem. Cytochem.* **1983**, *31*, 433-440.
15) Bendayan, M. *J. Electron Microsc. Techn.* **1984**, *1*, 243-270.
16) Bendayan, M. *J. Histochem. Cytochem.* **1982**, *30*, 81-85.
17) Benhamou, N. *J. Electron Microsc. Techn.* **1989**, *12*, 1-10.
18) Tolson, N. D.; Boothroyd, B.; Hopkins, C. R. *J. Microsc.* **1981**, *123*, 215-226.
19) Slot, J. W.; Geuze, H. J. *J. Cell Biol.* **1981**, *90*, 533-536.
20) Brada, D.; Roth, J. *Anal. Biochem.* **1984**, *142*, 79-83.
21) Horisberger, M. *Biol. Cellulaire* **1979**, *36*, 253-258.
22) Danscher, G.; Nörgaard, J. O. R. *J. Histochem. Cytochem.* **1983**, *31*, 1394-1398.
23) Springall, D. R.; Hacker, G. W.; Grimelius, L.; Polak, J. M. *Histochemistry* **1984**, *81*, 603-608.
24) Holgate, C. S.; Jackson, P.; Cowen, P. N.; Bird, C. C. *J. Histochem. Cytochem.* **1983**, *31*, 938-944.
25) Horisberger, M.; Clerc, M.-F. *Histochemistry* **1985**, *82*, 219-223.
26) Schönherr, H. *From Functional Group Ensembles to Single Molecules: Scanning Force Microscopy of Supramolecular and Polymeric Systems*; University of Twente: Enschede, The Netherlands, 1999.
27) Terlingen, J. G. A.; Hoffman, A. S.; Feijen, J. *J. Appl. Polym. Sci.* **1993**, *50*, 1529-1539.
28) Briggs, D.; Seah, M. P. *Practical Surface Analysis: by Auger and X-ray Photo-electron Spectroscopy*; Wiley: Chichester, 1983.
29) Weisbecker, C. S.; Merritt, M. V.; Whitesides, G. M. *Langmuir* **1996**, *12*, 3763-3772.
30) Baszkin, A.; Lyman, D. J. *J. Biomed. Mater. Res.* **1980**, *14*, 393-403.
31) Horbett, T. A.; Ratner, B. D.; Schakenraad, J. M.; Schoen, F. J. *Chapter 3: Some Background Concepts*; Ratner, B. D., Hoffman, A. S., Schoen, F. J. and Lemons, J. E., Ed.; Academic Press: San Diego, 1996.
32) van Damme, H. S. *Protein Adsorption at Solid-Liquid Interfaces - Influence of surface structure, hydrophobicity and charge*; University of Twente: Enschede, The Netherlands, 1990.

33) Bain, C. D.; Troughton, E. B.; Tao, Y. T.; Evall, J.; Whitesides, G. M.; Nuzzo, R. G. *J. Am. Chem. Soc.* **1989**, *111*, 321-335.
34) Ron, H.; Rubinstein, I. *Langmuir* **1994**, *10*, 4566-4573.
35) Ron, H.; Matlis, S.; Rubinstein, I. *Langmuir* **1998**, *14*, 1116-1121.

Chapter 8

Gas plasma etching of PEO/PBT segmented block copolymer films

M. B. Olde Riekerink, M. B. Claase, G. H. M. Engbers, D. W. Grijpma, J. Feijen

Department of Chemical Technology, Section Polymer Chemistry and Biomaterials and Institute for Biomedical Technology, University of Twente, P.O. Box 217, 7500 AE Enschede, The Netherlands

Poly(ethylene glycol) (PEG) and poly(butylene terephthalate) (PBT) were treated with a radio frequency (RF) carbon dioxide (CO_2) or argon (Ar) gas plasma to determine their etching rates (48-49 W, 0.06-0.10 mbar, 30 min). In both plasmas, PEG was etched significantly faster than PBT. Subsequently, a series of PEO/PBT block copolymer films was treated with an RF CO_2 plasma (1 and 30 min) or an Ar plasma (30 min) under similar treatment conditions. The effect of (preferential) etching on changes of surface structure, topography, chemistry and wettability was studied by Scanning Electron Microscopy (SEM), Atomic Force Microscopy (AFM), X-ray Photoelectron Spectroscopy (XPS) and contact angle measurements, respectively. In all cases, prolonged CO_2 plasma etching caused a substantial surface structural change. A granular-type nanostructure was formed, which could possibly be attributed to temperature induced surface reorientation of the phase separated copolymer system. Moreover, a surface lamellar structure (PBT) was gradually exposed after prolonged CO_2 or Ar plasma etching of the copolymer film containing 30 wt.% PEO segments (4000 g/mol), due to preferential removal of the 'soft' phase (PEO). Surface chemical changes upon plasma treatment were quite similar for most film compositions. CO_2 plasma treatment caused surface oxidation and oxidative degradation of the films, while Ar plasma etching mainly resulted in removal of PEO blocks. Generally, the wettability of the films significantly increased after plasma treatment due to creation of polar functional groups at the surface. Preliminary goat bone marrow cell (GBMC) compatibility experiments have shown that all plasma treated PEO/PBT films induced a greatly enhanced cell adhesion and/or growth compared to the untreated biomaterial. This improvement was attributed to changes of surface chemistry (introduction of polar surface groups) rather than to changes of surface structure during plasma etching. These results show that plasma treated PEO/PBT copolymers have a high potential as scaffolds for bone tissue regeneration.

8.1 Introduction

Gas plasma processes are extensively used for the chemical modification of polymer surfaces.[1-3] Plasma etching treatments have also been used to increase surface roughness without aiming for a specific surface structure, for instance to improve properties such as

adhesion.[4,5] Restructuring of polymer surfaces, i.e. changing surface structural characteristics (e.g. morphology, texture, roughness), on the nanoscale level is of interest for areas such as biomedical engineering.

In principle, gas plasma etching can be used for tailoring the surface structure of phase separated polymeric systems, i.e. semi-crystalline polymers, polymer blends or block copolymers, by removal of one polymer phase in preference to another. However, preferential etching will only succeed if the etching rates of the two phases differ substantially. In a recent study it was shown that during gas plasma etching of poly(ethylene), a semi-crystalline polymer, the amorphous phase was preferentially removed from the surface leading to surface restructuring.[6] To study the feasibility of this approach for block copolymers, several homopolymers (e.g. poly(styrene) (PS), poly(isoprene) (PIs), poly(butadiene) (PBd), poly(ethylene glycol) (PEG), poly(butylene terephthalate) (PBT)) were screened for their plasma etching behaviour in a preliminary study. PS, PIs and PBd are used as building blocks for PS/PIs and PS/PBd di- and triblock copolymer films. Due to their spontaneous self-assembly into well-ordered microdomain surface patterns, these block copolymers have a large potential as nanolithographic templates for semi-conductor applications. However, the homopolymers did not show substantially different etching rates in a gas plasma. In a CO_2 plasma, etching rates of 7.7, 7.2 and 7.8 nm/min were found for PS, PIs and PBd, respectively, while in an Ar plasma the respective values were 2.7, 2.0 and 2.3 nm/min as determined by a quartz crystal microbalance (QCM). Literature confirms that selective etching of PS/PIs or PS/PBd block copolymers is hardly possible when using only plasma techniques.[7] Alternative etching methods like ozonolysis have shown to be better suitable for the selective removal of the elastomeric phase (e.g. PIs, PBd) by preferential oxidation of the unsaturated bonds.[7-9]

In contrast to PS, PIs and PBd, preliminary data showed that plasma etching rates of PEG and PBT homopolymers differed significantly. The copolymers of these components, PEO/PBT segmented block copolymers, are a group of thermoplastic elastomers with a high biomedical potential. The physical and biological properties of these copolymers can be tailored by variation of the composition and the block length. In this way, they can be applied for a number of biomedical applications such as skin repair devices[10,11], alloplastic tympanic membrane materials[12], and protein release systems.[13] Besides soft tissue applications, PEO/PBT block copolymers also appear to be suitable as a biomaterial for bone tissue engineering.[14-16] PEO/PBT copolymers of certain compositions calcified and showed bone bonding after implantation in goat femurs.[15]

One interesting approach for bone tissue regeneration would be to culture host cells on biodegradable polymer scaffolds *in vitro* and subsequently implant the biocoated material.[17]

However, preliminary experiments have shown that *in vitro* bone cell adhesion and/or growth on a series of PEO/PBT copolymer films was generally quite poor. The cell-substrate properties of these polymers should therefore be improved without changing the (biodegradable) bulk properties of the biomaterial. Beumer *et al.* showed that gas plasma treatment of a skin substitute made of a PEO/PBT copolymer significantly improves the adherence and growth of epithelial cells seeded on the material's dense toplayer.[18] From literature it is also known that rough surfaces display higher levels of osteoblast attachment as compared to smooth surfaces.[19] Preferential gas plasma etching of one polymer phase of a PEO/PBT copolymer film is expected to induce an increase of surface roughness, while the films will be chemically modified at the same time. This combination of surface chemical and structural modification is believed to be a versatile tool for improving bone cell adhesion and/or growth on PEO/PBT block copolymers.

Therefore, the aim of the present study is to investigate the effect of (preferential) gas plasma etching on the surface properties (e.g. structure, chemistry, wettability) and bone cell compatibility of PEO/PBT block copolymer films. First, PEG and PBT homopolymers will be etched with a carbon dioxide (CO_2) or argon (Ar) gas plasma, the former being an oxidative etchant[2] while the latter is a slow, but potentially selective etchant.[20] Etching rates are measured *in situ* by a quartz crystal microbalance (QCM). Subsequently, a series of PEO/PBT block copolymer films with varying compositions is treated with a CO_2 or Ar plasma. Short treatment times (1 min) are used to study the effect of chemical surface changes, while prolonged etching (30 min) will give additional information on the effect of surface structural changes. The surface properties of the plasma treated films are studied by a number of surface analysis techniques (e.g. Scanning Electron Microscopy (SEM), Atomic Force Microscopy (AFM), X-ray Photoelectron Spectroscopy (XPS), captive bubble contact angle measurements). Finally, some preliminary goat bone marrow cell (GBMC) compatibility experiments are carried out to test the plasma treated films on their *in vitro* cell adhesion and/or growth.

8.2 Experimental

8.2.1 Materials

Poly(ethylene glycol) (PEG monoethyl; M_w = 5,000 g/mol; ρ = 1.1 g/cm^3) was purchased from Polysciences, Inc., Warrington, USA. Poly(1,4-butylene terephthalate) (PBT; ρ = 1.3 g/cm^3) was purchased from Sigma-Aldrich Chemie GmbH, Steinheim, Germany. A series of poly(ethylene oxide)/poly(butylene terephthalate)

(PEO/PBT) segmented block copolymers with varying compositions was prepared by polycondensation as previously described by Deschamps *et al.*.[21] These copolymers will be further addressed by the following codes: 4000/70/30 (with 4000 g/mol being the molecular weight of the starting PEG homopolymer, 70% being the weight percentage of PEO soft segment including one terephthalate unit (-(CH_2-CH_2-O)$_n$-OC-C_6H_4-COO-), and 30% being the weight percentage of PBT hard segment (-(CH_2)$_4$-OOC-C_6H_4-COO-), 1000/30/70, 1000/70/30, 300/55/45 and 300/70/30. Sympatex® film (type 30S; code 4000/30/70) was kindly supplied by Akzo Nobel, Arnhem, The Netherlands.

Chloroform (purity ≥ 99.9%) was obtained from Biosolve BV, Valkenswaard, The Netherlands. Ethanol (purity ≥ 99.8%) was purchased from Merck, Darmstadt, Germany. Trifluoroacetic acid (TFA) and hexafluoroisopropanol (HFIP) were purchased from Sigma-Aldrich Chemie GmbH, Steinheim, Germany. Argon (Ar) gas (purity ≥ 99.999%) and carbon dioxide (CO_2) gas (purity ≥ 99.995%) were purchased from Hoekloos, Amsterdam, The Netherlands. Quartz crystals (QS010, ∅=14 mm) were obtained from Balzers, Utrecht, The Netherlands. For all experiments ultra-pure water obtained from a Milli-Q Plus System (Millipore) was used.

8.2.2 Methods

Determination of etching rates of PEG and PBT homopolymers

The etching rates of PEG and PBT were determined by a quartz crystal microbalance (QCM) during gas plasma treatment of the homopolymers which were spincoated on quartz crystals (QC). PEG was dissolved in chloroform and PBT was dissolved in a 95/5 mixture of chloroform and TFA at concentrations of 2-5 w/v%. Subsequently, the homopolymer solutions were spincoated on QC at 1000-2000 rpm for 2 min with an IBIS spincoater (IBIS Technologies BV, Enschede, The Netherlands).

A polymer coated quartz crystal was then mounted in a water cooled QSK301 quartz crystal holder which was connected to a QSG301 film thickness monitor via an oscillator (Balzers). The crystal holder was mounted in the center region of a gas plasma tubular reactor (length 80 cm, internal diameter 6.5 cm). Three externally placed capacitively coupled copper electrodes were attached to the reactor: a 'hot' electrode in the center and a 'cold' electrode at both sides of the 'hot' electrode at 12 cm distance. The crystal holder was positioned between the 'hot' and 'cold' electrodes. The electrodes were connected to a RF (13.56 MHz) generator through a matching network. A detailed description of the plasma apparatus is given elsewhere.[20]

The reactor was evacuated to a pressure of 0.01 mbar. Subsequently, a CO_2 or Ar gas flow of 10 cm^3/min (STP) was established through the reactor for 5 min (pre-delay). The spincoated polymer layer was then exposed to the plasma (0.06-0.10 mbar, 48-49 W) for 30 min while maintaining a constant gas flow (10 cm^3/min) through the reactor. Subsequently, the gas flow was maintained for another 2 min (post-delay).

The thickness of the polymer coated quartz crystal was constantly monitored by the QSG301 unit during the plasma treatment. The average etching rate was calculated from the difference of thickness before and after plasma treatment divided by the treatment time.

Casting of PEO/PBT block copolymer films

The PEO/PBT block copolymers (± 4.5 g; excl. Sympatex®) were dissolved in 20 ml chloroform and cast on a glass plate using a 0.75 mm casting knife. Some HFIP (2-4 ml) was added to the 4000/70/30 and 1000/30/70 copolymer solutions for complete dissolution of the PBT segments. All films (incl. Sympatex®) were immersed in ethanol overnight to remove any residual chloroform and/or HFIP. The films were subsequently dried *in vacuo* under a small nitrogen flow for 5 days. Finally, the films were cut into 4x8 cm pieces.

Gas plasma treatment of PEO/PBT block copolymer films

Two cleaned films of the same composition were mounted in glass holders that were placed in the center region of the gas plasma tubular reactor described above. The configuration of the glass holders was such that the films were exposed to the plasma on both sides. The glass holders were positioned between the 'hot' and 'cold' electrodes. The films were either treated with an Ar plasma for 30 min, a CO_2 plasma for 1 min, or a CO_2 plasma for 30 min. Treatment conditions were similar to those used for the homopolymers (see previous section). After the post-delay (2 min), the reactor was brought to atmospheric pressure with air and the films were removed. The films were successively rinsed with water and ethanol, dried *in vacuo* overnight at RT, and stored at -20°C to suppress aging effects.[2]

SEM analysis

The surface structure of the plasma treated PEO/PBT block copolymer films was studied by Scanning Electron Microscopy (SEM). Prior to SEM analysis the samples were sputtered with a 20 Å thick gold-palladium layer (Polaron SEM Sputtering System, VG Microtek, East-Grinstead, UK). The coated samples were analysed with an S-800 Field Emission SEM (Hitachi, Tokyo, Japan; 2 kV, 20° tilt, 15,000x magnification).

AFM analysis

Atomic Force Microscopy (AFM) was used to study the surface topography of plasma treated PEO/PBT block copolymer films. The samples were analysed with a Nanoscope III microscope (Digital Instruments Inc., Santa Barbara, USA). AFM images were recorded in tapping mode at RT in air using silicon cantilevers (Digital Instruments). For each sample both height and phase images were recorded (2.5x2.5 μm) with the maximum available number of pixels (512x512). For image analysis the recorded scans were "flattened" using the Nanoscope image processing software. In addition, the mean surface roughness (R_a) was calculated for the scanned area by applying the formula:

$$R_a = \sqrt{\sum_{x,y=1}^{N} \frac{\left(Z_{x,y} - Z_{average}\right)^2}{N^2}} \qquad (8.1)$$

The roughness is defined as the normalised standard deviation calculated from the local heights ($Z_{x,y}$) and the average height ($Z_{average}$) determined over all x,y coordinates (N) measured in the AFM image.

XPS analysis

The chemical surface composition of the plasma treated PEO/PBT block copolymer films was investigated by high resolution X-ray Photoelectron Spectroscopy (XPS). The measurements were performed by an S probe (Surface Science Instruments, Mountain View, USA) with a monochromatic Al K_α source (1486.6 eV). The input power was 220 W and the analysed spot size was 250x1000 μm. Survey scans (0-1100 eV) were recorded with a pass energy of 150 eV. The concentrations of the various elements were calculated from the relative peak areas, using sensitivity factors known from literature.[22] Subsequently, high resolution detail scans of the C1s peak region (275-295 eV) were recorded with a pass energy of 50 eV. The C1s peak was normalised and the first subpeak (C-C) was set at 284.8 eV.

Contact angle measurements

Plasma treated PEO/PBT block copolymer films were characterized by static water contact angle measurements using the captive bubble method. The measurements were performed with a Video-based Optical Contact Angle Meter OCA 15 (DataPhysics Instruments GmbH, Filderstadt, Germany).

Samples were fixed onto glass slides with double-sided tape and immersed in water overnight. The sample slides were then mounted, with the polymer film facing downward, in an optical cuvette filled with water. Contact angles were determined by placing an air bubble (1-3 μl) on the sample with an electronically regulated syringe containing a hook-shaped needle. The contact angle was calculated by the provided SCA20 software (DataPhysics) using ellipse fitting. Contact angles were measured at five different spots on every sample.

Goat bone marrow cell (GBMC) compatibility experiments

The *in vitro* GBMC compatibility of the plasma treated PEO/PBT block copolymer films was tested by cell adhesion and/or growth experiments on these films. The experiments were performed by IsoTis NV (Bilthoven, The Netherlands) according to a standard operating procedure. A brief description is given here.

Sample discs (10 mm) were cut from the copolymer films and successively cleaned in 70% ethanol (15 min), distilled water (2x15 min), 70% ethanol (2 hrs) and PBS (rinsing twice). After washing, the samples were stored in α-MEM overnight at 37°C. Subsequently, GBMC's (passage 3) were seeded on the samples with a density of 10,000 cells/cm^2 in the presence of 3 ml culture medium (α-MEM, 15% Fetal Bovine Serum, 100 U/ml Peniciline/Streptomycine, 0.1 mM Asorbic acid-2-phosphate, 10^{-8} M Dexamethasone, 2 mM L-glutamine). After 6 days of culture at 37°C, the cells were fixed on the films with 1.5% glutaraldehyde and 0.14M cacodylate buffer (pH 7.2-7.4) and stained with methylene blue. The amount of adhered and proliferated cells was examined with a stereomicroscope.

8.3 Results and Discussion

8.3.1 Etching rates of homopolymers

PEG and PBT homopolymer layers were treated with a CO_2 or an Ar plasma to determine their etching rates. The results obtained with the QCM are presented in Figure 8.1. In a CO_2 plasma, PEG and PBT were etched at a rate of 19.8 and 8.0 nm/min, respectively. In an Ar plasma, the respective etching rates were substantially lower, 7.8 and 2.1 nm/min. At this point it should be noted that the etching rates of PEG in a CO_2 or Ar plasma did not change significantly at higher molecular weight (100,000 g/mol; data not shown). Since the aim of these experiments is to study the feasibility of preferential etching of PEO/PBT block copolymer films, most attention will be paid to the etching ratios of PEG vs. PBT rather than to the absolute values of the homopolymer's etching rates.

In a CO_2 plasma the PEG/PBT etching ratio was found to be 2.5, i.e. PEG was etched significantly faster in a CO_2 plasma than PBT. This etching ratio can be explained in both a physical and chemical way. PBT is a highly crystalline polymer with a high melting point (T_m>200°C), whereas PEG crystals already start melting at 55 °C. From literature it is known that the amorphous phase of a polymer is etched faster than the crystalline phase.[6,23-26] Also, a substantial surface temperature increase of the polymer layers can be expected during plasma

treatment[6,27-29], causing surface melting of polymers with a low T_m (PEG). A chemical explanation for the observed etching ratio can be found when comparing the chemical structure of the PEG backbone with that of the PBT backbone. The PEG and PBT backbone both contain relatively weak ether (C-O-C) sites which are more susceptible to dissociation in a reactive environment than the aliphatic C-C bonds and the aromatic ring structures that are only present in the PBT backbone.[30] Although ester linkages (PBT) are also vulnerable to oxidative degradation, the plasma susceptibility is suppressed by the attached aromatic ring structure.[30]

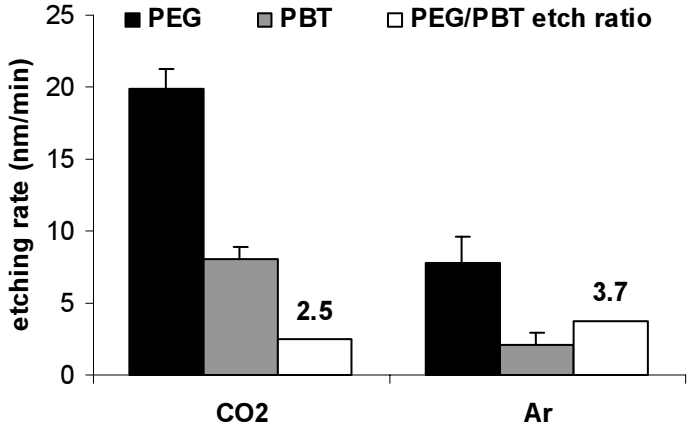

Figure 8.1: *QCM etching rates and etch ratios of PEG and PBT homopolymers in a CO_2 plasma and an Ar plasma (n=5, ±sd).*

In an Ar plasma, PEG was etched almost four times faster than PBT (PEG/PBT=3.7). Since Ar is a mild and non-oxidative etchant, the absolute etching rates were much lower than in a CO_2 plasma. Still, the etch selectivity of an Ar plasma was higher. Although the higher Ar plasma susceptibility of PEG as compared to PBT can be explained in a similar way as for a CO_2 plasma (see above), the higher etch selectivity should probably be attributed to a different chemical etch pathway. In an Ar plasma UV radiation plays a major role in the etching process[20,31,32], whereas in a CO_2 plasma oxidative degradation is mainly responsible for chemical etching.[2] UV bond cleavage is expected to be more selective (PEO vs. PBT) than oxidative degradation, since it does not affect the aromatic ring structures. On the other hand, UV radiation may induce crosslinking of PBT as well as PEO chains. Furthermore, the crystalline 'hard' phase (PBT) is likely to be less affected by UV etching than the amorphous 'soft' phase (PEO).

The results above indicate that preferential plasma etching can be expected in PEO/PBT block copolymer films, which may lead to surface restructuring. Besides changes of surface structure

(e.g. roughness) induced by preferential etching, changes of surface chemistry during plasma treatment could also have a large impact on the surface properties (e.g. wettability, biocompatibility) of the block copolymer films. Both aspects will be discussed in the following sections.

8.3.2 Surface structural changes during plasma treatment of PEO/PBT block copolymer films

Six different PEO/PBT block copolymer films, varying in composition and PEO block length, were treated with a CO_2 plasma (1 and 30 min) and an Ar plasma (30 min). Changes of surface structure during plasma treatment were studied by SEM analysis. Changes of surface topography and roughness were studied by AFM analysis. The resulting SEM pictures are presented in Figure 8.2, while Figure 8.3 shows some characteristic AFM height images of (un)treated PBT-rich copolymer films. The corresponding mean surface roughness data are presented in Table 8.1.

Table 8.1: Mean surface roughness (R_a) of untreated and 30 min CO_2 plasma treated PEO/PBT block copolymer films as calculated from AFM results (scanned surface area 2.5x2.5 μm; n=1).

Copolymer	R_a (nm) untreated	R_a (nm) 30 min CO_2
4000/30/70	8.8	9.9
4000/70/30	8.4	25.5
1000/30/70	19.8	15.6
1000/70/30	3.9	5.4
300/55/45	12.5	7.2
300/70/30	4.1	13.4

The untreated copolymer films had a varying surface roughness. Most PEO-rich films were quite smooth (1000/70/30, 300/70/30) while PBT-rich films seemed to be somewhat rougher (1000/30/70, 300/55/45). Crystalline regions in the PBT-rich 'hard' phase might explain the higher surface roughness of the PBT-rich films. The film preparation could also be partly responsible for an increased surface roughness. In this respect, it should be noted that all films were prepared by solution casting, except the 4000/30/70 film (Sympatex®) which was

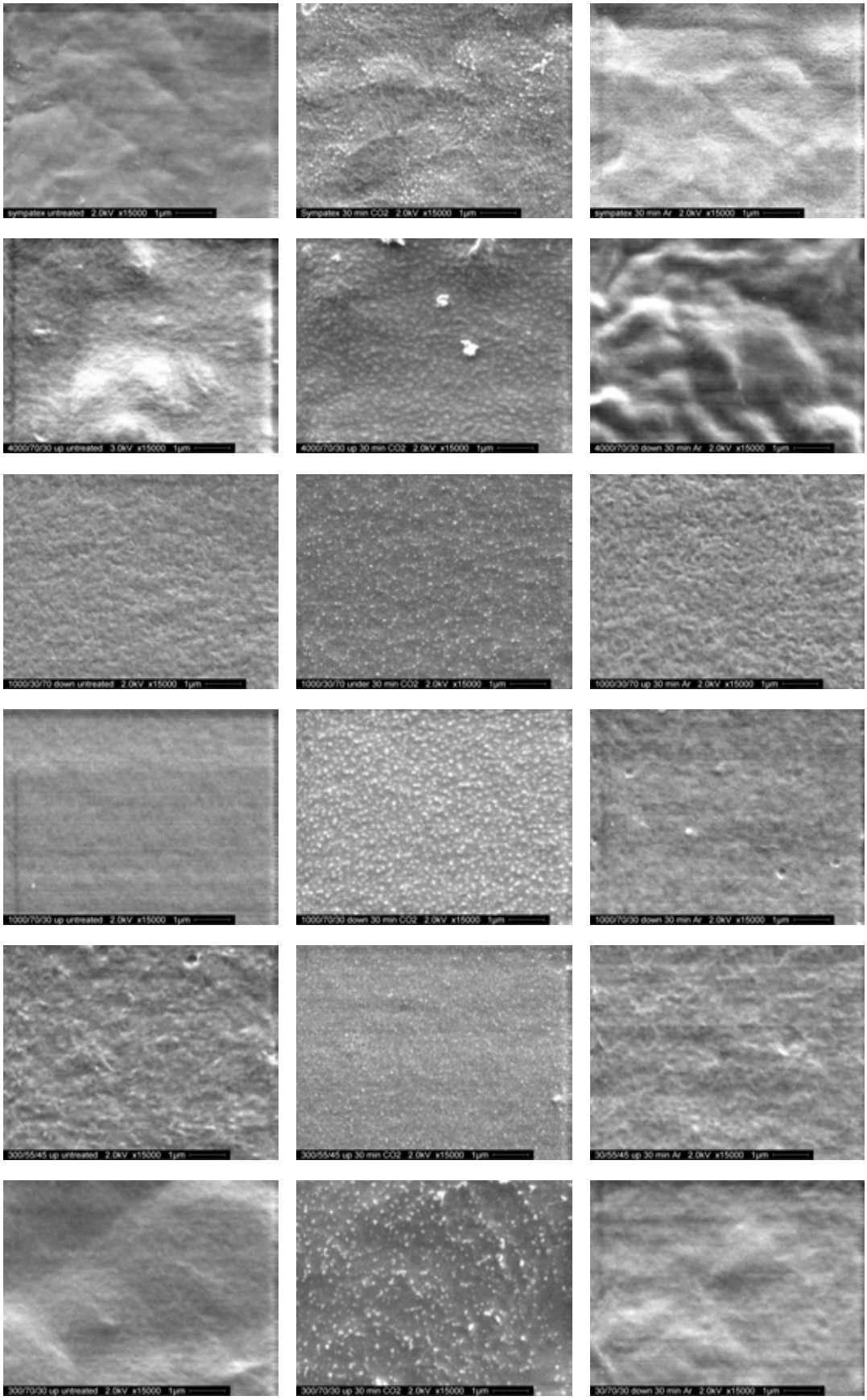

Figure 8.2: *SEM pictures of untreated (left), 30 min CO_2 plasma treated (middle), and 30 min Ar plasma treated (right) PEO/PBT block copolymer films (━━━ 2 μm).*

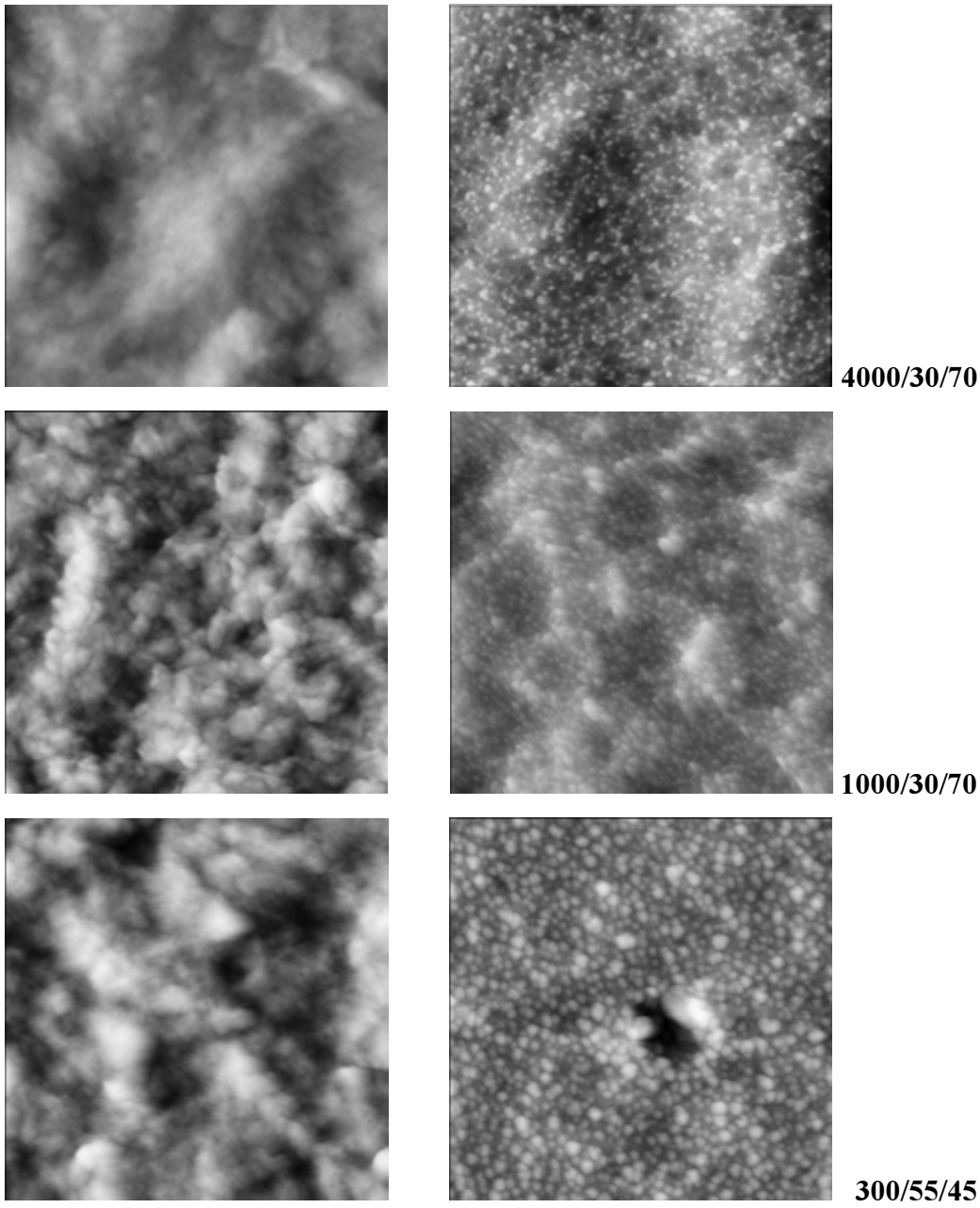

Figure 8.3: *AFM height images of untreated (left) and 30 min CO_2 plasma treated (right) PEO/PBT block copolymer films (scanned area 2.5x2.5 μm).*

prepared by melt extrusion.[33,34] The latter film preparation could also explain the relatively low surface roughness of the PBT-rich 4000/30/70 film as compared to the solution casted PBT-rich films (1000/30/70, 300/55/45). Generally, phase separation from the melt will result in a different surface structure than phase separation from solution. This should be kept in mind when comparing (un)treated 4000/30/70 films with the other copolymer samples.

After 1 min of CO_2 plasma treatment the surface structure of the copolymer films was not affected (pictures not shown). However, upon prolonged CO_2 plasma etching (30 min) the

surface nanostructure and topography changed quite drastically. In all cases a granular-type structure was observed at the surface, the granular size and density depending on the film composition. Table 8.1 shows that the surface roughness (R_a) of the PEO-rich films increased significantly upon CO_2 plasma etching, whereas R_a of the solution casted PBT-rich films decreased upon plasma etching. As discussed in the previous section, a general increase of surface roughness was expected upon preferential plasma etching of PEO/PBT block copolymers. However, the untreated 1000/30/70 and 300/55/45 films were already quite rough compared to the other samples (see also Figure 8.3), which could either be attributed to the 'rough' PBT-rich crystalline phase or to the film casting method ($R_a\uparrow$ due to solvent evaporation).

A closer look at the CO_2 plasma treated 4000/30/70 film (Figure 8.2) clearly reveals some crystalline regions (e.g. spherulites), originating from the PBT-rich 'hard' segments that were less affected by the etching process. However, the formed granular-type nanostructures at the surface of the solution casted films are less likely to be attributed to a plasma exposed crystalline phase. Although the origin of the granules cannot be explained in a straightforward way, temperature induced surface reorientation of the phase separated copolymer system upon plasma etching might be a probable cause. *In situ* temperature measurements (data not presented) have shown that the surface temperature of the films can easily exceed the melting temperature of the 'soft' PEO segments (30-60 ºC, depending on the molecular weight) during prolonged CO_2 plasma etching. Furthermore, when comparing the SEM pictures of plasma etched PEO-rich and PBT-rich films with the same PEO block length, it seems that the granular-type nanostructure is most pronounced for the former (cf. 1000/70/30 vs. 1000/30/70). This might suggest that PEO-rich films show a higher degree of phase separation than PBT-rich films. In a recent study, Deschamps *et al.* have shown that the extent of phase separation in PEO/PBT block copolymer films is strongly dependent on the polymer block length and the 'soft' to 'hard' segment ratio.[35] Microphase separation in these systems is enhanced by increasing the molecular weight of the starting PEG homopolymer (300 $\rightarrow$ 4000 g/mol) or by increasing the PBT content. The latter does not support the explanation given above, suggesting that PEO-rich films show a higher degree of phase separation than PBT-rich films. From the above it becomes clear that it is impossible to directly correlate the granular-type surface nanostructure of the CO_2 plasma etched copolymer films to the initial extent of microphase separation in the bulk of these materials.

Apart from some slight surface roughening, the surface structure of most PEO/PBT films did not change upon 30 min of Ar plasma treatment (Figure 8.2). The spherulitic surface structure, observed after CO_2 plasma etching of the 4000/30/70 film (see above), was hardly observed

after Ar plasma etching of this film. Apparently, longer Ar etching times are necessary to induce this kind of surface restructuring by preferential removal of the PEO-rich 'soft' phase. This was confirmed by trial treatments of 180 min (4000/30/70), after which the crystalline PBT regions were exposed more explicitly at the surface of the film (picture not shown). Thus, an Ar plasma should be considered as a very slow but preferential etchant for microphase separated, semi-crystalline copolymer systems, which is supported by the etching rate data presented before (Figure 8.1).

8.3.3 Surface chemical changes during plasma treatment of PEO/PBT block copolymer films

Besides changes of surface structure, plasma treatment undoubtedly leads to chemical modification of the polymer surface. High resolution XPS measurements were carried out on untreated and plasma treated PEO/PBT films to study these changes of surface chemistry. Before discussing the results presented in Figure 8.4 and Figure 8.5, the various processes that could affect the surface chemistry during or after plasma treatment will be addressed. At short treatment times the copolymer surface will strongly be oxidized by the CO_2 plasma due to the presence of highly reactive oxygen atoms. Surface oxygen incorporation is also expected after Ar plasma treatment by reaction of surface free radicals with oxygen in air (post-oxidation).

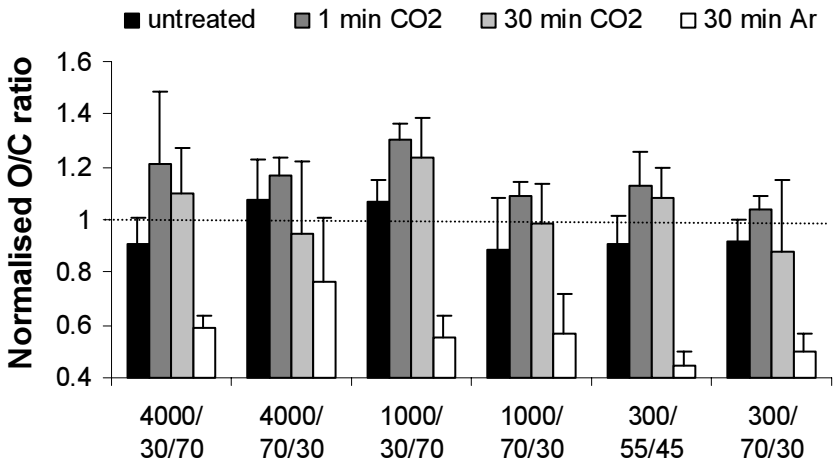

Figure 8.4: *Normalised O/C ratios of untreated and plasma treated PEO/PBT block copolymer films as determined by XPS measurements (n=4, ±sd). The normalised value is determined by dividing the measured O/C ratio through the theoretical (calculated) O/C ratio of the bulk copolymer.*

The effect of surface oxidation will be (partly) annulled by removal of oxygen containing fragments from the polymer backbone (etching) during plasma treatment. During prolonged

plasma treatment, preferential etching of PEO segments (as discussed in the previous sections) will result in surface enrichment of the PBT (crystalline) regions. Furthermore, after plasma treatment some kind of surface reorganisation (PEO enrichment) could possibly take place as a result of the rinsing procedure in a hydrophilic environment (water, ethanol). Yet, the latter effect may be undone by the drying step (*in vacuo*) following the rinsing procedure. Another, more probable rinsing effect could be the removal of oxidative degradation products from the surface of the films after plasma treatment.

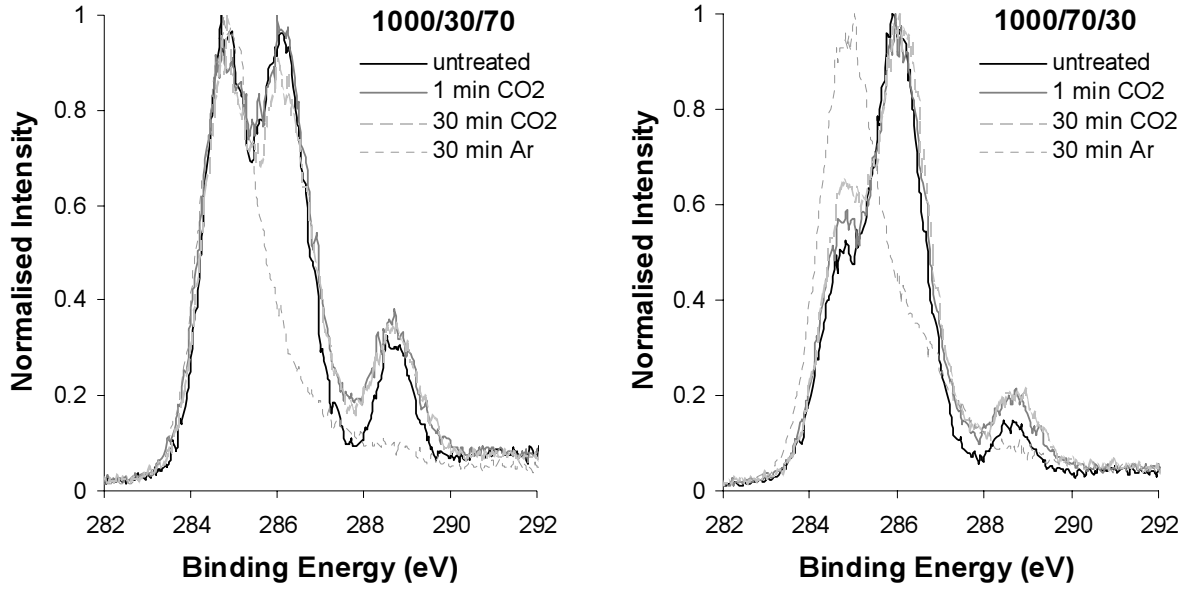

Figure 8.5: *Normalised high resolution XPS spectra of the C1s region of untreated and plasma treated 1000/30/70 (left) and 1000/70/30 (right) PEO/PBT block copolymer films.*

The interpretation of the XPS data will be based on the determined O/C ratios (Figure 8.4) and the high resolution XPS spectra of the C1s region (Figure 8.5). The theoretical (calculated) O/C ratio that is used for normalisation of the measured O/C ratios (Figure 8.4), is based on the initial PEO/PBT film composition taking into account one terephthalate unit at the end of every PEO block. Figure 8.5 shows two representative examples of the C1s region of (un)treated PBT-rich (1000/30/70) and PEO-rich (1000/70/30) films. Generally, the C1s region of the untreated copolymers can be deconvoluted into three different peaks (not shown). The first peak (284.8 eV)[36] is attributed to aromatic and aliphatic carbon bonds (C-C) primarily originating from the PBT blocks. The second peak (286.2-286.4 eV)[36] is ascribed to ether bonds (C-O) originating from the PEO as well as the PBT blocks. The third peak (288.7 eV)[36] is attributed to ester bonds (O-C=O) primarily originating from the PBT blocks.

Figure 8.4 shows the average results of four series of XPS measurements. Since the errors are rather large, the interpretation of the XPS results will be focussed on the trends that are observed for all block copolymer compositions. In this respect, it should be noted that these trends (i.e. an increase of the O/C ratio after CO_2 plasma treatment and a substantial O/C decrease after Ar plasma treatment) were observed for each series of measurements. The measured and normalised surface O/C ratios of most untreated films are fairly close to unity (0.9-1.1). This indicates that the chemical surface and theoretical composition of these films were quite similar. In principle, PBT is energetically favoured at the surface of a PEO/PBT film. Indeed, Figure 8.4 suggests a slight enrichment of PBT (i.e. normalised O/C ratio < 1) at the surface of most untreated copolymer compositions. Yet, the data in Figure 8.4 are not unambiguous with respect to this tentative conclusion.

Generally, it should be noted that minor surface contaminations were observed on a few of the (un)treated samples (e.g. Si). Control experiments have shown that these contaminations, in most cases not exceeding 1 at.%, are arbitrary and most probably introduced during sample handling. One exception was found for the 4000/30/70 film, which contained higher amounts of silicon (2-4 at.%) inherent to its industrial preparation (Sympatex®). The contact angle data in Figure 8.6 (discussed in the next section) clearly indicate that surface contamination, if present at all, did not have any (significant) effect on the surface properties of the films (i.e. silicon contamination would have induced much higher contact angles). Therefore, no further attention will be paid to this matter.

Upon plasma treatment the changes of the O/C ratio were quite similar for most copolymer films. These changes are nicely reflected in the C1s region of the high resolution XPS spectra shown in Figure 8.5. After 1 min of CO_2 plasma treatment an increase of the O/C ratio was observed (Figure 8.4), generally corresponding to a relative increase of carboxyl functionalities (Figure 8.5). Possibly, a fourth type of functionality was introduced during CO_2 (and Ar) plasma treatment of the films. This is believed to be an epoxide or carbonyl (C=O) functionality, since the corresponding peak was observed between the ether and ester carbon peaks at 287.0-287.5 eV.[36] Epoxide as well as carbonyl functionalities are known to occur after oxidative plasma treatment of polymer surfaces, due to the variety of chemical reactions in the plasma.[2] Since no surface structural changes occurred during short plasma treatment (see previous section), changes of surface chemistry are predominant at short treatment times. The relative increase of oxygen containing functionalities like C=O and O-C=O can therefore be attributed to surface oxidation by the CO_2 plasma. However, the stagnated (or even somewhat decreased) contribution of ether bonds indicates that the effect of surface oxidation

on the O/C ratio is being annulled by etching (oxidative degradation) of mainly PEO segments (C-O) during CO_2 plasma treatment.

The relative decrease of C-O bonds in comparison to C-C and O-C=O bonds becomes more obvious after prolonged CO_2 plasma etching (30 min; Figure 8.5). Preferential PEO removal is further supported by the slight decrease of O/C ratio (1 min CO_2 $\rightarrow$ 30 min CO_2) for all copolymer compositions (Figure 8.4). Obviously, surface oxidation has already reached its maximum after short treatment times, subsequently accompanied by oxidative degradation during the advanced stages of CO_2 plasma etching.

The O/C ratio was by far lowest after 30 min of Ar plasma etching. The strong relative increase of C-C bonds at the expense of ether functionalities (Figure 8.5) clearly illustrates preferential removal of PEO blocks during Ar plasma etching. Also, the Ar etched surfaces showed a substantial decrease of O-C=O groups, which was probably caused by radical formation at the ester linkage leading to removal of volatile CO_2 (decarboxylation). Decarboxylation is known to occur during Ar plasma treatment of polymers containing pendant carboxylic acid groups.[31,32] Therefore, it can also be expected (to a lesser degree) for polymers with ester bonds in the backbone.

Generally, the XPS data in Figure 8.4 and Figure 8.5 could be correlated to the expected processes that can occur during plasma treatment. Initial surface oxidation was succeeded by removal of oxidated degradation products and preferential etching of PEO blocks, the latter being most obvious after Ar plasma etching. The rinsing procedure that was applied after all plasma treatments may also have contributed to the removal of etched (degraded) material.

8.3.4 Wettability of plasma treated PEO/PBT block copolymer films

Water contact angle measurements were performed on all PEO/PBT films to study their wettability before and after plasma treatment. The captive bubble method was used since the water uptake of the films is in equilibrium under these conditions. Moreover, this aqueous environment resembles the conditions in which the films are tested for their GBMC compatibility (see next section). The water contact angles are plotted in Figure 8.6.

All untreated films were moderately hydrophilic with contact angles ranging from 35° for PEO-rich films (4000/70/30) to 48° for PBT-rich films (4000/30/70). Generally, the wettability of the films increased significantly after 1 min of CO_2 plasma treatment. A further increase of wettability to contact angles of 23° for PEO-rich films was observed upon prolonged CO_2 plasma etching. Ar plasma etching also induced an increase of surface wettability, although in most cases this increase was less pronounced than observed after CO_2 plasma treatment.

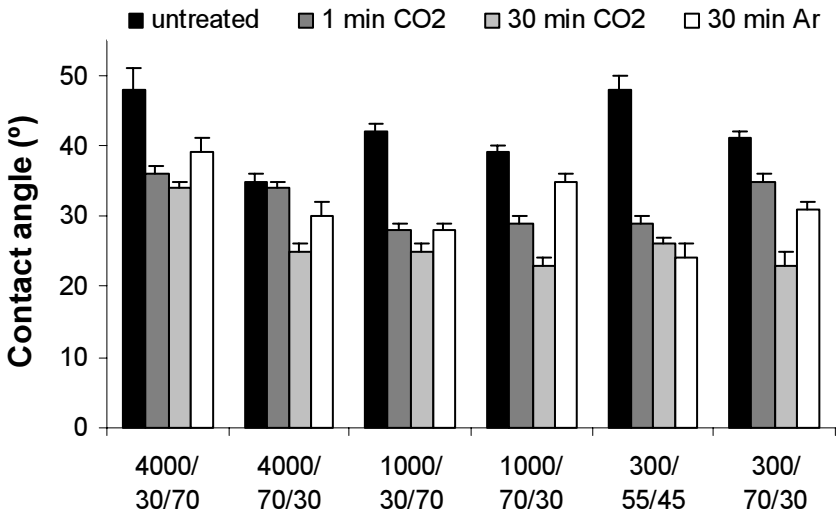

Figure 8.6: *Static water contact angles of untreated and plasma treated PEO/PBT block copolymer films as determined by the captive bubble method (n=5, ±sd).*

Although changes of surface chemistry are largely responsible for the general increase of wettability (discussed below), the results found by contact angle measurements cannot be directly correlated to the surface chemical data discussed previously (Figure 8.4 and Figure 8.5). This can be explained by substantial differences in the analysis depth and the physical state of the samples during contact angle measurements and XPS analysis. XPS analyses a relatively thick and dry surface layer of 5-10 nm, whereas the contact angle is determined by the outermost surface (<1 nm) of hydrated films. A straightforward comparison is therefore impossible.

When comparing the contact angles of untreated films with the same PEO block length it is obvious that in all three cases the PEO-rich film (70%) was more hydrophilic. PEO is a hydrophilic polymer due to its polar backbone while PBT is hydrophobic, resulting in an average surface wettability for the PEO/PBT block copolymers depending on the PEO/PBT ratio. After 1 min of CO_2 plasma treatment these initial differences have largely disappeared. In most cases, the wettability increased substantially, irrespective of the initial PEO/PBT ratio. This wettability increase can be directly attributed to oxidation during CO_2 plasma treatment. It is generally known that CO_2 plasma treatment of polymer films causes an increase of surface wettability, due to introduction of polar functional groups at the surface.[2] When a surface comes into contact with an aqueous (polar) environment the outward directed surface polar groups (e.g. OH, COOH), introduced by plasma oxidation, mainly determine the contact angle. In this respect, the initial surface PEO/PBT ratio is of minor importance for the final surface properties of the films after CO_2 plasma treatment. Extensive oxidation and subsequent

degradation of the polymer backbone during prolonged CO_2 plasma etching resulted in a further decrease of contact angles.

Also, the increase of wettability caused by Ar plasma etching can be attributed to surface oxidation.[37] In this case the polar functional groups were mainly introduced after plasma treatment by reactions of surface free radicals with oxygen in air (post-oxidation). Still, it is obvious that the overall effect of an Ar plasma is less extreme than that of a CO_2 plasma, since in most cases the induced wettability increase was less pronounced after the former treatment. Preferential etching of PEO blocks may have influenced the surface wettability after Ar plasma etching, although the exact contribution of surface structural changes to the resulting contact angles was not clear from the data in Figure 8.6.

Generally, it can be concluded that surface oxidation during or after plasma treatment was mainly responsible for the substantial increase of wettability, thereby reducing the initial contact angle differences related to the PEO/PBT ratio of the films. The XPS data in Figure 8.4 confirm that surface oxidation of the films took place during CO_2 plasma treatment (O/C ratio ↑). However, surface post-oxidation of the films upon Ar plasma etching, as suggested above, clearly did not result in a net increase of O/C ratio (Figure 8.4).

8.3.5 *In vitro* GBMC compatibility of plasma treated PEO/PBT block copolymer films

Finally, some *in vitro* cell adhesion and/or growth experiments were carried out to study the effect of surface chemical and structural changes on the GBMC compatibility of untreated vs. plasma treated PEO/PBT films. The (qualitative) results of these experiments are presented in Table 8.2.

Most untreated copolymer films did not show any substantial cell adhesion and/or growth, with the exception of the 300/55/45 film and (to a lesser extent) the 300/70/30 film. After CO_2 plasma treatment of the films cell adhesion and/or growth was greatly enhanced, irrespective of the film composition and treatment time. Also, Ar plasma etching substantially improved the GBMC compatibility of PEO/PBT films with a PEO block length of 1,000 g/mol.

The cell adhesion and/or growth on untreated PEO/PBT films seemed to be somewhat related to the film composition. Still, the surface structure, chemistry and wettability of untreated, compatible 300/55/45 and 300/70/30 films (Figure 8.2 to Figure 8.6) did not differ substantially from the surface characteristics of the non-compatible copolymers. Based on these data, it is not directly clear which surface property is responsible for the GBMC compatibility of the untreated 300- films. One phenomenon that plays a major role in the initial stage of all cell adhesion processes is protein adsorption. The type, amount and conformation

of a protein adsorbed onto a biomaterial largely determines the ability of cells to adhere onto the biocoated surface. Thus, some change in protein adsorption induced by a specific film composition or surface morphology could be one possible explanation for the GBMC compatibility of the 300- films. In this respect, the degree of phase separation, being lowest for the 300- films as shown by Deschamps *et al.*[35] and discussed in section 8.3.2, may be (partly) responsible for the observed differences in GBMC compatibility.

Table 8.2: Goat bone marrow cell adhesion and/or growth on untreated and plasma treated PEO/PBT block copolymer films after 6 days of culture.

Copolymer	Untreated	1 min CO_2	30 min CO_2	30 min Ar
4000/30/70	-	nd	++	nd
4000/70/30	-	nd	+	nd
1000/30/70	-	++/+++	+++	+/++
1000/70/30	-	+++	+/++	+/++
300/55/45	+	nd	+/++	nd
300/70/30	±	nd	+++	nd

- : no cell adhesion/growth
+ : cell adhesion/growth
nd : not determined

The initial differences of GBMC compatibility largely disappeared after CO_2 plasma treatment. Although subtle differences of cell adhesion and/or growth were still present after plasma treatment, no clear relation could be found between the initial film composition and the GBMC compatibility. Since the cell adhesion and/or growth was greatly enhanced already after short CO_2 plasma treatment times, changes of surface chemistry (oxidation) rather than changes of surface structure (roughness) must have been responsible for this drastic improvement. Currently, it is believed that the introduction of polar functional groups at the PEO/PBT surface during plasma treatment, causing a general increase of surface wettability (Figure 8.6), is mainly responsible for the enhanced cell adhesion and/or growth on all films. These polar surface groups most probably induced substantial changes of protein adsorption (amount, type, conformation) at the surface of the oxidized films, which inherently results in changes of cell adhesion (see above). The introduction of polar surface groups would also explain the increased GBMC compatibility of PEO/PBT films after Ar plasma etching and post-oxidation.

The above results clearly point out that CO_2 or Ar plasma treatment is a versatile tool to improve the GBMC compatibility of PEO/PBT films, irrespective of their initial composition. In other words, an optimal copolymer composition can be chosen on the basis of the desired bulk properties (e.g. physical, mechanical, biodegradable) of the biomaterial that can be subsequently compatibilised for bone cells by plasma treatment. Future experiments should further optimise plasma treatment conditions in order to extrapolate these promising results to porous PEO/PBT copolymer scaffolds that are suitable for bone tissue regeneration.

8.4 Conclusions

This study has shown that gas plasma etching (CO_2 or Ar) significantly changed the surface properties (chemistry, structure, wettability) of a series of PEO/PBT segmented block copolymer films, which resulted in a greatly enhanced GBMC compatibility of this biomaterial. Short CO_2 plasma treatment (1 min) mainly caused oxidation of the films without changing the surface structure. During prolonged CO_2 plasma etching (30 min) of the films surface oxidation and oxidative degradation was observed besides the formation of a granular-type nanostructure. Ar plasma etching resulted in preferential removal of PEO blocks without strongly affecting the surface structure of the films. In all cases, the surface wettability of the films significantly increased upon plasma treatment, which was mainly attributed to the introduction of polar surface groups. The latter is considered to be responsible for the drastic increase of GBMC adhesion and/or growth on all plasma treated films in comparison to the untreated biomaterial. Plasma treated PEO/PBT copolymers therefore seem to be good candidates for bone tissue regeneration, without changing the biomaterial's desired bulk properties (e.g. strength, biodegradability).

8.5 Acknowledgements

Joop de Vries (Department of Biomedical Engineering, University of Groningen) is acknowledged for performing the high resolution XPS measurements. Mark Smithers and Clemens Padberg (MESA+ Institute, University of Twente) are acknowledged for performing the SEM and AFM measurements. IsoTis NV (Bilthoven) is acknowledged for performing the *in vitro* GBMC compatibility experiments. This study was financed by the Netherlands Foundation for Chemical Research (NWO-CW).

8.6 References

1) Terlingen, J. G. A. *Introduction of functional groups at polymer surfaces by glow discharge techniques*; University of Twente: Enschede, The Netherlands, 1993.
2) Takens, G. A. J. *Functionalization of polymeric surfaces by oxidative gas plasma treatment*; University of Twente: Enschede, The Netherlands, 1997.
3) Dewez, J. L.; Humbeek, E.; Everaert, E.; Doren, A.; Rouxhet, P. G. *Plasma treated polymer films: Relationship between surface composition and surface hydrophilicity*; Pireaux, J. J., Bertrand, P. and Brédas, J. L., Ed.; IOP Publishing Ltd: Bristol, 1992, pp 463-474.
4) Wu, S. *Polymer Interface and Adhesion*; Marcel Dekker, Inc.: New York, 1982.
5) Choi, D. M.; Park, C. K.; Cho, K.; Park, C. E. *Polymer* **1997**, *38*, 6243-6249.
6) Olde Riekerink, M. B.; Terlingen, J. G. A.; Engbers, G. H. M.; Feijen, J. *Langmuir* **1999**, *15*, 4847-4856.
7) Park, M.; Harrison, C.; Chaikin, P. M.; Register, R. A.; Adamson, D. H. *Science* **1997**, *276*, 1401-1404.
8) Mansky, P.; Harrison, C. K.; Chaikin, P. M.; Register, R. A.; Yao, N. *Appl. Phys. Lett.* **1996**, *68*, 2586-2588.
9) Avgeropoulos, A.; Chan, V. Z.-H.; Lee, V. Y.; Ngo, D.; Miller, R. D.; Hadjichristidis, N.; Thomas, E. L. *Chem. Mater.* **1998**, *10*, 2109-2115.
10) Beumer, G. J.; van Blitterswijk, C. A.; Ponec, M. *J. Biomed. Mater. Res.* **1994**, *28*, 545-552.
11) Dorp, A. G. M. v.; Verhoeven, M. C. H.; Koerten, H. K.; van Blitterswijk, C. A.; Ponec, M. *J. Biomed. Mater. Res.* **1999**, *47*, 292-300.
12) Grote, J. J.; Bakker, D.; Hesseling, S. C.; van Blitterswijk, C. A. *Am. J. Otology* **1991**, *12*, 329-335.
13) Bezemer, J. M. *Protein Release Systems based on Biodegradable Amphiphilic Multiblock Copolymers*; University of Twente: Enschede, The Netherlands, 1999.
14) van Blitterswijk, C. A.; Brink, J. v. d.; Leenders, H.; Bakker, D. *Cell. Mater.* **1993**, *3*, 23-36.
15) Radder, A. M.; Leenders, H.; van Blitterswijk, C. A. *J. Biomed. Mater. Res.* **1996**, *30*, 341-351.
16) Meijer, G. J.; Dooren, A. v.; Gaillard, M. L.; Dalmeijer, R.; Putter, C. d.; Koole, R.; van Blitterswijk, C. A. *Int. J. Oral Maxillofacial Surg.* **1996**, *25*, 210-216.
17) Marler, J. J.; Upton, J.; Langer, R.; Vacanti, J. P. *Adv. Drug Delivery Rev.* **1998**, *33*, 165-182.
18) Beumer, G. J.; van Blitterswijk, C. A.; Ponec, M. *J. Mater. Sci.-Mater. Medicine* **1994**, *5*, 1-6.
19) Bowers, K. T.; Keller, J. C.; Wick, D. G.; Randolph, B. A. *J. Dental Res.* **1990**, *69*, 370.
20) Terlingen, J. G. A.; Hoffman, A. S.; Feijen, J. *J. Appl. Polym. Sci.* **1993**, *50*, 1529-1539.
21) Deschamps, A. A.; Claase, M. B.; Sleijster, W. J.; de Bruijn, J. D.; Grijpma, D. W.; Feijen, J. *J. Controlled Release* **2001**, accepted.
22) Wagner, C. D.; Davis, L. E.; Zeller, M. V.; Taylor, J. A.; Raymond, R. H.; Gale, L. H. *Surf. Interface Anal.* **1981**, *3*, 211-225.
23) Herbert, S.; Shinozaki, D. M.; Collacott, R. J. *J. Mater. Sci.* **1996**, *31*, 4655-4661.
24) Okuno, T.; Yasuda, T.; Yasuda, H. *Textile Res. J.* **1992**, *62*, 474-480.
25) Friedrich, J.; Gähde, J.; Frommelt, H.; Wittrich, H. *Faserforsch. Textiltechnik* **1976**, *27*, 604-608.
26) Friedrich, J.; Gähde, J. *Acta Polymerica* **1980**, *31*, 52-58.
27) Durandet, A.; Joubert, O.; Pelletier, J.; Pichot, M. *J. Appl. Phys.* **1990**, *67*, 3862-3866.
28) ter Beek, M. *Immobilisatie van enzymen aan oppervlakte gemodificeerde polyethyleen membranen (not published)*; University of Twente: Enschede, The Netherlands, 1994.
29) Olde Riekerink, M. B.; Engbers, G. H. M.; Feijen, J. *Chapter 4 of this thesis.*
30) Yasuda, H.; Lamaze, C. E.; Sakaoku, K. *J. Appl. Polym. Sci.* **1973**, *17*, 137-152.

31) Terlingen, J. G. A.; Takens, G. A. J.; Gaag, F. J. v. d.; Hoffman, A. S.; Feijen, J. *J. Appl. Polym. Sci.* **1994**, *52*, 39-53.
32) Groenewoud, L. M. H.; Terlingen, J. G. A.; Engbers, G. H. M.; Feijen, J. *Langmuir* **1999**, *15*, 5396-5402.
33) Gebben, B. *J. Membr. Sci.* **1996**, *113*, 323-329.
34) Gebben, B. *Thermoplastic Elastomers Course*: University of Twente, Enschede, The Netherlands, 1997.
35) Deschamps, A. A.; Grijpma, D. W.; Feijen, J. *Polymer* **2001**, *42*, 9335-9345.
36) Beamson, G.; Briggs, D. *High resolution XPS of organic polymers: the Scienta ESCA300 database*; Wiley: Chichester, 1992.
37) Lens, J. P. *Gas plasma immobilization of surfactants to improve the blood compatibility of polymeric surfaces*; University of Twente: Enschede, The Netherlands, 1996.

Summary

Nowadays, polymeric materials are used for a wide variety of applications. The choice for a specific polymer is usually based on its bulk properties (e.g. mechanical, physical), which are mainly determined by the bulk chemistry and structure of the processed material. For many applications the polymer's surface properties are of major importance. Gas plasma treatment has proven to be a versatile tool for surface modification of polymeric materials. Besides being a dry (solvent-free) and time-efficient process, the main advantage of this technique is its confinement to the surface layer of a material. Structural and chemical surface modification of phase separated polymer systems (e.g. semi-crystalline polymers, block copolymers, organic-inorganic hybrid materials) by means of gas plasma treatment is of great interest for tailoring a wide variety of interfacial properties without affecting the material's desired bulk properties (e.g. strength, toughness, biodegradability). Surface characteristics like wettability, adhesion, printability, friction, fouling, and biocompatibility largely determine the applicability of polymeric materials (e.g. thermoplastic objects, coatings, films, membranes, fibers, textiles, biomaterials) in various industrial areas (e.g. automotive, packaging, filtration, clothing, biomedical technology). Furthermore, nanostructuring of phase separated polymer systems has become increasingly important for the fast growing area of nanotechnology. Nanopatterned polymer templates have a huge potential as etching masks in nanolithographic processing.
The objective of the study described in this thesis is to explore the possibilities of gas plasma etching as a tool to tailor the surface properties of polymeric and hybrid systems. The primary goal is to induce surface nanostructuring by preferential etching of one component from a two-phase system (e.g. crystalline vs. amorphous, organic vs. inorganic, polymer A vs. polymer B). Inherently, chemical surface modification will occur during gas plasma etching. The basic principles of this complicated process are outlined in **Chapter 2**. Furthermore, a literature survey on (preferential) etching of polymer surfaces is given and the factors that determine the plasma etching rate of a polymer are discussed in more detail. Finally, the current status of developing nanostructured polymer surfaces and its (potential) applications in areas like nanotechnology, membrane technology and biomedical technology are described in this chapter.

The first experimental part of this thesis (chapters 3-5) is focussed on gas plasma etching of a semi-crystalline polymer, poly(ethylene) (PE). In **Chapter 3**, a series of commercial PE films with varying crystallinity is treated with a CF_4 gas plasma. The etching behaviour and surface

chemical and structural changes of the PE films upon plasma etching were studied by weight measurements, X-ray Photoelectron Spectroscopy (XPS), water contact angle measurements, Scanning Electron Microscopy (SEM) and Atomic Force Microscopy (AFM). Besides preferential etching of the amorphous phase, the PE films were highly fluorinated during CF_4 plasma treatment ($F/C \leq 1.6$). Moreover, prolonged CF_4 plasma treatment of PE ($\geq$ 15 min) resulted in extremely hydrophobic surfaces ($\theta_a \leq 150°$), which was mainly caused by a pronounced surface restructuring. The lamellar surface structure of low density PE (LDPE) changed into a nanoporous-like structure with uniform pores and grains on the order of tens of nanometers. This structural change during continuous CF_4 plasma treatment was attributed to a combined effect of etching and an increase of surface temperature, resulting in phase separation of PE-like and poly(tetrafluoroethylene)-like material of which the latter is surface oriented.

The surface chemical and structural modification of LDPE upon CF_4 plasma treatment is further described in **Chapter 4**. The effect of temperature rise (*in situ* fluoroptic temperature measurements) and fluorination (XPS) on the surface structure (SEM), wettability (contact angle measurements) and stability (aging) of LDPE films was studied as a function of the plasma treatment time. Initially, the surfaces were rapidly fluorinized (< 15 s) leading to increased surface heterogeneity. Substantial surface restructuring took place between 5 and 15 min of treatment. This drastic change of surface structure was attributed to a temperature induced phase separation (or demixing) of fluorinated and non-modified LDPE domains. In contrast to continuous treatment, no substantial surface temperature increase was observed during pulsed treatment, thus preventing surface restructuring. The fluorinated, superhydrophobic films were not susceptible to aging, but did show a large hysteresis due to an increased surface heterogeneity and roughness.

In **Chapter 5**, some bio-interfacial properties of CF_4 plasma etched LDPE films are discussed. The effect of surface energy, roughness and charge on the fouling behaviour of these superhydrophobic films was investigated by performing *in vitro* adhesion experiments with several microbes (four different bacterial strains and one yeast strain). Microbial adhesion onto superhydrophobic LDPE was compared with adhesion onto three reference materials (untreated LDPE, fluorinated ethylene propylene copolymer (FEP) and poly(ethylenimine) (PEI) coated LDPE). Surprisingly, in most cases superhydrophobization of LDPE films did not lead to a substantial decrease of microbial adhesion. Changes of surface roughness and energy did not seem to affect the bioadhesive properties of the films, whereas inverting the film surface charge (from negative to positive) led to a much higher initial microbial adhesion.

Gas plasma etching of polymeric membranes is described in **Chapter 6**. The aim of this study was to explore the possibilities to tailor the properties of asymmetric, cellulose acetate membranes (e.g. permeability, wettability, retention, fouling) by gradual etching of the membrane's toplayer with oxidative (CO_2) or fluorinizing (CF_4) gas plasma treatment. SEM, XPS and contact angle measurements were used to characterize the membrane's toplayer, while the membrane properties (e.g. permeability, selectivity, fouling) were studied by water flux measurements, molecular weight cutoff (MWCO) measurements and fouling experiments. CO_2 plasma treatment resulted in gradual etching of the membrane's dense toplayer, which led to significant changes of permeation and selectivity. Both the water flux and MWCO of cellulose triacetate (CTA) membranes increased with treatment time, the latter increase being linear. Moreover, CTA membranes were hydrophilized during CO_2 plasma treatment, whereas CF_4 plasma treatment led to hydrophobic surfaces due to strong fluorination of the toplayer. By simultaneously modifying the chemistry and structure of the toplayer, the membrane properties could be tailored with gas plasma etching without affecting its low fouling character.

Surface nanostructuring of a two-phase hybrid system (organic vs. inorganic) by using oxidative plasma etching (CO_2, air) is described in **Chapter 7**. Protein-gold nanocolloids (10-20 nm) were adsorbed onto various substrates (e.g. glass, silicon, poly(styrene), LDPE) from an aqueous solution in a one-step procedure. Besides the role as adsorbate, the protein could also serve as a spacer, maintaining a lateral distance between the adsorbed particles. After adsorption the protein was removed from the gold nanoparticles by selective plasma etching. Subsequently, the substrates were characterized by SEM, AFM and XPS to study the surface nanoparticle distribution, topography and chemistry, respectively. Adsorption of albumin-gold (AGC) and protein A-gold (PAGC) nanocolloids and subsequent protein removal was succesful on most substrates, the surface nanoparticle density being highest for AGC adsorbed onto glass. On all substrates AGC was randomly distributed at the surface. Selective chemical modification of these heterogeneous, nanostructured surfaces is feasible as was shown by selective thiol chemisorption onto silane physisorbed gold control substrates.

Chapter 8 is directed to a study in which a block copolymer system was subjected to oxidative (CO_2) and mild (Ar) gas plasma etching. The effect of chemical (XPS) and structural (SEM, AFM) surface modification on the wettability (contact angle measurements) and biocompatibility (bone cell adhesion and growth) of a series of segmented poly(ethylene oxide)/poly(butylene terephthalate) (PEO/PBT) block copolymer films was investigated in this

final chapter. In all cases, prolonged CO_2 plasma etching caused a substantial surface structural change. A granular-type nanostructure was formed, which could possibly be attributed to temperature induced surface reorientation of the phase separated copolymer system. Surface chemical changes upon plasma treatment were quite similar for most film compositions. CO_2 plasma treatment caused surface oxidation and oxidative degradation of the films, while Ar plasma etching mainly resulted in preferential removal of PEO blocks. Generally, the wettability of the films significantly increased after plasma treatment due to creation of polar functional groups at the surface. Preliminary goat bone marrow cell compatibility experiments have shown that all plasma treated PEO/PBT films induced a greatly enhanced cell adhesion and/or growth compared to the untreated biomaterial. This improvement was attributed to changes of surface chemistry rather than to changes of surface structure during plasma etching. These results show that plasma treated PEO/PBT copolymers have a high potential as scaffolds for bone tissue regeneration.

Samenvatting

Tegenwoordig worden polymeren gebruikt voor een grote verscheidenheid aan toepassingen. De keuze voor een bepaald polymeer is meestal gebaseerd op zijn bulkeigenschappen (mechanisch, fysisch) die vooral worden bepaald door de bulkchemie en -structuur van het verwerkte materiaal. Voor veel toepassingen zijn echter ook de oppervlakte-eigenschappen van het polymeer van groot belang. Gasplasmabehandeling blijkt een zeer geschikte techniek te zijn voor de oppervlaktemodificatie van polymeren. Deze snelle en oplosmiddelvrije techniek heeft als groot voordeel dat de behandeling zich beperkt tot het oppervlak van een materiaal. Structurele en chemische oppervlaktemodificatie van fasengescheiden polymeersystemen (bijv. semi-kristallijne polymeren, blokcopolymeren, organisch-anorganische hybride materialen) door middel van gasplasmabehandeling is erg interessant voor het afstemmen van diverse oppervlakte-eigenschappen zonder daarbij de gewenste bulk-eigenschappen van het materiaal (bijv. sterkte, taaiheid, biodegradeerbaarheid) aan te tasten. Oppervlaktekarakteristieken zoals bevochtigbaarheid, hechting, afdrukbaarheid, wrijving, bevuiling en biocompatibiliteit bepalen grotendeels de toepasbaarheid van polymeren (bijv. thermoplastische voorwerpen, coatings, films, membranen, vezels, textielen, biomaterialen) in diverse industriële gebieden (bijv. automobiel- en verpakkingsindustrie, filtratie, kleding, biomedische technologie). Bovendien wordt het nanostructureren van fasengescheiden polymeersystemen steeds belangrijker voor de snel groeiende nanotechnologie sector. Polymeersjablonen met een bepaald nanopatroon zouden heel goed als etsmaskers kunnen fungeren voor nanolithografische processen.

Het doel van de in dit proefschrift beschreven studie is om te onderzoeken wat de mogelijkheden van gasplasmabehandeling zijn als etstechniek voor het afstemmen van de oppervlakte-eigenschappen van polymeer- en hybridesystemen. Daarbij wordt primair gestreefd naar het induceren van nanostructurering van het oppervlak door preferentieel etsen van één component uit een tweefasensysteem (bijv. kristallijn en amorf, organisch en anorganisch, polymeer A en polymeer B). Tijdens het etsen met een gasplasma wordt het oppervlak van een materiaal altijd chemisch gemodificeerd. De basisprincipes van dit gecompliceerde proces worden besproken in **hoofdstuk 2**. Tevens wordt een literatuur-overzicht gegeven van het (preferentieel) etsen van polymeeroppervlakken. Ook de factoren die de etssnelheid van een polymeer in een plasma bepalen, zullen nader worden besproken. Tenslotte zullen de huidige status van de ontwikkeling van nanogestructureerde polymeer-

oppervlakken en de (mogelijke) toepassingen in gebieden zoals nanotechnologie, membraantechnologie en biomedische technologie in dit hoofdstuk worden beschreven.

Het eerste experimentele gedeelte van dit proefschrift (hoofdstukken 3 t/m 5) is gericht op het etsen van een semi-kristallijn polymeer, polyetheen (PE), met een gasplasma. In **hoofdstuk 3** wordt een serie commerciële PE films behandeld met een CF_4 plasma. Het etsgedrag van de PE films en de chemische en structurele veranderingen aan het oppervlak als gevolg van de plasmabehandeling werden bestudeerd met gewichtsmetingen, röntgen geïnduceerde foto-electron spectroscopie (XPS), randhoekmetingen met water, elektronenmicroscopie (SEM) en atomaire krachtmicroscopie (AFM). Tijdens CF_4 plasmabehandeling werd de amorfe fase van de PE films preferentieel weggeëtst en vond tevens sterke fluoridering van het oppervlak plaats (F/C $\leq$ 1,6). Bovendien resulteerde langdurige CF_4 plasmabehandeling van PE ($\geq$ 15 min) in zeer hydrofobe oppervlakken ($\theta_a \leq 150°$), hetgeen voornamelijk werd veroorzaakt door een uitgesproken verandering van de oppervlaktestructuur (herstructurering). De lamellaire oppervlaktestructuur van lage dichtheid PE (LDPE) veranderde in een nanoporeus-achtige structuur bestaande uit uniforme poriën en korrels in de orde van grootte van tientallen nanometers. Deze structurele verandering tijdens continu CF_4 plasmabehandeling werd toegeschreven aan een gecombineerd effect van etsen en een temperatuurtoename aan het oppervlak, hetgeen resulteerde in fasenscheiding van PE-achtig en polytetrafluoretheen-achtig materiaal, waarvan laatstgenoemde zich aan het oppervlak bevond.
De chemische en structurele modificatie van het LDPE oppervlak als gevolg van CF_4 plasmabehandeling wordt nader beschreven in **hoofdstuk 4**. Het effect van temperatuur-toename (*in situ* fluoroptische temperatuurmetingen) en fluoridering (XPS) op de oppervlakte-structuur (SEM), bevochtigbaarheid (randhoekmetingen) en stabiliteit (veroudering) van LDPE films werd bestudeerd als functie van de plasmabehandelingstijd. In eerste instantie werden de oppervlakken snel gefluorideerd (< 15 s), hetgeen leidde tot een toename van de heterogeniteit aan het oppervlak. Een aanzienlijke herstructurering van het oppervlak trad op tussen 5 en 15 minuten behandeling. Deze drastische verandering van de oppervlaktestructuur werd toegeschreven aan een door temperatuur geïnduceerde fasenscheiding (of ontmenging) van gefluorideerde en niet-gemodificeerde LDPE domeinen. In tegenstelling tot continu behandeling werd er geen substantiële temperatuurtoename waargenomen tijdens gepulseerde behandeling, waardoor herstructurering van het oppervlak werd voorkomen. De gefluorideerde, superhydrofobe films waren niet gevoelig voor veroudering, maar lieten wel een grote hysterese zien vanwege de toegenomen heterogeniteit en ruwheid van het oppervlak.

In **hoofdstuk 5** wordt een aantal biologische oppervlakte-eigenschappen van met CF_4 plasma geëtste LDPE films besproken. Het effect van de oppervlakte-energie, -ruwheid en -lading op het bevuilingsgedrag van deze superhydrofobe films werd onderzocht door het uitvoeren van *in vitro* hechtingsexperimenten met diverse microben (vier verschillende bacteriestammen en een gist). Microbiële hechting op superhydrofoob LDPE is vergeleken met de hechting op drie referentiematerialen (onbehandeld LDPE, gefluorideerd etheen propeen copolymeer (FEP) en LDPE voorzien van een polyetheenimine (PEI) coating). In de meeste gevallen leidde superhydrofobisering van LDPE films niet tot een duidelijke afname van de microbiële hechting. Veranderingen van de oppervlakteruwheid en -energie leken de biohechtingseigenschappen van de films niet te beïnvloeden, terwijl het omkeren van de oppervlaktelading van de films (van negatief naar positief) een veel hogere initiële microbiële hechting veroorzaakte.

Het etsen van polymere membranen met een gasplasma wordt beschreven in **hoofdstuk 6**. Het doel van deze studie is om de mogelijkheden te onderzoeken voor het afstemmen van de eigenschappen van asymmetrische celluloseacetaat membranen (permeabiliteit, bevochtigbaarheid, retentie, bevuiling) door middel van het geleidelijk etsen van de toplaag van het membraan met een oxidatieve (CO_2) of fluoriderende (CF_4) gasplasmabehandeling. SEM, XPS en randhoekmetingen werden gebruikt om de toplaag van het membraan te karakteriseren, terwijl de membraaneigenschappen (permeabiliteit, selectiviteit, bevuiling) werden bestudeerd met waterfluxmetingen, retentiemetingen (MWCO) en bevuilingsexperimenten. CO_2 plasmabehandeling leidde tot het geleidelijk etsen van de toplaag van het membraan, hetgeen resulteerde in significante veranderingen van de permeabiliteit en de selectiviteit. Zowel de waterflux als de MWCO van cellulosetriacetaat (CTA) membranen namen toe als functie van de behandelingstijd, waarbij de laatstgenoemde toename lineair bleek te zijn. CTA membranen werden gehydrofiliseerd tijdens CO_2 plasmabehandeling, daar waar CF_4 plasmabehandeling resulteerde in hydrofobe oppervlakken vanwege sterke fluoridering van de toplaag. Door tegelijkertijd de chemie en de structuur van de toplaag te modificeren met behulp van een etsende gasplasmabehandeling, konden de membraaneigenschappen worden afgestemd zonder daarbij het lage bevuilingskarakter van het membraan aan te tasten.

Nanostructurering van het oppervlak van een tweefasen hybridesysteem (organisch en anorganisch) door middel van oxidatief etsen met een gasplasma (CO_2, lucht) wordt beschreven in **hoofdstuk 7**. Eiwit-goud nanocolloïden (10-20 nm) werden vanuit een waterige oplossing in een eenstapsprocedure op diverse substraten (glas, silicium, polystyreen, LDPE)

geadsorbeerd. Het eiwit dient daarbij als adsorbaat, maar kan ook als 'spacer' fungeren die de geadsorbeerde gouddeeltjes onderling op een bepaalde afstand houdt. Na adsorptie werd het eiwit selectief weggeëtst van de gouddeeltjes door middel van gasplasmabehandeling. De substraten werden daarna gekarakteriseerd met SEM, AFM en XPS om respectievelijk de verdeling van de nanodeeltjes, de topografie en de chemie aan het oppervlak te bestuderen. Adsorptie van albumine-goud (AGC) en eiwit A-goud (PAGC) nanocolloïden met daaropvolgend het verwijderen van het eiwit was succesvol op de meeste substraten, waarbij de deeltjesdichtheid het hoogst was voor AGC geadsorbeerd op glas. Op alle substraten was AGC willekeurig verdeeld over het oppervlak. Uit selectieve thiol chemisorptie op silaan gefysisorbeerde goud controlesubstraten is gebleken dat het haalbaar is om deze heterogene, nanogestructureerde oppervlakken chemisch selectief te modificeren.

Hoofdstuk 8 is gericht op een studie waarin een blokcopolymeersysteem werd onderworpen aan oxidatief (CO_2) en mild (argon) etsen met een gasplasma. In dit laatste hoofdstuk is het effect van chemische (XPS) en structurele (SEM, AFM) oppervlaktemodificatie op de bevochtigbaarheid (randhoekmetingen) en de biocompatibiliteit (botcelhechting en -groei) van een serie gesegmenteerde polyetheenoxide/polybuteentereftalaat (PEO/PBT) blokcopolymeer films onderzocht. Langdurig etsen met een CO_2 plasma veroorzaakte in alle gevallen een aanzienlijke verandering van de oppervlaktestructuur. Er ontstond een korrelachtige nanostructuur die mogelijk kan worden toegeschreven aan een door temperatuur geïnduceerde heroriëntatie van het oppervlak van het fasengescheiden copolymeersysteem. Voor de meeste filmsamenstellingen waren de veranderingen van de oppervlaktechemie als gevolg van plasmabehandeling redelijk vergelijkbaar. CO_2 plasmabehandeling veroorzaakte oppervlakte-oxidatie en oxidatieve degradatie van de films, terwijl etsen met een argonplasma hoofdzakelijk leidde tot het preferentieel verwijderen van PEO blokken. Over het algemeen nam de bevochtigbaarheid van de films aanzienlijk toe na plasmabehandeling vanwege het ontstaan van polaire functionele groepen aan het oppervlak. Inleidende compatibiliteits-experimenten met geitenbeenmergcellen hebben laten zien dat alle met plasma behandelde PEO/PBT films een sterk verhoogde celhechting en/of -groei induceerden ten opzichte van het onbehandelde biomateriaal. Deze verbetering werd vooral toegeschreven aan veranderingen van de oppervlaktechemie en niet zozeer aan veranderingen van de oppervlaktestructuur tijdens het etsen met een gasplasma. Deze resultaten laten zien dat met plasma behandelde PEO/PBT blokcopolymeren geschikte kandidaten zijn voor gebruik bij botweefselregeneratie.

Curriculum Vitae

Mark Olde Riekerink kwam op 6 september 1972 in het Twentse dorp Losser ter wereld als oudste van een tweeling. Na achtereenvolgens de peuterspeelzaal, de kleuterschool, het basisonderwijs en het voortgezet onderwijs (VWO) probleemloos te hebben doorlopen, begon hij in 1990 aan de studie Chemische Technologie op de Universiteit Twente.

Na een leuke studieperiode en een interessante stage bij de Rode Kruis Bloedbank Groningen-Drenthe studeerde hij in april 1996 af bij de vakgroep 'Polymeerchemie en Biomaterialen' van prof. dr. Jan Feijen op het onderwerp 'Immobilisatie van heparine op polyetheen door gasplasmabehandeling'.

Zijn belangstelling voor de biomedische wetenschap en de gasplasmatechniek vormde de aanleiding om na zijn studie verder te gaan met een promotieonderzoek. Ook dit onderzoek, waarvan het resultaat nu voor u ligt, werd uitgevoerd aan de UT in de groep van prof. dr. Jan Feijen onder de bezielende leiding van dr. ir. Leon Terlingen en dr. ir. Gerard Engbers. Op dit proefschrift hoopt hij op 21 september 2001 te promoveren.

Sinds 1 mei 2001 is hij als ontwikkeltechnoloog werkzaam bij Philips Centre for Industrial Technology in Eindhoven.